Transposition of IS*Aba*13 in *Acinetobacter baumannii* AB5075

By

CHARLES COOPER

A thesis submitted to the University of Birmingham for the degree of
DOCTOR OF PHILOSOPHY

School of Biosciences
College of Life and Environmental Sciences
University of Birmingham
May 2024

Statement of contribution

This thesis and the preprint “H-NS is a bacterial transposon capture protein” doi: https://doi.org/10.1101/2024.02.16.580519 were written in parallel, and some parts of the text I have written for my thesis were adapted for the preprint by Prof. David Grainger.

Abstract

Acinetobacter baumannii is a critical priority category pathogen for which new drug treatments are urgently required. A major cause of nosocomial infection, *A. baumannii* is able to colonise and persist for long periods of time in hospital environments. Here we have characterised a novel colony variant of the well-studied, highly virulent, and drug-resistant, model strain AB5075.

We determined the biological mechanism for formation of these rare colonies; insertion sequence IS*Aba*13 disrupts gene *gtr52* of the capsule synthesis locus. As a consequence, there are profound phenotypic effects. We also probed the effects of IS*Aba*13 on transcription of adjacently located genes. This led to the discovery of the first bidirectional promoter within a bacterial insertion sequence.

Finally, we developed a method termed native Tn-Seq to map genome-wide natural insertions of IS*Aba*13 across a population of AB5075. This highlighted a propensity for insertion into AT-rich DNA, and a pivotal role for the chromosome folding protein H-NS in directing transposition to these regions. We show that the ability of H-NS to bridge DNA is required for directing these transposition events. To our knowledge, this is the first example of a bacterium dictating its own downstream evolution by manipulating patterns of transposition.

Acknowledgements

First and foremost, I would like to thank Prof. David Grainger who has been the best supervisor I could have ever dreamed of having. Thank you for always being so supportive and for helping to calm my constant worries.

I thank my lab colleagues and good friends including Andrew, Ksenia, Rachel, Matt, Al, Lucas, Ali, Tom, and Simon. I would like to extend a further thank you to Dr. Prateek Sharma, Dr. Emily Warman and especially Dr. James Haycocks, for their words of encouragement, unwavering support, and lab assistance. I would like to extend an even further special thanks to Dr. David Forrest who has been more than a best friend, but a true mentor to me. I would like to thank my undergraduate supervisor Dr. Emeline Lawaree for inspiring me to continue with science. I thank the members of my AAMR cohort Hannah, Sam, Lilly and Lizzy, and my gym buddy Oscar as well as Natalie. Thank you to the Wellcome Trust for funding this research and giving me this opportunity.

Finally, and most importantly, I would like to thank my family. My mother Aideen, father Mike, brother Alexander, sister-in-law Liza, Aunt Irene and grandparents Tom & Deirdre. You have all always been so incredibly supportive of me and I cannot thank you enough for everything you have done for me. I dedicate this work to all of you.

Abstract iii

Acknowledgements iv

List of Tables xi

List of Figures xii

Abbreviations xvi

Chapter 1: Introduction 1

1.1. The *Acinetobacter* genus 2
1.1.1. Infections caused by *A. baumannii* 3
1.1.2. *A. baumannii* model strains 3
1.1.3. Phase switch in *A. baumannii* 4

1.2. Virulence factors of *A. baumannii* 6
1.2.1. Capsular polysaccharide 6
1.2.2. Type IV pilus 12
1.2.3. Csu pilus 12
1.2.4. Type VI secretion system (T6SS) 13
1.2.5. OmpW 13

1.3. Biofilm formation 14

1.4. Motility 15

1.5. Natural transformation 16

1.6. Antibiotic resistance 17

1.7. Transposable elements 20
1.7.1. Insertion sequences and their derivatives 21
1.7.2. The IS5 family of insertion sequences 23
1.7.3. Mechanisms of transposition 24
1.7.4. Target site selection 26
1.7.5. Regulation of transposition 28
1.7.6. Transposition shapes genomes 30
1.7.7. Consequences of transposition on transcription 31

1.8. Transcription 32
1.8.1. RNA polymerase 33
1.8.2. Promoter structure 35
1.8.3. Transcription initiation 35
1.8.4. Transcription termination 36
1.8.5. Transcription factors 37

1.9. H-NS 38
1.9.1. The structure of H-NS 39
1.9.2. The role of H-NS in chromosome organization 39
1.9.3. The role of H-NS in transcriptional regulation 43
1.9.4. The function of H-NS *in A. baumannii* 45

1.10. Objectives of the project 46

Chapter 2: Materials and Methods 47

2.1. Materials 48
2.1.1. Strains 48
2.1.2. Plasmids 48
2.1.3. Oligonucleotides 48
2.1.4. Buffers and reagents 48

2.2. Growth of bacterial strains 48
2.2.1. Antibiotics 62
2.2.2. Storage as glycerol stocks 62
2.2.3. Generating pure stocks of colony phase variants 62

2.3. Gel electrophoresis 63
2.3.1. Agarose gel electrophoresis 63
2.3.2. Polyacrylamide gel electrophoresis (PAGE) 63
2.3.3. Sodium dodecylsulphate-polyacrylamide gel electrophoresis (SDS-PAGE) 63

2.4. DNA purification 64
2.4.1. PCR product purification 64
2.4.2. Agarose gel extraction 64
2.4.3. Plasmid purification 64
2.4.4. Phenol-chloroform extraction 65
2.4.5. Genomic DNA (gDNA) extraction 65

2.4.6. AMPure XP bead cleanup 65

2.5. DNA sequencing 66
2.5.1. Sanger sequencing 66
2.5.2. Whole genome sequencing 66

2.6. RNA purification 66

2.7. RNA sequencing 67

2.8. Cloning 67
2.8.1. PCR 67
2.8.2. Restriction digestion 70
2.8.3. Ligation 70
2.8.4. Gibson assembly 72
2.8.5. Preparation of chemically competent cells 72
2.8.6. Heat shock transformation 72
2.8.7. Natural transformation 73
2.8.8. Conjugation 73
2.8.9. Generation of scarless *ompW*::IS*Aba*13 chromosomal mutant 74

2.9. Phenotypic assays 74
2.9.1. Capsule production assay 74
2.9.2. Growth curves 76
2.9.3. Broth microdilution MIC 76
2.9.4. Congo Red binding assay 76
2.9.5. Biofilm assay 77
2.9.6. Surface-associated motility assay 77
2.9.7. Twitching motility assay 78
2.9.8. Natural transformation assay 78
2.9.9. Desiccation assay 78

2.10. *LacZ* assay 79

2.11. Native Tn-seq 80

2.12. *In vitro* transcription (IVT) 83

2.13. Radiolabelling of DNA fragments 84

2.14. Electrophoretic mobility shift assay (EMSA) 84

2.15. Bacterial two hybrid (BACTH) assay 84

2.16. Protein expression and purification 86
2.16.1. Measurement of protein concentration 86
2.16.2. Attempted protein purification of IS*Aba*13 encoded transposase 86
2.16.3. Native protein purification of H-NS 87
2.16.4. Peptide synthesis of H-NS^{39aa} 87

2.17. DNA bridging assay 88
2.17.1. Radiolabelling of prey DNA 88
2.17.2. DNA Bridging 88

2.18. Bioinformatics analysis 90
2.18.1. Genome sequence assembly 90
2.18.2. RNA-seq analysis 90
2.18.3. Conserved domain search 91
2.18.4. Native Tn-seq analysis 92
2.18.5. Data visualisation and statistics 92

Chapter 3: Insertion of IS*Aba*13 into the K-locus has diverse phenotypic implications 94

3.1. Introduction 95

3.2. Discovery of a novel colony morphology of AB5075 96

3.3. IS*Aba*13 inserts into the K-locus of grey cells 96

3.4. Insertion of IS*Aba*13 modulates the transcriptome of grey cells 98

3.5. Phenotypic impact of insertion of IS*Aba*13 at the K-locus 104
3.5.1. Grey cells have decreased capsule production 104
3.5.2. Grey cells show increased growth under standard laboratory conditions but decreased growth in human serum 106
3.5.3. Grey cells show increased susceptibility to gentamicin 108
3.5.4. Grey cells have reduced motility 110
3.5.5. Grey cells have an increased capacity to form biofilms 112
3.5.6. Grey cells have a reduced capacity for natural transformation 114
3.5.7. Grey cells are more hydrophobic and susceptible to desiccation 114

3.6. Discussion 117

Chapter 4: The IS*Aba*13 promoter is bidirectional and impacts transcription of adjacent genes 121

4.1. Introduction 122

4.2. Insertion of IS*Aba*13 blocks transcription of the K-locus 123

4.3. Annotation of TSSs and promoter elements across the K-locus 123

4.4. The impact of IS*Aba*13 orientation on transcription termination of adjacent genes *in vivo* 126

4.5. The bidirectional promoter of IS*Aba*13 is active *in vivo* 127

4.6. IS*Aba*13 does not block transcription *in vitro* 131

4.7. Discussion 134

Chapter 5: Locations and consequences of global insertions of IS*Aba*13 137

5.1. Introduction 138

5.2. Mapping global insertion sites of IS*Aba*13 in a population with native Tn-seq 139

5.3. Preferential insertion of IS*Aba*13 into the K-locus 142

5.4. IS*Aba*13 inserts into *ompW* and *ABUW_1221* 144
5.4.1. Phenotypes of IS*Aba*13 insertion into *ompW* and *ABUW_1221* 146
5.4.2. The impact of *ompW*::IS*Aba*13 on transposition 146

5.5. IS*Aba*13 inserts into *hns* 150
5.5.1. Phenotypes of the *hns*::T26 mutant 150

5.6. Discussion 154

Chapter 6: H-NS directs transposition of IS*Aba*13 by DNA bridging 162

6.1. Introduction 163

6.2. H-NS directs transposition of IS*Aba*13 to AT-rich regions..... 166

6.3. Attempted purification of IS*Aba*13 transposase 169

6.4. H-NS does not interact with IS*Aba*13 encoded transposase..... 173

6.5. Purification of *A. baumannii* H-NS 175

6.6. H-NS binds to IS*Aba*13 insertion hotspots *in vitro* 175

6.7. H-NS bridges DNA *in vitro* 179

6.8. H-NS^{39aa} disrupts bridging of H-NS *in vitro* 181

6.9. H-NS^{39aa} disrupts bridging of H-NS *in vivo* 181

6.10. H-NS^{39aa} does not inhibit H-NS binding to DNA 184

6.11. Discussion 184

Chapter 7: Final discussion 191

Appendices 195

References 209

List of Tables

Table 1.1. Well characterised virulence factors of *A. baumannii* and their functions 8

Table 2.1. Strains used in this study 50

Table 2.2. Plasmids used in this study 52

Table 2.3. Oligonucleotides used in this study..... 59

Table 2.4. Buffers and reagents used in this study..... 61

Table 2.5. PCR parameters used for Q5 polymerase 69

Table 2.6. PCR parameters used for colony PCR 71

Table 2.7. PCR parameters used for 1st PCR in native Tn-seq 82

Table 3.1. Conserved domain search of hypothetical proteins upregulated/downregulated in RNA-seq..... 103

Table 3.2. MIC of VIR-O, AV-T and grey cells measured by broth microdilution 109

Table 5.1. MIC of WT and *ompW*::IS*Aba*13 measured by broth microdilution 149

Table 5.2. MIC of WT and *hns*::T26 measured by broth microdilution 156

List of Figures

Fig.1.1. Colony morphology of AB5075 VIR-O and AV-T variants 7

Fig.1.2. Illustration of a selection of well characterised virulence factors of *A. baumannii* 7

Fig.1.3. Arrangement of the K-locus in *A. baumannii*..... 10

Fig.1.4. Synthesis of capsular polysaccharide 11

Fig.1.5. Illustration of resistance mechanisms of *A. baumannii* 19

Fig.1.6. Illustration of ISs and their derivatives..... 22

Fig.1.7. Mechanisms of transposition of IS5 family IS903 25

Fig.1.8. DNA elements associated with RNAP binding 34

Fig.1.9. The structure of H-NS 40

Fig.1.10. Stiffening and bridging modes of H-NS..... 42

Fig.2.1. Illustration of RNA-seq methods..... 68

Fig.2.2. Illustration of creation of scarless chromosomal *ompW*::IS*Aba*13 mutant 75

Fig.2.3. Illustration of BACTH assay..... 85

Fig.2.4. Illustration of DNA bridging assay..... 89

Fig.3.1. Colony morphology of different AB5075 variants on LBA plates..... 97

Fig.3.2. VIR-O and grey genome sequences assembled from long read genome sequencing 99

Fig.3.3. Illustration of IS*Aba*13 insertion into the K-locus 100

Fig.3.4. RNA-seq of differentially expressed genes between VIR-O and grey cells 101

Fig.3.5. Capsule production in VIR-O, AV-T and grey cells..... 105

Fig.3.6. Growth curves of VIR-O, AV-T and grey cells 107

Fig.3.7. Motility of VIR-O, AV-T and grey cells 111

Fig.3.8. Biofilm formation of VIR-O, AV-T and grey cells 113

Fig.3.9. Natural transformation of VIR-O, AV-T and grey cells . Error! Bookmark not defined.

Fig.3.10. Hydrophobicity and desiccation tolerance of VIR-O, AV-T and grey cells 116

Fig.4.1. TSS, total RNA and TTS compared at the K-locus..... 124

Fig.4.2. DNA sequence of promoter elements of *gtr52* and IS*Aba*13 125

Fig.4.3. *lacZ* assay with different orientations of IS*Aba*13 128

Fig.4.4. *lacZ* assay with IS*Aba*13 promoter element mutations 129

Fig.4.5. *lacZ* assay with bidirectional activity of IS*Aba*13 130

Fig.4.6. IVT of IS*Aba*13 K-locus constructs 132

Fig.5.1. The method of native Tn-seq 140

Fig.5.2. Global insertion of IS*Aba*13 in AB5075 141

Fig.5.3. Insertion of IS*Aba*13 into the K-locus identified by native Tn-seq ... 143

Fig.5.4. IS*Aba*13 insertion into *ompW* and *ABUW_1221* 145

Fig.5.5. Growth curves of *ompW*::IS*Aba*13 and *ABUW_1221*::T26 cells 147

Fig.5.6. *ompW*::IS*Aba*13 and *ABUW_1221*::T26 biofilm assay 148

Fig.5.7. IS*Aba*13 insertion in *ompW*::IS*Aba*13 151

Fig.5.8. IS*Aba*13 insertion into *hns* 152

Fig.5.9. Growth curves of wild-type and *hns*::T26 cells 153

Fig.5.10. *hns*::T26 biofilm assay 155

Fig.6.1. Sequence and putative structure of *A. baumannii* H-NS 165

Fig.6.2. IS*Aba*13 hotspots are lost in an *hns*::T26 mutant 168

Fig.6.3. SDS-PAGE of pET21-IS*Aba*13 and pET28-IS*Aba*13 expression 171

Fig.6.4. SDS-PAGE of MBP-IS*Aba*13 fusion expression 172

Fig.6.5. BACTH assay for H-NS and IS*Aba*13 encoded transposase 174

Fig.6.6. SDS-PAGE of expression of *A. baumannii* H-NS 176

Fig.6.7. SDS-PAGE of *A. baumannii* H-NS purification 177

Fig.6.8. H-NS EMSA for *csuAB* and T6SS intergenic regions. 178

Fig.6.9. *in vitro* bridging assay of H-NS 180

Fig.6.10. *in vitro* bridging assay of H-NS with H-NS^{39aa} 182

Fig.6.11.Native Tn-seq with wild-type cells expressing H-NS^{39aa} 183

Fig.6.12. H-NS^{39aa} does not impair H-NS binding to DNA 185

Fig.6.13. Potential models for how H-NS directs transposition 188

Abbreviations

Name	Abbreviation
3C-seq	Chromosome conformation capture sequencing
ATP	Adenosine triphosphate
ACB complex	*Acinetobacter baumannii* complex
Ata	Autotransporter adhesin
APS	Ammonium persulphate
AV-T	Avirulent translucent
BACTH	Bacterial two hybrid assay
Bap	Biofilm associated protein
BSA	Bovine serum albumin
CFU	Colony forming units
ChIP-seq	Chromatin immunoprecipitation sequencing
CIP	Calf intestinal phosphatase
CTD	C-terminal domain
DNA	Deoxyribonucleic acid
dRNA-seq	Differential RNA-seq
dsDNA	Double stranded DNA
DTR	Direct target repeat
EMSA	Electrophoretic mobility assay
GFP	Green fluorescent protein
GST	Glutathione-S-transferase
H-NS	Histone-like nucleoid structuring protein
HGT	Horizontal gene transfer
HPLC	High-performance liquid chromatography
HSA	Human serum albumin
ICU	Intensive care unit
ICE	Integrative conjugative element
IHF	Integration host factor
IME	Integrative mobilizable element
IPTG	isopropyl β-d-1-thiogalactopyranoside
IR	Inverted repeat

IRL	Left inverted repeat
IRR	Right inverted repeat
IS	Insertion sequence
ISs	Insertion sequences
IS-seq	Insertion sequence sequencing
IVT	*In vitro* transcription
LB	Lysogeny broth
LBA	Lysogeny broth agar
LOS	Lipooligosaccharide
LPS	Lipopolysaccharide
MBP	Maltose binding protein
MDR	Multidrug resistant
MGE	Mobile genetic element
MIC	Minimal inhibitory concentration
MITE	Miniature inverted repeat transposable element
NAP	Nucleoid associated protein
nt	nucleotides
NTP	Nucleoside triphosphate
mRNA	Messenger RNA
OMV	Outer membrane vesicle
ONPG	2-nitrophenyl-ß-D-galactopyranoside
ORF	Open Reading Frame
PAGE	Polyacrylamide gel electrophoresis
PNAG	poly-β-1,6-N-acetylglucosamine
PNK	Polynucleotide kinase
polyU	polyuridine
REPs	Repetitive extragenic palindromic sequences
RNA	Ribonucleic Acid
RNA-seq	RNA sequencing
RNAP	RNA polymerase
rRNA	Ribosomal RNA
SD	Shine-Dalgarno
SDS	Sodium dodecylsulphate
SDS-PAGE	Sodium dodecylsulphate polyacrylamide gel electrophoresis
SIDD	stress-induced duplex destabilization
SNP	Single nucleotide polymorphism

sRNA	Small RNA
SUMO	Small ubiquitin-like modifier
S-layer	Surface layer
T4P	Type IV Pilus
T6SS	Type VI secretion system
TE	Transposable Element
TIR	Terminal inverted repeat
tIS	Transporter insertion sequence
Tn-seq	Transposon sequencing
tRNA	Transfer RNA
TSS	Transcription start site
TSSs	Transcription start sites
TTS	Transcription termination site
TTSs	Transcription termination sites
UDP-diNAcBac	UDP-N,N-diacetylbacillosamine
UDP-GalNAc	UDP-N-acetylgalactosamine
UDP-GlcNAc	UDP-N-acetylglucosamine
Und-P	Undecaprenyl-pyrophosphate
VAP	Ventilator associated pneumonia
VIR-O	Virulent opaque
WT	Wild-type
XDR	Extensively drug resistant

Chapter 1: Introduction

1.1. The *Acinetobacter* genus

The genus *Acinetobacter* is comprised of aerobic, Gram-negative, non-fermentative, catalase-positive and oxidase-negative coccobacilli (Juni, 1978; Lee *et al.*, 2017). Within this genus are diverse non-pathogenic and commensal species which have been isolated from environments including soil, water, sewage and the skin/upper respiratory tract of humans (Juni, 1978; Bergogne-Bérézin and Towner, 1996; Jung and Park, 2015). Currently, six phenotypically/genetically related species, indistinguishable by simple biochemical tests, have been grouped together into the *Acinetobacter calcoaceticus-Acinetobacter baumannii* complex (ACB complex) (Vijayakumar, Biswas and Veeraraghavan, 2019). These include the environmental species *Acinetobacter calcoaceticus* and the human pathogens *Acinetobacter baumannii, Acinetobacter pittii, Acinetobacter seifertii, Acinetobacter dijkshoorniae and Acinetobacter nosocomialis* (Vijayakumar, Biswas and Veeraraghavan, 2019). Pathogenic *Acinetobacter* species which are not members of the ACB complex are less commonly isolated from clinical specimens (less than 30 % of specimens containing *Acinetobacter* compared with ACB complex members), and include *Acinetobacter lwoffi*, *Acinetobacter haemolyticus*, *Acinetobacter junii*, *Acinetobacter radioresistens*, and *Acinetobacter johnsonii* (Gupta *et al.*, 2015; Vijayakumar, Biswas and Veeraraghavan, 2019; Sheck *et al.*, 2023). Globally, the most frequently isolated pathogenic *Acinetobacter* species are three members of the ACB complex, *A. nosocomialis, A. pittii*, and *A. baumannii* (Weber, Harding and Feldman, 2016). The latter is most prevalent and associated with the greatest mortality (Visca, Seifert and Towner, 2011; Park *et al.*, 2014; Lee *et al.*, 2017; Mohd Rani *et al.*, 2018; Rebic *et al.*, 2018). In 2019, *A. baumannii* was estimated to cause over 450,000 deaths (Ikuta *et al.*, 2022).

1.1.1. Infections caused by *A. baumannii*

A. baumannii is most frequently found within hospital environments and is an opportunistic pathogen of immunocompromised individuals and patients in intensive care units (ICUs) (Visca, Seifert and Towner, 2011). Although predominantly a nosocomial pathogen, community-acquired infections are increasingly prevalent, particularly in tropical climates, with up to 88 % of patients presenting during humid months (Dexter *et al.*, 2015). The organism causes meningitis, and can infect the skin, wounds, urinary tract, blood, and most commonly, the lungs, often manifesting as ventilator-associated pneumonia (VAP) (Ayoub Moubareck and Hammoudi Halat, 2020). Interestingly, a high incidence of infection has been reported in wounded military personnel serving in Iraq/Afghanistan (Johnson *et al.*, 2007; Calhoun, Murray and Manring, 2008). The propensity of *A. baumannii* to cause nosocomial infections is enabled by its ability to colonise multiple surfaces, survive desiccation, resist the host immune response, and resist multiple antibiotics (Monem *et al.*, 2020). First-line antibiotic treatments for *A. baumannii* include β-lactams such as penicillin's, cephalosporins and carbapenems with β-lactamase inhibitors, while second-line treatments include aminoglycosides, polymyxins, trimethoprim/sulfamethoxazole and tetracycline and related derivatives (Rafailidis *et al.*, 2024).

1.1.2. *A. baumannii* model strains

Antibiotic resistance can vary drastically between *A. baumannii* isolates. For example, the model strain ATCC 17978 is susceptible to aminoglycosides, cephalosporins and fluoroquinolones, whereas the commonly studied strain AYE is classified as resistant to these

antibiotics (Harris *et al.*, 2013). Strain *A. baumannii* AB5075, isolated from a tibial osteomyelitis infection, is susceptible only to tetracycline, doxycycline, erythromycin, hygromycin, tigecycline and polymyxin B (Jacobs *et al.*, 2014; Cheng *et al.*, 2019). AB5075 was chosen as the model strain in this study because it has been shown to be highly drug resistant, genetically tractable, and highly virulent in both *Galleria mellonela* and murine pulmonary models, making it an infectious isolate of interest (Jacobs *et al.*, 2014).

1.1.3. Phase switch in *A. baumannii*

Previously, it was reported that AB5075 can undergo a phase switch in colony opacity (Tipton, Dimitrova and Rather, 2015). The two forms, virulent opaque (VIR-O) and avirulent translucent (AV-T) must be distinguished using oblique indirect lighting with a stereo dissecting microscope (Fig.1.1) (Tipton, Dimitrova and Rather, 2015). At a particular angle of incident light, VIR-O colonies have a rainbow shine around half of the colony (Fig.1.1a), whereas AV-T colonies have a thicker blue outer layer surrounding the entire colony, and a paler inner area (Fig.1.1b). Intermediate colonies undergoing switching between the two phases can occasionally be observed (Fig.1.1c). This phase switch is not limited to AB5075, with 3/4 strains, and all of 54 isolates in a separate study, found to produce translucent colonies (in the context of a majority opaque morphology) when plated on LB agar (Tipton, Dimitrova and Rather, 2015; Ahmad *et al.*, 2019). Recently, a low-switching opaque variant, with a 1000-fold decrease in switching frequency compared to a typical VIR-O cell, has been discovered (Anderson *et al.*, 2020). This variant has only one copy of an amplified region of a

(a)

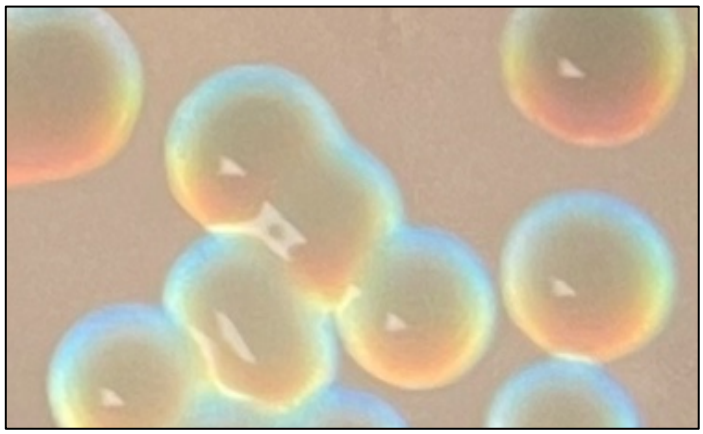

(b)

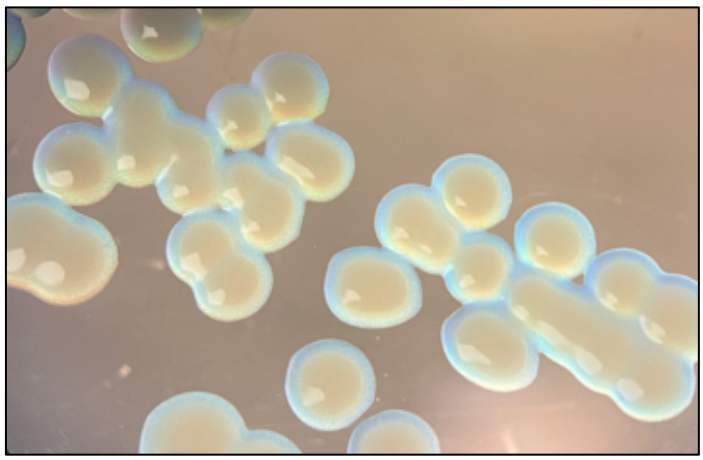

(c)

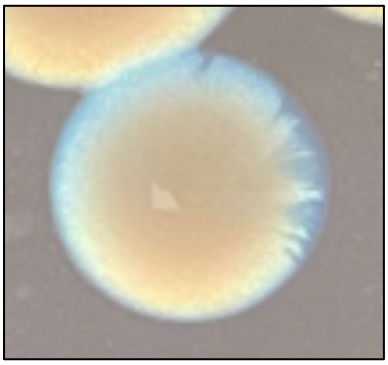

Fig.1.1. Colony morphology of AB5075 VIR-O and AV-T variants
Colonies viewed using an SMZ1000 Nikkon stereomicroscope with oblique indirect illumination (a) VIR-O variants (b) AV-T variants (c) colony undergoing 'switching' between VIR-O and AV-T.

plasmid integron locus (compared to two copies in typical VIR-O cells), with switching to AV-T regulated by part of the amplified region encoding a putative global regulator small RNA (sRNA) (Anderson *et al.*, 2020). VIR-O and AV-T cells show differences in capsule thickness, virulence, host antimicrobial susceptibility, antibiotic susceptibility, desiccation survival, biofilm formation, and motility (Tipton, Dimitrova and Rather, 2015; Chin *et al.*, 2018). These phenotypes may provide advantages in different environments. A TetR-like transcriptional regulator (ABUW_1645) has been identified as a key factor in maintaining the AV-T phase, initially identified as an essential gene for growth in the *G. mellonella* infection model (Gebhardt *et al.*, 2015; Chin *et al.*, 2018).

1.2. Virulence factors of *A. baumannii*

In order to successfully colonise a host, *Acinetobacter* species use a large arsenal of virulence factors. The most well-known virulence factors are illustrated in Fig.1.2 with functions outlined in Table 1.1. The most relevant virulence factors to this study are described in the subsections following.

1.2.1. Capsular polysaccharide

The cell capsule is the outermost exopolysaccharide layer of *A. baumannii*, formed of repeating oligosaccharide subunits (K-units) (Singh, Adams and Brown, 2019). Genes involved in capsule biosynthesis are organised into a genetic region called the K-locus (Fig.1.3a) (Kenyon and Hall, 2013). Strain AB5075 has a K-locus designated as type KL25, as illustrated in Fig.1.3b. In multiple strains of *A. baumannii*, K-unit synthesis starts with the production of the

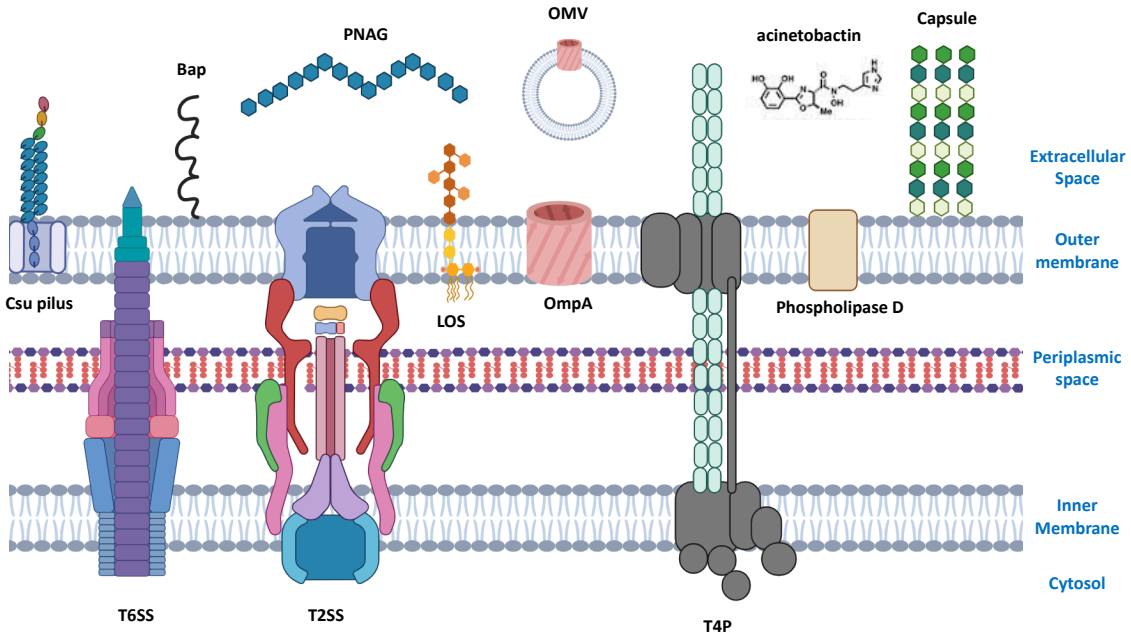

Fig.1.2. Illustration of a selection of well characterised virulence factors of *A. baumannii*
Bap = Biofilm associated protein, PNAG = poly-β-1,6-N-acetylglucosamine, OMV = outer membrane vesicle, LOS = lipooligosaccharide, T6SS = type 6 secretion system, T2SS = type 2 secretion system, T4P = Type IV pilus. Figure created with Biorender.

Factor	Function	Reference
Phospholipase D	Acts on phosphatidylcholine of eukaryotic membranes for epithelial cell invasion	(Jacobs *et al.*, 2010; Stahl *et al.*, 2015)
OmpA	Adherence and invasion of epithelial cells, induction of apoptosis of host cell, adhesion to abiotic surfaces	(Choi *et al.*, 2005, 2008; Gaddy, Tomaras and Actis, 2009)
OMV	Small spherical proteoliposomes formed from outer membrane which release OmpA and other virulence factors into target cells	(Jun *et al.*, 2013)
Acinetobactin	High affinity iron chelator essential for utilising host iron	(Sheldon and Skaar, 2020)
LOS	Formed of a lipid A anchor glycosylated with core oligosaccharides, without an O-antigen repeat as seen in lipopolysaccharide (LPS). Confers rigidity and permeability.	(Morris *et al.*, 2019; Simpson *et al.*, 2021)
Capsular polysaccharide	Provides resistance from desiccation, disinfectants, antibiotics, and antimicrobials	(Singh, Adams and Brown, 2019)
Csu pilus	Attachment to abiotic and biotic surfaces, biofilm maturation, epithelial cell adhesion	(Tomaras *et al.*, 2003; Ahmad *et al.*, 2023)
T2SS	Secretion of protein effectors (toxins lipases, proteases)	(Johnson *et al.*, 2016)
T6SS	Injection of proteins to kill neighbouring bacterial competitors	(Carruthers *et al.*, 2013)
Bap	Formed of immunoglobulin-like domains, involved in biofilm formation and adhesion to epithelial cells and abiotic surfaces	(Brossard and Campagnari, 2012)
PNAG	Attachment to abiotic surfaces and biofilm formation	(Choi *et al.*, 2009)
T4P	Twitching motility, natural transformation, epithelial cell adherence	(Vesel and Blokesch, 2021; Ahmad *et al.*, 2023)

Table 1.1. Well characterised virulence factors of *A. baumannii* and their functions

(a)

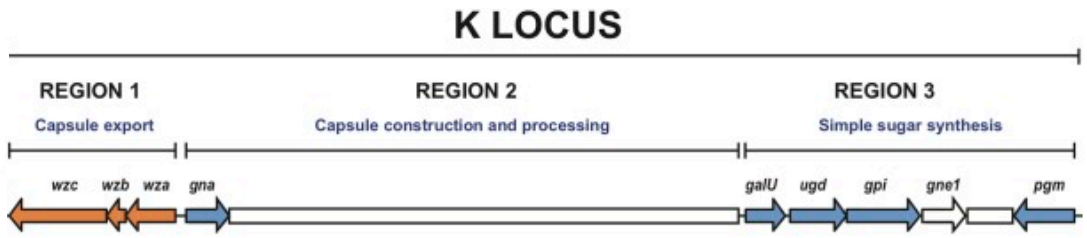

(b)

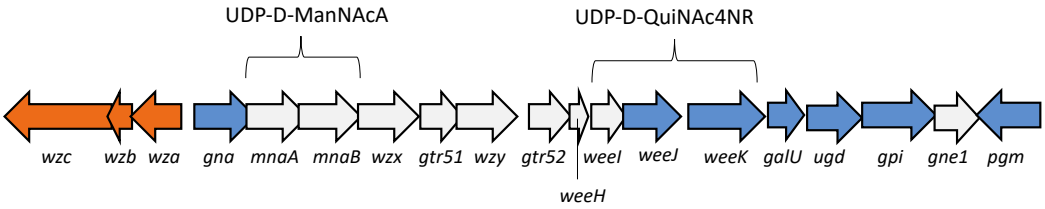

Fig.1.3. Arrangement of the K-locus in *A. baumannii*

(a) General arrangement of the K-locus in *A. baumannii.* Capsule production and processing region (white box) shows less conservation than the other two regions, indicating a high variability of genes. Figure adapted from (Wyres *et al.*, 2020)**.** (b) KL25 capsule biosynthesis locus of AB5075. Note synonyms for genes include *itrA1/pglC* (*weeH*), *qhbA* (*weeI*), *qhbB* (*weeJ*). The genes *mnaA* and *mnaB* are for synthesis of the sugar UDP-D-ManNAcA, and the genes, *weeI*, *weeJ* and *weeK* are used for synthesis of UDP-D-QuiNAc4NR. Figure adapted from (Senchenkova *et al.*, 2015)**.**

sugar nucleotide UDP-N,N-diacetylbacillosamine (UDP-diNAcBac), also known as UDP-D-QuiNAc4NAc) (Fig1.4a) (Morrison and Imperiali, 2013). Phospho-diNAcBac is added by the initial phosphoglycosyltransferase (*itr,* also known as *pglC/weeH*) onto the lipid carrier undecaprenyl-pyrophosphate (Und-P) to give Und-PP-diNAcBac (Morrison and Imperiali, 2013; Singh, Adams and Brown, 2019). Note that some strains of *A. baumannii* can use UDP-N-acetylglucosamine (UDP-GlcNAc) or UDP-N-acetylgalactosamine (UDP-GalNAc) as starting phosphorylated monosaccharides for transfer onto the Und-P scaffold (Harding *et al.*, 2018). Additional sugars are then added to this scaffold by further glycosyltransferase enzymes (for example *gtr51* and *gtr52* in AB5075) to produce the final K-unit (Singh, Adams and Brown, 2019). In AB5075 K-units are a trisaccharide repeat, as illustrated in Fig. 1.4b. Note that in AB5075, WeeI can add either an acetyl group or an (S)-3-hydroxybutanoyl group (Fig.1.4b). K-units are translocated to the periplasm by the flippase Wzx, polymerized by Wzy, and exported through the outer membrane for presentation on the surface by the Wza/Wzb/Wzc complex (Singh, Adams and Brown, 2019). Alternatively, K-units can be used for O-linked protein glycosylation of selected surface proteins. The O-oligosaccharyltransferase, PglL, attaches the sugar unit to the target protein via a serine/threonine residue (Lees-Miller *et al.*, 2013).

The capsule is a barrier against disinfectants, antibiotics, antimicrobials and complement, and protects from desiccation (Singh, Adams and Brown, 2019). The propensity of *Acinetobacter* to persist and survive in the hospital environment is greatly enabled by its ability to survive long periods of desiccation. Capsule forms a negatively charged hydrophilic layer at the

(a)

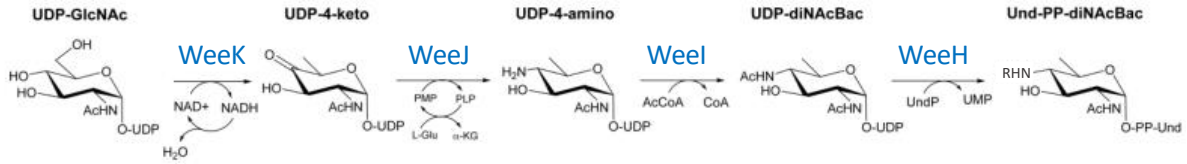

(b)

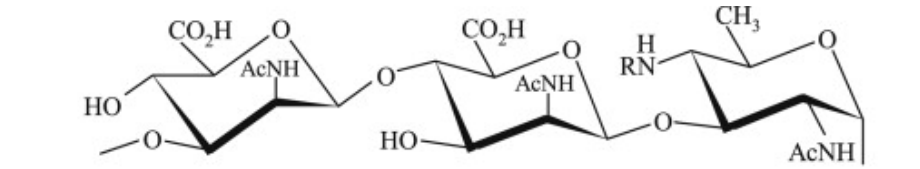

→3)-β-D-Man*p*NAcA-(1→4)-β-D-Man*p*NAcA-(1→3)-α-D-Qui*p*NAc4NR-(1→

R = (*S*)-3-hydroxybutanoyl or acetyl (~2.5:1)

Fig.1.4. Synthesis of capsular polysaccharide

(a) Pathway of UDP-diNAcBac synthesis in *A. baumannii*. WeeK catalyses oxidation of the 4-hydroxyl of UDP-GlcNac to a ketone by NAD^+, with loss of water and subsequent reduction of the alkene bond at C6 to give UDP-4-keto. The aminotransferase WeeJ attaches an amino group from glutamic acid at C4 using pyridoxal 5'-phosphate (PMP) to create UDP-4-amino. The acetyltransferase WeeI uses Acetyl coenzyme A (AcCoA) to attach an acetyl group at C4 to generate UDP-diNAcBac, which is attached to Und-P by WeeH. Figure adapted from (Morrison and Imperiali, 2013). (b) Biochemical structure of capsular polysaccharide K-unit in AB5075. R group can be either (S)-3-hydroxybutanoyl or an acetyl group. Figure from (Senchenkova *et al*., 2015).

surface which helps to retain water (Singh, Adams and Brown, 2019; Kon *et al.*, 2020). *A. baumannii* clones with greater hydrophobicity show decreased desiccation tolerance, reduced virulence and an increased biofilm forming propensity (Vesel and Blokesch, 2021). Interestingly, the oxidoreductase thioredoxin A decreases cell surface hydrophobicity by maintaining levels of the Type IV pilus (T4P) (May *et al.*, 2019).

1.2.2. Type IV pilus

The T4P is a multi-protein helical fibre structure critical for twitching motility, natural transformation, adhesion and infection (Vesel and Blokesch, 2021). The backbone of the T4P consists of multiple units of the major pilin subunit PilA. These polymerise to extend, and depolymerise to retract, the pilus (Ellison *et al.*, 2021). The cytoplasmic AAA+ ATPase motor proteins, PilB and PilT, mediate extension and retraction respectively via interactions with integral membrane protein PilC (Ellison *et al.*, 2021). There is large functional diversity of PilA in terms of sequence and glycosylation patterns (Ronish *et al.*, 2019). While some strains carry a designated type IV pilus glycosylation enzyme (TfpO) others, such as AB5075, do not (Harding *et al.*, 2015; Ronish *et al.*, 2019). Variation of PilA properties such as surface charge, between different *Acinetobacter,* may indicate a choice between motility and biofilm formation (Ronish *et al.*, 2019).

1.2.3. Csu pilus

The Csu chaperone-usher type pili are longer than T4P, and are encoded by an operon formed of the genes *CsuA/B, csuA, csuB, csuC, csuD and csuE* (Ahmad *et al.*, 2023). Csu pili are key

mediators of biofilm maturation at abiotic surfaces. Unlike deletion of genes encoding the T4P major subunit *pilA*, deletion of *csuA* or *csuC* significantly reduces pellicle biofilm formation (Ahmad *et al.*, 2023). The CsuA/B subunit was discovered to be the most abundant protein of air-liquid interface pellicles of three morphologically different clinical isolates (Chabane *et al.*, 2014). Csu pili were also shown to reduce surface motility, enhance murine bacterial colonization, and mediate adherence to A549 epithelial cells (Ahmad *et al.*, 2023).

1.2.4. Type VI secretion system (T6SS)

The T6SS secretion system is a multi-protein contractile structure mediating the contact-dependent injection of effector proteins into neighbouring cells. These can be other bacteria or eukaryotic hosts. Initially, T6SS of *A. baumannii* were only thought to target bacterial cells (Carruthers *et al.*, 2013; Morris *et al.*, 2019). However, recently, three yeast species were shown to be killed by *A. baumannii* using a T6SS secreted DNase called TafE (Luo *et al.*, 2023). However, the utility of the T6SS appears strain-dependent; the system is lost from some clinical isolates (Wright *et al.*, 2014). One study found that, despite expression of the T6SS in five *A. baumannii* strains, including three clinical isolates, only one non-clinical isolate could kill *E. coli* in a T6SS-dependent manner (Repizo *et al.*, 2015). This non-clinical isolate also showed dependency on the T6SS for virulence in *G. mellonela* (Repizo *et al.*, 2015).

1.2.5. OmpW

Though less well studied than other *A. baumannii* virulence factors, the β-barrel porin OmpW is significantly up-regulated in persister cells (quiescent bacteria which can survive transient

exposure to bactericidal antibiotics), which may partly explain increased virulence of persisters in *G. mellonella* (Schmitt *et al.*, 2023). Deletion of *ompW* decreases adherence, invasion, and cytotoxicity whilst the minimum lethal dose of *A. baumannii* in a mouse sepsis infection model increases (Gil-Marqués, Pachón and Smani, 2022). OmpW is also involved in the uptake of iron, and is found in OMVs with the potential to elicit a strong immune response, making it an attractive vaccine target (Huang *et al.*, 2015; Catel-Ferreira *et al.*, 2016). OmpW interacts with the OXA-23 carbapenamase, and is down-regulated in the carbapenem resistant strain ABRS307, and some colistin-resistant *A. baumannii* (Vila, Martí and Sánchez-Céspedes, 2007; Tiwari et al., 2012). This suggests levels of OmpW could play a role in susceptibility to carbapenems, and/or colistin. While deletion of *ompW* decreases susceptibility to multiple antibiotics in *E. coli*, in *A. baumannii* only a change in minimal inhibitory concentration (MIC) is seen for meropenem (Catel-Ferreira *et al.*, 2016; Wu *et al.*, 2016). Additionally, OmpW has been shown to play a positive role in biofilm formation in ATCC 17978 (Gil-Marqués, Pachón and Smani, 2022).

1.3. Biofilm formation

Biofilms are a population of surface-associated bacterial cells surrounded by a matrix of exopolysaccharides, extracellular DNA, proteins, and OMVs. When in a biofilm, bacteria are more resistant to antibiotic treatments, disinfectants, desiccation, and the host immune response (Gunn, Bakaletz and Wozniak, 2016). Biofilm formation on medical equipment such as catheters, prosthetic joints, pacemakers, and dry surfaces enables persistence of *A. baumannii* in the nosocomial environment (Pour *et al.*, 2011; Espinal, Martí and Vila, 2012; Upmanyu, Haq and Singh, 2022). In *A. baumannii* the main mediators of biofilm formation are

the aforementioned T4P and CsuA/BABCDE chaperone-usher complex, as well as OmpA, biofilm associated protein (Bap) and the exopolysaccharide poly-β-1,6-N-acetylglucosamine (PNAG) (Vijayakumar *et al.*, 2016). The latter is the glue holding the matrix together. Regulation of biofilm formation depends on many external factors including light, iron availability, oxygen, cell density, antibiotics and growth conditions (Upmanyu, Haq and Singh, 2022). The secondary messenger cyclic di-GMP, and two component system BfmR/S, have been identified as central regulators, coordinating the sensing of environmental conditions to biofilm production (Upmanyu, Haq and Singh, 2022). Additionally, environmental temperature can influence biofilm formation. In ATCC 17978, Csu is upregulated at 28 °C compared to 37 °C, leading to greater biofilm production (De Silva *et al.*, 2017). Conversely, surface-associated motility was reduced at this lower temperature, reinforcing the antagonism between biofilm formation and motility (De Silva *et al.*, 2017).

1.4. Motility

Although lacking a flagellum and classified as “non-motile”, *Acinetobacter* species are able to move across semi-solid surfaces by twitching motility and surface-associated motility (Vijayakumar *et al.*, 2016). Twitching motility, mediated by the T4P, is the movement of bacteria at the interface between two surfaces (Harding *et al.*, 2013). The T4P can extend, attach to a surface, and retract to pull the bacterium along towards the point of attachment (Harding *et al.*, 2013).

Surface-associated motility is less well understood, but is believed to be appendage-independent, and possibly driven by secretion of extrapolymeric material (Corral *et al.*, 2021). There is some discrepancy in results between whether the T4P also plays a role in surface-associated motility (Clemmer, Bonomo and Rather, 2011; Harding *et al.*, 2013; Wilharm *et al.*, 2013; Ahmad *et al.*, 2023). Overall however, it seems multiple genes, involved in nucleoside metabolism, stress response, RNA modification, outer membrane proteins, and natural transformation, are needed (Blaschke, Skiebe and Wilharm, 2021).

1.5. Natural transformation

Many *A. baumannii* strains are naturally transformable, able to take up DNA from the environment and incorporate it into their genome. In one study, 86/142 (36 %) clinical isolates were naturally competent (Hu *et al.*, 2019). Whereas, an even greater incidence (27/61, or 44 %) of environmental avian isolates were found to be naturally transformable (Wilharm *et al.*, 2017). This process is thought to involve the T4P, with *pilT,* the ATPase required for retraction, essential for natural transformation (Wilharm *et al.*, 2013). Additional essential components include PilQ, the secretin which allows DNA translocation through the outer membrane, and the ComEC channel, which allows passage through the inner membrane into the cell (Vesel and Blokesch, 2021). In *A. baumannii* A118, production of T4P is correlated with cell density, with maximum rates of transformation coinciding with an OD_{600} of 0.6 (Vesel and Blokesch, 2021). The propensity to undergo natural transformation has enabled horizontal gene transfer (HGT) of sequences involved in drug resistance, with homologous recombination driving strain

divergence (Snitkin *et al.*, 2011). This has led to the widespread acquisition, upregulation, exchange, and dissemination of antibiotic resistance determinants.

1.6. Antibiotic resistance

Antimicrobial resistance is a significant cause of global mortality, with almost 5 million deaths associated with, and 1.3 million deaths directly caused by bacterial antimicrobial resistance in 2019 (Murray *et al.*, 2022). The rapid development of resistance has been catalysed by a lack of new antibiotic research and development, poor stewardship, limited surveillance, and overuse of antibiotics in the clinic and agricultural industries. The ESKAPE pathogens (*Enterococcus faecium*, *Staphylococcus aureus, Klebsiella pneumoniae, Acinetobacter baumannii, Pseudomonas aeruginosa* and *Enterobacter* species) encompass a group of increasingly prevalent, virulent bacteria which have become particularly difficult to treat, given their formidable resistance to our current arsenal of antibiotics (Rice, 2008; Santajit and Indrawattana, 2016).

While general resistance to antibiotics is of increasing concern, carbapenem-resistant *A. baumannii* are classified as a critical priority for research and development of new antimicrobials by the World Health Organization (Tacconelli *et al.*, 2018). The alarming rise in multidrug resistant (MDR) *A. baumannii* has limited treatment options, leaving only antibiotics of last resort – colistin and tigecycline. Extensively drug resistant (XDR) and Pan-resistant strains are also emerging, with some infections essentially untreatable with current antibiotics (Karakonstantis, 2021). In 2019, over 100,000 deaths were attributable to *A. baumannii*

antimicrobial resistance, with the highest fraction of such deaths (relative to other bacterial pathogens) most prevalent in Southeast Asia, east Asia and Oceania (Murray *et al.*, 2022).

Resistance to antibiotics can be achieved by reducing their intracellular concentration. This can be done by efflux or by reducing entry. Antibiotic Inactivating/modifying enzymes, and modification/loss of the antibiotic target, can also play a role. The classical drug resistance mechanisms to antibiotics, with examples in *A. baumannii* are outlined in Fig.1.5. *A. baumannii* has a high degree of intrinsic resistance, that is resistance conferred as a consequence of the structural and functional characteristics of the bacterium. Important factors include low permeability outer membrane protein OmpA, along with constitutively expressed β-lactamases and efflux pumps (Sugawara and Nikaido, 2012; Ayoub Moubareck and Hammoudi Halat, 2020). Acquired resistance is when *Acinetobacter* obtains the ability to resist an antimicrobial to which it was previously susceptible. For example, the acquisition of metallo-β-lactamases contained in class I integrons (Ayoub Moubareck and Hammoudi Halat, 2020). The rapid dissemination of antimicrobial resistance genes in *A. baumannii* can be partially explained by the propensity for *Acinetobacter* to undergo HGT via conjugation, transformation, transduction and OMV transfer (Da Silva and Domingues, 2016). These processes often involve the exchange and movement of MGEs containing antibiotic resistance determinants. These include plasmids, bacteriophages, transposons, integrons, miniature inverted repeat transposable elements (MITEs) and insertion sequences (ISs) (Da Silva and Domingues, 2016).

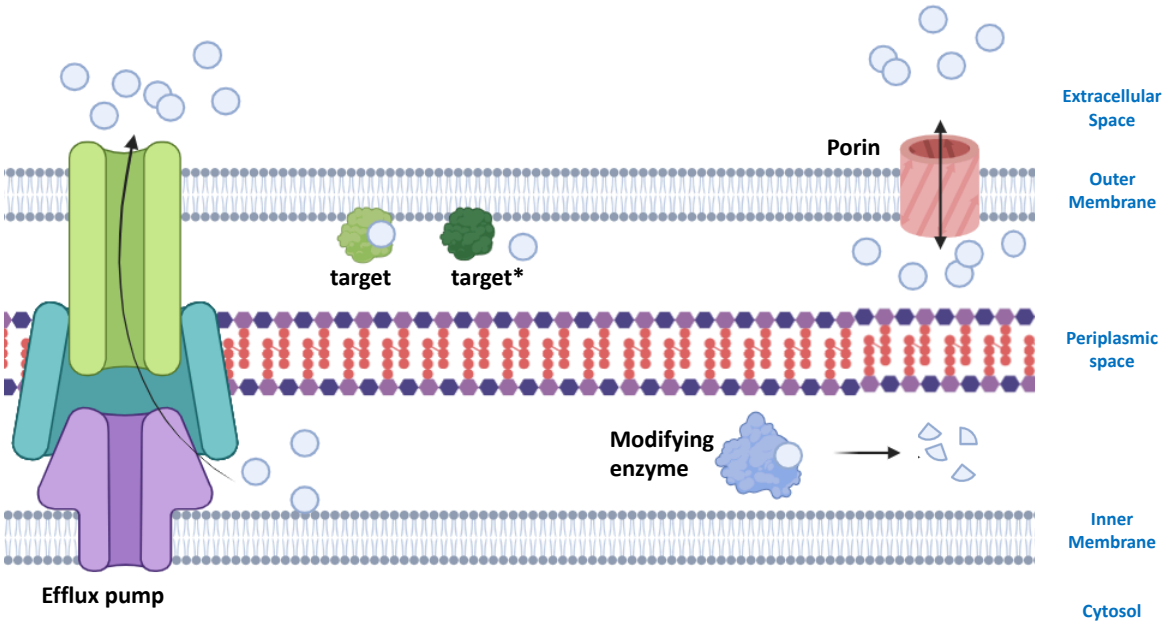

Fig.1.5. Illustration of resistance mechanisms of *A. baumannii*
Decreased expression of porins on the outer membrane e.g. OmpA reduces β-lactam entry into the cell (Sugawara and Nikaido, 2012). Increased efflux pump activity e.g. AdeIJK reduces intracellular tetracyline concentration (Saranathan *et al.*, 2017). Target alteration/loss, for example loss of LpxA stops lipid A synthesis targeted by polymyxins (Chamoun *et al.*, 2021). Destruction/modification of the antibiotic, e.g. β-lactamases such as carbapenamases that hydrolyse carbapenems (Turton *et al.*, 2006).

1.7. Transposable elements

MGEs can be classed as either intercellular, able to transfer from cell to cell (plasmids, phage) or intracellular, able only to reposition themselves within the cell (transposons, ISs, integrons and introns) (Siguier, Gourbeyre and Chandler, 2014). Note that intracellular MGEs may be moved between cells if integrated into intercellular MGEs. All intracellular MGEs are defined as transposable elements (TEs) (Siguier, Gourbeyre and Chandler, 2014). The boundaries between these classes of MGEs has become increasingly muddied in recent years by the discovery of conjugative transposons, also known as integrative conjugative elements (ICEs), integrative mobilizable elements (IMEs) and genomic islands, which have similarities to both intracellular and intercellular classes (Siguier, Gourbeyre and Chandler, 2014; Guédon *et al.*, 2017).

TEs are found in every domain of life and were first discovered as the cause of differently coloured corn kernels, in maize, by Barbara McClintock in 1948 (Feschotte, 2023). Autonomous TEs encode their own machinery for movement to new genomic locations. Conversely, non-autonomous TEs rely on trans-encoded proteins (Curcio and Derbyshire, 2003). Whilst TEs constitute a large fraction of eukaryotic DNA, these elements typically form less than 5 % of bacterial genomes (Curcio and Derbyshire, 2003). This could be because bacterial genomes have a more compact genetic architecture. Compared with eukaryotes, most bacterial TEs use DNA, rather than RNA, intermediates and are therefore classed as type II TEs (Siguier, Gourbeyre and Chandler, 2014).

1.7.1. Insertion sequences and their derivatives

The general structure of ISs, and closely related derivatives, is shown in Fig.1.6a. Insertion sequences are the simplest transposable elements of bacteria, consisting of short sequences (< 2.5 kb) and encoding a transposase (Ross *et al.*, 2021). Initially, ISs were said to only encode a transposase, whereas transposons were larger and defined by the carriage of passenger genes of additional function unrelated to transposition (Siguier *et al.*, 2015). The original definition of ISs no longer holds, following the discovery of transporter insertion sequences. These contain passenger genes for transcriptional regulators, methyltransferases, or antibiotic resistance factors (Siguier, Gagnevin and Chandler, 2009; Siguier *et al.*, 2015). If a transporter insertion sequence (tIS) loses its transposase gene, it becomes the non-autonomous transposable element known as a mobile insertion cassette. If an insertion sequence (IS) loses its transposase gene, it becomes a non-autonomous MITE (Siguier, Gourbeyre and Chandler, 2014).

Transposons (Fig.1.6b) can be subdivided into unit transposons and composite (also known as compound) transposons. In unit transposons, passenger genes are carried with a transposase (and typically a resolvase) as part of the transposon (Siguier *et al.*, 2015). ICEs represent a further group which resemble unit transposons but additionally contain genes for conjugative transfer into other bacteria (Siguier, Gourbeyre and Chandler, 2014). In composite transposons, passenger genes reside in a region between two copies of potentially different ISs. The IS copies encode the transposase necessary for transposition. For example, the IS5 family member IS903 flanks either side of a kanamycin resistance phosphotransferase gene in the composite transposon Tn903 (Grindley and Joyce, 1980).

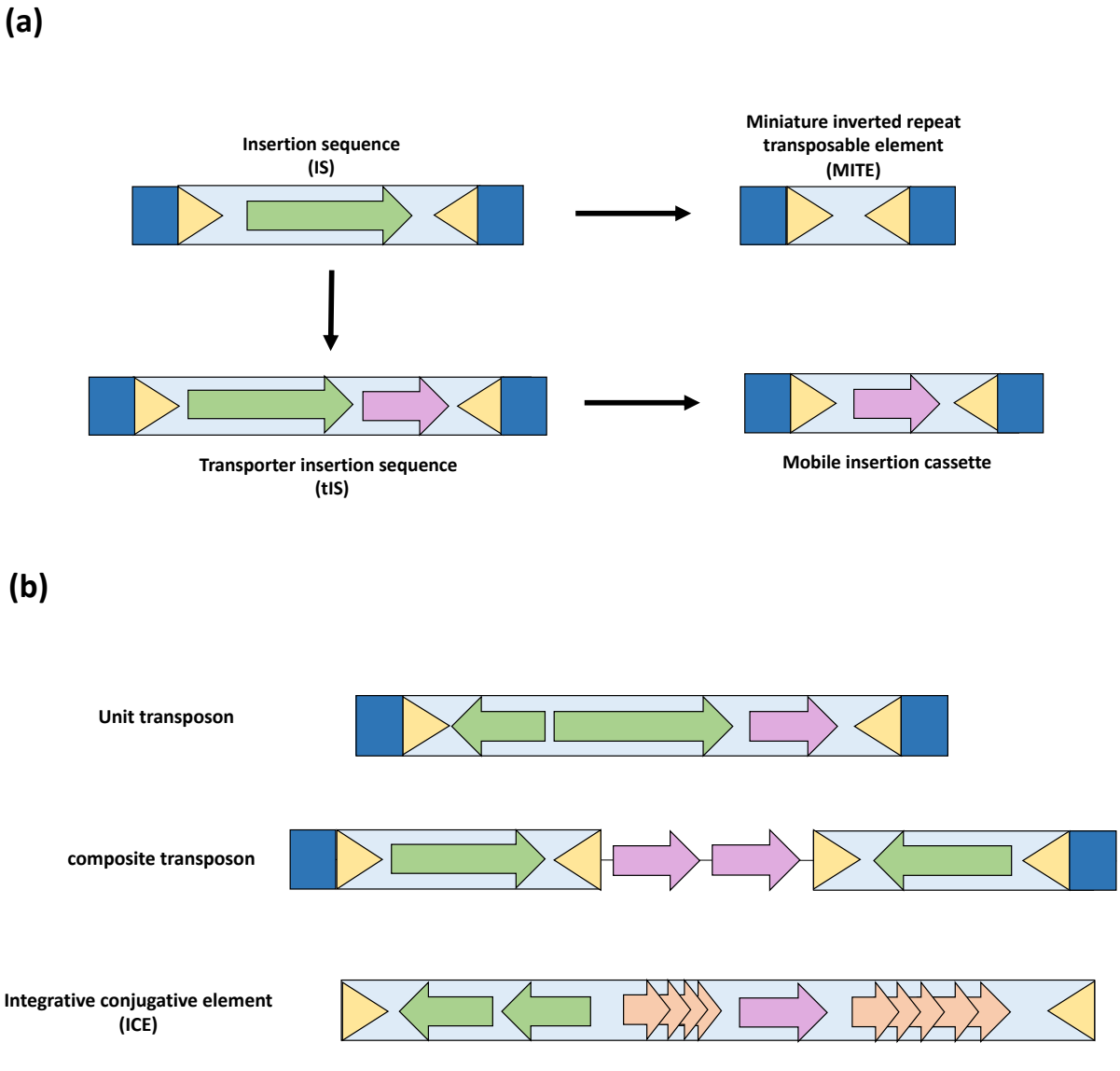

Fig.1.6. Illustration of ISs and their derivatives

Green arrow = transposase open reading frame (ORF), yellow triangles = terminal inverted repeats (TIR), dark blue square = direct target repeat (DTR), pink arrow = passenger gene, orange arrow = transfer genes. (a) Insertion sequences, MITEs, tIS and mobile insertion cassette. (b) Unit transposon, composite transposon and ICE. Figure inspired from (Siguier *et al.*, 2015)

1.7.2. The IS5 family of insertion sequences

IS5 was initially discovered as an insertion in bacteriophage lambda, disrupting the AT-rich cI gene which encodes the transcriptional factor regulating the lysogenic-lytic switch (Engler and Van Bree, 1981). Further studies concluded insertion of IS5 near the *bgl* promoter can activate expression of the H-NS repressed *bgl* operon in *E. coli* (Reynolds, Felton and Wright, 1981; Schnetz and Rak, 1992). The IS5 family is now relatively diverse and formed of six groups: IS5, IS427, ISH1, ISLL2, IS1031 and IS903, with most members containing only a single transposase open reading frame (ORF) (Siguier *et al.*, 2015).

Members of the IS5 family (including IS*Aba*5, IS*Aba*12, IS*Aba*13, IS*Aba*59 and IS*Aba*62) frequently make up a large proportion of the total IS elements in many *A. baumannii* genomes (Jung and Park, 2015; Adams, Bishop and Wright, 2016; Hamidian *et al.*, 2019; Guo *et al.*, 2022). IS*Aba*13 in particular is the most abundant of the IS5 family, found in 38 % of 1035 genomes analysed, and having the second greatest number of total sites identified (3,639) out of 37 IS elements surveyed (Adams, Bishop and Wright, 2016). Massive clonal expansion of some IS5 family elements is seen in some isolates, for example 22 copies of IS*Aba*13 in the hypervirulent isolate LAC-4, and 14 copies in the environmental isolate NCIMB8209 (Ou *et al.*, 2015; Hamidian *et al.*, 2019). Very little is known about the mechanism of transposition for IS5 family members, with the only currently characterised member being IS903 from *E. coli* (Tavakoli and Derbyshire, 2001).

1.7.3. Mechanisms of transposition

Transposases generally catalyse transposition by one of two mechanisms, non-replicative (also known as cut-and-paste or simple insertion) or replicative (also known as copy-and-paste). Both mechanisms have similar chemistry and start with cleavage of the 3' end of the IS at the donor site. With non-replicative transposition, 5' cleavage also occurs to produce a double stranded break. IS903 moves predominantly by a non-replicative mechanism but, intriguingly, can also move by a replicative mechanism called cointegrate formation (Tavakoli and Derbyshire, 2001). The mechanisms of transposition of IS903 are illustrated in Fig.1.7.

The first step in transposition is recognition of, and binding to, the terminal inverted repeats (TIR) by the transposase. Typically, two transposase monomers bind to the ends of the IS and oligomerise, bringing the ends together to form a synaptic complex or transpososome. Often, the transposase bound to one end catalyses cleavage at the other end, ensuring coordinated simultaneous cleavage at both ends (Nagy and Chandler, 2004; Hickan and Dyda, 2015). Insertion sequences can be grouped largely by the amino acids at the catalytic site of the transposase. The HUH transposases use tyrosine as a nucleophile, and have a conserved pair of histidine residues (H) between a large non-polar amino acid (U) (Siguier *et al.*, 2015). The DDE-transposases are much more common in IS transposition. All IS5 family members use a DDE transposase, which has a conserved catalytic triad of two aspartic acid (D) residues and one glutamic acid (E) residue (Siguier *et al.*, 2015). These residues coordinate divalent metal ions which activate the H_2O nucleophile for initial DNA cleavage at the donor site IS ends (hydrolysis), or the nucleotide 3'OH nucleophile during strand transfer into a new target site (transesterification) (Hickman and Dyda, 2015). During strand transfer, nucleophilic attack on

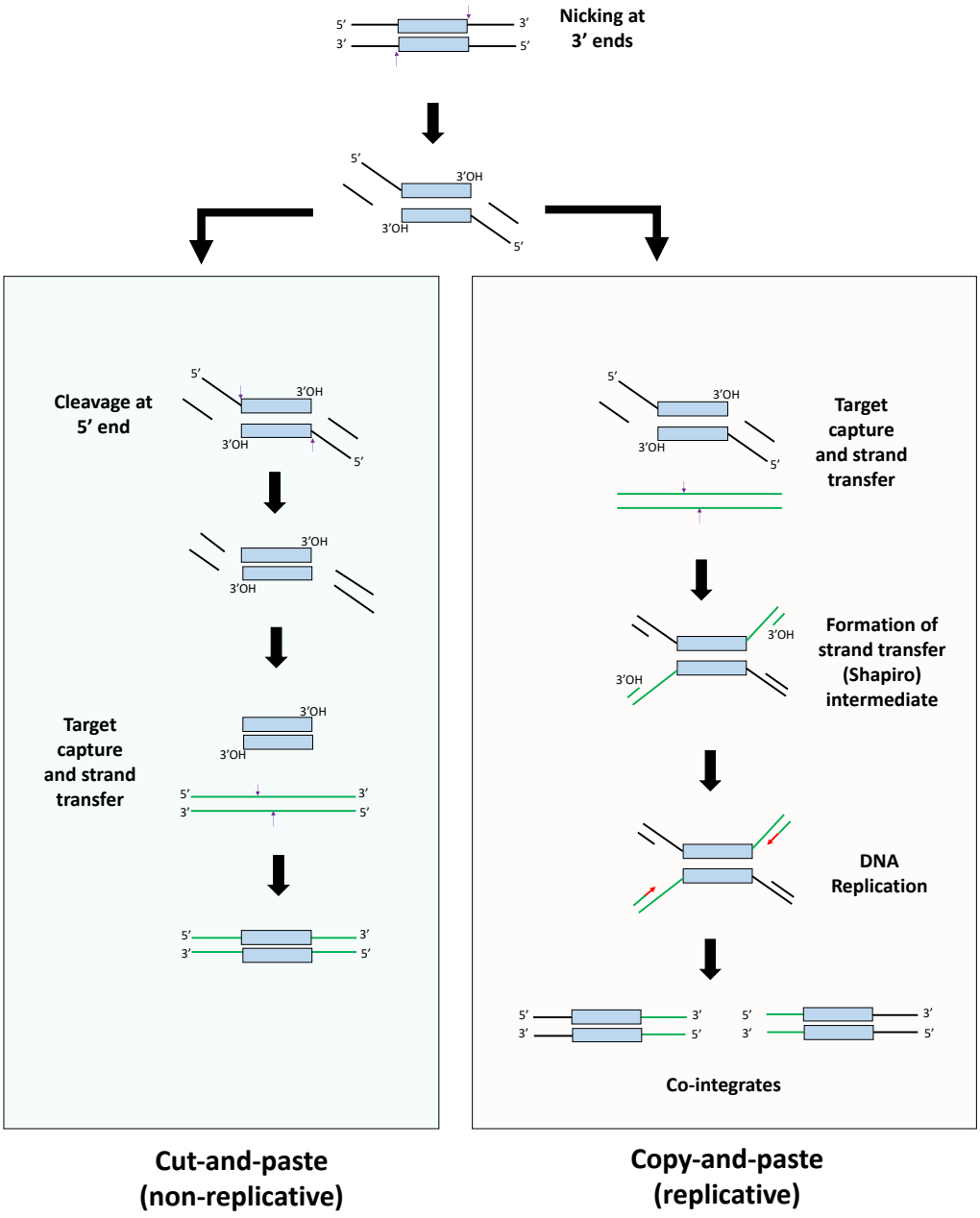

Fig.1.7. Mechanisms of transposition of IS5 family IS903

IS903 can move by either a non-replicative/cut-and-paste pathway (left) or replicative/copy-and-paste pathway (right). Purple arrows represent sites of cleavage. Blue boxes represent IS. Green lines represent target site DNA. Red arrows indicate DNA replication. Replicative transposition leads to formation of co-integrates which are resolved. In both pathways, transposase catalyses nicking to generate a free 3’ end which is used in strand transfer. These 3’OH ends act as nucleophiles to attack the phosphodiester DNA backbone of the target creating the final product. In replicative transposition, the free 3’OH end of the target in the Shapiro intermediate primes DNA replication. Figure inspired from (Tavakoli and Derbyshire, 2001).

each strand occurs in a staggered manner. The resultant gaps are filled in by host replication or repair machinery, generating the characteristic target site duplications, known as direct target repeats (DTRs) (Tavakoli and Derbyshire, 2001). The end result is homology-independent movement of the IS across the genome (Tavakoli and Derbyshire, 2001). Following replicative transposition, homologous recombination or a resolvase is used to resolve cointegrates and regenerate the donor and target molecules each carrying a copy of the IS (Haren, Ton-Hoang and Chandler, 1999). It is important to note that a non-replicative mechanism can also give rise to an increase in copy number of the IS. Bacteria have multiple copies of a chromosome in one cell prior to division. The donor locus, prior to excision, can be used as a template to restore the excised site by homologous recombination (Hagemann and Craig, 1993).

1.7.4. Target site selection

Biases have been observed in target selection by ISs (Siguier *et al.*, 2015). Particular sequence motifs can guide certain elements, for example IS630 inserts at TA dinucleotides, whilst IS10 inserts preferentially into the sequence 5'-GCTNAGC-3' (Lee, Butler and Kleckner, 1987; Tenzen, Matsutani and Ohtsubo, 1990). More general nucleotide content biases have also been identified, including preferential insertion of IS186 into GC-rich DNA, and IS903 into AT-rich DNA. (Chong *et al.*, 1985; Hu and Derbyshire, 1998). Preferential insertion into AT-rich DNA may partially explain the greater IS prevalence in conjugative bacterial plasmids compared to chromosomes, facilitating propagation by HGT (Siguier *et al.*, 2015). Intriguingly, hotspots of IS903 insertion within a conjugative plasmid coincided with regions involved in

conjugative transfer (Hu and Derbyshire, 1998). Furthermore, genomic context may influence insertion frequency. For example, analysis of 155 archaeal genomes showed a bias for intragenic insertion between convergently oriented genes, whereas insertion between divergently oriented genes is disfavoured (Florek, Gilbert and Plague, 2014). In *A. baumannii*, intragenic insertion can vary dramatically from 30 % to 70 % depending on the IS (Adams, Bishop and Wright, 2016). However, these observations may not reflect a preference for insertion into these regions, but rather an evolutionary advantage for these insertions which drives selection.

Commonly, sites of insertion also manifest as inverted repeat sequences (Lee, Butler and Kleckner, 1987; Tenzen, Matsutani and Ohtsubo, 1990; Hu and Derbyshire, 1998). This has been suggested to facilitate target sequence recognition by a dimeric or multimeric transposase (Hu and Derbyshire, 1998). Secondary structures, such as hairpin loops, likely formed by repetitive extragenic palindromic sequences (REPs), or DNA replication forks have also been identified as hotspots for IS insertion (Tobes and Pareja, 2006; Gómez *et al.*, 2014). Host proteins implicated in directing transposition include integration host factor (IHF) and the Histone-like nucleoid structuring protein (H-NS). IHF promotes channelling of Tn10, where transposon ends are directed to insertion within the transposon, forming intratransposon inversion circles (Chalmers *et al.*, 1998). Intriguingly, H-NS directly antagonises the channelling of Tn10 by IHF, by competitively binding the transpososome and preventing such intramolecular transposition (Singh *et al.*, 2008). H-NS has additionally been shown to influence targeting of IS903 in *E. coli.* In an *hns* mutant, hotspots of IS903 insertion are lost, with more even distribution across the *E. coli* chromosome (Swingle et al., 2004). The authors

proposed that H-NS was acting as an exclusionary factor, and that deletion of *hns* would make more sites available for IS903 insertion. As well as targeting, IHF and H-NS have also been shown to contribute to regulation of transposition efficiency.

1.7.5. Regulation of transposition

Transposition must be tightly regulated, as widespread aberrant insertion would likely be fatal. The amount of active transposase is a rate-limiting factor and can be regulated at the level of transcription, translation, or transpososome formation.

Low levels of transposase transcription can be maintained by the presence of an intrinsically weak or inefficient promoter (Nagy and Chandler, 2004). IS1 has a weak promoter, with two consecutive overlapping ORFs in different reading phases. The IS1 transposase (InsAB') is produced by a programmed translational frameshift, however the N-terminal DNA binding portion of the transposase, made by only the first ORF (InsA) can bind to the TIR and further downregulate transcription of the transposase (by repression of the promoter) as well as occlude InsAB' binding to form the synaptic complex (Ton-Hoang, Turlan and Chandler, 2004). Additionally, premature rho-dependent termination of IS1 offers another level of transposase expression control, with mRNA produced lacking the required catalytic site (*insB* frame) for the full length transposase (Hübner, Iida and Arber, 1987).

In terms of translational regulation, various mechanisms exist. For example, IS10 transposase expression is inhibited by an antisense transcript made from a stronger, outwardly directed

promoter, located further inside the IS (Ma and Simons, 1990). The antisense transcript sequesters the sense transcript Shine-Dalgarno (SD) sequence and AUG start codon, blocking ribosome binding and translation (Ma and Simons, 1990). Inefficient translation of transposase mRNA can also occur if RNA secondary structure occludes the SD. Alternatively, the SD sequence may be absent, as occurs with IS186 (Nagy and Chandler, 2004).

At the level of transpososome formation, many transposases act preferentially at the immediately adjacent TIR, rather than at a distal IS (described as cis-acting.) This is partly explained by transposase instability. For example, the ability of IS903 to act in trans increases 100-fold in *E. coli* lacking Lon protease (Derbyshire, Kramer and Grindley, 1990). Alternatively, the Tn5 inhibitor protein (Inh) is an N-terminally truncated transposase variant, that forms heterodimers with the true transposase to stimulate DNA binding without transposition (de la Cruz *et al.*, 1993). The Tn5 transposase may also form inactive multimers thought to mask the DNA binding domain (Weinreich, Gasch and Reznikoff, 1994). For correct function, DNA binding must occur before oligomerization.

As well as impacting IS903 target preference, H-NS can modulate transposition efficiency. For instance, H-NS can alter transcription, varying the amount of transposase produced, impacting transpososome formation. This is evident for bacteriophage Mu, where H-NS decreases Mu transcription and stabilizes Mu repressor-DNA complexes (Falconi *et al.*, 1991). Post-transcriptional control occurs for IS1. In an *hns* mutant, levels of the IS1 transposase are almost undetectable, with transcription and mRNA levels unchanged compared to wild-type. This suggests loss of H-NS either reduces translation or increases transposase degradation

(Rouquette, Serre and Lane, 2004). H-NS also binds to, and encourages formation of, the Tn5 and Tn10 transpososomes (Wardle *et al.*, 2005; Ward *et al.*, 2007; Whitfield, Wardle and Haniford, 2009). In Tn10 transposition, IHF binds flanking DNA adjacent to the TIR and induces DNA bending, stabilizing the transpososome as a compensatory mechanism for lack of negative supercoiling (Chalmers *et al.*, 1998). Other nucleoid proteins implicated in regulating transposition include HU, Fis, StpA, and Dps (Swingle *et al.*, 2004).

Environmental conditions such as oxidative stress, metal ions, spermine, antibiotics, temperature, radiation and conjugation have all be shown to regulate transposition of various ISs (Vandecraen *et al.*, 2017). Such environmental stresses may encourage transposition to increase genomic variability and increase chances of population survival. For example, ciprofloxacin and tetracycline treatment, and oxidative stress from H_2O_2 exposure, have been shown to promote increased transposition of multiple IS elements in *A. baumannii* (Wright *et al.*, 2017; Penesyan *et al.*, 2019).

1.7.6. Transposition shapes genomes

TEs play important roles in shaping genomes, they contribute to genome size expansion and reductive evolution, by driving large-scale rearrangements, insertions, deletions and inversions (Vandecraen *et al.*, 2017; Consuegra *et al.*, 2021). The latter two are facilitated by either direct intramolecular transposition by replicative transposition, or recombination of homologous regions generated by transposition at distant loci (Haren, Ton-Hoang and Chandler, 1999; Curcio and Derbyshire, 2003; He *et al.*, 2015). Indeed, *Acinetobacter* genus

diversification has been driven by genome plasticity facilitated by ISs (Touchon *et al.*, 2014; Li *et al.*, 2015; Álvarez *et al.*, 2020). Plasmids frequently harbour TEs, facilitating the spread of these elements into other bacteria. This enables the dissemination of antibiotic resistance genes, heavy metal resistance genes and virulence factors (Maslova *et al.*, 2022; Noel, Petrey and Palmer, 2022). As a consequence of their insertion, ISs can also impact the expression of adjacent genes at the locus in which they insert into.

1.7.7. Consequences of transposition on transcription

The movement of ISs can have different impacts on transcription depending on the locus and orientation of insertion. For example, a strong promoter sequence can be brought close to, and up-regulate, expression of a gene. This is exemplified by *A. baumannii* IS*Aba*1 inserting upstream of β-lactamase genes *ampC* and $bla_{\text{OXA-51-like}}$ (Turton *et al.*, 2006; Hamidian and Hall, 2013). The internal promoter of IS*Aba1* in this context drives increased resistance to cephalosporins and carbapenemases (Turton *et al.*, 2006; Hamidian and Hall, 2013). Insertion of IS*Aba*1 at either side of *ampC* creates transposon Tn6168, which can mobilise and confer cephalosporin resistance in different strains (Hamidian and Hall, 2014).

Insertion of an IS into a gene can inactivate its function. For example, insertion of IS*Aba*1, IS*Aba*125 or IS*Aba*27 can occur into *adeN*, which encodes a negative regulator of the efflux pump AdeIJK (Gerson *et al.*, 2018). Disruption of *adeN* by IS*Aba*1 is correlated with increased *adeJ* expression, virulence, antibiotic resistance, and decreased biofilm formation (Saranathan *et al.*, 2017). Depending on the locus of insertion, there is a possibility of far-reaching

downstream effects. For example, a change in the genome plasticity of ST78A *A. baumannii* isolates is theorised to be due to a high rate of IS66 proliferation, insertion into *comEC/rec2*, and subsequent impairment of natural transformation (Gaiarsa *et al.*, 2019).

As well as locus position, polarity is important. If the IS inserts antisense to nearby genes or operons, this could block transcription. This has been studied using the synthetic minimal bacterial cell system JCVI-syn2.0 (Hutchison *et al.*, 2019). Here, Tn5-puromycin resistance insertions were examined with 3.3 % of genes showing an asymmetry preference. Of these, 62.5 % were located within operons upstream of essential genes, favouring insertion in the same orientation to enable transcriptional readthrough. Plausible explanations for a "transcriptional conflict" include RNA polymerase (RNAP) collisions, antisense RNA interference, or introduction of a terminator sequence (Hutchison *et al.*, 2019).

1.8. Transcription

Transcription is the process of converting information in DNA into a temporary readable form as either messenger RNA (mRNA), transfer RNA (tRNA) or ribosomal RNA (rRNA). Regulation of transcription is a highly efficient way of regulating gene expression; resources are expended if points of control are post-transcriptional. Transcription begins with the enzyme RNAP recognising and binding to specific regions of DNA called promoter sequences.

1.8.1. RNA polymerase

The DNA-dependent RNAP is a highly conserved enzyme essential to all domains of life. In bacteria, the core enzyme is composed of four subunits, $\alpha_2\beta\beta'$, as illustrated in Fig.1.8 (Zhang *et al.*, 1999; Borukhov and Nudler, 2008). β and β', the largest subunits, form pincers of a crab claw shape with the active site at the bottom of the intersubunit cleft (Sutherland and Murakami, 2018). Nucleoside triphosphate (NTP) substrates enter the catalytic site via the secondary channel, where an essential Mg^{2+} ion catalyses attachment to the elongating RNA chain by nucleophilic attack (Sutherland and Murakami, 2018). The homodimeric α subunit is the scaffold for assembly of the core enzyme. The alpha N-terminal domain (α-NTD) dimerises and recruits the β and β' subunits, while the alpha C-terminal domain (α-CTD), which binds DNA, is joined by a flexible linker (Sutherland and Murakami, 2018). Many bacteria, including *A. baumannii,* contain a subunit called omega (ω), which is non-essential and believed to assist in RNAP stabilization (Mukherjee *et al.*, 1999).

The σ subunit, formed of four independently folded domains, is required for recognition of specific DNA sequences (Busby, 2019). When the core RNAP binds σ, the resulting complex is called the holoenzyme. Most σ factors belong to the σ^{70} family, and are related to the housekeeping σ^{70} factor of *E. coli* (Paget and Helmann, 2003). This is a factor required for general transcription during exponential growth. However, σ^{70} can be replaced by other σ factors, in response to environmental stresses (Paget and Helmann, 2003). Alternative σ factors recognise different DNA sequences, and so regulate different sets of genes. For example, σ^{54} coordinates the response to nitrogen starvation (Danson *et al.*, 2019).

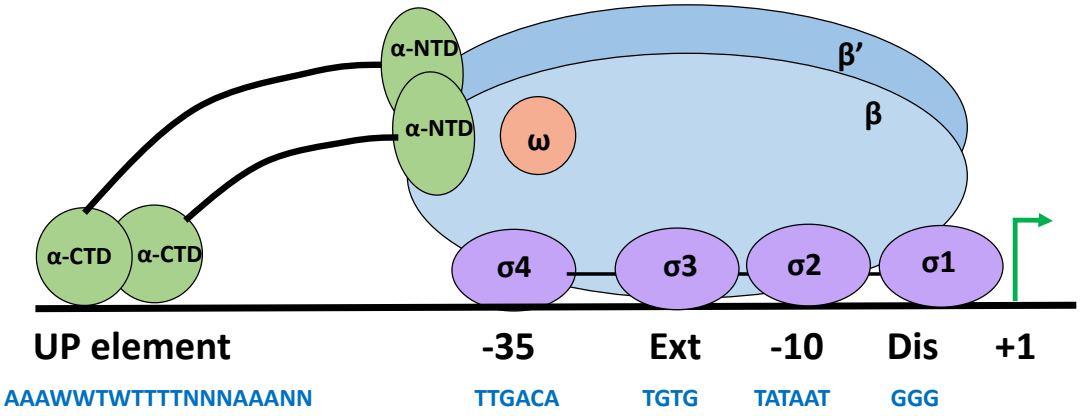

Fig.1.8. DNA elements associated with RNAP binding
σ factor domains 1-4 of σ^{70} and the α-CTD of RNAP bind to the highlighted regions. Figure modified from (Browning and Busby, 2016).

1.8.2. Promoter structure

Transcription begins with the recognition of specific "promoter" DNA sequences by regions of the σ factor (Busby, 2019). The typical housekeeping promoter sequences are the -10 and -35 elements upstream of the transcription start site (TSS) (+1), illustrated in Fig.1.8 (Borukhov and Nudler, 2008). The first 'T', second 'A' and last 'T' of the -10 element are the most important components, as they interact with RNAP to facilitate DNA unwinding (Feklistov and Darst, 2011). The housekeeping σ factor can also recognise the extended -10 element (Ext) and Discriminator element (Dis) (Fig.1.8) (Browning and Busby, 2016). At some promoters, the α-CTD contacts DNA sequences called UP-elements (Fig.1.8) (Browning and Busby, 2016). It was recently shown that promoters often act bidirectionally, driving divergent transcription (Warman et al., 2021). This phenomenon, widespread in bacteria, is due to inherent -10 element AT-richness, and symmetry (Warman et al., 2021).

1.8.3. Transcription initiation

Regions 2 and 4 of σ^{70} are highly conserved and contact the promoter -10 and -35 regions respectively. Initially, a closed complex forms with DNA remaining double stranded (Borukhov and Nudler, 2008). Transition to open complex is mediated by region 2 of σ^{70}, which causes DNA duplex melting, and formation of a transcription bubble (Paget and Helmann, 2003). NTPs are added to the elongating RNA chain, which translocates towards the RNAP exit channel. Early in transcription, the concurrent build-up of free energy within the RNAP-promoter complex results in either short transcripts being released in cycles of abortive initiation, or RNAP escape from the promoter (Borukhov and Nudler, 2008). Elongation

continues until a terminator site is reached and newly formed transcripts are released (Chen, Boyaci and Campbell, 2021).

1.8.4. Transcription termination

Transcription termination occurs when the elongating RNAP pauses, nucleotide addition stops, and RNAP dissociates from DNA template and RNA transcript (Ray-Soni, Bellecourt and Landick, 2016). There are two main mechanisms of termination of transcription in bacteria; intrinsic termination, driven by DNA sequence, and factor-dependent termination, driven by proteins such as Rho or Mfd (Roberts, 2019).

Intrinsic termination depends on specific DNA sequences and resulting RNA structures. In DNA, GC-rich inverted repeat sequences are followed by approximately 8 (mostly thymidine) nucleotides, while in RNA, the GC-rich inverted repeats base pair to form a hairpin loop, followed by a polyuridine (polyU) tract of 7 – 8 nucleotides (Gusarov and Nudler, 1999). The weak base-pairing of the polyU tract is believed to pause RNAP (Roberts, 2019). This is followed by hairpin formation in the RNAP exit channel, which weakens upstream RNA-DNA hybrid interactions (You *et al.*, 2023). Subsequent rewinding of the transcription bubble and complete formation of the hairpin destabilise the elongation complex and initiate the release of newly formed RNA transcripts (You *et al.*, 2023).

Factor-dependent termination in bacteria is mostly mediated by Rho, with Mfd causing termination at sites of RNAP pausing caused by DNA damage (Peters, Vangeloff and Landick,

2011; Ray-Soni, Bellecourt and Landick, 2016). Recent evidence has shown that Rho can recycle stalled RNAP at damaged sites, complementing the action of Mfd if the latter is absent (Jain, Gupta and Sen, 2019). Rho is a highly conserved, hexameric, ATP-dependent, ring shaped, RNA translocase/helicase (Murayama *et al.*, 2023). Rho uses its primary RNA binding site to recognise RNA with a lack of secondary structure and high proportion of cytosine nucleotides (Mitra *et al.*, 2017). A secondary RNA binding site, within the hexameric channel, binds pyrimidine rich RNA, causing the ring to close (Murayama *et al.*, 2023). This is followed by ATP-dependent translocation of the now catalytically active Rho towards the elongating RNAP, where Rho induces disruption and dissociation of nucleic acids (Molodtsov *et al.*, 2023; Murayama *et al.*, 2023). Termination is aided by a bridging interaction of Rho with RNAP, mediated by the transcription elongation factor NusG, which stimulates formation of the active Rho closed ring form (Molodtsov *et al.*, 2023). Additionally, Rho has an important role (along with NusG, which binds the small ribosomal subunit NusE) in coupling transcription to translation (Saxena *et al.*, 2018). If translation stops, Rho binding sites on RNA and NusG, which were previously occupied by ribosomes, become free. This causes Rho to bind and terminate transcription (Mitra *et al.*, 2017).

1.8.5. Transcription factors

Transcription factors are regulatory proteins which help to dictate the expression of genes transcribed by RNAP. Transcription factors can bind regions of DNA, to either activate or repress transcription, achieving their desired effects through mechanisms such as direct RNAP interaction or steric occlusion of other regulatory proteins (Browning and Busby, 2016).

Transcription factors frequently bind to palindromic DNA sequences, as a consequence of their dimeric organisation, and often have DNA binding and regulatory domains (Browning and Busby, 2016). The latter can coordinate conformational changes in response to environmental conditions (Browning, Butala and Busby, 2019).

Transcription activators increase the rate of transcription. Typically, they bind DNA and recruit RNAP by contacting α-CTD (class I), or α-NTD or σ region 4 (class II), whereas some activators modulate the conformation of the promoter (Browning and Busby, 2004). Repressors are transcription factors which downregulate transcription. This can occur either by steric hindrance and occlusion of RNAP, DNA looping, RNAP trapping at the promoter, or interfering with activator activity (Browning and Busby, 2016; Browning, Butala and Busby, 2019). Some transcription factors function as global regulators of gene expression, enabling the coordinated regulation of multiple genes. One well known example of a global repressor is the histone-like nucleoid structuring protein, H-NS (Wan *et al.*, 2016).

1.9. H-NS

H-NS, like other nucleoid associated proteins (NAPs), is a small, abundant protein found in all γ-proteobacteria and some α and β-proteobacteria (Fitzgerald *et al.*, 2020). Functional analogues of H-NS include Rok, MvaT and LsrT found in *Bacillus, Pseudomonas,* and *Mycobacterium* species respectively (Qin *et al.*, 2019). H-NS does not have a stringent sequence specificity, typically binding DNA at a nucleation site (with a thermally unstable and flexible T-A base step) before oligomerising in filaments across AT-rich DNA (Lang *et al.*, 2007).

H-NS plays important roles in both transcriptional regulation and chromosome compaction and organisation, based on its ability to form unique protein-DNA structures.

1.9.1. The structure of H-NS

H-NS is composed of a C-terminal winged helix-turn-helix DNA binding domain, connected to an N-terminal oligomerisation domain via a flexible unstructured linker region (Fig.1.9) (Arold et al., 2010). The only current partial crystal structure of H-NS comes from *Salmonella enterica* Serovar Typhimurium where the N-terminal portion of the protein (encompassing residues 1-87) was diffracted to 3.7 Angstroms (Fig.1.9a) (Arold *et al.*, 2010). This structure showed H-NS can dimerise via its N-terminal helices (H1 and H2), also called site 1, in "head-to-head" interactions (Arold *et al.*, 2010). These dimers oligomerise via N-terminal helices H3 and H4, also called site 2, in "tail-to-tail" interactions (Arold *et al.*, 2010). Oligomers are predicted to be in antiparallel coiled coils. Additionally, NMR has shed light on the *S. enterica* Serovar Typhimurium C-terminal domain in solution (Fig.1.9b) (Gordon *et al.*, 2011). H-NS type proteins have a conserved motif in the C-terminal domain of TWTGXGRXP (Bertin *et al.*, 2001). The residues Q112, G113 and R114 (illustrated Fig. 1.9b) form the hook motif which interacts with the DNA minor groove to facilitate binding (Gordon *et al.*, 2011).

1.9.2. The role of H-NS in chromosome organization

NAPs such as H-NS form higher order structures with DNA in order to compact the chromosome, altering the local nucleoid structure through bending, looping, wrapping, twisting and bridging DNA (Dillon and Dorman, 2010). Overexpression of H-NS produces a

(a)

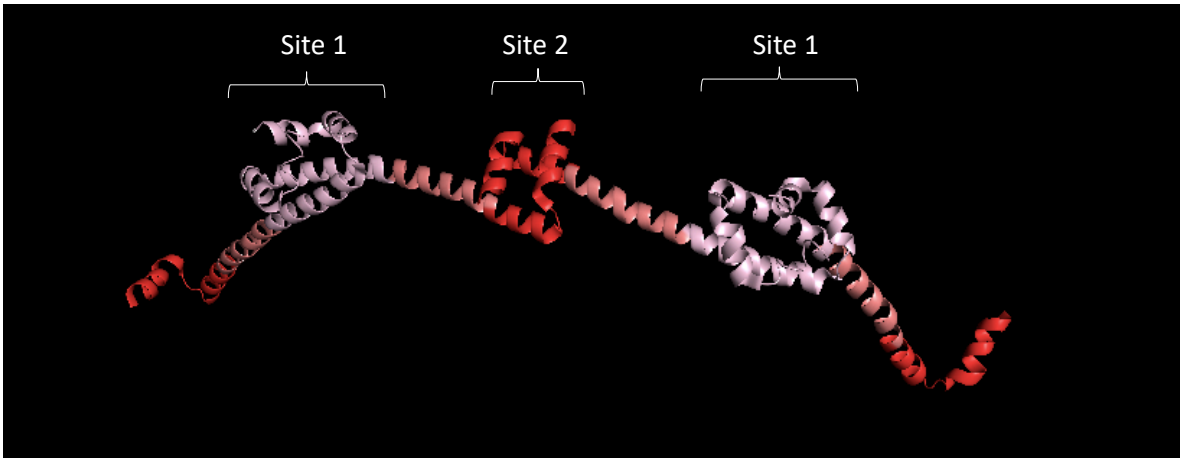

(b)

(c)

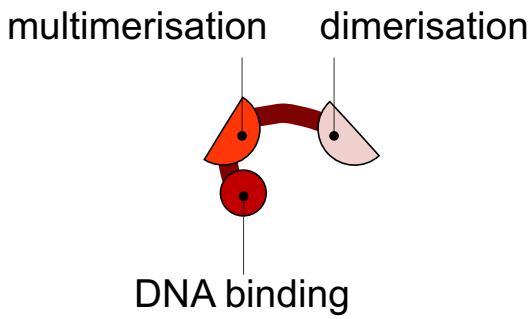

Fig.1.9. The structure of H-NS

N-terminal portion of *S. enterica* Serovar Typhimurium H-NS determined by X-ray crystallography, PDB: 3NR7. Viewed in PyMOL v2.5.3. Four monomers of H-NS are shown, with pairs dimerised at site 1 and dimers oligomerised at site 2. (b) C-terminal DNA binding domain of *S. enterica* Serovar Typhimurium H-NS obtained by NMR in solution. PDB: 2L93. Viewed in PyMOL v2.5.3. Residues which interact with DNA minor groove highlighted in green. (c) Cartoon schematic of domains in an H-NS monomer.

highly condensed, compact, spherically shaped nucleoid, and cells lacking H-NS have a decreased amount of DNA condensation (Spurio *et al.*, 1992; Helgesen, Fossum and Skarstad, 2016). The crystal structure of the *S. enterica* Serovar Typhimurium NTD suggests that H-NS can condense DNA into a super helical structure (Arold et al., 2010).

H-NS can form long nucleoprotein filaments that stiffen and extend DNA (Fig.1.10a) (Amit, Oppenheim and Stavans, 2003). Alternatively H-NS can bridge two DNA duplexes and form loops if this interaction is intramolecular (Dame, Noom and Wuite, 2006; Liang *et al.*, 2017) (Fig.1.10b). H-NS has been shown to either constrain or promote the supercoiling state of DNA, depending on whether it is in its linear or bridged form respectively (Lim, Kenney and Yan, 2014). Whilst DNA stiffening is sensitive to changes in pH (range of 6.5 to 8) or temperature (range of 24°C to 37°C), bridging is not (Liu *et al.*, 2010). Bridging does however appear to be disrupted at temperatures exceeding 37°C (Kotlajich *et al.*, 2015). The conformational change in H-NS, to drive the switch from linear state to bridged state, is dependent on an increase in cation concentration, offering a mechanism for H-NS and its associated activities in different forms to act as an environmental sensor (Liu *et al.*, 2010; van der Valk *et al.*, 2017).

Using atomic force microscopy (AFM), individual H-NS-DNA complexes have been shown to create loops of DNA *in vitro* (Dame, Wyman and Goosen, 2000; Shin *et al.*, 2005; Liu *et al.*, 2010). Loops have the potential to form microdomain boundaries of chromosome structure (on the scale of 10 kb) (Qin *et al.*, 2019). Evidence for this comes from topological domain size

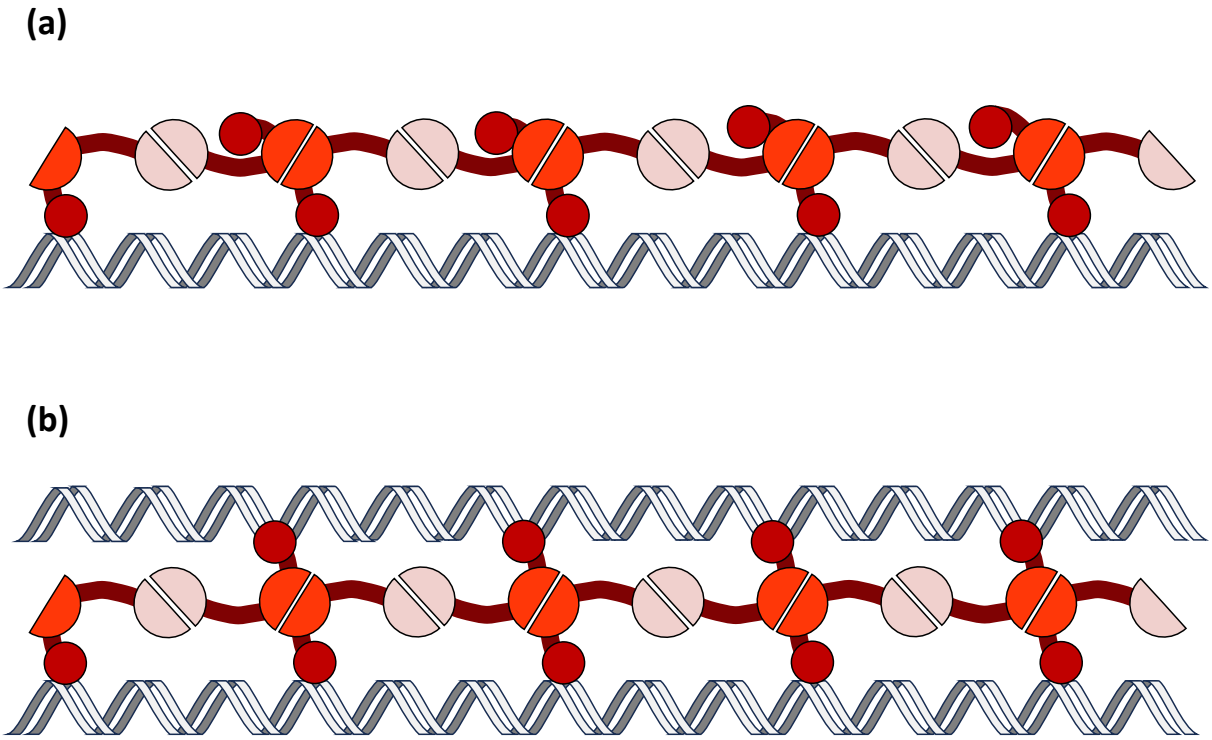

Fig.1.10. Stiffening and bridging modes of H-NS
(a) Filamentation of H-NS along one piece of dsDNA leads to stiffening. (b) Bridging of two strands of dsDNA by alternate binding of the CTD. This can create DNA loops if done intramolecularly.

matching the distance between H-NS binding regions, and an *hns* mutant displaying phenotypes of disrupted domain barriers (Hardy and Cozzarelli, 2005; Noom *et al.*, 2007). However, the precise role of H-NS in loop and domain formation is still unclear, and the scale at which loop formation occurs may be important. For example, a Hi-C contact map in an *hns* mutant revealed no large scale changes to chromosomal interaction domains (CIDs) compared with wild-type, but an increase in short range contacts in the absence of H-NS (Lioy *et al.*, 2018). Similarly, chromosome conformation capture (3C) showed H-NS binding sites did not significantly cluster spatially, and instead suggested a role for localized rather than global structuring, in contrast to previous chromosome capture results (Wang *et al.*, 2011; Cagliero *et al.*, 2013). H-NS was shown to unexpectedly decrease loop formation on a very short scale (order of < 100 bp) using a *lacZ* reporter-operator system (Becker, Kahn and Maher, 2007). However, it was recently shown using 3C-qPCR that changes in osmolarity can modulate local chromosome architecture through H-NS. At high K^+ concentration, H-NS mediated bridging of regulatory elements is disrupted, enabling expression of the *proVWX* operon (Rashid *et al.*, 2023).

1.9.3. The role of H-NS in transcriptional regulation

Silencing of genes by H-NS can be achieved by general condensation of chromosome structure, constraining DNA topology, and modulating the accessibility of promoters (Tupper *et al.*, 1994). Additionally, H-NS can interfere with transcription initiation by occlusion of RNAP, direct interaction with and masking of RNAP α-CTD, or through DNA bridges which trap RNAP initiation complexes, preventing promoter escape (Dame *et al.*, 2002; Shin *et al.*, 2012; Singh and Grainger, 2013). As well as impacting transcription initiation, bridged H-NS filaments

have been shown to stall RNAP during elongation, leading to rho-dependent termination (Kotlajich *et al.*, 2015). In contrast, H-NS can act as a positive regulator at the post-transcriptional level via an RNA-mediated interaction. Here, H-NS binds to mRNA with a poor SD sequence and shifts the 30S ribosomal subunit in the 3' direction to an alternative and more efficient site of translation initiation (Park et al., 2010) .

As mentioned previously, H-NS preferentially binds to AT-rich regions. Often, these are horizontally acquired. Therefore, an important role of H-NS is xenogeneic silencing of horizontally acquired DNA (Lucchini *et al.*, 2006). Such AT-rich DNA is toxic because of spurious intragenic transcription that titrates RNAP (Lamberte *et al.*, 2017). H-NS mediated repression enables the acquisition of foreign DNA whilst maintaining integrity of the genome and regulome, and reducing spurious transcription (Navarre *et al.*, 2007; Singh *et al.*, 2014). For example, in *Shigella* and enteroinvasive *E. coli*, H-NS represses the plasmid encoded virulence master regulator *virF* (Porter and Dorman, 1994). In *S. enterica,* H-NS represses two horizontally acquired pathogenicity islands required for host infection, reducing the fitness cost associated with expenditure of resources on unnecessary gene expression (Lucchini *et al.*, 2006).

The ability of H-NS to modulate its activity according to environmental conditions (such as pH, temperature and osmolarity) enables de-repression of genes when appropriate (Arold et al., 2010). For example, at 37 °C, anti-silencing of H-NS repression of *virF* is achieved by a DNA conformational change, reducing a cooperative H-NS interaction between two sites and relieving repression (Falconi *et al.*, 1998). Further regulation and anti-silencing of H-NS can be

achieved in *Enterobacteriaceae* by interaction with H-NS-like proteins, which show sequence similarity to the site 2 interacting N-terminal domain of H-NS. For example, depression of H-NS in enteropathogenic *E. coli* occurs when H-NS binds to a truncated version of H-NS called H-NST, which lacks a C-terminal DNA binding domain (Williamson and Free, 2005). Alternatively Hha, which also shows sequence similarity to the N-terminal domain of H-NS, can form co-complexes that stabilise DNA bridging and repression by H-NS (Nieto *et al.*, 2002; van der Valk *et al.*, 2017).

1.9.4. The function of H-NS *in A. baumannii*

H-NS from *Acinetobacter* has a very similar structure to *E. coli* H-NS, and likely has a similar role in chromosome organization, but studies so far on *Acinetobacter* H-NS have focused on its role in gene regulation. One study showed H-NS from *Acinetobacter* can complement the phenotypes of an *E. coli hns* mutant, including *lacZ* metabolism, motility and mucoidy (Tendeng et al., 2003). The genome of *Acinetobacter* species is more AT-rich than many other Gram-negative bacteria, with a typical GC-content of just under 40 % (Touchon *et al.*, 2014; Bohlin *et al.*, 2017). IS*Aba*12 disruption of *hns* in ATCC 17978 increased motility, biofilm formation, A549 alveolar cell adherence, surface hydrophobicity and virulence in *C. elegans* (Eijkelkamp *et al.*, 2013). These phenotypes were accompanied by a 4-fold change in the expression of over 150 genes, including significant up-regulation of components of the horizontally acquired T6SS (360-fold increased expression of the first gene of the cluster), highlighting the role of H-NS in xenogeneic silencing (Eijkelkamp *et al.*, 2013). Other genes with significantly altered expression in the *hns* mutant include the quorum sensing regulator

abaR, the gene encoding the autotransporter adhesin (Ata) and the type I pilus (Eijkelkamp *et al.*, 2013). IS*Aba*125-mediated disruption of *hns* in a clinical isolate of *A. baumannii* also modulated expression of over 150 genes (including increased expression of Csu pili and genes for synthesizing PNAG) and significantly decreased susceptibility to colistin (Deveson Lucas *et al.*, 2018). However, the influence of H-NS in antibiotic resistance varies between strains. Deletion of *hns* in strains AB5075 and A118 did not change susceptibility to colistin, but did increase susceptibility to amikacin, meropenem, imipenem and gentamicin (Rodgers *et al.*, 2021). Additionally, H-NS has also been shown to help cells survive stress from metallo-β-lactamase expression or DNA damage, and increases the capacity for natural transformation (Huang *et al.*, 2020; Le *et al.*, 2021). Recently, a plasmid-encoded H-NS (50 % identical to the chromosomal copy) found in the multidrug resistant urinary isolate UPAB1, was shown to decrease PNAG formation and expression of a CsgG homologue, decreasing biofilm formation (Benomar, Di Venanzio and Feldman, 2021). In terms of the regulation of H-NS in *A. baumannii*, *hns* expression is repressed in response to human serum albumin (HSA), and this may represent an important coordinated switch in global transcription in the context of human infection (Martinez *et al.*, 2019; Escalante *et al.*, 2022).

1.10. Objectives of the project

The aim of this project was to investigate the mechanism behind the formation of newly identified colony types of AB5075, and to characterise phenotypic differences relative to wild-type cells. Upon learning IS*Aba*13 insertion drives this change, we next wanted to investigate how IS*Aba*13 impacts transcription of adjacent genes, where else IS*Aba*13 inserts globally, and why IS*Aba*13 inserts preferentially into particular genomic hotspots.

Chapter 2: Materials and Methods

2.1. Materials

2.1.1. Strains

Bacterial strains used in this study are listed in Table 2.1.

2.1.2. Plasmids

Plasmids used in this study are listed in Table 2.2.

2.1.3. Oligonucleotides

Oligonucleotides used in this study are listed in Table 2.3.

2.1.4. Buffers and reagents

Buffers and reagents used in this study are listed in Table 2.4.

2.2. Growth of bacterial strains

Unless otherwise stated, strains were routinely grown in in low-salt Lysogeny broth (LB) medium (Sigma) (20 g/L) at 37 °C with shaking for liquid cultures, or on low-salt LB agar (LBA) (Sigma) (35 g/L) at 37 °C. For selection of positive *lacZ* clones, MacConkey agar (Sigma) (52 g/L) was used. To avoid phase switching of AB5075, strains were grown at room temperature overnight without shaking to an OD_{600} ~ 0.1.

Strain	Description	Source
AB5075	Highly virulent and drug resistant isolate from an osteomyelitis tibial infection	(Jacobs *et al.*, 2014)
AB5075::*gtr52*::IS*Aba*13	Streaked from wild-type AB5075. Natively formed insertion of IS*Aba*13 into *gtr52* (*ABUW_3824*)	This study
AB5075::*ompW*::IS*Aba*13	*ompW* with IS*Aba*13 inserted, made using the scarless genome editing strategy	This study
AB5075 *ABUW_1221*::T26	Obtained from T26 transposon mutant library. Tet^R	(Gallagher *et al.*, 2015)
AB5075 *hns*::T26	Obtained from T26 transposon mutant library. Tet^R	(Gallagher *et al.*, 2015)
E. coli JCB387	Strain used for general cloning. Genotype: Δ*nirB* Δ*lac*	(Page, Griffiths and Cole, 1990)
E. coli DH5α	Strain used for general cloning. Genotype: *fhuA2Δ(argF-lacZ)U169 phoA glnV44 Φ80Δ(lacZ)M15 gyrA96 recA1 relA1 endA1 thi-1 hsdR17*	New England Biolabs (NEB)
E. coli BTH101	Strain used in bacterial 2 hybrid (BACTH) assay. Genotype: F-, *cya-99, araD139, galE15, galK16, rpsL1 (Str r), hsdR2, mcrA1, mcrB1*	(Karimova *et al.*, 1998)
E. coli ATCC 25922	Control strain used in MIC	American Type Culture Collection (ATCC)
E. coli NCTC 10418	Control strain used in MIC	National Collection of Type Cultures (NCTC)
E. coli Lemo21 DE3	Strain used for tuneable expression of N/C-terminal His_6-tagged IS*Aba*13 transposase.	NEB

	Genotype: *fhuA2 [lon] ompT gal (λ DE3) [dcm] ΔhsdS/ pLemo(CamR) λ DE3 = λ sBamHIo ΔEcoRI-B int::(lacI::PlacUV5::T7 gene1) i21 Δnin5pLemo = pACYC184-PrhaBAD-lysY*	
E. coli NEBExpress	Strain used for non-T7 protein expression of MBP-IS*Aba*13 transposase fusion. Genotype: *fhuA2 [lon] ompT gal sulA11 R(mcr-73::miniTn10--TetS)2 [dcm] R(zgb-210::Tn10--TetS) endA1 Δ(mcrC-mrr)114::IS10*	NEB
E. coli T7 express	Strain used for T7 protein expression of H-NS. Genotype: *fhuA2 lacZ::T7 gene1 [lon] ompT gal sulA11 R(mcr-73::miniTn10--*TetS*)2 [dcm] R(zgb-210::Tn10--*TetS*) endA1 Δ(mcrC-mrr)114::IS10*	NEB

Table 2.1. Strains used in this study

Plasmid	Description	Source
pRW50T	Low copy number, broad host range, EcoRI and HindIII/BamHI restriction sites upstream of *lacZ*, Tet^R. Contains OriT origin of transfer for conjugation.	(Lodge *et al.*, 1992)
pSR	EcoRI/HindIII restriction sites upstream of λoop terminator. Amp^R. Used for in i*n vitro* transcription.	(Kolb *et al.*, 1995)
pVRL1Z	High copy number plasmid, Zeo^R. Contains *parE2-paaA2* toxin-antitoxin system	(Lucidi *et al.*, 2018)
pVRL2Z	High copy number plasmid, Zeo^R. Contains *parE2-paaA2* toxin-antitoxin system. Contains arabinose inducible *araC*-P_{BAD} promoter.	(Lucidi *et al.*, 2018)
pMHL-2	Template for PCR containing *apra*^{R}::*sacB* counter selection and resistance cassette for use in genome editing	(Godeux *et al.*, 2020)
pUT18	Used in BACTH assay. High copy number. N-terminal fusion to T18. Amp^R	(Karimova *et al.*, 1998)
pUT18C	Used in BACTH assay. High copy number. C-terminal fusion to T18, Amp^R	(Karimova *et al.*, 1998)
pKT25	Used in BACTH assay. Low copy number. Kan^R C-terminal fusion to T25	(Karimova *et al.*, 1998)
pKNT25	Used in BACTH assay. Low copy number, Kan^R N-terminal fusion to T25	(Karimova *et al.*, 1998)
pJ414	Used for protein expression of H-NS. High copy number. IPTG inducible T7 lac promoter. Amp^R.	DNA 2.0
pET21	Used for attempted protein expression of IS*Aba*13 transposase. C-terminal His_6-tag. IPTG inducible T7 lac promoter. Amp^R	Novagen
pET28	Used for attempted protein expression of IS*Aba*13	Novagen

	transposase. N-terminal His_6-tag. IPTG inducible T7 lac promoter. Kan^R.	
pMAL-c6T	MBP fusion to protein of interest. His_6-tag and TEV protease recognition site. Amp^R	NEB
pRK2013	Helper plasmid for conjugation. Kan^R	(Figurski and Helinski, 1979)
pEX-A128	Contains codon optimised H-NS flanked with restriction sites NdeI/XhoI. Amp^R.	Eurofins

Table 2.2. Plasmids used in this study

Oligonucleotide name	Description	Sequence (5'→3')
Primers for creating *gtr52*::IS*Aba*13 constructs in pRW50T for lacZ assays		
P8	To create constructs *gtr52* and *gtr52*::IS*Aba*13. BamHI restriction site underlined.	atgcgaggatccgactatttgagtat ggcaact
P9	To create constructs *gtr52* and *gtr52*::IS*Aba*13. EcoRI restriction site underlined.	gtgcgagaattcaggtggactaattt attgg
P11	To create construct *gtr52*::IS*Aba*13 -10 k.o. BamHI restriction site underlined. Mutated residues in red.	gtgcgaggatccgactatttgagtat ggcaactcaaattggctttgttgcaca aacctatctctaaaggcttattccaca agctaagtttcaaatgaata
P16	To create IS*Aba*13 bidirectional only. EcoRI restriction site underlined.	gtgagagaattcttgagtggctttgtt gc
P29	To create construct *gtr52*::IS*Aba*13 truncated. BamHI restriction site underlined.	gtaatcggatccaaacttactccgac gca
P13	To create construct IS*Aba*13 only. EcoRI restriction site underlined.	atgcgagaattcgactatttgagtatg gcaact
P56	To create construct IS*Aba*13 only. BamHI restriction site underlined.	ttgataggatccaatttgagtggcttt gttgc
P57	To create *gtr52*::IS*Aba*13 inverted.	cttgagtccacgctagatctgaattca ggtggactaatttattgg
P58	To create *gtr52*::IS*Aba*13 inverted.	taggtttgtgcaacaaagccactcaa attcaataatatca
P59	To create *gtr52*::IS*Aba*13 inverted.	tgatattattgaatttgagtggctttgt tgcacaaaccta
P60	To create *gtr52*::IS*Aba*13 inverted.	aagcttggctgcaggtcgacggatcc gactatttgagtatggcaactcaaatt ggctttgttgcacaaagatt
Primers for creating IS*Aba*13 constructs in pSR for IVT assays		
P21	To make construct 1	gaggccctttcgtcttcaagaggtgg actaatttattggtttatc
P22	To make construct 1	gatcctgctacccgagttgtcacttaa atttg
P23	To make construct 1	acaactcgggtagcaggatcaaacc aaatg
P24	To make construct 1	actggaggggatggggagtagacta tttgagtatggcaac

P25	To make construct 2	gaggccctttcgtcttcaagaggtgg actaatttattgg
P26	To make construct 2	actggaggggatggggagtagacta tttgagtatggcaac
P38	To make construct 3. EcoRI restriction site underlined.	cttcaagaattcgactaatttattggtt tatc
P39	To make construct 3. HindIII restriction site underlined.	gcatccaagcttccacaatataatttt c
P40	To make construct 5. EcoRI restriction site underlined	tgtagtgaattctttattgcgagagga ag
P41	To make construct 5. HindIII restriction site underlined.	ggatggaagcttgactatttgagtatg gcaac
P42	To make construct 4. Mutations to -10 element highlighted in red. EcoRI restriction site underlined.	ttcgtcgaattcaggtggactaattta ttggtttatcatgcctatatttttgcgta ggtgtatttttattgcgag
P43	To make construct 6	gaggccctttcgtcttcaagaggtgg actaatttattggtttatc
P44	To make construct 6	gatcctgctacccgagttgtcacttaa atttg
P45	To make construct 6	acaactcgggtagcaggatcaaacc aaatg
P46	To make construct 6	actggaggggatggggagtagttgtt gtcgcaaatacaac

To create *ompW*::IS*Aba*13 mutant		
P5	To amplify *apra*^{R}*::sacB* cassette	cgactcactatagggcgaattgggcc gctt tccagtcgggaaacctg
P6	To amplify *apra*^{R}*::sacB* cassette	catatgccaccgacccgagcaaaccc cgccagggttttcccagtcacgac
P62	To create fragment 1	cagcagtcacataatagatagc
P63	To create fragment 1	ggcccaattcgccctatagtgagtcg attggcaagtaaaatttggg
P64	To create fragment 2	gggtttgctcgggtcggtggcatatgg gctttgttgcacaaagatttaaaag
P65	To create fragment 2	attggcaagggctttgttgcacaaac ctatctc
P66	To create fragment 3	caacaaagcccttgccaattaccagc a
P71	To create fragment 3	cgttatgcgcaatgtccagt
P70	To amplify Gibson assembly product	taagccatcaagcaaagtgag

P74	To amplify Gibson assembly product and create fragment used in 2nd recombination	ctcagagctaataagtgactg
P72	For creating fragment used in 2nd recombination	ccgtactaccttctacacggt
P157	For creating fragment used in 2nd recombination	acttgccaatggctttgttgcacaaag atttaaaagttaag
P158	For creating fragment used in 2nd recombination	caacaaagccattggcaagtaaaatt tggg

Primers for attempted protein expression of IS*Aba*13 transposase		
P119	To put IS*Aba1*3 transposase into pET28	cagccatatgaataagtcgacaccta aaatttatc
P120	To put IS*Aba1*3 transposase into pET28	ggtgctcgagttaagtgacaactcgg gtatg
P121	To put IS*Aba*13 transposase into pET28	tgtcacttaactcgagcaccaccacc ac
P122	To put IS*Aba*13 transposase into pET28	tcgacttattcatatggctgccgcgcg g
P99	To put IS*Aba*13 transposase into pET21	agatatacatatgaataagtcgacac ctaaaatttatc
P100	To put IS*Aba*13 transposase into pET21	ggtgctcgagagtgacaactcgggta tg
P101	To put IS*Aba*13 transposase into pET21	agttgtcactctcgagcaccaccacc ac
P102	To put IS*Aba*13 transposase into pET21	acttattcatatgtatatctccttctta aagttaaacaaaattatttctagagg
P150	To put IS*Aba*13 transposase into pMAL-c6T. AlwNI restriction site underlined.	tagcgacagatgctgatgaataagtc gacacct
P151	To put IS*Aba*13 transposase into pMAL-c6T. SbfI restriction site underlined.	cgatacctgcaggttaagtgacaac tcgggta

Primers for protein expression of H-NS		
P129	To amplify codon optimised AB5075 H-NS, to put in pJ414. NdeI restriction site underlined.	gcaagccatatgaaaccggacatta gc
P146	To amplify codon optimised AB5075 H-NS to put in pJ414. XhoI restriction site underlined.	gcaggtctcgagttaaatcaggaaat c

Primers for BACTH assay		
P103	To put *hns* in pKT25. PstI restriction site underlined.	gagtgactgcagtaatgaaaccggatattagtg
P104	To put *hns* in pUT18c, pKNT25 and pUT18. PstI restriction site underlined.	gagtgactgcagaatgaaaccggatattagtg
P105	To put *hns* in pKT25 and pUT18C. KpnI restriction site underlined.	gctgtaggtaccttagattaagaaatcttcaagttttgcacc
P106	To put *hns* in pKNT25 and pUT18. KpnI restriction site underlined.	gctgtaggtaccgcgattaagaaatcttcaagttttgcacc
P107	To put IS*Aba*13 transposase in pKT25. PstI restriction site underlined.	cgtgtactgcagcaatgaataagtcgacacc
P108	To put IS*Aba*13 transposase in pUT18c, pKNT25 and pUT18. PstI restriction site underlined.	cgtgtactgcagaatgaataagtcgacacc
P109	To put IS*Aba*13 transposase in pKT25 and pUT18C. KpnI restriction site underlined.	gctgtaggtaccttaagtgacaactcgggt
P111	To put IS*Aba*13 transposase in pKNT25 and pUT18. KpnI restriction site underlined.	gctgtaggtaccgcagtgacaactcgggt

Primers for creating H-NS^{39aa} construct		
P134	To create fragment 1, XhoI restriction site underlined	ccccctcgagataaatattaagaaaatatattacaattataattactaatg
P135	To create fragment 1	tgatctttttttcattaataaatactccagtcttac
P136	To create fragment 2	tttattaatgaaaaaagatcaagcaatcg
P137	To create fragment 2, PstI restriction site underlined	cgggctgcagttatgttgttttcttacgtttttg

Primers for *in vitro* bridging assay/EMSA		
P162	To create IS*Aba*13 bait fragment	**biotin**-cttattaaatggctttgttgcac
P163	To create IS*Aba*13 bait fragment	taatttaataaggctttgttgcac
P164	To create T6SS bait fragment	**biotin**-caacacaactttcattcc
P171	To create T6SS fragment	caacacaactttcattcc
P172	To create T6SS fragment	agggtatctatatcagcca

P173	To create *csuAB* fragment	tcattatccagcctgtaag
P174	To create *csuAB* fragment	gcaactattaatgctgcaag

Oligonucleotides for use in native Tn-seq		
Adaptor 1.2	To ligate to end repaired DNA	taccacgacca
Adaptor 2.2	To ligate to end repaired DNA	atgatggccggtggatttgtgtggtcg tggtat
JelAP1	For 1st PCR, binds adapter 2.2 sequence	atgatggccggtggatttgtg
IS*Aba*13_out	For 1st PCR binds end of IS*Aba*13 sequence	caaagccaagtcaatgagattcatgc
Staggered_1	For 2nd hemi-nested PCR of P5 end, binding site to IS*Aba*13 underlined. Staggered T in red added for heterogeneity.	aatgatacggcgaccaccgagatcta cactctttccctacacgacgctcttcc gatctgaccacatacccgagttgtca c
Staggered_2	For 2nd hemi-nested PCR of P5 end, binding site to IS*Aba*13 underlined. Staggered TT in red added for heterogeneity.	aatgatacggcgaccaccgagatcta cactctttccctacacgacgctcttcc gatcttgaccacatacccgagttgtca c
Staggered_3	For 2nd hemi-nested PCR of P5 end, binding site to IS*Aba*13 underlined. Staggered TGATA in red added for heterogeneity.	aatgatacggcgaccaccgagatcta cactctttccctacacgacgctcttcc gatctgatagaccacatacccgagtt gtcac
Staggered_4	For 2nd hemi-nested PCR of P5 end, binding site to IS*Aba*13 underlined. Staggered TATCTA in red added for heterogeneity.	aatgatacggcgaccaccgagatcta cactctttccctacacgacgctcttcc gatctatctagaccacatacccgagtt gtcac
AP1_P7_tagged_1	For 2nd hemi-nested PCR of P7 end, binding site to adaptor underlined. Barcode: CGTGAT in blue.	caagcagaagacggcatacgagata tcacggtgactggagttcagacgtgt gctcttccgatctgtcaatgatggccg gtggatttgtg
AP1_P7_tagged_2	For 2nd hemi-nested PCR of P7 end, binding site to adaptor underlined. Barcode: ACATCG in blue.	caagcagaagacggcatacgagatc gatgtgtgactggagttcagacgtgt gctcttccgatctgtcaatgatggccg gtggatttgtg
AP1_P7_tagged_3	For 2nd hemi-nested PCR of P7 end, binding site to adaptor underlined. Barcode: GCCTAA in blue.	caagcagaagacggcatacgagatt taggcgtgactggagttcagacgtgt gctcttccgatctgtcaatgatggccg gtggatttgtg
AP1_P7_tagged_4	For 2nd hemi-nested PCR of P7 end, binding site to adaptor underlined. Barcode: TGGTCA in blue.	caagcagaagacggcatacgagatt gaccagtgactggagttcagacgtgt

		gctcttccgatctgtcaatgatggccg gtggatttgtg
AP1_P7_tagged_5	For 2nd hemi-nested PCR of P7 end, binding site to adaptor underlined. Barcode: CACTGT in blue.	caagcagaagacggcatacgagata cagtggtgactggagttcagacgtgt gctcttccgatctgtcaatgatggccg gtggatttgtg
AP1_P7_tagged_6	For 2nd hemi-nested PCR of P7 end, binding site to adaptor underlined. Barcode: ATTGGC in blue.	caagcagaagacggcatacgagatg ccaatgtgactggagttcagacgtgt gctcttccgatctgtcaatgatggccg gtggatttgtg
AP1_P7_tagged_7	For 2nd hemi-nested PCR of P7 end, binding site to adaptor underlined. Barcode: CATAGC in blue.	caagcagaagacggcatacgagatg ctatggtgactggagttcagacgtgt gctcttccgatctgtcaatgatggccg gtggatttgtg
AP1_P7_tagged_8	For 2nd hemi-nested PCR of P7 end, binding site to adaptor underlined. Barcode: CTAGCT in blue.	caagcagaagacggcatacgagata gctaggtgactggagttcagacgtgt gctcttccgatctgtcaatgatggccg gtggatttgtg
AP1_P7_tagged_9	For 2nd hemi-nested PCR of P7 end, binding site to adaptor underlined. Barcode: TTCGAC in blue.	caagcagaagacggcatacgagatg tcgaagtgactggagttcagacgtgt gctcttccgatctgtcaatgatggccg gtggatttgtg
AP1_P7_tagged_10	For 2nd hemi-nested PCR of P7 end, binding site to adaptor underlined. Barcode: CTCGTA in blue.	caagcagaagacggcatacgagatt acgaggtgactggagttcagacgtgt gctcttccgatctgtcaatgatggccg gtggatttgtg

Primers for checking and sequencing		
pRW50_F	To check pRW50T constructs	gttctcgcaaggacgagaatttc
pRW50_R	To check pRW50T constructs	aatcttcacgcttgagatac
pSR_F	To check pSR constructs	gcatttatcagggttattgtctc
pSR_R	To check pSR constructs	catcaccgaaacgcgcgagg
pVRL1Z_F	To check pVRL1Z constructs	tgagcggataacaatttcac
pVRL1Z_R	To check pVRL1Z constructs	gctgcaaggcgattaagt
pVRL2Z_F	To check natural transformants	gattatttgcacggcgtcac
pVRL2Z_R	To check natural transformants	gctgcaaggcgattaagttg
P31	Sequencing primer for *lacZ*/IVT constructs	aggtaacaatggtttgtgg
P32	Sequencing primer for *lacZ*/IVT constructs	attccatcaaccacaccac

P47	To confirm *ompW* region	gtgaggtgcctgaatctagg
P48	To confirm *ompW* region	tgggatactgtgataccaac
P49	To confirm *ABUW_1221* region	cataactcttcagcccattg
P50	To confirm *ABUW_1221* region	catttgtttggcgtctgg
P51	To confirm *hns* region	cgtctcgctaaagactataag
P52	To confirm *hns* region	tgtcagtaagactggagta
P112	To sequence pKT25 constructs	cggatatcgacatgttcg
P113	To sequence pKT25 constructs	tgctgcaaggcgattaag
P114	To sequence pUT18C constructs	tgtcttctacgagaaccg
P115	To sequence pUT18C constructs	ttgtctgtaagcggatgc
P116	To sequence pKNT25 and pUT18 constructs	cgcaacgcaattaatgtg
P117	To sequence pKNT25 constructs	gttgaccaggcggaacatc
P118	To sequence pUT18 constructs	attcatgtcgccgtcgtag
P123	To check codon optimised *hns* in pJ414	tgtgagcggataacaattcc
P124	To check codon optimised *hns* in pJ414	gattgacgcgtctcagg
Pgro-172_Tn26	To check T26 mutants	tgagctttttagctcgactaatccat

Table 2.3. Oligonucleotides used in this study

Buffer/Reagent	Constituents
DNA purification	
Phenol:chloroform:isoamyl alcohol	Phenol 50 % (v/v) Chloroform 48 % (v/v) Isoamyl alcohol 2 % (v/v)
General protein purification	
Coomassie stain	50 % methanol (v/v) 10 % acetic acid (v/v) 0.2 % Brilliant blue R (w/v)
2 x Laemmli buffer	100 mM Tris-HCl pH 6.8 2 % SDS (w/v) 20 % glycerol (v/v) 4% ß-mercaptoethanol (v/v) 0.005 % Bromophenol blue (w/v)
Protein purification of His_6-IS*Aba*13 transposase and MBP-IS*Aba*13 transposase	
Buffer NTA	20 mM Tris pH 7.9 5 % glycerol 600 mM NaCl
Protein purification of H-NS	
Protein buffer A	20 mM Tris-HCl pH 7.2 1 mM EDTA 10 % glycerol
Protein buffer B	20 mM Tris-HCl pH 7.2 1 mM EDTA 10 % glycerol 1 M NaCl
Dialysis buffer	20 mM Tris-HCl pH 7.2 50 % glycerol 300 mM KCl
***lacZ* assay**	
Z-buffer	30 mM $NaH_2PO_4.2H_2O$ 60 mM $NaPO_4$ 1 mM $MgSO_4.7H_2O$ 10 mM KCl
IVT/EMSA	
10 x TNSC buffer	400 mM Tris-acetate pH 7.9 100 mM $MgCl_2$ 1 M KCl
2 x Stop solution	7 M Urea 0.01 M EDTA 80 % (v/v) Deionised formamide 1 % (v/v) Bromophenol blue 1 % (v/v) Xylene cyanol

NTP mix	1.25 mM ATP 1.25 mM CTP 1.25 mM GTP 62.5 µM UTP
5 % Polyacrylamide gel for IVT	16.7 % (v/v) Protogel (30%, Geneflow) 6 M Urea 0.5 x TBE 3.5 mM Ammonium persulphate (APS) 0.05 % (v/v) N,N,N',N'-Tetramethylethylenediamine (Temed)
5 % Polyacrylamide gel for EMSA	16.7 % (v/v) Protogel 0.5 x TBE 3.6 mM APS 0.083 % (v/v) Temed
Bridging assay	
10 x Renaturation buffer (RB)	200 mM Tris-HCl pH 9.5 10 mM spermidine 1 mM EDTA
10 x Labelling buffer (LB)	500 mM Tris-HCl pH 9.5 100 mM $MgCl_2$ 40 % (v/v) glycerol
Coupling buffer (CB)	20 mM Tris-HCl pH 7.9 2 mM EDTA 2 M NaCl 2 mg/ml acetylated BSA 0.04 % (v/v) Tween-20
Incubation buffer (IB)	10 mM Tris-HCl pH 7.9 0.02 % Tween-20 1 mg/ml acetylated BSA 1.25 mM spermidine 12.5 mM $MgCl_2$ 6.25 % (v/v) glycerol 1.25 mM DTT
Stop buffer	10 mM Tris-HCl pH 7.9 1 mM EDTA 200 mM NaCl 0.2 % sodium dodecylsulphate (SDS)
DNA storage buffer (DSB)	10 mM Tris-HCl pH 7.9 50 mM KCl 10 mM $MgCl_2$

Table 2.4. Buffers and reagents used in this study

2.2.1. Antibiotics

All antibiotics were purchased from Sigma, filter sterilised (0.45 µm) and stored short term at 4 °C or long term at -20 °C. For *A. baumannii,* antibiotics were used to a final concentration of 10 µg/ml for tetracycline, 30 µg/ml for apramycin, 250 µg/ml for zeocin in liquid culture and 500 µg/ml for zeocin on agar plates. For *E. coli*, antibiotics were used to a final concentration of 35 µg/ml for tetracycline, 25 µg/ml for zeocin, 100 µg/ml for gentamicin, 50 µg/ml for kanamycin, 100 µg/ml for streptomycin, 30 µg/ml for chloramphenicol, and 100 µg/ml for ampicillin.

2.2.2. Storage as glycerol stocks

For long term storage at -80 °C, 500 µl of overnight culture was mixed with 500 µl 50 % glycerol for a final concentration of 25 % for *E. coli*. 625 µl of overnight culture was mixed with 375 µl 80 % glycerol for a final concentration of 30 % for *A. baumannii*.

2.2.3. Generating pure stocks of colony phase variants

Strains were streaked onto 0.5 x LBA plates where the correct phase was chosen under oblique illumination with a Nikkon SMZ-1000 microscope. Single colonies were streaked on 1 x LBA and grown for 6 h at 37 °C. Following this, single colonies were picked and used to inoculate LB, grown overnight at room temperature. Stocks were tested for purity by streaking onto 0.5 x LBA to check that the correct phase had been generated.

2.3. Gel electrophoresis

2.3.1. Agarose gel electrophoresis

Agarose electrophoresis was used to check DNA size, integrity and preceding gel extraction. Typically, 1 % (w/v) agarose gels were made with agarose (Bioline) in 1 x TBE. The solution was microwaved at full power with intermittent mixing until dissolved. 1 % (v/v) Sybr Safe was added and the gel left to cool on the bench. DNA was mixed with DNA loading dye (Qiagen) and run at 120 V for 20 – 40 minutes in 1 x TBE running buffer, before visualisation with a blue light transilluminator.

2.3.2. Polyacrylamide gel electrophoresis (PAGE)

PAGE was used to visualise band sizes for IVT and EMSA assays. A 5 % denaturing polyacrylamide gel was made with SequaGel UreaGel system (National Diagnostic). APS and TEMED were added and the gel allowed to set at room temperature. For IVT the gel was run in 1 x TBE at 80 W for 1 h to prewarm before loading samples. After adding samples to the wells, the gel was run at 80 W. For EMSA the gel was run in 0.5 x TBE at 150 V.

2.3.3. Sodium dodecylsulphate-polyacrylamide gel electrophoresis (SDS-PAGE)

To check the presence and size of protein, soluble and insoluble fractions following sonication were run on SDS-PAGE gels. Samples were mixed with Laemmli buffer and loaded onto a NUPAGE 4–12 % Bis-tris gel with acrylamide gradient (Invitrogen) run with 1 x MES buffer (Invitrogen) at 200 V for 1 h. Gels were microwaved with Coomassie stain for 30 s and

incubated for 20 minutes shaking. Gels were washed with destain and incubated 20 minutes a total of three times before imaging on a GS-800 calibrated Denistometer (Biorad).

2.4. DNA purification

2.4.1. PCR product purification

PCR products were purified using the QIAquick PCR Purification Kit (Qiagen) following the manufacturer's instructions.

2.4.2. Agarose gel extraction

Gel slices were excised with a clean scalpel and purified using the QIAquick Gel Extraction Kit (Qiagen) following the manufacturer's instructions.

2.4.3. Plasmid purification

For general cloning, plasmids were purified using the QIAprep Spin Miniprep kit (Qiagen). For generating large stocks of plasmid or for use in IVT assays, plasmids were purified by either using the ZymoPURE II Plasmid Midiprep Kit (Zymo Research) or the Qiagen Maxiprep kit (Qiagen).

2.4.4. Phenol-chloroform extraction

Due to its large size (17.2 kbp), pRW50T was purified following restriction digestion by phenol-chloroform extraction. An equal volume of phenol:chloroform:isoamyl alcohol was added to pRW50T purified by Maxiprep or Miniprep. The mixture was vortexed for 15 s, followed by centrifugation in a 5PRIME phase-lock gel heavy tube (Quantabio) at 17,900 x g for 3 minutes. The upper aqueous phase was removed to a fresh tube and 20 µl 3 M NaAc pH 5.2 was added. 600 µl of ice-cold 100 % ethanol was added and the tube put at -80 °C for 30 minutes. This was followed by centrifugation at 17,900 x g, 4 °C for 45 minutes. Supernatant was removed leaving the pellet undisturbed, which was washed with 750 µl ice-cold 70 % ethanol followed by centrifugation at 17,900 x g, 4 °C for 10 minutes. Supernatant was removed, the pellet was dried by vacuum (Savant120 speedvac, Thermofisher) on the medium/run setting, followed by resuspension in H_2O .

2.4.5. Genomic DNA (gDNA) extraction

gDNA was extracted using the DNeasy Blood & Tissue kit (Qiagen) according to the manufacturer's instructions for Gram-negative bacteria. The optional RNase A step was included. A final elution in 100 µl H_2O was used rather than 200 µl in elution buffer.

2.4.6. AMPure XP bead cleanup

An appropriate amount of beads for each assay was aliquoted out and left at room temperature for > 30 minutes. 100 µl DNA in H_2O was mixed with different amounts of beads depending on the ratio required, and incubated at room temperature for 5 minutes. Tubes

were placed on a magnetic rack and supernatant removed. Beads were washed 2 x with 200 µl freshly prepared 70 % ethanol. To elute DNA off beads, tubes were taken off the rack, H_2O was added, mixed, and tubes were incubated at room temperature for 2 minutes. Then tubes were placed back on the rack and supernatant containing eluted DNA removed into a fresh Eppendorf.

2.5. DNA sequencing

2.5.1. Sanger sequencing

All plasmids and mutants generated were confirmed by Sanger sequencing done by either the Genomics Facility at the University of Birmingham or by Eurofins.

2.5.2. Whole genome sequencing

Strains were grown to mid-exponential phase and 10^9 cells were collected by centrifugation. Cells were washed with 1 ml PBS and resuspended in 0.5 ml 1 x DNA/RNA shield (Zymo). MicrobesNG performed long read genome sequencing using Oxford Nanopore and short read genome sequencing with Illumina (2 x 250 bp paired ends, 30 x depth coverage).

2.6. RNA purification

Strains were grown to mid-exponential phase, and RNA extraction was done with the Qiagen RNeasy kit following the manufacturer's instructions. Tapestation (Agilent) was used to assess RNA integrity and concentration.

2.7. RNA sequencing

Library preparation for RNA-seq was done by Vertis Biotechnologie (Fig.2.1). Samples were depleted of rRNA, fragmented ultrasonically, and an adapter ligated to the 3' end. M-MLV reverse transcriptase was used to generate cDNA that was then amplified by PCR. Libraries were sequenced using an Illumina NextSeq 500 system with 75 bp read length.

2.8. Cloning

2.8.1. PCR

PCR was done with Q5 polymerase (NEB) according to the manufacturer's instructions in a final volume of 50 µl. For gDNA template, 100 ng was used, for plasmid template 10 ng was used. Thermocycling parameters used are given in Table 2.5, which were modified as appropriate depending on the annealing temperature of primers and the length of product to be amplified (30 s per kb).

For overlap extension PCR, Q5 polymerase was used as above with the appropriate fragments added for 15 cycles without primers to enable annealing, followed by addition of flanking primers and a further 30 cycles. This method was used to join the native H-NS promoter to the DNA sequence encoding the 39 amino acids of H-NS^{39aa}, including a start codon for translation initiation.

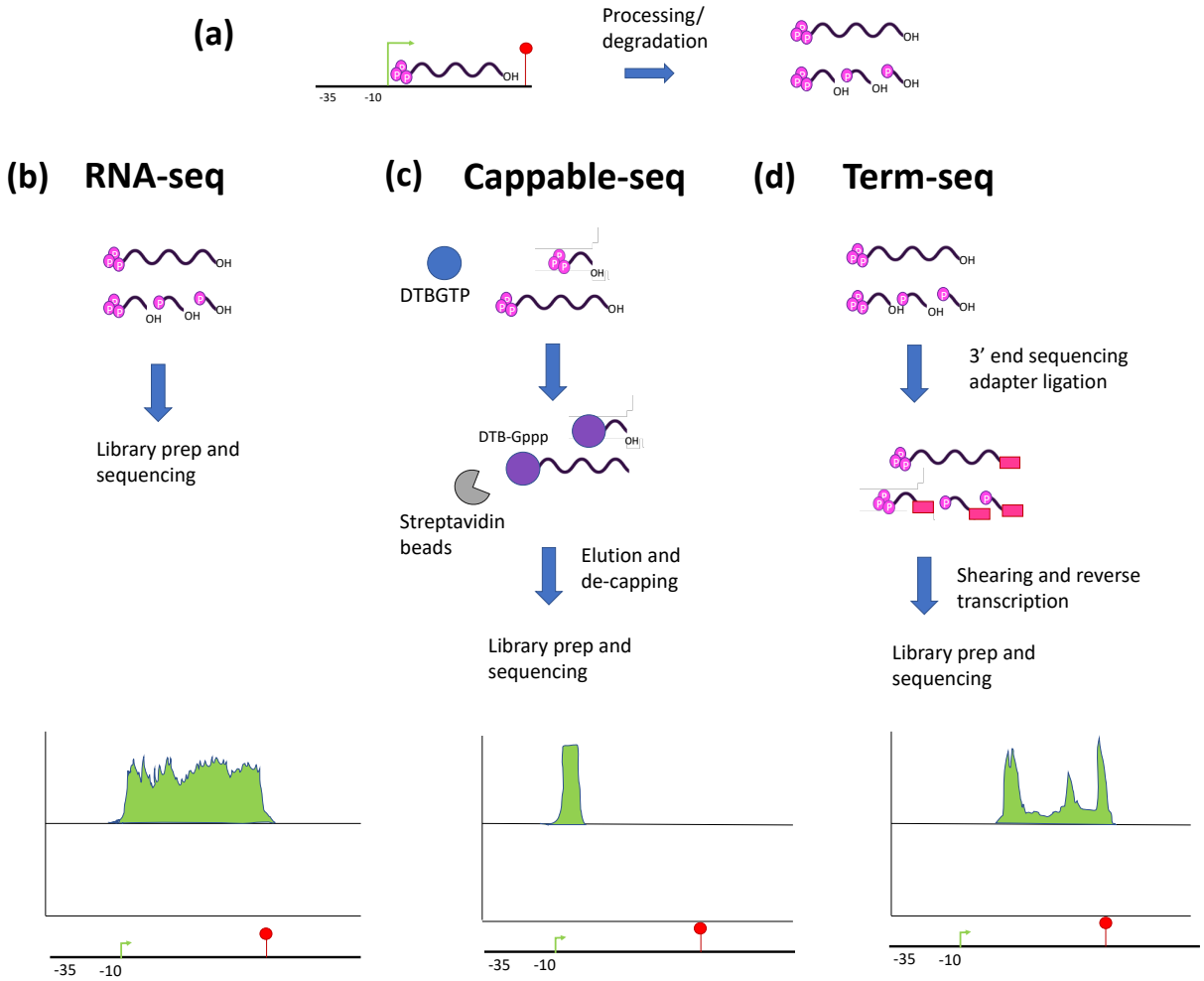

Fig.2.1. Illustration of RNA-seq methods

(a) RNA processing and degradation give rise to a heterogenous population of RNA species of different lengths making annotation of transcription start and stop sites difficult. (b) Standard RNA-seq sequences all mRNA species in the transcriptome. (c) In Cappable-seq, RNA is capped using desthiobiotin-TEG-guanosine 5'triphosphate (DTBGTP) and the vaccinia capping enzyme, followed by capture with streptavidin beads. This enables enrichment of 5' ends of RNA. (d) In Term-seq, a 5' sequencing adapter is ligated to the 3'OH at the ends of RNA. Bottom: examples of expected traces following alignments of reads to a reference genome.

Step	Description	Temperature (°C)	Time	Number of cycles
1	Initial denaturation	98	30 s	1
2	Denaturation	98	10 s	30
	Annealing	50-72	20 s	
	Elongation	72	30 s	
3	Final elongation	72	2 minutes	1

Table 2.5. PCR parameters used for Q5 polymerase

Colony PCR with MyTaq red (Bioline) was used to confirm positive transformants, with a sterile tip used to stab a single colony and add it to the master mix. Thermocycling parameters used are given in Table 2.6, which were modified as appropriate depending on the annealing temperature of primers and the length of product to be amplified (10 s per kb).

2.8.2. Restriction digestion

All restriction enzymes were purchased from NEB. Digestion reactions were carried out with 3 µl of each restriction enzyme for plasmid and 1.5 µl of each restriction enzyme for PCR products, in a total volume of 50 µl with 1 x rCutSmart buffer. Reactions were incubated at 37 °C for at least 1 h. For plasmid digestion, 5 µl calf intestinal phosphatase (CIP) (NEB) was added, with incubation at 37 °C for 30 minutes. Complete plasmid digestion was confirmed by electrophoresis on a 1.5 % agarose gel, compared alongside single digest reactions.

2.8.3. Ligation

In a PCR tube, digested plasmid DNA and digested PCR product were mixed in a 1:3 molar ratio with 2 µl ligation buffer, 1 µl T4 DNA ligase (NEB) and made up to 20 µl with H_2O. No more than 100 ng digested plasmid was used. Ligation reactions were incubated overnight at 16 °C. Reactions always included a negative control of digested plasmid without insert.

Step	Description	Temperature (°C)	Time	Number of cycles
1	Boiling	95	5 minutes	1
2	Initial denaturation	95	30 s	1
3	Denaturation	95	30 s	30
	Annealing	50-72	30 s	
	Elongation	72	30 s	
4	Final elongation	72	10 minutes	1

Table 2.6. PCR parameters used for colony PCR

2.8.4. Gibson assembly

Gibson assembly was used to join multiple DNA fragments together, either as a linear product for natural transformation or as a closed circular plasmid. Less than a total of 0.2 pmol was used in each reaction. For assembly of 2-3 linear fragments, a molar ratio of 1:1 of each fragment was used. Whereas, for assembly of 2-3 linear fragments into a vector, a molar ratio of 1:2 of vector:insert was used with 100 ng total vector. DNA was mixed with NEBuilder HiFi DNA assembly master mix (NEB) and incubated at 50 °C for 1 h.

2.8.5. Preparation of chemically competent cells

An overnight culture was subcultured into 50 ml LB and grown at 37 °C to OD_{600} = 0.5. Cells were incubated on ice for 10 minutes followed by centrifugation at 3,500 x g for 5 minutes at 4 °C. Pellets were gently resuspended in 25 ml ice-cold 0.1 M $CaCl_2$ and incubated on ice for at least 30 minutes. Cells were collected by centrifugation at 3,500 x g for 10 minutes at 4 °C, supernatant removed, and pellet resuspended in 3.3 ml 0.1 M $CaCl_2$. Cells were left at 4 °C overnight on ice and the following day 1.2 ml of 50 % glycerol was added. This mixture was aliquoted and stored at -80 °C.

2.8.6. Heat shock transformation

Competent cells were left on ice for at least 30 minutes with ligation product or digested plasmid as a negative control. Cells were heated at 42 °C for either 2 minutes (JCB387), 30 seconds (NEB DH5α) or 10 seconds (NEB Lemo21), put on ice for 3 minutes and incubated at 37 °C for 1 h shaking in SOC medium before selection on LBA with the appropriate antibiotic.

2.8.7. Natural transformation

Cells were first streaked on 1 x LBA or selective LBA if appropriate and incubated overnight at 37 °C. Next, 1 ml of motility medium (2 % agarose (w/v) (Euromedex), 5 g/L tryptone (Difco)) was heated, added to a sterile Eppendorf tube, and left to cool on the bench. A single colony was resuspended in 2 ml LB and incubated at 37 °C until OD_{600} = 1. The culture was diluted 100-fold in sterile PBS and 2.5 µl mixed with an equal volume of transforming DNA. This mixture was spotted onto motility medium and incubated at 37 °C overnight. The next day, 100 µl PBS was added to the Eppendorf tubes, and cells were resuspended using a vortex mixer for 5 s. The resulting mixture was plated on appropriate media.

2.8.8. Conjugation

Triparental conjugation was carried out as follows. 1 ml of overnight culture grown at 37 °C underwent centrifugation for 5 minutes at 2,500 x g. Cell pellets were washed twice with 500 µl 0.9 % sterile NaCl followed by centrifugation for 5 minutes at 2,500 x g. Cell pellets were resuspended in 1 ml LB and 100 µl donor *E. coli* DH5α was mixed with 100 µl recipient AB5075 and 200 µl *E. coli* DH5α containing the helper plasmid pRK2013. 50 µl of this mixture was spotted onto a fresh LBA plate and incubated overnight at 30 °C. The next morning, clumps were scraped with a sterile plastic inoculation loop and resuspended in 100 µl 0.9 % sterile NaCl. This suspension was plated onto selective LBA plates, incubated overnight at 37 °C and restreaked on selective media followed by incubation again overnight at 37 °C.

2.8.9. Generation of scarless *ompW*::IS*Aba*13 chromosomal mutant

To insert IS*Aba*13 at the *ompW* locus, PCR was used to generate 2 kb fragments flanking *ompW*. Two further fragments, containing IS*Aba*13 and *sacB*-*apra*^{R} respectively, were also generated. The different sections of DNA were then combined by Gibson assembly, purified, and used to transform AB5075 cells (Fig.2.2). To remove the *sacB*-*apra*^{R} cassette from the locus, leaving a scarless IS*Aba*13 insertion, we first extracted genomic DNA from a successful transformant. This was used as a template to generate fragments, that could be fused by overlap extension PCR, to create a copy of the *ompW* locus lacking the *sacB*-apra^{R} cassette (Fig.2.2). Following transformation, successful recombinants were plated on media without NaCl containing 20 % (w/v) sucrose for counter selection, with incubation overnight at 30 °C.

2.9. Phenotypic assays

2.9.1. Capsule production assay

We followed the protocol of (Whiteway *et al.*, 2022). Cells were collected from an overnight culture by centrifugation at 5,000 x g. Cells were resuspended in 1 ml PBS and 875 µl of resuspended bacteria were mixed with 125 µl of 30 % (w/w) Ludox LS colloidal silica (Merck), followed by centrifugation at 9,000 x g for 30 minutes with band distances recorded photographically.

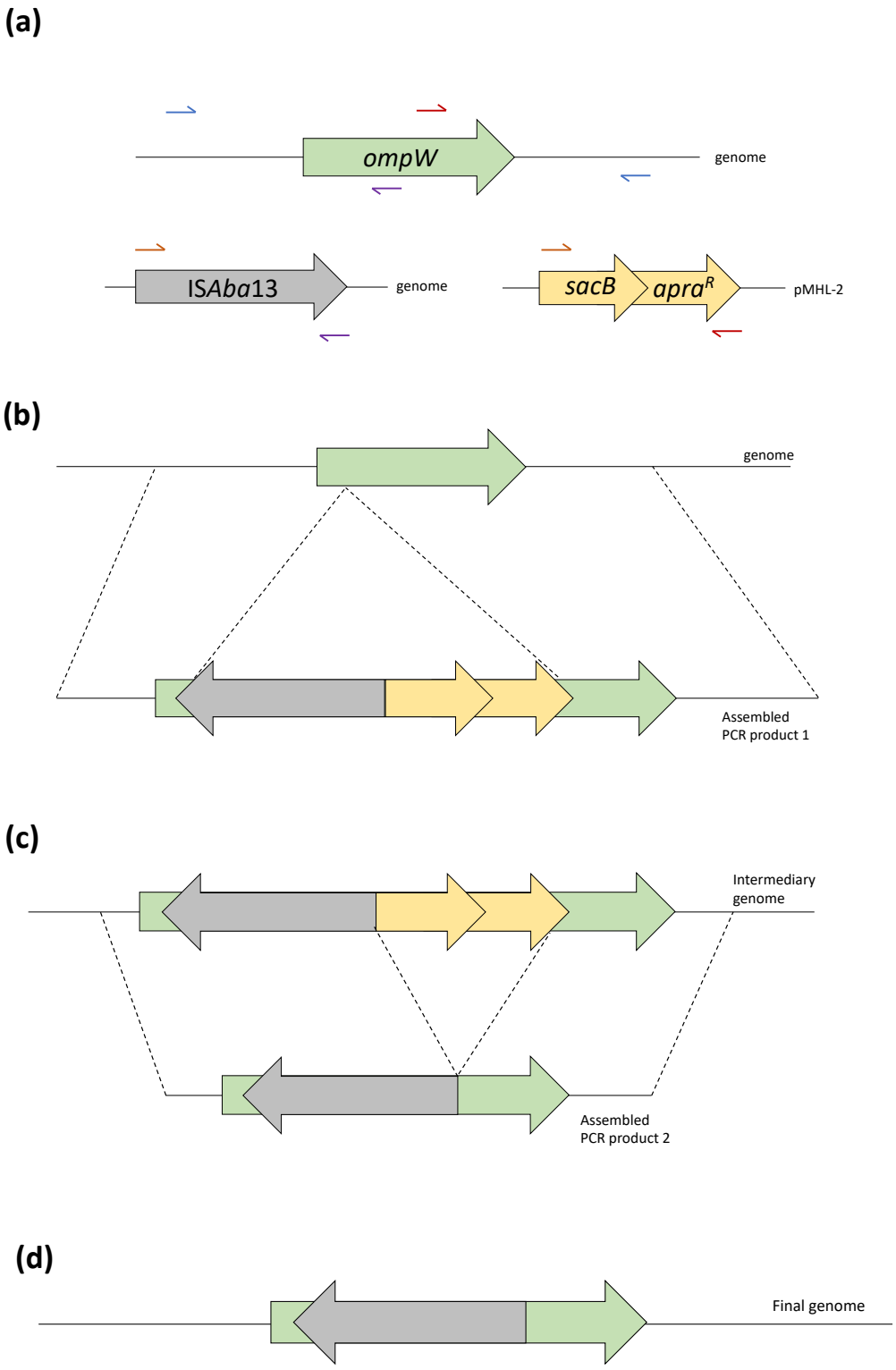

Fig.2.2. Illustration of creation of scarless chromosomal *ompW*::IS*Aba*13 mutant
(a) PCR is used to generate the four fragments with overlapping regions to be stitched together. (b) The 1st recombination inserts the *sacB-apra*^{R} cassette into the chromosome with the desired rearrangements. (c) A second recombination is used to remove the *sacB-apra*^{R} cassette. (d) The final scarless mutant generated contains IS*Aba*13 in the desired location.

2.9.2. Growth curves

Overnight cultures were serially diluted to a starting OD_{600} = 0.05 in LB medium, in a 96-well plate (Costar). Plates were incubated at 37 °C with shaking, and measurements taken every hour for 24 hours in a microplate reader (Fluostar). For growth in serum, human serum type AB (Sigma) was diluted 1:2 in LB medium. For heated control human serum, aliquots were treated at 56 °C for 30 minutes before dilution 1:2 in LB medium.

2.9.3. Broth microdilution MIC

To prepare serial dilutions of the antibiotic to be tested, 50 µl of LB was added to each row of a 96-well plate (Costar), excluding the first column. Next, 50 µl of antibiotic diluted in LB at twice the required concentration was added to the first two columns, and a multichannel pipette was used to create double dilutions of each sequential column, starting from column two, by transferring 50 µl of mixture from one column to the next, with 50 µl removed and discarded from the final column. Overnight cultures were diluted to OD_{600} = 0.05 in sterile distilled water, and then diluted further in a 1:20 dilution in LB medium. 50 µl of this dilution was added to each well to create a final volume of 100 µl. The plate was grown at 37 °C, stationary, for 18 hours and growth in each well was assessed.

2.9.4. Congo Red binding assay

Congo Red plates were made from Congo Red solution added to warm LBA made without salt, to a final concentration of 40 µg/ml. Overnight cultures were diluted 1:10,000 in LB made

without salt, and 5 µl was spotted in triplicate onto the Congo Red agar plates. Plates were incubated at 30 °C for 48 hours before being photographed.

2.9.5. Biofilm assay

The procedure was adapted from the work of (López-Martín *et al.*, 2021). Bacteria were grown to mid-log phase and 750 µl of culture added to a 1.5 ml polypropylene Eppendorf tube. After incubation at 37 °C or room temperature for 24 h, the culture was removed, and tubes washed twice with 1 ml PBS. Next, 850 µl of 0.1 % (w/v) crystal violet was added to the tube. Following incubation at room temperature for 15 minutes, the dye was removed, and tubes were washed three times with 1 ml PBS. After drying, tubes were photographed as a qualitative measure of biofilm production. For quantification, the dye was dissolved by adding 1 ml of 100 % ethanol to each tube, followed by vortexing and incubation for 10 minutes at room temperature. The A_{585} was recorded to measure amount of crystal violet dye.

2.9.6. Surface-associated motility assay

Five bacterial colonies were resuspended in 100 µl LB medium, and 1 µl of the resulting mixture spotted onto 0.3 % agarose (Bioline) plates. These were sealed with parafilm and incubated, agar surface up at 37 °C for 16 h inside a sealed plastic bag. Plate images were recorded photographically, and motility was quantified by measuring the colonised area of the plate with ImageJ software.

2.9.7. Twitching motility assay

Strains to be tested were streaked on 1 x LBA and incubated overnight at 37 °C. Twitching agar was prepared as 1 % tryptone (w/v), 0.5 % yeast extract (w/v), 0.25 % NaCl (w/v) and 1 % agar (w/v). 10 ml of twitching agar was poured into a Petri dish and left to solidify by a Bunsen burner for 10 minutes. A single colony was picked from the agar plate using a sterile pipette tip and stabbed until contacting the plastic. Plates were incubated at 37 °C for 48 h, and the twitching halo photographed, with areas measured by ImageJ software.

2.9.8. Natural transformation assay

Natural transformation was conducted as described above, with bacteria grown to OD_{600} = 0.6 instead of OD_{600} = 1. Before incubation, 250 ng of plasmid DNA was mixed with bacteria. Following incubation, 300 µl sterile PBS was added to tubes and vortexed for 5 seconds. A range of serial dilutions were made by mixing 30 µl of culture with 270 µl LB in a 96 well plate. 100 µl of dilutions were plated onto selective agar to enumerate transformants and 100 µl plated on LBA at various dilutions to enumerate total colony forming units (CFU).

2.9.9. Desiccation assay

Overnight cultures were grown to OD_{600} = 0.15. Next, 25 µl was spotted into the wells of a 96-well flat-bottomed polystyrene plate (Corning). The plate was allowed to dry in a biosafety cabinet for 1 h, and then incubated on the bench at room temperature. At appropriate times,

100 µl PBS was mixed thoroughly into the wells and incubated for 30 minutes to allow bacteria to rehydrate. Mixtures were serially diluted and plated to enable CFU enumeration.

2.10. *LacZ* assay

150 µl of overnight culture grown in selective LB medium was used to inoculate 3 ml fresh selective LB medium. Strains were grown to OD_{600} = 0.3 - 0.5. Cultures were lysed by adding 2 drops of 1 % (w/v) sodium deoxycholate and 2 drops of toluene, followed by vortexing for 20 seconds. Tubes were left to incubate in a biosafety cabinet for at least 1 hour to allow toluene to evaporate. Z-buffer was prepared with 8 mg/ml 2-nitrophenyl-ß-D-galactopyranoside (ONPG) and 0.27 % ß-mercaptoethanol. Next, 2.5 ml of this solution was mixed with 100 µl of lysate in glass test tubes to begin the reaction. Following incubation at 37 °C for 20 minutes, the assay was stopped with 1 ml of 1 M Na_2CO_3. A_{420} was measured and activity (Miller units) calculated with the equation below:

$$Activity = \frac{(2.5 * 1000 * A * A_{420})}{(4.5 * T * V * OD_{650})}$$

Where, A = final assay volume (ml), T = reaction time (min), and V = volume of lysate used (ml).

2.11. Native Tn-seq

At least two biological replicates were done for each genetic background. Following overnight growth, cells were sub-cultured in 50 ml LB and grown to mid exponential phase (OD_{600} = 0.5). Genomic DNA was extracted from 13 ml of the culture using a DNeasy Blood & Tissue kit (Qiagen) according to the manufacturer's instructions for Gram-negative bacteria, as described above (section 2.4.5.). The extracted DNA was further purified with Agencourt AMPure XP magnetic beads (Beckman Coulter), using a 1.8:1 ratio of beads:DNA as described above (section 2.4.6.) NEBnext dsDNA fragmentase (NEB) was used to digest 6 µg of gDNA. Reactions were incubated for 10 - 15 minutes at 37 °C and stopped by the addition of 5 µl 0.5M EDTA. Fragmented DNA, between 400 – 650 bp in size, was extracted from a 1 % (w/v) agarose gel following electrophoresis. Gel slices were stored at -20 °C for > 30 minutes and DNA extracted using the Qiagen minelute kit according to the manufacturer's instructions, with an extra PE buffer wash. Next, 1 µg of DNA was mixed with 7 µl NEBnext Ultra II end prep reaction buffer (NEB) and 3 µl Ultra II end prep enzyme mix (NEB), and incubated at 20 °C for 30 min, followed by 65 °C for 30 min.

Next, 48 µl of 100 µM stock DNA adaptors 1.2 and 2.2 was mixed with 4 µl 50 mM $MgCl_2$, heated at 95 °C for 10 minutes, and allowed to cool to room temperature overnight. Adaptor 1.2 has a 3' C3-amino modification to protect against exonuclease degradation and block strand extension during PCR. The longer adaptor 2.2 creates a 3' overhang of a single thymine base, facilitating ligation to genomic DNA fragments. Hybridised adapters were attached to DNA fragments using either a Fastlink DNA ligation kit (Cambio), or following discontinuation of this reagent, the NEBnext ultra II ligation module (NEB). For the Fastlink DNA ligation kit,

four reactions were done per sample: 11.25 µl of DNA was mixed with 1 µl of adaptor mix, 1.5 µl of ligase buffer, 0.75 µl 10mM ATP and 1 µl ligase, and incubated at room temperature for 1 h. Then to each sample an additional 1 µl ligase buffer, 7.5 µl H_2O, 0.5 µl 10 mM ATP and 1 µl ligase was added and incubated for a further 2 h at room temperature. For the NEBnext Ultra II ligation module, 2.5 µl of adaptor mix above was added to the completed end repair reaction mixture, with 30 µl NEBnext Ultra II ligation master mix and 1 µl NEBnext ligation enhancer incubated at 20 °C for 15 minutes. After ligation, products were purified with a 0.7:1 ratio of AMPure XP beads to DNA.

Purified products were used as template for 50 µl PCR reactions containing 1 x GoTaq mix (Promega), 0.3 µM of each oligonucleotide JelAP1 and IS*Aba*13_out, and 5 % DMSO. For each experiment, 8 reactions were done using 100 ng of DNA template in each. Thermocycling parameters used are given in Table 2.7. The JelAP1 oligonucleotide anneals to adaptor 2.1 and results in extension products directed toward the isolated genomic DNA fragment. The IS*Aba*13_out oligonucleotide anneals close to the 3' end of the IS*Aba*13 transposase coding sequence and results in extension products across the boundary of IS*Aba*13 and the associated chromosomal DNA, towards the site of adaptor 2.1 attachment. Thus, all products of the PCR reaction capture boundaries between IS*Aba*13 and chromosomal DNA at insertion sites. Following PCR, each set of 8 equivalent reactions was pooled and products separated on a 2 % (w/v) agarose gel. Products in the region of 400 – 650 bp were excised in a gel slice that was then stored at -20 °C for 30 minutes. The DNA was then recovered using a minelute gel extraction kit (Qiagen) using four PE buffer washes.

Step	Description	Temperature (°C)	Time	Number of cycles
1	Initial denaturation	95	10 minutes	1
2	Denaturation Annealing Elongation	95 58 72	30 s 30 s 45 s	20
3	Final elongation	72	5 minutes	1

Table 2.7. PCR parameters used for 1st PCR in native Tn-seq

In a second round of PCR reactions, we used an oligonucleotide (Ap_P7_tagged_1) that anneals to the JelAP1 sequence and introduces a DNA barcode. This was in conjunction with a mixture of four oligonucleotides, all annealing to the same site towards the 5' end of the IS*Aba*13 sequence, and containing different stagger lengths to improve complexity of the final library. Resulting PCR products should contain the final 78-83 bp (depending on the stagger length) of IS*Aba*13 at the 5' end. The PCR conditions were the same as those used in step one above, except without DMSO, and the cycle number was reduced to 8. After PCR, DNA was recovered using a 1:0.75 ratio of AMPure XP beads. The size and purity of DNA fragments were assessed using a Tapestation (Agilent) and concentration assessed by qPCR, before sequencing with an Illumina HiSeq or NovaSeq instrument (2 x 150 bp) with a 5 % PhiX spike in.

2.12. *In vitro* transcription (IVT)

IVT master mix was made with 2 µl 10x TNSC buffer, 0.1 µl 20 mg/ml BSA, 3 µl NTP mix and 0.2 µl α ^{32}P-UTP (5 µCi). Next, 300 ng of pSR template was made up to 12.7 µl in H_2O. RNAP mix was prepared per reaction as 2 µl RNAP holoenzyme (NEB) added to 0.2 µl σ^{70}. 5.3 µl of master mix was added to each DNA template with 2 µl RNAP mix and incubated at 37 °C for 10 minutes. 20 µl Stop solution was added and samples were loaded onto a prewarmed polyacrylamide gel and run for several hours. Gels were dried at 80 °C for 1 h before exposure to a Fuji phosphor screen overnight and imaging by a BioRad Molecular Imager FX.

2.13. Radiolabelling of DNA fragments

Fragments generated by Q5 PCR were incubated with [γ-^{32}] adenosine triphosphate (ATP) (10 µCi/ul, Perkin Elmer) and T4 PNK (NEB) following the manufacturer's protocol. Unincorporated nucleotides were removed by centrifugation through a Micro Bio-spin P-30 gel column (Bio-Rad) at 1,000 x g for 4 minutes.

2.14. Electrophoretic mobility shift assay (EMSA)

Experiments were done according to the protocol of (Haycocks *et al.*, 2019). Briefly, radiolabelled DNA fragments were mixed with herring sperm DNA (12.5 mg/ml) and indicated proteins in 1 x TNSC buffer. After incubation at 37 °C for 10 minutes, samples were analysed by electrophoresis using a 5 % (w/v) polyacrylamide gel. After drying, gels were exposed to a Fuji phosphor screen overnight and imaged using an Amersham Typhoon (Cytiva).

2.15. Bacterial two hybrid (BACTH) assay

Plasmids pKT25, pKNT25, pUT18 and pUT18C were digested with KpnI and PstII, and ligated with genes encoding the proteins of interest digested with the same restriction enzymes. This created in frame fusions of the genes encoding the protein of interest with the T25 or T18 catalytic domains of the adenylate cyclase *from Bordetella pertussis* (Fig.2.3). Positive controls of leucine zipper fused to the catalytic domains was included. The plasmids were used to transform BTH101, prepared as chemically competent as above (section 2.8.5). To assess cyclic AMP (cAMP) synthesis and subsequent *lacZ* expression, a *lacZ* assay was done as above (section 2.10).

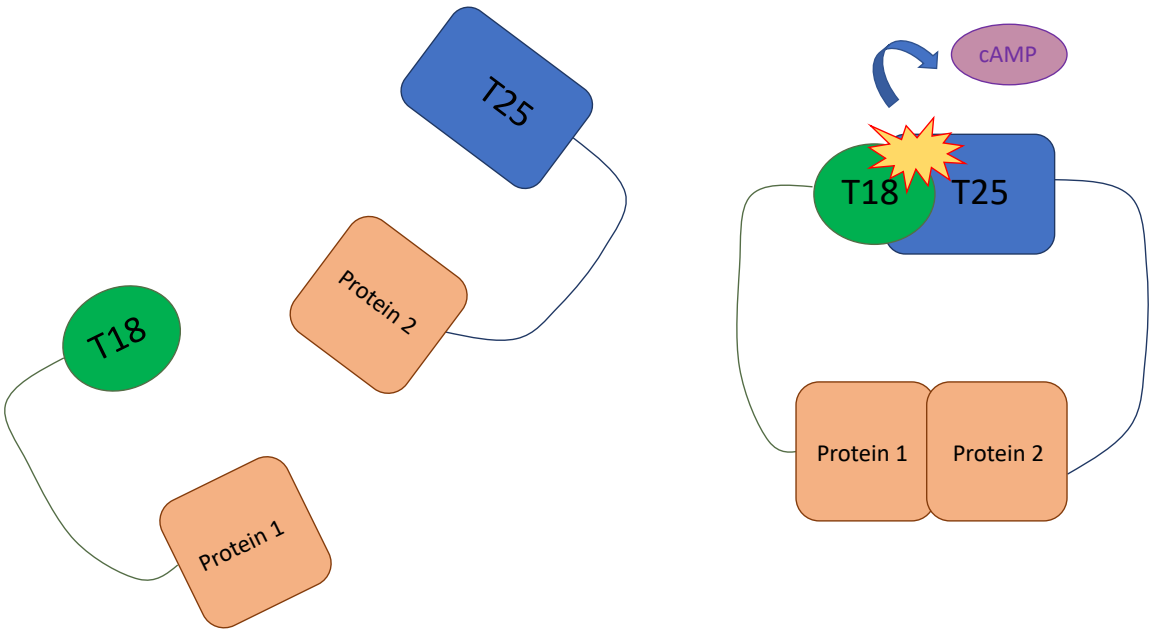

Fig.2.3. Illustration of BACTH assay
Proteins of interest are fused in frame to the catalytic domains (T18 and T25) of adenylate cyclase. If the two proteins interact spatially, the catalytic domains are brought close together and can catalyse the production of cAMP. This signalling molecule binds the regulator cAMP receptor protein (CRP) which induces expression of *lacZ.*

2.16. Protein expression and purification

2.16.1. Measurement of protein concentration

Protein concentrations were measured on a Qubit 2.0 fluorometer (Life technologies) using the Quantit protein assay kit (Thermofisher). Diluted dye was prepared 1:200 along with three standards. 1 µl or 10 µl sample was diluted with 199 µl diluted dye or 190 µl diluted dye respectively.

2.16.2. Attempted protein purification of IS*Aba*13 encoded transposase

For small scale protein expression, overnight cultures were diluted 1:50 in fresh LB with appropriate antibiotics, and with or without L-rhamnose for Lemo21 DE3 cells. Cultures were grown to OD_{600}= 0.4–0.5 at 37 °C, induced with or without isopropyl β-d-1-thiogalactopyranoside (IPTG) (400 µM) and grown further at 37 °C for a few hours or overnight at 18 °C. OD_{600} was measured and normalised amounts of bacteria were collected by centrifugation at 13,000 rpm for 1 minute. Pellets were resuspended in 200 µl 1 x Bugbuster protein extraction reagent (Merck) in NTA buffer. One tablet of cOmplete Mini EDTA-free protease inhibitor cocktail (Sigma) was added and dissolved. Suspensions were sonicated using a Bio-rupter (Diagenode) with 15 cycles on for 30 s, 15 cycles off for 30 s. This was followed by centrifugation for 3 minutes at 13,000 rpm. For the supernatant soluble fraction, Qubit was used to measure protein concentration. Laemmli dye was added to 5 µg of protein per tube. For the insoluble fraction, pellets were resuspended in 50 µl NTA buffer A + 8M Urea

with Laemmli dye. All samples were vortexed and boiled for 5 minutes and loaded on an SDS-PAGE gel.

2.16.3. Native protein purification of H-NS

The *A. baumannii hns* sequence was cloned into plasmid pJ414 under the control of an IPTG-inducible promoter, and the construct was used to transform *E. coli* T7 Express cells. Transformants were grown to mid-log phase before induction of H-NS expression with 1 mM IPTG for 2 h. Cells were collected by centrifugation and resuspended in 30 ml of buffer A with 100 mM NaCl with one cOmplete Mini EDTA-free protease inhibitor cocktail tablet. Cells were lysed by sonication and lysates cleared by centrifugation at 13,000 rpm for 1h at 4 °C. Supernatant was filtered (0.4 µm pore size) and loaded onto a HiTrap heparin HP1 5 ml column (Cytiva). The protein was eluted with a gradient to 1 M NaCl using an Akta™. Fractions containing H-NS were identified by SDS-PAGE, pooled and dialysed overnight at 4 °C in SnakeSkin tubing (Thermofisher) with 2 L of buffer A. The resulting sample was loaded onto and eluted from a HiTrap SP XL 5 ml column (Cytiva) as described above. Fractions containing H-NS were pooled and concentrated with a Vivaspin 20 MWCO 5000 column (Cytiva) by centrifugation at 4,000 x g, 4 °C. The purified protein was then dialysed overnight into dialysis buffer for storage at –20 °C.

2.16.4. Peptide synthesis of H-NS^{39aa}

Lyophilized peptide (> 95 % purity) was prepared by Thermofisher using Fmoc solid-phase technology, purified by high-performance liquid chromatography (HPLC). Peptide sequence

was confirmed by mass spectrometry, and purity determined by analytical HPLC. Upon receipt, peptide was dissolved in H_2O, aliquoted and stored at –20 °C.

2.17. DNA bridging assay

This assay is based on the procedure of (van der Valk *et al.*, 2017) illustrated in Fig.2.4.

2.17.1. Radiolabelling of prey DNA

Q5 PCR was used to generate bait and prey DNA. DNA bands were checked on a 1 % agarose gel and subsequently purified with a PCR purification kit. 2 pmol of purified DNA was mixed with 10 x RB to a final volume of 15 µl in H_2O. Next, 10 µl kinase mix was prepared per DNA labelling as follows: 2.5 x LB, 25 mM DTT, 2 µl ATP $\gamma^{32}P$, 1 U/µl Polynucleotide kinase (PNK). DNA was incubated at 80 °C for 10 minutes and kept on ice. 10 µl of the kinase mix made above was added to the DNA sample and incubated at 37 °C for 30 minutes. The reaction was stopped with the addition of 1µl 0.5M EDTA and incubated at 75 °C for 15 minutes. Unincorporated nucleotides were removed by centrifugation through a Micro Bio-spin P-30 gel column at 1,000 x g for 4 minutes. Radiolabelled DNA was made to a final volume of 100 µl with DSB.

2.17.2. DNA Bridging

For each reaction, 3 µl of MyOne streptavidin T1 Dynabeads (Thermofisher) were added to a microfuge tube, washed once with 50 µl PBS and twice with 50 µl CB. The beads were then

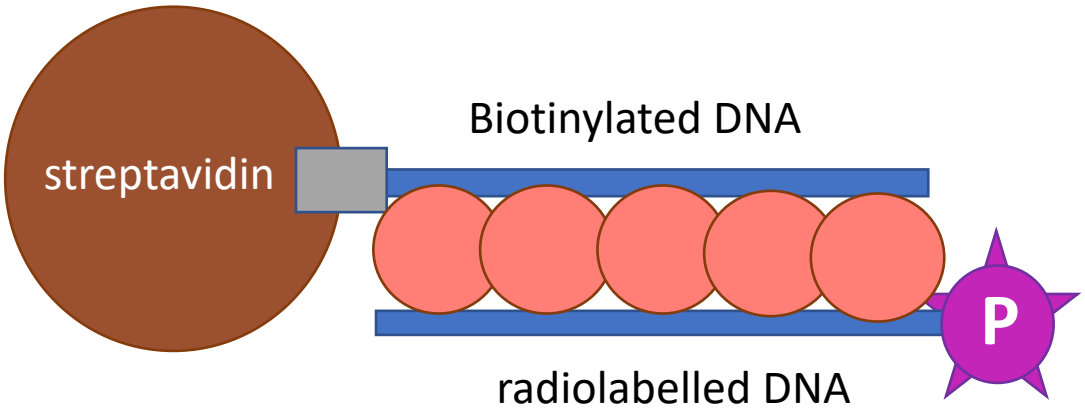

Fig.2.4. Illustration of DNA bridging assay
Biotinylated "bait" DNA is bound to the streptavidin bead. Upon addition of a bridging protein, free radiolabelled "prey" DNA is tethered to bait DNA bound to beads. The greater the amount of bridging, the greater the amount of radiolabelled DNA retained following washing, and the greater the radioactive signal.

resuspended in 3 µl CB. 100 fmol of biotinylated bait DNA in 3 µl of DSB was added to the resuspended beads and incubated at 25 °C for 20 minutes with shaking at 1000 rpm. Proteins and radiolabelled prey DNA (minimum counts 5000/min) were then added, and samples incubated at room temperature for 20 min. Beads were washed with 20 µl of reaction buffer and resuspended in 12 µl stop buffer. A 5 µl aliquot of each reaction was spotted onto a nitrocellulose filter paper and exposed to a Fuji phosphor screen overnight. After imaging with an Amersham Typhoon instrument, spot intensity was quantified using ImageJ. Each assay included negative controls of no biotinylated DNA and no H-NS.

2.18. Bioinformatics analysis

2.18.1. Genome sequence assembly

Bioinformatics on the reads obtained from long and short read genome assembly were done by MicrobesNG. The short and long read data was combined in a hybrid assembly to produce a complete bacterial genome. Kraken was used to identify a reference genome and reads mapped using BWA mem. A *de novo* assembly was performed with SPAdes and reads mapped back to contigs with BWA mem. Variant calling was done with VarScan and automated gene annotation with Prokka.

2.18.2. RNA-seq analysis

All sequencing reads were processed as described by (Forrest et al., 2022). Briefly, reads were aligned against the reference genome (CP008706.1) using Bowtie 2 (Langmead and Salzberg, 2012; Afgan *et al.*, 2018) (Galaxy v2.4.2) and coverage extracted using the genomcov function

of BedTools (Quinlan and Hall, 2010) (Galaxy v2.30.0). For differential expression analysis, FeatureCounts (Liao, Smyth and Shi, 2019) was used to determine gene read counts, which were input into edgeR (Robinson, McCarthy and Smyth, 2010) to determine differential gene expression, using the R script in Appendix 1, written by Dr. David Forrest. For Cappable-seq, coverage files were used in the script in Appendix 2, written in R by Dr. David Forrest and Zuzana Palečková. Briefly, If the number of Cappable-seq reads at a single position is four times greater than the previous one and greater than 4 reads, it is assigned as a TSS. For Term-seq, identification of TTS using coverage files was done using Logic functions in Microsoft Excel. TTS were defined if the following criteria were met. Firstly, the read depth of the position of interest divided by the read depth 4 nucleotides prior must be greater than 2. Secondly, the read depth at 4 nucleotides prior must be at least 20, and three times greater than the read depth 5 nucleotides after the position of interest. Thirdly, these two conditions must apply for several consecutive bases and the last base is called as the site of termination.

2.18.3. Conserved domain search

Conserved domain search was carried out to identify potential functional domains of hypothetical proteins with no annotated function. Searches were conducted against database CDD v3.20-59693 PSSMs with expected value threshold of 0.01 and composition based statistics adjustment (Marchler-Bauer *et al.*, 2017)

2.18.4. Native Tn-seq analysis

The FASTQ files were parsed using Barcode Splitter (Hannon and Assaf, 2010) (Galaxy v1.0.1) to identify reads having the final 83 nucleotides of IS*Aba*13 at the 5' end. To account for differences introduced by the staggered oligonucleotides up to 4 mismatches and 2 deletions were allowed. Once selected, the first 83 nucleotides of each read were removed using dada2:filterAndTrim (Callahan *et al.*, 2016) (Galaxy v1.20). Only remaining reads 20 or more nucleotides in length were retained. These were then mapped to the reference genome using Bowtie 2 (Galaxy v2.4.2). Read depths for each DNA strand were the calculated using the BAM to Wiggle function of the RSeQC package (Wang, Wang and Li, 2012) (Galaxy v5.0.1). Subsequent analysis of wiggle files to identify sites of transposition, was done using logic functions in Microsoft Excel. First, chromosomal locations were identified where reads were detected, but no reads mapped to at least 2 positions upstream. These were recorded as sites of IS*Aba*13 insertion unless the read depth 1 position downstream was greater by 2-fold or more. In such cases, the latter position was used. Insertion sites identified in each biological replicate were then combined. Note that we did not expect, nor did we detect, the same sites of transposition in both replicates. Rather, we observed similar patterns of transposition (e.g., a bias towards H-NS bound DNA).

2.18.5. Data visualisation and statistics

RNA-seq differential analysis was plotted in R with ggplot (v3.3.3) (Wickham, 2009). BAM files were viewed in Artemis (v18.1.0) (Carver et al., 2012) and genomes in Mauve (v2.4.0) (Darling et al., 2004). All other graphs and statistical analysis were done in Prism 9 (v9.4.1).

In all graphs, (ns) represents $p > 0.05$, (*) represents $p \leq 0.05$, (**) represents $p \leq 0.01$, (***) represents $p \leq 0.001$, and (****) represents $p \leq 0.0001$.

Chapter 3: Insertion of IS*Aba*13 into the K-locus has diverse phenotypic implications

3.1. Introduction

The behaviour of bacterial colonies on agar plates is a useful tool. For example, *Staphylococcus aureus* haemolytic activity can be assessed using blood agar, with a haemolytic ring around colonies indicating a haemolytic phenotype (Zhang *et al.*, 2016). Colony morphology can also identify variants within a species of bacteria. For example, in *Vibrio cholerae,* a phase switch occurs between smooth and rugose forms. The latter produces more exopolysaccharide, increasing the capacity to form biofilms (Beyhan and Yildiz, 2007). In *Streptococcus pneumoniae*, phase variation creates opaque and translucent forms with differential production of capsule and pilus (Li and Zhang, 2019).

Mechanisms of phase variation in bacteria include recombination, inversion, DNA methylation, and transposition (van der Woude and Bäumler, 2004). For example, transposition of IS1301 inactivates the sialic acid encoding biosynthetic gene *siaA* in *Neisseria menigingitids* (Hammerschmidt *et al.*, 1996). In the case of *A. baumannii* AB5075, there is a well characterised, high frequency, phase switch between VIR-O and AV-T colonies (Tipton, Dimitrova and Rather, 2015). A complex regulatory network is believed to be involved in the switch, involving stochastic activation of multiple TetR-like transcriptional regulators and the small RNA SrvS (Pérez-Varela *et al.*, 2022). AV-T colonies produce less capsule than their VIR-O counterparts and the two colony types show differences in biofilm formation, antibiotic susceptibility and motility (Tipton, Dimitrova and Rather, 2015).

In this chapter we describe a novel colony morphology of AB5075. We identify transposition as the underlying genetic mechanism and show diverse phenotypes resulting from this genetic change.

3.2. Discovery of a novel colony morphology of AB5075

VIR-O and AV-T colony types can only be distinguished by oblique illumination. When we generated pure stocks of these two colony types, occasionally different variants were observed which appeared clearly translucent by eye under room lighting (Fig.3.1). Under a microscope, with oblique illumination, the colonies lack the usual mucoid phenotype and have a dull grey colour. These colonies were hence named “grey” variants. Grey colonies rarely appeared from a pure stock of wild-type cells and were stably maintained, with revertants infrequent. This contrasts to the high frequency phase switch between VIR-O and AV-T (Tipton, Dimitrova and Rather, 2015).

3.3. IS*Aba*13 inserts into the K-locus of grey cells

To understand the genetic basis for the grey colony morphology, we used genome sequencing. Short-read Illumina genome sequencing revealed no major differences between VIR-O and grey colony types, other than a selection of mostly synonymous single nucleotide polymorphisms (SNPs) described in Appendix 3. Next, we used long read Oxford Nanopore sequencing, aiming to capture any large-scale rearrangements, including transposition events, and inversion or duplication of DNA regions. Long read genome sequencing identified an extra copy of the IS5 family insertion sequence IS*Aba*13. In grey colonies, the third copy of IS*Aba*13

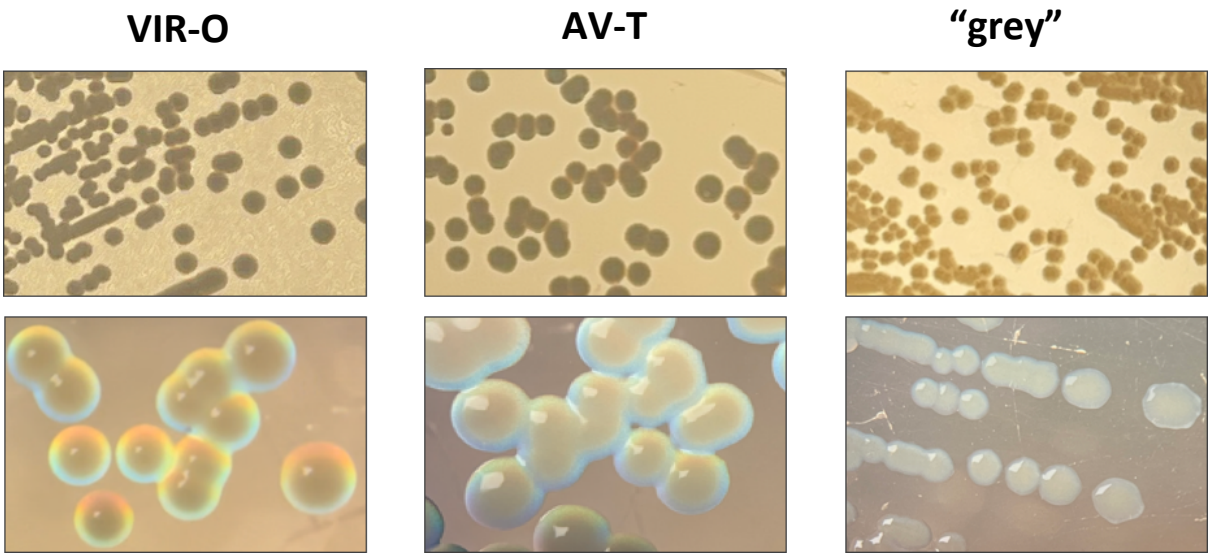

Fig.3.1. Colony morphology of different AB5075 variants on LBA plates
Top: colonies viewed on 1 x LBA plates under room lighting by eye. Bottom: colonies viewed on 0.5 x LBA plates under oblique illumination using a Nikkon SMZ1000 microscope with the same light aperture setting.

Interrupts the gene *gtr52* (*ABUW_3824*) of the capsule biosynthetic operon (Fig.3.2a, grey arrow). As shown in Fig.3.3, IS*Aba*13 inserts in the opposite orientation to *gtr52* of the K-locus, which encodes the enzymes required for synthesising and assembling exopolysaccharide capsule. Upon insertion, IS*Aba*13 generates a 9 bp DTR (ACTCAAATT) as a consequence of the transposition mechanism. We also observed duplication of a small section of prophage (Fig.3.2a, purple arrow). The duplicated genes are shown in Appendix 4 and annotated in Appendix 5. The gene duplications create an extra 17 kb of DNA at the locus. Given that there are no gene interruptions, and that these regions are already highly duplicated in the wild-type chromosome, additional gene copies are unlikely to induce phenotypic change. These are the only substantial changes in the grey colony genome. We conclude that the grey colony phenotype most likely results from loss of capsule production.

3.4. Insertion of IS*Aba*13 modulates the transcriptome of grey cells

Next, we compared the transcriptomes of the starting strain and grey derivative using RNA-seq. Cells were grown to mid exponential phase in LB broth. RNA reads were aligned to the AB5075 reference genome. Differential gene expression patterns were then calculated. The results are shown as a volcano plot in Figure 3.4. Significantly up and down regulated genes are labelled red and blue respectively.

As predicted, we observed decreased transcription of K-locus genes, *weeH* and *weeI,* immediately adjacent to the site of IS*Aba*13 insertion. The genes encode a phosphoglycosyltransferase and acetyltransferase respectively, which are needed to make

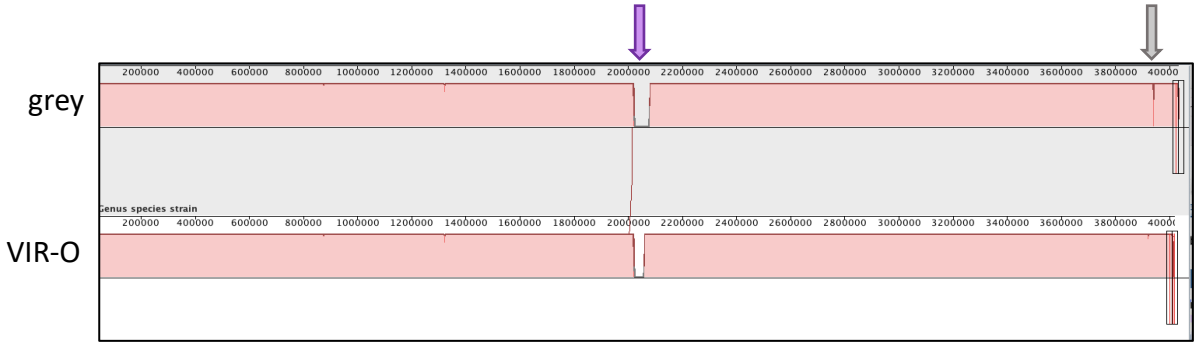

Fig.3.2. VIR-O and grey genome sequences assembled from long read genome sequencing
Contigs were aligned with ProgressiveMauve (v2.4.0). Full chromosome of both grey (top) and VIR-O (bottom) colonies shown by red bar. Red interconnecting line show both chromosomes as a single localised co-linear block which is conserved. Purple arrow highlights prophage sequence duplication, grey arrow highlights novel IS*Aba*13 insertion. Numbers indicate chromosomal coordinates.

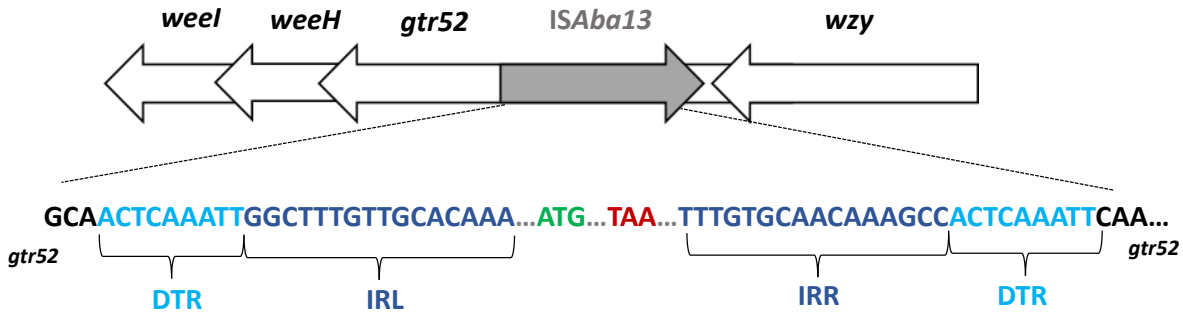

Fig.3.3. Illustration of IS*Aba*13 insertion into the K-locus
DTR = direct target repeat, IRL = left inverted repeat, IRR = right inverted repeat. Start codon ATG for transposase highlighted in green and stop codon TAA highlighted in red.

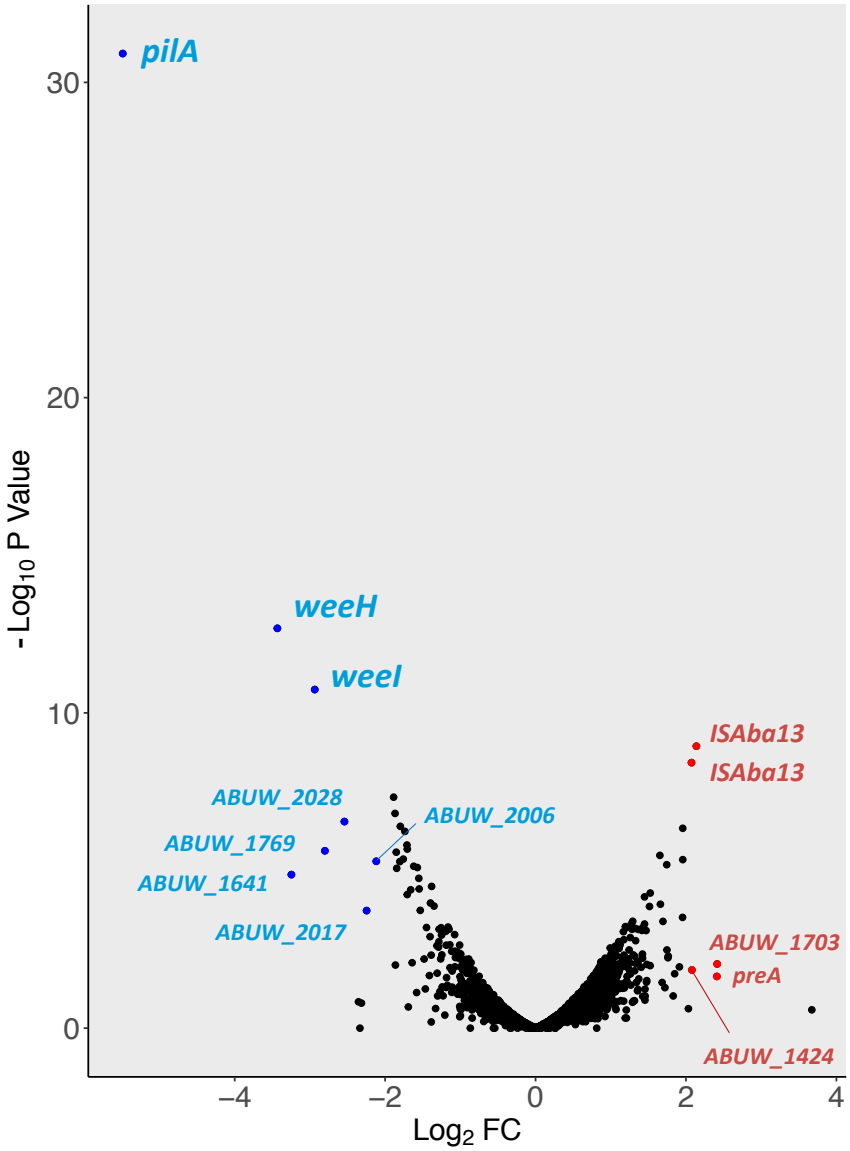

Fig.3.4. RNA-seq of differentially expressed genes between VIR-O and grey cells
In blue are genes statistically significantly downregulated in grey compared to VIR-O, in red are genes statistically significantly upregulated in grey compared to VIR-O. EdgeR assessed statistical significance using a threshold of $p \leq 0.05$. Genes labelled "*ABUW*" encode hypothetical proteins.

UDP-diNAcBac. This is the starting molecule for K-unit synthesis, used for both capsular polysaccharide and general O-linked protein glycosylation (Morrison and Imperiali, 2013; Singh, Adams and Brown, 2019). Therefore, disrupting *weeH* and *weeI* could affect both capsule production and the glycosylation of other surface proteins. Whilst *gtr52,* encoding a K-locus glycosyltransferase, is downregulated, the change does not reach statistical significance. This is because RNA-seq reads still map to the start of *gtr52,* before IS*Aba*13 insertion. Hence, over the whole gene body, the overall change in read depth is insufficient. Unexpectedly, *pilA* was the most significantly downregulated gene. This gene encodes the major subunit of the type IV pilus, a structure involved in biofilm formation, adherence, twitching motility and natural transformation (Ronish *et al.*, 2019). *ABUW_1769,* which is also downregulated in grey cells, is annotated as a PEGA domain containing protein, showing similarity to surface layer (S-layer) proteins.

The most upregulated gene encodes the IS*Aba*13 transposase. This could be a consequence of higher IS*Aba*13 copy number in the grey cell type (3 rather than 2). However, the > 4-fold up-regulation of IS*Aba*13 is greater than expected based on this change in gene dosage. A further complication is that many reads corresponding to IS*Aba*13 are unlikely to map correctly as each copy has the same sequence. Also significantly upregulated is *preA*, a 4Fe4S cluster binding oxidoreductase protein.

Despite an increase in prophage sequence copy number in grey variants, transcripts from this region appear to be 4-fold downregulated in grey cells (Table 3.1, genes *ABUW_2028, ABUW_2017, ABUW_2006*). However, upon close inspection the absolute transcript levels are

Gene name	Conserved protein domains identified	Log_2 Fold change
ABUW_2028	Phage coat protein B. Major protein of capsid of filamentous phage	-2.54
ABUW_1769	Peptidase associated/ transthyretin-like domain-containing protein	-2.80
ABUW_1641	None	-3.25
ABUW_2017	Phage coat protein B. Major protein of capsid of filamentous phage (same as *ABUW_2028*)	-2.25
ABUW_2006	Phage coat protein B. Major protein of capsid of filamentous phage (same as *ABUW_2028*)	-2.12
ABUW_1703	None	2.41
ABUW_1424	None	1.85

Table 3.1. Conserved domain search of hypothetical proteins upregulated/downregulated in RNA-seq.

very low (~ 60 reads). Hence, the region overall is poorly transcribed. This could give rise to aberrant fold changes between cell types.

3.5. Phenotypic impact of insertion of IS*Aba*13 at the K-locus

3.5.1. Grey cells have decreased capsule production

Given reduced transcription of K-locus genes, we expected a decrease in capsule production. To assess the impact of IS*Aba*13 insertion on capsule production, a semi-quantitative density gradient assay was used to compare VIR-O, AV-T and grey cells. In this assay, Ludox colloidal silica beads are mixed with cells. The amount of capsule synthesised is inversely proportional to the migration of cells during centrifugation (visible as a white band of cellular density). High density *A. baumannii* migrate faster and have a lower capsulation level, conversely low-density *A. baumannii* migrate slower and have a greater level of capsulation. As expected, VIR-O cells produce the most amount of capsule (Fig.3.5). In agreement with the literature, AV-T cells produce less capsule than VIR-O, though this does not reach statistical significance ($p = 0.094$). However, grey cells produce a significantly reduced amount of capsule compared with both VIR-O ($p < 0.0001$) and AV-T ($p < 0.0001$). This supports the hypothesis that IS*Aba*13 insertion, into the K-locus, impairs capsule production in grey cells.

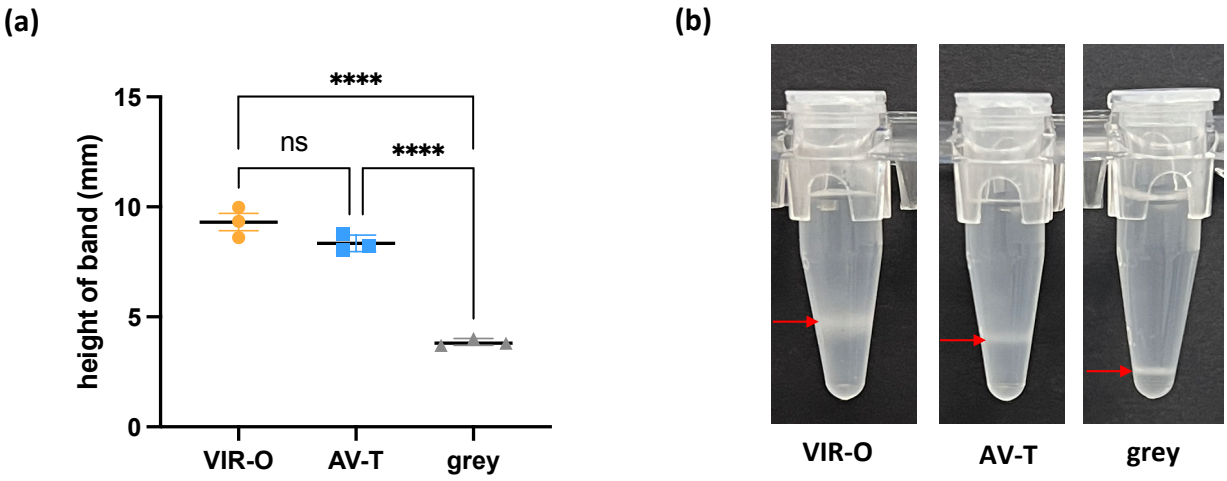

Fig.3.5. Capsule production in VIR-O, AV-T and grey cells

(a) Distance of band measured from bottom of 1.5 ml Eppendorf for VIR-O, AV-T and grey cells. Ordinary one-way ANOVA with Tukey's multiple comparisons test used to assess significance. Horizontal black lines represent the mean of three biological replicates. Error bars represent standard deviation. (b) Photographs of band positions following centrifugation (red arrows).

3.5.2. Grey cells show increased growth under standard laboratory conditions but decreased growth in human serum

Next, we searched for less obvious phenotypic impacts of K-locus disruption. The first assay was growth in LB medium (Fig. 3.6a). Note that although growth was assessed by OD_{600} measurement and not CFU/ml, AB5075 cells with a similar colony morphology to grey cells, which also have K-locus disruption by IS*Aba*13, show no significant difference in CFU/ml compared to wild-type when both strains are plated at the same OD_{600} (Whiteway *et al.*, 2022). Grey cell types reached their maximum OD_{600} approximately 5 h quicker than AV-T cells or VIR-O cells. Grey cells also have a greater growth rate constant (k = 0.651, 95 % confidence intervals = 0.623 to 0.681) compared with VIR-O cells (k = 0.486, 95 % confidence intervals = 0.453 to 0.522).

Human serum is blood plasma which does not contain cells or clotting factors but does contain complement; a group of proteins which form part of the innate immune system. These proteins opsonise pathogens, marking them for targeting, increasing susceptibility to phagocytes. Additionally, complement activates inflammation to support phagocytosis, and forms the membrane attack complex, leading to pathogen cell death. The capsule of wild-type cells protects *A. baumannii* from complement-mediated killing (Kamuyu *et al.*, 2022). Since grey cells have reduced capsule production, we predicted a growth defect in the presence of human serum. Grey cells have impaired growth in 50 % normal human serum compared to wild-type cells (Fig.3.6b). Grey cells also have smaller growth rate constant (k = 0.116, with 95% confidence intervals unable to be calculated) compared with VIR-O cells (k = 0.344, 95 %

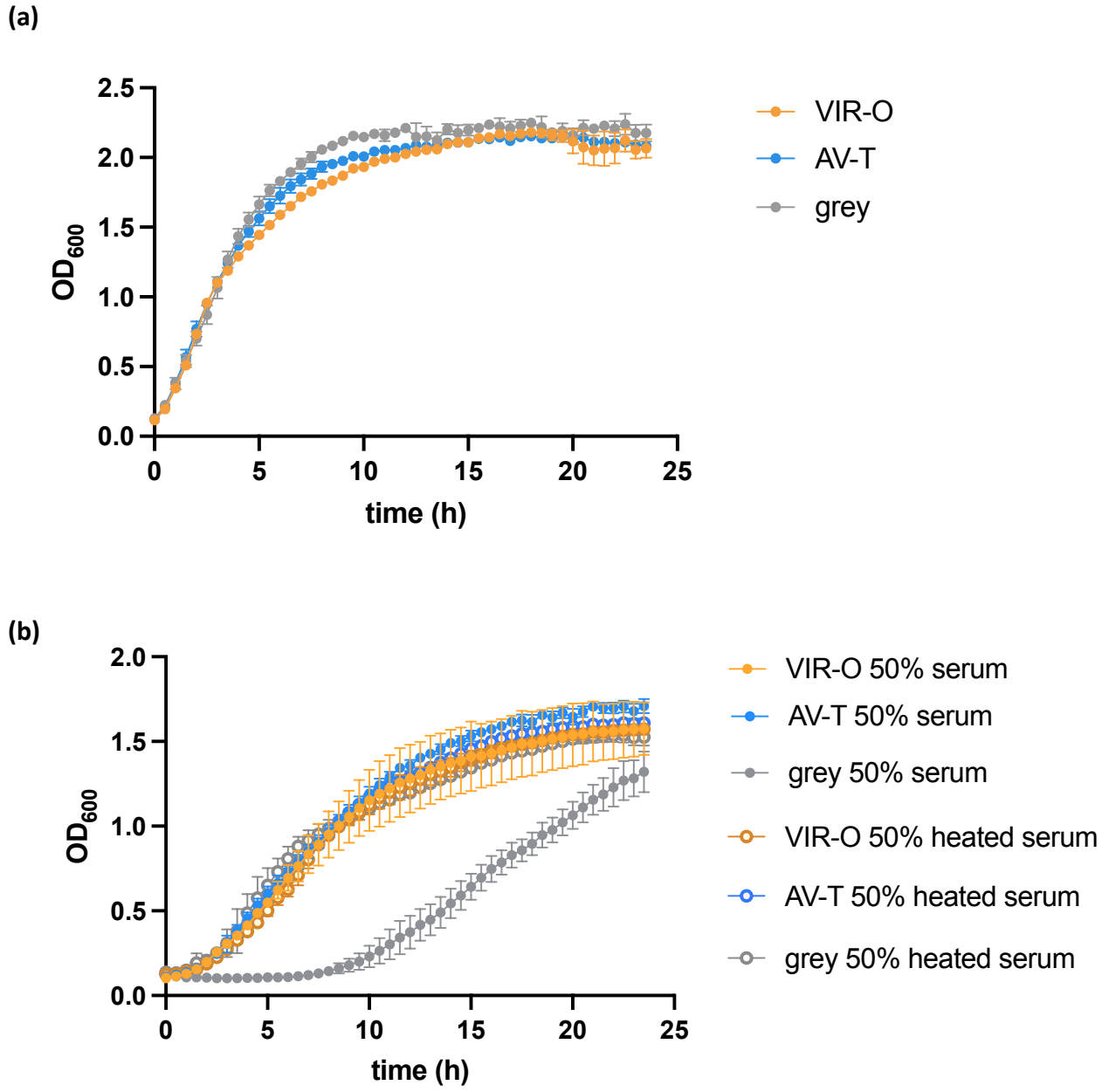

Fig.3.6. Growth curves of VIR-O, AV-T and grey cells

OD_{600} was measured by a plate reader in a 96-well plate for 24 hours in (a) LB medium or (b) 50 % normal human serum or 50 % heat-treated normal human serum. Points represent the mean of three biological replicates, error bars represent standard deviation. Logistic growth analysis using nonlinear regression was used to calculate the growth rate constant (k).

confidence intervals = 0.305 to 0.389). An exaggerated lag phase is observed after which grey cells eventually reach the same final OD_{600} as VIR-O and AV-T cells. Growth in heated human serum is unperturbed, likely due to complement inactivation. Intriguingly AV-T cells, which produce less capsule, do not show impaired growth in human serum. This could be because VIR-O and AV-T cell types phase switch more often as culture density increases. Alternatively, the amount of capsule produced by AV-T cells could be enough to confer protection.

3.5.3. Grey cells show increased susceptibility to gentamicin

Given the intrinsically high resistance of AB5075 to antibiotics, we tested whether grey cells had altered susceptibility. For example, this could result from lack of capsule providing easier access of antibiotics to the cytoplasm in grey cells. MIC assays were done in 96-well polystyrene plates, at 37 °C for 18 hours, without shaking. Grey cells showed a reduced MIC For gentamicin, with an 8-fold increased susceptibility, whereas only a 2-fold decrease was seen for polymyxin B and zeocin, and no difference in MIC was observed for tetracycline (Table 3.2). There may be a greater than 2-fold change in MIC with kanamycin, however this could not be deduced from the range of concentrations used. Interestingly we did not observe a difference in susceptibility to gentamicin for AV-T compared to VIR-O as previously reported, though measurements appear to differ between sources (Tipton, Dimitrova and Rather, 2015; Anderson *et al.*, 2018).

Strain	MIC of antibiotic (μg/ml)				
	gentamicin	kanamycin	polymyxin B	zeocin	tetracycline
VIR-O	4096	>1024	2	64	0.5
AV-T	4096	>1024	2	64	0.5
grey	512	512	1	32	0.5

Table 3.2. MIC of VIR-O, AV-T and grey cells measured by broth microdilution
Strains were tested in a 96-well plate in at least triplicate on at least two separate occasions, with the modal value reported. Reference ATCC 25922 and NCTC10418 control strains were included as controls.

3.5.4. Grey cells have reduced motility

In *A. baumannii*, motility is an important property for virulence. AV-T cells show a decreased surface-associated motility compared with VIR-O cells (Tipton, Dimitrova and Rather, 2015). To assess differences in movement across the surface of the agar (surface-associated motility) between VIR-O, AV-T and grey cells, we undertook a surface motility assay (Fig.3.7a). During incubation, a sealed plastic bag was used to enclose the plates, as changes in humidity cause variability between replicates. Grey cells show a significantly reduced area of surface-associated motility compared with VIR-O cells ($p < 0.0001$). As expected, AV-T cells also showed significantly impaired motility compared with VIR-O cells ($p < 0.0001$), however AV-T cells showed no significant difference compared with grey cells ($p = 0.9976$).

Many *Acinetobacter* species have the ability to undergo subsurface twitching motility at solid interfaces using their T4P. This involves a hook and pull motion, enabling movement across the surface. Given the large downregulation of *pilA,* encoding the major subunit of the T4P, we hypothesised that grey cells would have reduced twitching motility. Twitching assays were used to assess twitching motility at the agar-plastic interface of Petri dishes. As seen in Fig.3.7b, grey cells have significantly impaired twitching motility compared with VIR-O ($p < 0.0001$). AV-T cells are also impaired relative to VIR-O, but to a reduced extent ($p = 0.0008$). The difference in twitching motility between AV-T and grey cells does not reach statistical significance ($p = 0.0722$).

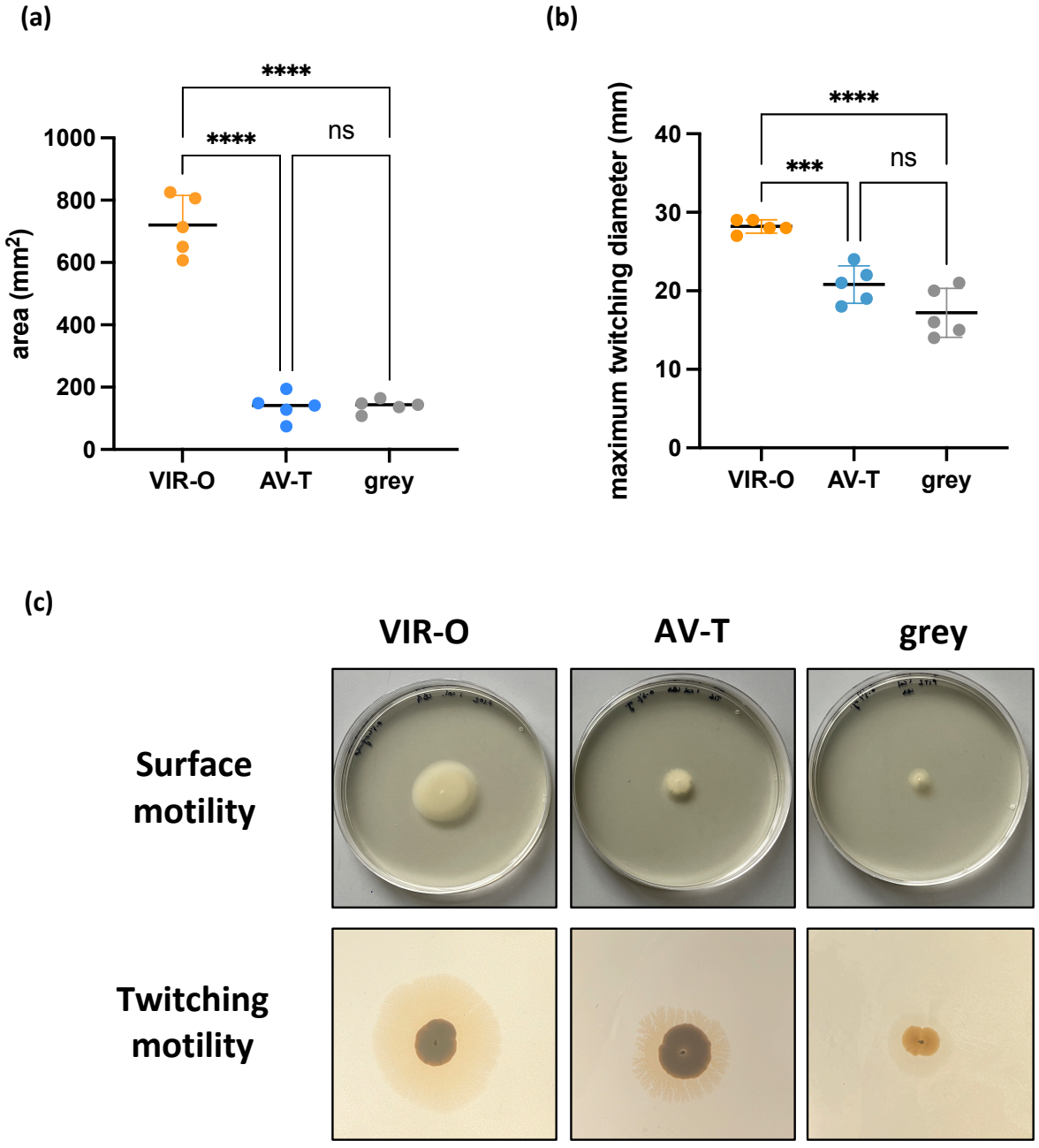

Fig.3.7. Motility of VIR-O, AV-T and grey cells

(a) Surface motility assay on soft (0.3 %) agarose plates with horizontal black line representing mean of five biological replicates with error bars representing standard deviation. Ordinary one-way ANOVA with Tukey's multiple comparisons test used to assess significance. (b) Twitching motility assay on LBA plates, Horizontal black line represents mean of five biological replicates with error bars representing standard deviation. Ordinary one-way ANOVA with Tukey's multiple comparisons test used to assess significance. (c) Top: Area of surface motility on agarose plates was photographed and quantified in ImageJ. Bottom: Maximum diameter of the halo generated around the point of inoculation on LBA plates was measured and photographed.

3.5.5. Grey cells have an increased capacity to form biofilms

The T4P plays a negative role in biofilm formation at the air-liquid interface (Ronish *et al.*, 2019; Ahmad *et al.*, 2023). Additionally, a Δ*weeH* (*pglC*) mutant of *A. baumannii* 17978 produces a significantly thicker and heterogenous biofilm compared to wild-type at the air-liquid interface (Lees-Miller *et al.*, 2013). Given that grey cells express less *pilA* and *weeH*, we expected an improved capacity to form biofilms at the air-liquid interface, where *Acinetobacter* species involved in nosocomial infections typically form biofilms (Martí *et al.*, 2011; López-Martín *et al.*, 2021; Robin *et al.*, 2022). Hence, we used an air-liquid interface crystal violet staining assay. As seen in Fig.3.8a, grey cells have a greater capacity to form biofilms, compared to VIR-O cells, at room temperature ($p = 0.0009$) or 37 °C ($p = 0.0003$). Conversely, no significant difference was found for biofilm formation between VIR-O and AV-T cells. Members of the ACB complex have been reported to form a greater biofilm at the air-liquid interface at 25 °C compared to 37 °C (Martí *et al.*, 2011). However, in this study, for AB5075, no substantial difference was found between room temperature and 37 °C for any of the variants tested.

Recently, it was shown that *pilA* expression in *A. baumannii* strain A118 peaks at OD_{600} = 0.6-0.7 (Vesel and Blokesch, 2021). To investigate whether starting OD_{600} of the inoculum could affect the amount of biofilm formed at the air-liquid interface, the assay was modified to include a range of starting optical densities (OD_{600} 0.1, 0.3 or 0.6.) As seen in Fig. 3.8b, there is no significant difference in biofilm formation for VIR-O cells. However, for grey cells, there is significantly more biofilm formation at $OD_{600} = 0.6$ ($p < 0.0001$).

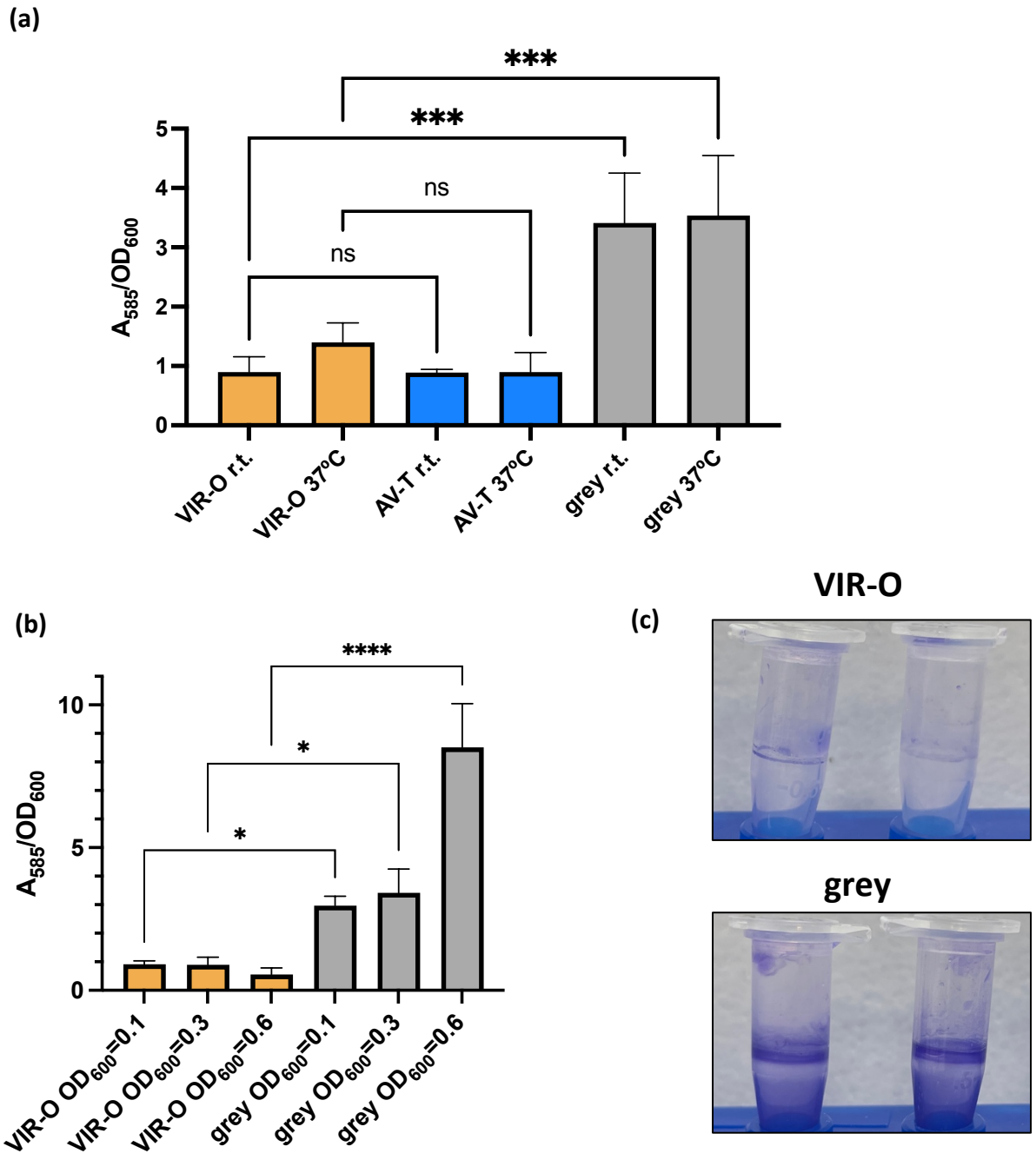

Fig.3.8. Biofilm formation of VIR-O, AV-T and grey cells

(a) Crystal violet staining measured by absorbance at A_{585} and normalised by OD_{600}. Initial inoculum for overnight culture was OD_{600} = 0.3. tubes were incubated overnight at 37°C or room temperature. Ordinary one-way ANOVA with Tukey's multiple comparisons test used to assess significance. Bars represent mean of three biological replicates with error bars representing standard deviation. (b) Initial inoculum was varied, and all tubes incubated at room temperature overnight. Ordinary one-way ANOVA with Tukey's multiple comparisons test used to assess significance. Bars represent mean of three biological replicates with error bars representing standard deviation. (c) Photographs showing thick band of crystal violet staining at the air-liquid interface of polystyrene Eppendorfs.

3.5.6. Grey cells have a reduced capacity for natural transformation

Given the pivotal role of the T4P in natural transformation, we compared the ability of AV-T and grey cells to take up exogenously supplied plasmid DNA compared with VIR-O cells (Fig.3.9). The high intrinsic resistance of AB5075 to multiple antibiotics means there is a limited selection of available antibiotic markers to use. This assay uses the plasmid pVRL2Z, containing the *bleo* gene conferring resistance to zeocin (Lucidi *et al.*, 2018). AB5075 still has a relatively high intrinsic resistance to zeocin and background colonies were seen even at 250 µg/ml. Hence, 500 µg/ml was used to ensure accurate selection of transformants. Compared to VIR-O, AV-T cells show a small reduction in the ability to undergo natural transformation ($p = 0.0005$). Grey cells are significantly more impaired (roughly 100-fold), ($p < 0.0001$) consistent with reduced expression of *pilA* and the T4P.

3.5.7. Grey cells are more hydrophobic and susceptible to desiccation

In *A. baumannii*, down-regulation of T4P components in a *trxA* mutant (lacking the redox protein Thioredoxin-A) is associated with increased cell surface hydrophobicity, as measured by Congo Red binding (May *et al.*, 2019). Congo Red is an azo amyloid dye previously used to assess the degree of curli fibre formation in *E. coli* and *Salmonella* (Reichhardt *et al.*, 2015). The dye offers a qualitative measure of surface hydrophobicity. The bacterial capsule is negatively charged and so, if no or reduced capsule is made, as in grey colonies, an increase in hydrophobicity is expected. When spotted onto a Congo red plate (Fig.3.10a) grey colonies appear darker red, suggesting greater uptake of Congo red and a more hydrophobic surface.

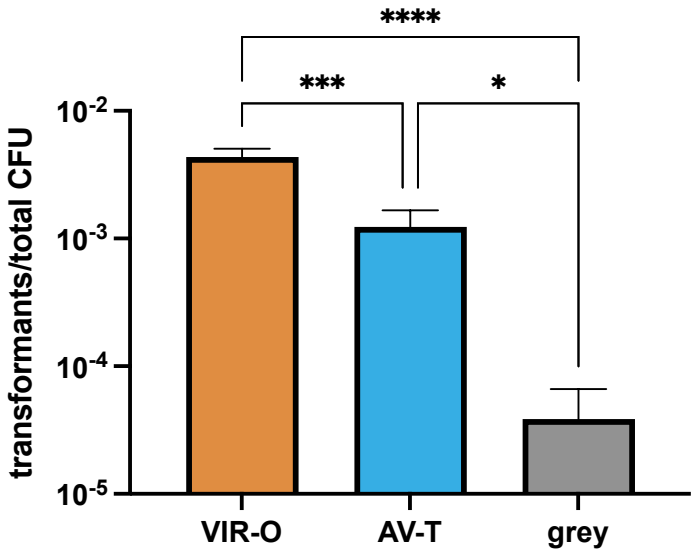

Fig.3.9. Natural transformation of VIR-O, AV-T and grey cells
Cells were mixed with pVRL2Z and incubated at 37 °C overnight. PBS was added and serial dilutions plated on either LBA or LBA-zeocin (500 µg/ml) to select for transformants. Ordinary one-way ANOVA with Tukey's multiple comparisons test used to assess significance. Bars represent mean of three biological replicates, error bars = standard deviation.

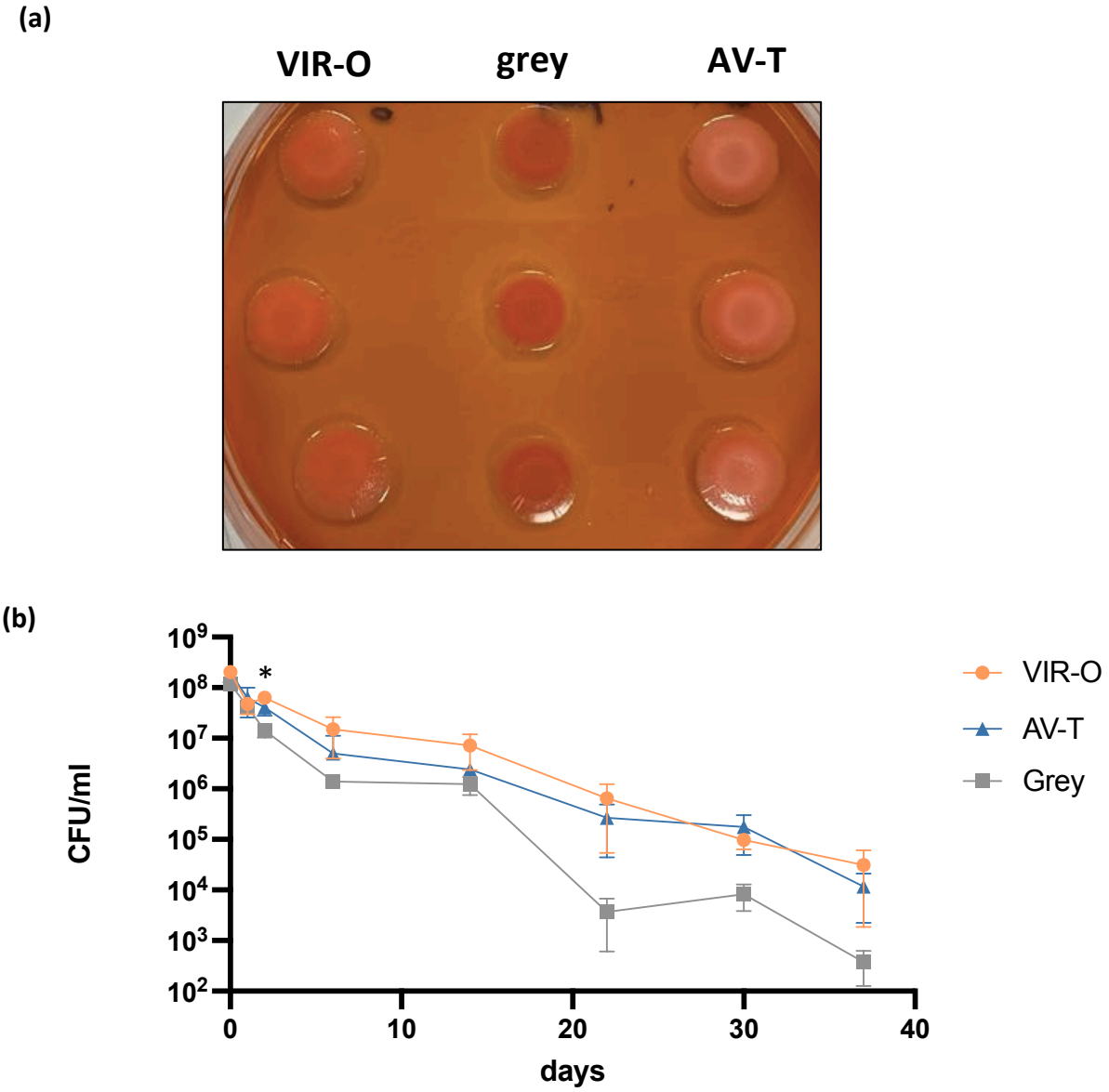

Fig.3.10. Hydrophobicity and desiccation tolerance of VIR-O, AV-T and grey cells
(a) Congo red binding to macrocolonies spotted onto Congo red agar plates. (b) Survival of bacteria following desiccation on a polystyrene 96-well plate incubated at room temperature. Points represent the mean of three biological replicates, error bars = standard deviation. Two-way ANOVA with Bonferroni's multiple comparisons test used to assess significance.

The ability to persist on hospital surfaces for long periods of time makes *A. baumannii* difficult to eradicate in nosocomial settings. Capsule is known to be an important factor in protecting against desiccation (Singh, Adams and Brown, 2019). To test the ability of AB5075 to survive on dry surfaces, a desiccation assay was done (Fig.3.10b). Grey cells have a reduced ability to survive desiccation, with a reduced number of recoverable CFU following rehydration at various time points. AV-T cells, with their reduced capsule compared to VIR-O cells, are only slightly less defective in their ability to resist desiccation. A statistically significant difference is observed between VIR-O and grey cells at time t = 2 days ($p = 0.0136$).

3.6. Discussion

In this chapter, we have shown that a simple genetic change can have far reaching effects on multiple clinically relevant phenotypes. IS*Aba*13 inserts into the capsule operon of AB5075, downregulating the expression of genes involved in capsule synthesis. Many of these phenotypes could confer selective advantages under particular conditions. For example, the grey variant may be better able to persist as a biofilm on medical equipment. On the other hand, the VIR-O form may better survive antibiotic treatment and desiccation. Note that many of the antibiotics used in the MIC assay to investigate a difference in resistance between VIR-O and grey cells are of limited clinical relevance for *A. baumannii* treatment. Future work should include testing the MIC of the variants with cephalosporins, carbapenems and colistin.

Unlike the high frequency phase switch between VIR-O and AV-T, grey cells are more stably maintained. Whilst the VIR-O to AV-T switch is determined by fluctuations in TetR

transcriptional regulators and an sRNA (Pérez-Varela *et al.*, 2022), the switch from VIR-O to grey is determined by transposition of IS*Aba*13 to the K-locus. Insertion prevents transcription of three genes, *gtr52*, *weeI* and *weeH*. In most phenotypic assays, grey variants have a similar, but more extreme phenotype compared to AV-T cell types. This is expected given the differences in capsule production; AV-T variants produce a capsule half as thick as VIR-O variants, while grey cells likely produce almost no capsule (Chin *et al.*, 2018). Throughout assays, as cell number increases, interconversion occurs. Therefore, even though assays start with a pure stock of one phase variant, inevitably the population will become mixed. A further interesting phenotype to test would be susceptibility to bacteriophage; a promising alternative therapy for multidrug resistant *A. baumannii* (Nir-Paz *et al.*, 2019). The bacterial capsule is typically a target for phage adsorption. Mutations arising in the K-locus confer phage resistance *in vivo*, with 11/11 phage resistant isolates which evolved during a murine infection model found to have a frameshift or substitution in K-locus genes (Gordillo Altamirano *et al.*, 2022; Liu *et al.*, 2022). For example, frameshifts in the glycosyltransferase *gtr29* in strain AB900 and the isomerase *gpi* in strain A9844, abolish capsule production and endow resistance to phage infection (Gordillo Altamirano *et al.*, 2021). Interestingly, disrupted capsular branching resulting from IS*Aba*13 insertion into *gtr6* results in decreased phage adsorption, phagocytosis and complement deposition, and increased virulence in a murine bacteremia model (Talyansky *et al.*, 2021; Bai *et al.*, 2023). For the model strain AB5075, used in this study, a known phage, LK01, is able to infect and lyse only the AV-T form. The phage is difficult to work with because of phase switching in the presence of phage selection pressure creating an immune VIR-O population (Jeremy Barr personal communication, Gordillo Altamirano *et al.*, 2021).

Grey variants grow to a higher culture density compared to VIR-O cells (Fig.3.6a). This may help explain the propensity for this capsule mutant to form under laboratory conditions. A possible advantage for grey variants is reduced resource expenditure on capsule components or the T4P major subunit *pilA,* which may not be necessary during growth in rich nutrient medium at 37°C. Indeed, many phenotypic differences may be due to downregulation of *pilA* (decreased twitching motility and natural transformation, and increased biofilm forming capacity.) In terms of genomic position, the *pilA* locus is > 400 kbp from the K-locus, pointing towards an indirect mechanism altering expression of *pilA*. It was recently reported that overexpression of the TetR transcriptional regulator *ABUW_1645,* which is more highly expressed in the AV-T colony form, drastically reduces expression of T4P components, including *pilA,* by more than 60-fold (Pérez-Varela *et al.*, 2022). In grey cells, it is possible that the lack of glycosylation by *weeH* changes regulation of a factor that regulates *pilA.* Unlike in other strains of *A. baumannii*, PilA itself is not glycosylated in AB5075, so K-locus disruption of *weeH,* and *pilA* downregulation, are not directly linked in this way (Ronish *et al.*, 2019).

During this study, another group simultaneously and independently found a similar grey colony. In this instance, IS*Aba*13 inserts into the gene *weeH*, downstream of *gtr52*, generating the 9 bp DTR CCTATAAAG (Whiteway *et al.*, 2022). The authors show that, in *weeH*::IS*Aba*13, capsule formation, and virulence in a *Galleria* model, are decreased. In this study, we have shown that insertion at the gene beforehand (*gtr52*) also creates translucent appearing colonies which produce less capsule. Given that in *gtr52*::IS*Aba*13, the location of insertion occurs at the start of the operon and downregulates both *weeI* and *weeH*, It is plausible that the grey cells in this study are also avirulent. A different study also noted disruption of *gtr52*

and *wzy* by IS*Aba*13, in biofilm cells subjected to ciprofloxacin/tetracycline, but did not investigate these mutants (Penesyan *et al.*, 2019). IS*Aba*13 targeting of genes involved in cell surface components is a common theme. A study from Cleveland, Ohio, found 35 % of 425 clinical isolates of *A. baumannii* had IS*Aba*13 disrupting the glycosyltransferase gene *gtrOC11*, which forms part of the OC locus for biosynthesis of the outer core component of lipooligosaccharide (Adams *et al.*, 2019). This extends to other ISs, with IS*Aba*1 and IS*Aba*23 disruption of the OC locus of different global clones leading to the production of reduced molecular weight lipooligosaccharide (Kenyon *et al.*, 2014).

Due to the presence of identical DTRs either side of the IS, upon colistin exposure, IS*Aba*13 can excise itself from *weeH* and restore the native sequence (Whiteway *et al.*, 2022). Insertion sequence mediated inactivation of genes represents an attractive mechanism to quickly and effectively change phenotype, potentially conferring an advantage in different environmental conditions. The added bonus being this change is fully reversible if unfavourable. The reversibility of the transposition event may in part explain some of the data generated. For example, during growth in human serum (Fig.3.6b), the long lag phase for grey cells could be explained by the occurrence of revertants, generated by scarless excision of IS*Aba*13 from *gtr52* using the identical DTR repeats. Another explanation could be that the grey cells more readily form a population of persister cells which could prove beneficial to surviving antibiotic treatment in a human host.

Chapter 4: The IS*Aba*13 promoter is bidirectional and impacts transcription of adjacent genes

4.1. Introduction

Insertion sequences can inactivate target genes and, depending on polarity, have differing effects on the expression of adjacent genes. For example, as shown in the previous chapter, insertion of IS*Aba*13 into *gtr52* of the K-locus reduces transcription of downstream genes for capsule synthesis. We wanted to understand how different IS*Aba*13 position and orientation, with respect to coding DNA, might alter transcription of adjacent genes. First, we used Cappable-seq and Term-seq to annotate transcription start sites (TSSs) and transcription termination sites (TTSs) associated with IS*Aba*13 at the K-locus. This showed IS*Aba*13 lacks an intrinsic terminator but has a bidirectional promoter at the 5' end of the element. Bidirectional promoters are pseudo-symmetrical DNA sequences that stimulate transcription in both the forward and reverse directions. Their occurrence is widespread in diverse bacteria and archaea (Warman *et al.*, 2021). The main driver of divergent transcription is inherent symmetry of the promoter -10 element (Warman *et al.*, 2021).

To understand the absence of a termination signal, and presence of a bidirectional promoter, we placed the *gtr52*::IS*Aba*13 region upstream of *lacZ* to measure transcription from the region. For comparison we did equivalent *in vitro* transcription assays. We discovered that IS*Aba*13 insertion in either orientation into *gtr52* reduces transcriptional readthrough. We also found that the bidirectional promoter of IS*Aba*13 is active *in vivo* when fused to *lacZ*, and that transcription termination resulting from IS*Aba*13 insertion only occurs *in vivo*.

4.2. Insertion of IS*Aba*13 blocks transcription of the K-locus

Our RNA-seq analysis (Fig.3.4) showed both *weeH* and *weeI* are downregulated in grey cells; transcription is prematurely terminated at the point IS*Aba*13 inserts in *gtr52* (Fig.4.1). To better understand IS*Aba*13 mediated transcriptional effects, we used Cappable-seq and Term-seq. Cappable-seq enriches for the 5' triphosphorylated initiating RNA nucleotide, and therefore the 5' edge of Cappable-seq read enrichment corresponds to the precise transcription start site (TSS) (Ettwiller et al., 2016). This strategy is more accurate and more sensitive than the alternative RNA-seq (dRNA-seq) method (Ettwiller *et al.*, 2016). Term-seq enriches for the OH at RNA 3' ends, and therefore the 3' edge of Term-seq read enrichment corresponds to TTSs (Dar *et al.*, 2016). One caveat for Term-seq is that RNA processing creates noise because RNA 3'OH ends are created by endoribonuclease and exoribonuclease processing (Dar *et al.*, 2016). Global TSSs and TTSs were mapped using the criteria outlined in the methods section (2.18.2), and TSSs were annotated at the K-locus around the site of IS*Aba*13 insertion (Fig.4.1). There were no clear TTSs within IS*Aba*13, suggesting termination is initiated by Rho, across a series of consecutive bases, rather than at a specific site.

4.3. Annotation of TSSs and promoter elements across the K-locus

The *gtr52* TSS, identified by Cappable-seq, is on the bottom DNA strand inside the upstream *wzy* gene (Fig.4.1.) The sequence of the associated promoter is illustrated in Fig.4.2a. There is a further TSS in the middle of *wzy,* which might also contribute to *gtr52* expression, and a TSS on the top DNA strand inside *gtr52*. Note that it is not unusual to find intragenic TSSs in horizontally acquired AT-rich DNA (Singh *et al.*, 2014). The start point of the IS*Aba*13

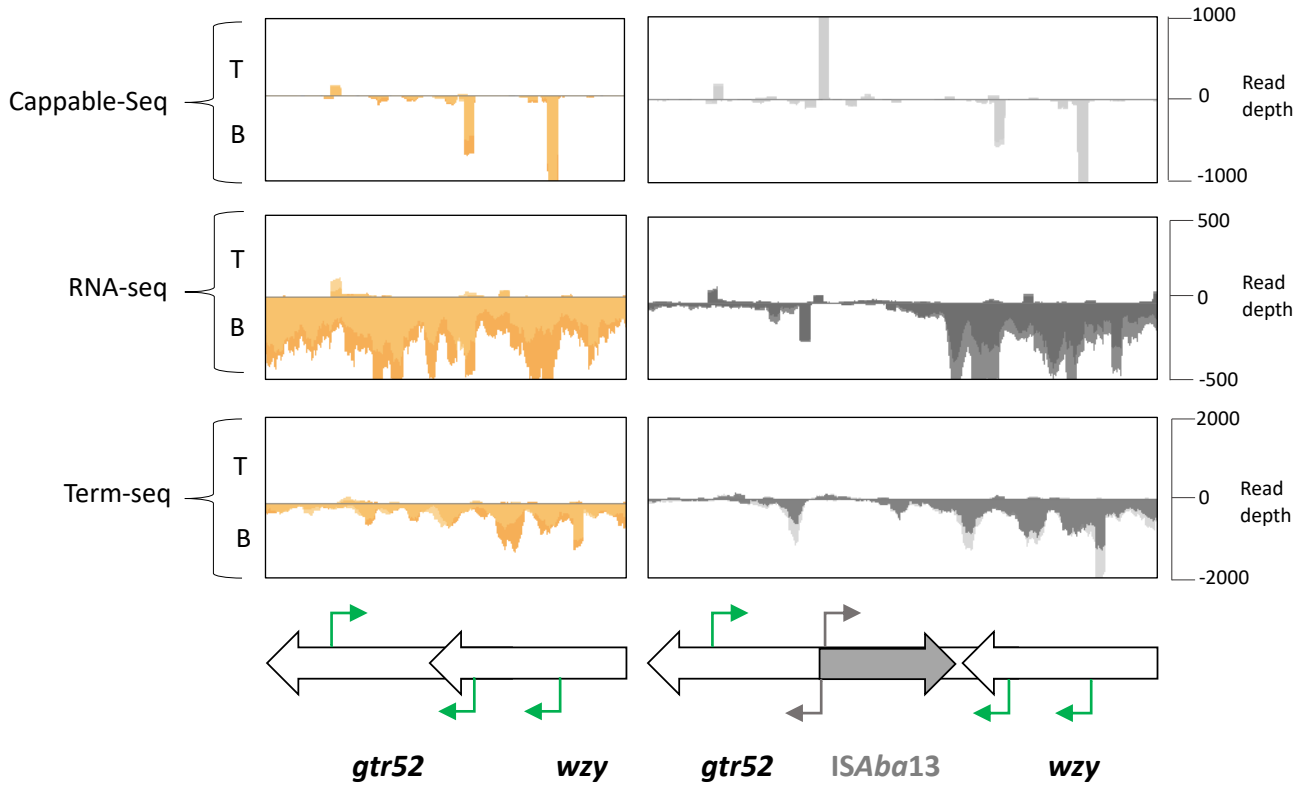

Fig.4.1. TSS, total RNA and TTS compared at the K-locus
Cappable-seq shows TSS, RNA-seq shows total RNA reads, Term-seq shows TTS. K-locus genes shown below with green arrows showing TSS in wild-type cells and grey cells and grey arrows showing TSS at this locus following IS*Aba*13 insertion in grey cells. Peaks pointing upwards show reads on the top (T) DNA strand, peaks pointing downwards show reads on the bottom (B) DNA strand. Cappable-seq coverage cut-off set to 1000, standard RNA-seq coverage cut-off set to 500, Term-seq coverage cut off set to 2000. Two biological replicates are shown in each panel by light and dark shades. Viewed on Artemis v18.1.0.

(a)

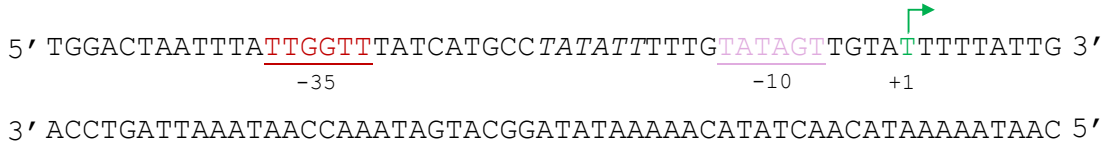

(b)

Fig.4.2. DNA sequence of promoter elements of *gtr52* and IS*Aba*13
(a) DNA sequence of promoter elements of gene *gtr52*. Green arrow = TSS, pink = -10 element, red = -35 element. Sequence in italics indicates a further potential upstream -10 element. (b) DNA sequence of promoter elements for IS*Aba*13 at the point of insertion into the K-locus. dark blue = ILL, pink = -10 element, red= -35 element, green = start codon of transposase, green arrow = TSS for top DNA strand transcription, light blue = transposase ORF, orange = initiating nucleotide for bottom DNA strand transcription, dark green dotted arrow = TSS for bottom DNA strand transcription. Purple nucleotides with asterisk indicate mutations used in mutated -10 construct.

transposase mRNA is at the 5' end of the IS*Aba*13 sequence. There is an additional TSS in IS*Aba*13, on the bottom DNA strand, 23 bp upstream of the TSS for the transposase mRNA. This indicates the presence of a bidirectional promoter, controlling both transposase expression and outward transcription from IS*Aba*13 (Fig.4.2b). The -10 element is pseudo-symmetrical and matches the consensus perfectly in the forward direction (Fig.4.2b). The initiating nucleotide for the transposase mRNA is the 'A' of the ATG start codon for translation. This means there is no 5' leader sequence, and no Shine-Dalgarno (SD) sequence, to initiate transposase translation. A strong Cappable-seq signal is observed for the 5' end of the mRNA. However, RNA-seq data suggests low levels of complete IS*Aba*13 transposase transcript. This indicates premature transcription termination and/or low mRNA stability. This is consistent with poor translation, which otherwise protects RNAs from premature termination by Rho, and degradation by RNAses. This is likely a mechanism to reduce transposase expression and prevent excessive transposition.

4.4. The impact of IS*Aba*13 orientation on transcription termination of adjacent genes *in vivo*

Although RNA-seq shows premature termination of K-locus transcription, within IS*Aba1*3, we found no specific site of termination. Further, no DNA sequence for an intrinsic terminator is evident, either upon visual sequence inspection or using ARNold (Naville *et al.*, 2011). This indicates a Rho-dependent mechanism of termination, less dependent on DNA sequence, targeting untranslated RNA. If there is no intrinsic terminator, and transcription is indeed blocked by Rho, then IS*Aba*13 should have similar effects on *gtr52* transcription, regardless of insertion orientation. To test this, sections of the K-locus, with IS*Aba*13 in either possible

orientation were fused to *lacZ*. A schematic of the different constructs is shown in Fig.4.3a. Our starting fusion, called *gtr52,* has only the *gtr52* promoter, within *wzy*, upstream of *lacZ*. We made derivatives of this with IS*Aba*13 inserted in *gtr52*, either as in grey cell types (*gtr52*::IS*Aba*13), or in the opposite direction (*gtr52*::IS*Aba*13 inverted). The final construct (IS*Aba*13 only) contains the transposable element only. Results of *lacZ* assays are shown in Fig.4.3b. The starting DNA construct, containing just *gtr52* and its upstream promoter, stimulated the highest *lacZ* expression. Transcription decreased 4-fold upon IS*Aba*13 insertion regardless of orientation ($p < 0.0001$) and reduced only slightly further upon loss of the *gtr52* promoter ($p < 0.0017$). Overall, this is consistent with the absence of an intrinsic terminator, with transcription instead being prevented by Rho due to a lack of translation.

4.5. The bidirectional promoter of IS*Aba*13 is active *in vivo*

We next wanted to understand the bidirectional IS*Aba*13 promoter. To do this, we made further derivatives of the *gtr52*::IS*Aba*13 construct (Fig.4.4a). In these variants, the bidirectional promoter was removed by deletion or mutation. The mutations are shown in Fig.4.2b above the wild-type sequence. Both changes abolished *lacZ* expression ($p < 0.0001$, Fig.4.4b). Our interpretation is that, when IS*Aba*13 is present, most *lacZ* expression is due to outward transcription from the bidirectional IS*Aba*13 promoter; transcription from the *gtr52* promoter inside *wzy* is expected to terminate prematurely. To confirm this, we deleted the *gtr52* promoter and, as expected, this had no impact on *lacZ* expression (Fig.4.5).

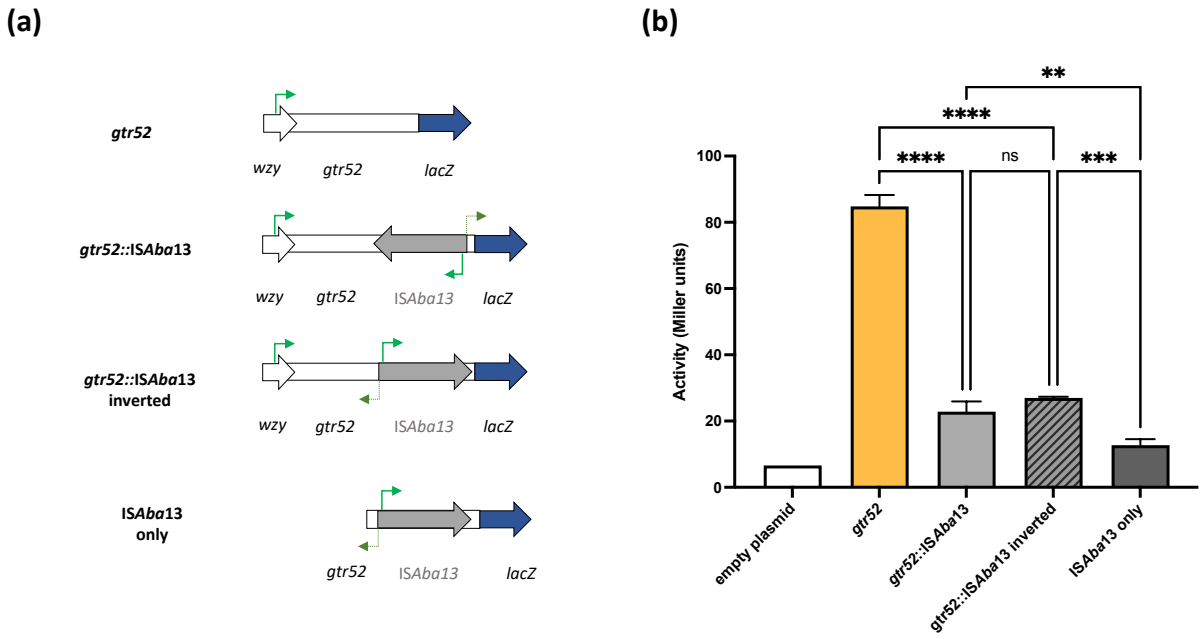

Fig.4.3. *lacZ* assay with different orientations of IS*Aba*13

(a) Schematic cartoons represent constructs used in *lacZ* assay. Green arrows represent TSSs. (b) *lacZ* activity of different constructs. Empty plasmid represents pRW50T with no insert to show background *lacZ* activity. Ordinary one-way ANOVA with Tukey's multiple comparisons test used to assess significance. Bars represent mean of three biological replicates, error bars = standard deviation.

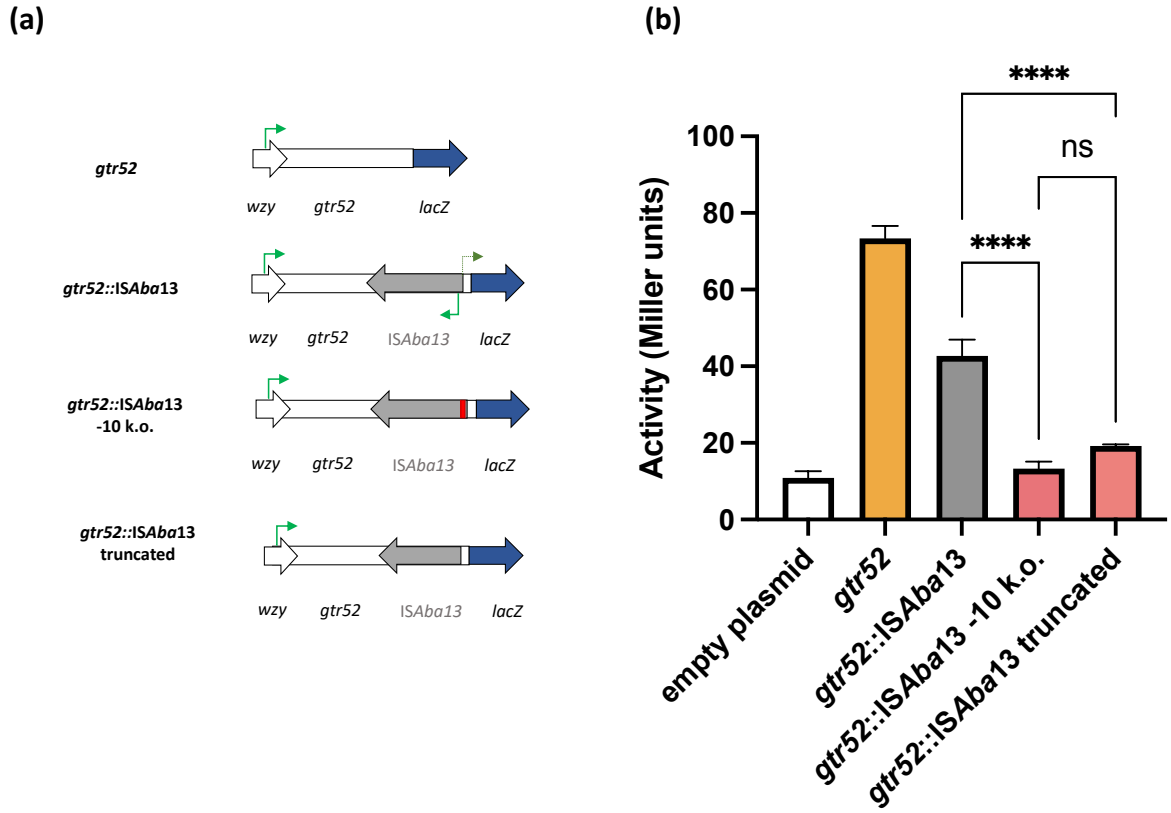

Fig.4.4. *lacZ* assay with IS*Aba*13 promoter element mutations

(a) Schematic cartoons represent constructs used in *lacZ* assay (b) *lacZ* activity of different constructs. Empty plasmid represents pRW50T with no insert to show background *lacZ* activity. Ordinary one-way ANOVA with Tukey's multiple comparisons test used to assess significance. Bars represent mean of three biological replicates, error bars = standard deviation.

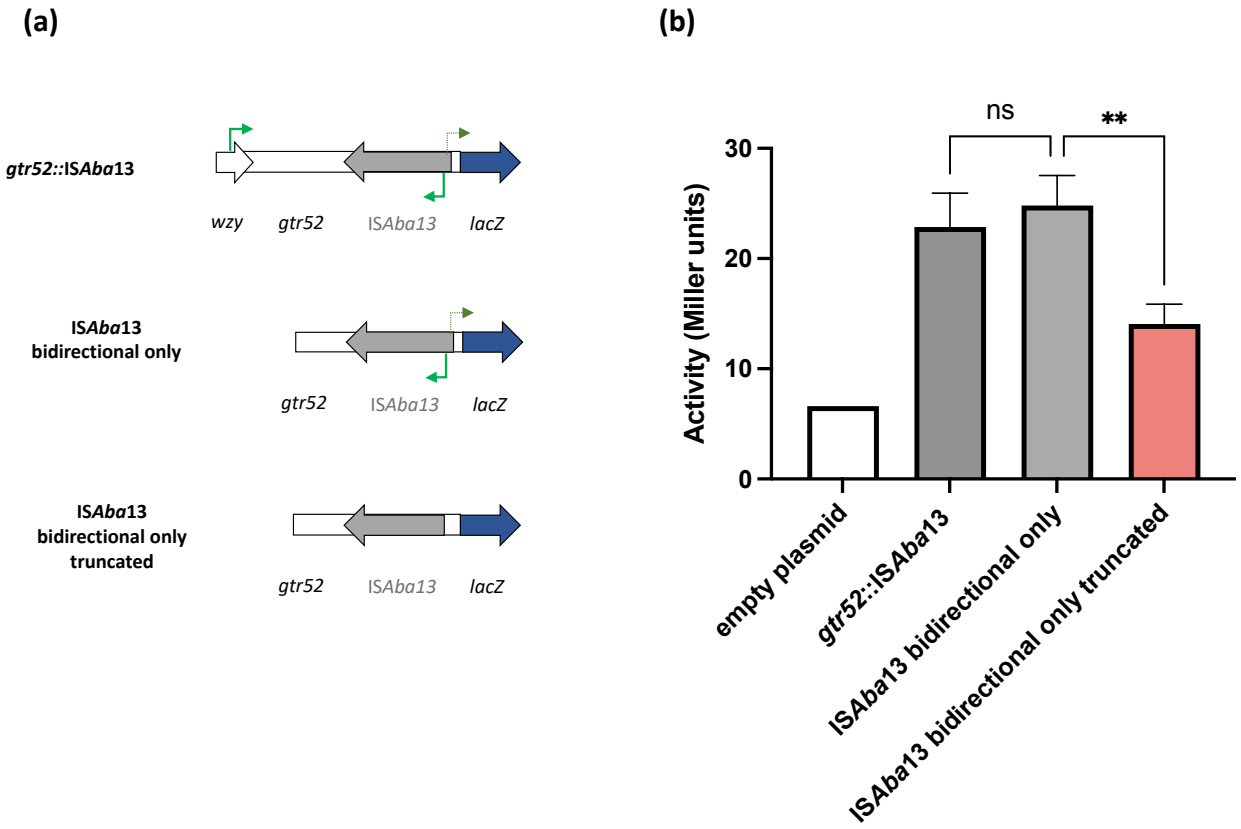

Fig.4.5. *lacZ* assay with bidirectional activity of IS*Aba*13
(a) Schematic cartoons represent constructs used in *lacZ* assay. (b) Empty plasmid represents pRW50T with no insert to show background *lacZ* activity. Ordinary one-way ANOVA with Tukey's multiple comparisons test used to assess significance. Bars represent mean of three biological replicates, error bars = standard deviation.

4.6. IS*Aba*13 does not block transcription *in vitro*

LacZ assays show IS*Aba*13 has an active bidirectional promoter *in vivo*, and transcription from the bidirectional promoter does not impact premature termination of *gtr52* transcription (Fig.4.4, Fig.4.5). We also found no evidence of an intrinsic terminator within IS*Aba*13. To confirm these observations, we used *in vitro* transcription assays. We expected that the absence of Rho *in vitro* would greatly reduce the effect of IS*Aba*13 on transcription from the *gtr52* promoter. DNA regions were cloned in plasmid pSR, upstream of a λoop terminator sequence, and used as the template for *in vitro* transcription. The various constructs, and expected transcript sizes, are illustrated in Fig.4.6a. Results of the assays are in Fig.4.6b. Note that IS*Aba*13 is shortened so that RNAs produced are a size suitable for separation by denaturing PAGE. The RNAI transcript serves as an internal control. For construct 1 (lane 1) RNAs 669 nt and 143 nt in length are observed (Fig.4.6b red and blue triangles respectively). The longer transcript is from the *gtr52* promoter in *wzy.* The shorter is the outward RNA from the bidirectional IS*Aba*13 promoter. Hence, premature *gtr52* termination does not occur *in vitro*, as predicted. This also confirms that (i) there is no intrinsic terminator within IS*Aba*13, and (ii) that inward IS*Aba*13 transcription does not completely block transcription of *gtr52*. Construct 2 (lane 2) lacks the bidirectional IS*Aba*13 promoter and the amount of *gtr52* transcript does increase (Fig.4.6b, red triangle). This suggests that transcriptional interference from the bidirectional IS*Aba*13 promoter may reduce *gtr52* transcription. An increase in the amount of free RNAP, because the bidirectional IS*Aba*13 promoter has been removed, is likely to contribute. Results from experiments with construct 3 (lane 3) are inconclusive, as no expected RNAs were present. However, it is possible to still see the RNAI control band, and

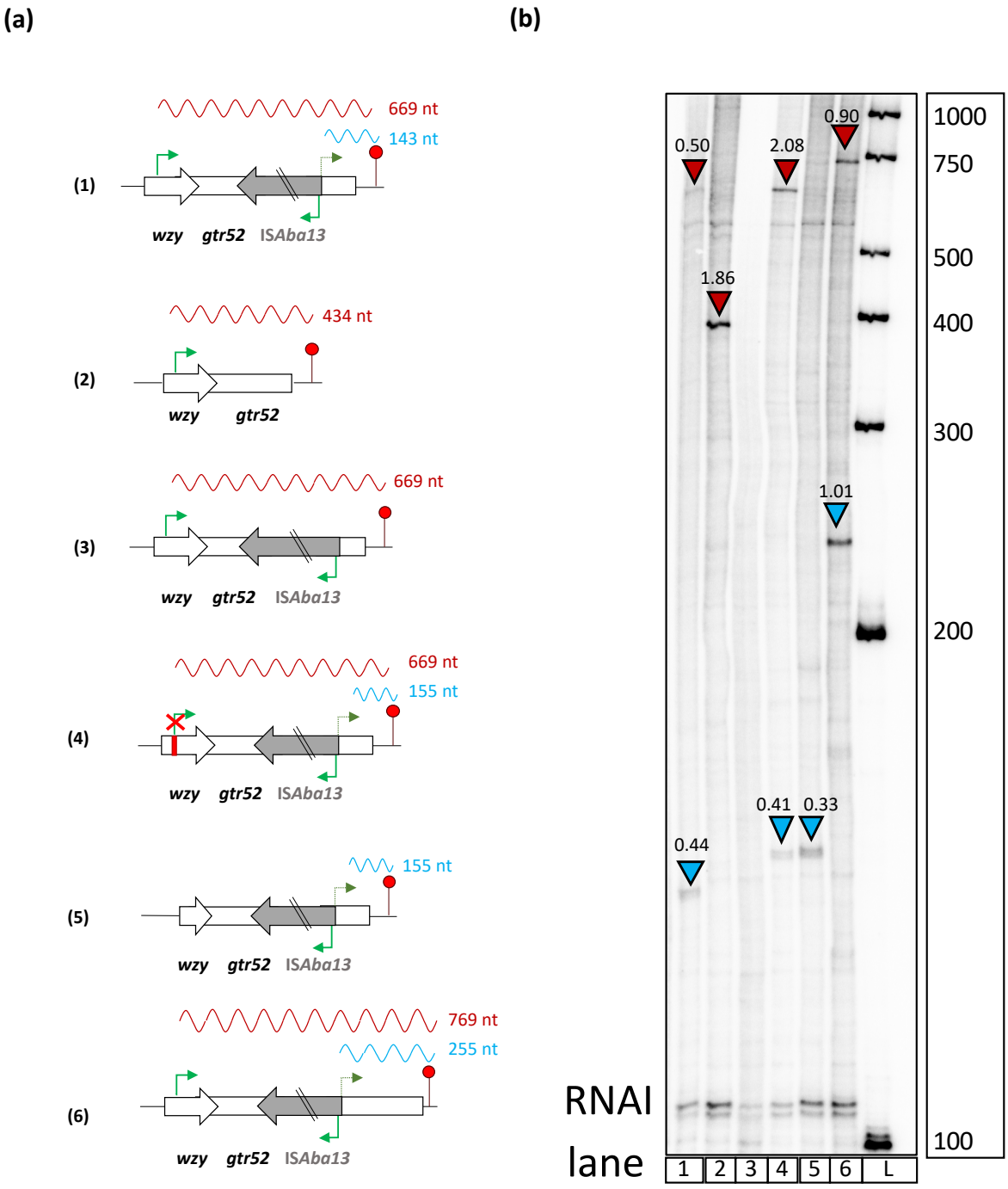

Fig.4.6. IVT of IS*Aba*13 K-locus constructs

(a) Schematic cartoons represent constructs used in IVT. Two hyphens indicate broken IS*Aba*13 gene. Red circle indicates λoop transcriptional terminator on pSR. Green arrows represent TSSs. (b) IVT gel of transcripts produced by constructs. L = ladder. Coloured arrows represent transcripts of various lengths corresponding to cartoon depictions with ratios relative to RNAI control band indicated as number above arrow.

other non-specific bands at the bottom of the gel. Construct 3 has the start of IS*Aba*13 removed, causing the initiating nucleotide of the outward TSS to change from 'A' to 'T'. This suggests the identity of the initiating nucleotide (or the specific sequence between the – 10 element and the TSS) is important for outward transcription of IS*Aba*13. In construct 4 (lane 4), an unexpected band, similar in size to the RNA from the *gtr52* promoter, is still present (Fig.4.6b, red triangle). This is likely due to a sequence, upstream of the *gtr52* promoter, containing an almost perfect -10 element (Fig. 4.2b, sequence in italics). It is interesting that there are no Cappable-seq reads corresponding to a start site for this additional promoter *in vivo* (Fig.4.1). Most likely, this "phantom" promoter is occluded by the real *gtr52* promoter. To confirm the additional -10 element was responsible for the unexpected RNA, both -10 elements were removed by truncation in construct 5 (lane 5). Accordingly, the band is lost. Finally, to confirm all bands were correctly identified, construct 6 (lane 6) has an extra 100 bp of DNA between IS*Aba*13 and the λoop terminator. As expected, the bands we had annotated shifted position because larger RNAs are produced from the template. Other bands, likely due to transcripts generated from other pSR sites did not. Note that the outward IS*Aba*13 transcript (Fig.4.2b, blue arrows) is larger in assays with constructs 4, 5 and 6 because they were made by restriction digestion of an insert, and ligation into pSR, instead of Gibson assembly. The former method added 12 nt to transcript length because two 6 bp restriction sites are included

4.7. Discussion

Overproduction of a transposase is likely to cause aberrant widescale transposition across the chromosome. Therefore, transposase levels must be tightly regulated. For example, IS256 in *Enterococcus faecalis* and *Enterococcus faceium* is regulated at the transcriptional and translational level by an antisense RNA and a second TSS that produces a truncated transposase (Kirsch *et al.*, 2023). In this study, we show that the IS*Aba*13 transposase mRNA is leaderless. The lack of an SD sequence likely results in low levels of ribosome recruitment, as leaderless mRNAs are not common in γ-proteobacteria including *A. baumannii* (Beck and Moll, 2018). This could explain the lack of RNA-seq reads mapping to the transposase ORF; without ribosome recruitment Rho will terminate transcription (Fig.4.1).

The presence of IS*Aba*13 prematurely terminates *gtr52* transcription. Three mechanisms could explain this: (i) Rho-dependent termination (ii) intrinsic termination or (iii) RNAP collisions due to transcription in the opposing direction. An intrinsic terminator should generate an RNA 3' end detectable by Term-seq, but none was evident (Fig.4.1). Further, if IS*Aba*13 contained an intrinsic terminator or RNAP collisions were important, altering IS*Aba*13 orientation would likely have an effect on *gtr52* termination. Since this is not the case (Fig.4.3), the most plausible explanation is Rho-dependent transcription termination. This is also in agreement with no precise *gtr52* termination being observed *in vitro,* where no Rho is present (Fig.4.6). It is important to note that *in vitro* assays are conducted with RNAP, a highly conserved enzyme, purified from *E. coli*. It is possible, but unlikely, that a feature of *A. baumannii* RNAP is important for termination along this sequence. To test the importance of

Rho in termination, *lacZ* assays could be repeated in the presence of bicyclomycin which inhibits Rho (Skordalakes *et al.*, 2005).

Upon IS insertion, an intrinsic promoter element can drive adjacent gene expression. For example a strong outward directed promoter in IS*Aba*1 has been shown to drive expression of the beta-lactamase genes *ampC*, *bla* $_{\text{OXA-23}}$ and *bla* $_{\text{OXA-27}}$ (Turton *et al.*, 2006). Additionally, transposition of one IS into another can create a composite promoter. Insertion of IS*Aba*825 into an IS*Aba*3-like element brings -35 and -10 elements into correct juxtaposition to drive expression of bla_{OXA-58} , conferring carbapenem resistance (Ravasi *et al.*, 2011). Insertion sequences can also form hybrid promoters, with existing sequences at the site of insertion. For example, a -35 element found in the IRL of IS*Aba*125 forms a promoter with a -10 element in plasmid p271A of *E. coli* to drive expression of $bla_{\text{NDM-1}}$ (Poirel, Bonnin and Nordmann, 2011). Until this work, nothing was known about the role of IS*Aba*13 in driving the expression of adjacent genes. This can occur in two ways, transcriptional readthrough into downstream genes, following transposase expression, or outward transcription due to the bidirectional promoter.

This is, to our knowledge, the first example of a bidirectional promoter within a prokaryotic IS. The bidirectional promoter identified has a 23 bp spacing between the divergent TSSs. This is the second most common configuration in *E. coli* and most other bacteria (Warman *et al.*, 2021). As noted above, such a promoter offers the potential to drive expression of adjacent genes, if in the opposite orientation to IS*Aba*13. Additionally, there could be co-expression of divergent genes. It is also possible that bidirectionality impacts the rate of transposition. For

example, Warman *et al*. demonstrated competition between RNAP molecules attempting to bind bidirectional promoters in each possible direction.

Chapter 5: Locations and consequences of global insertions of IS*Aba*13

5.1. Introduction

The discovery of IS*Aba*13 at the K-locus was a fortuitous consequence of the discernible colony morphology. We next searched for other sites of IS*Aba*13, and the phenotypic heterogeneity that could be generated. To do this we developed a method called native transposon sequencing (Tn-seq). This method differs from the well-established method of Tn-seq. In Tn-seq, the chromosome of interest has no copies of the transposon being introduced. Instead, the genome is exposed to reconstituted transpososomes *in vitro,* or subject to overexpression of a transposon *in vivo* (van Opijnen and Levin, 2020). This results in a similar number of insertions in each cell and, at the population level, a reasonably even distribution of the transposon genome wide. If insertions occur into genes essential under the specific conditions used, during subsequent outgrowth, these variants are outcompeted.

In native Tn-seq, chromosomal copies of the IS are allowed to transpose naturally during normal growth. There are two challenges with this approach. First, all cells carry the IS at the same starting position. Hence, most sequencing reads will map to the IS starting location and rare instances of transposition are easily missed. Second, transposition is a rare event. To overcome this, libraries of a large cell population are sequenced to a high depth. Further, steps are taken during library preparation to avoid further biases arising (see below for details).

Previous work developed a similar method called IS-seq. However, this study used the isolate LAC-4, that already has 22 copies of IS*Aba*13 (Wright *et al.*, 2017). Thus, a very high proportion of total library reads will map to these starting locations. Additionally, this study used low

sequencing depth, and, consequently, only 14 novel insertion sites were identified. As described below, our approach mapped thousands of IS*Aba*13 insertions.

5.2. Mapping global insertion sites of IS*Aba*13 in a population with native Tn-seq

The process of native Tn-seq is outlined in Fig.5.1. Wild-type cells are subcultured and grown to mid-exponential phase to generate a sufficiently large population for analysis. After growth, genomic DNA is extracted (step 1) and randomly fragmented using a fragmentase (step 2). The ends of enzymatically sheared DNA are repaired, with a dA nucleotide added to the 3' end (step 3), facilitating ligation of adapter containing a dT nucleotide overhang at the 3' end (step 4). PCR is then done with an IS*Aba*13 specific primer, and an adaptor specific primer (step 5). A second PCR is then done using a different IS*Aba*13 specific primer which binds further downstream from the first primer used in step 5, increasing specificity (step 6). To mitigate bias, introduced by preferential amplification of IS*Aba*13 insertions at the starting loci, we reduced the number of PCR cycles. Additionally, we used staggered primers (Staggered_1 - Staggered_4, Table 2.3) in step 5. This increases library diversity, and final sequencing quality.

Using native Tn-seq we were able to map 8,026 unique IS*Aba*13 insertions across the AB5075 chromosome in a population of *A. baumannii* cells. The distribution of insertions is illustrated as a heat map in Fig.5.2a (top panel). Darker regions correspond to parts of the chromosome where there is a high density of IS*Aba*13 insertions. Note that, in this analysis, each insertion site is counted equally, no matter how many reads are detected at that specific location. Interestingly, regions around the two starting copies of IS*Aba*13 are hotspots for

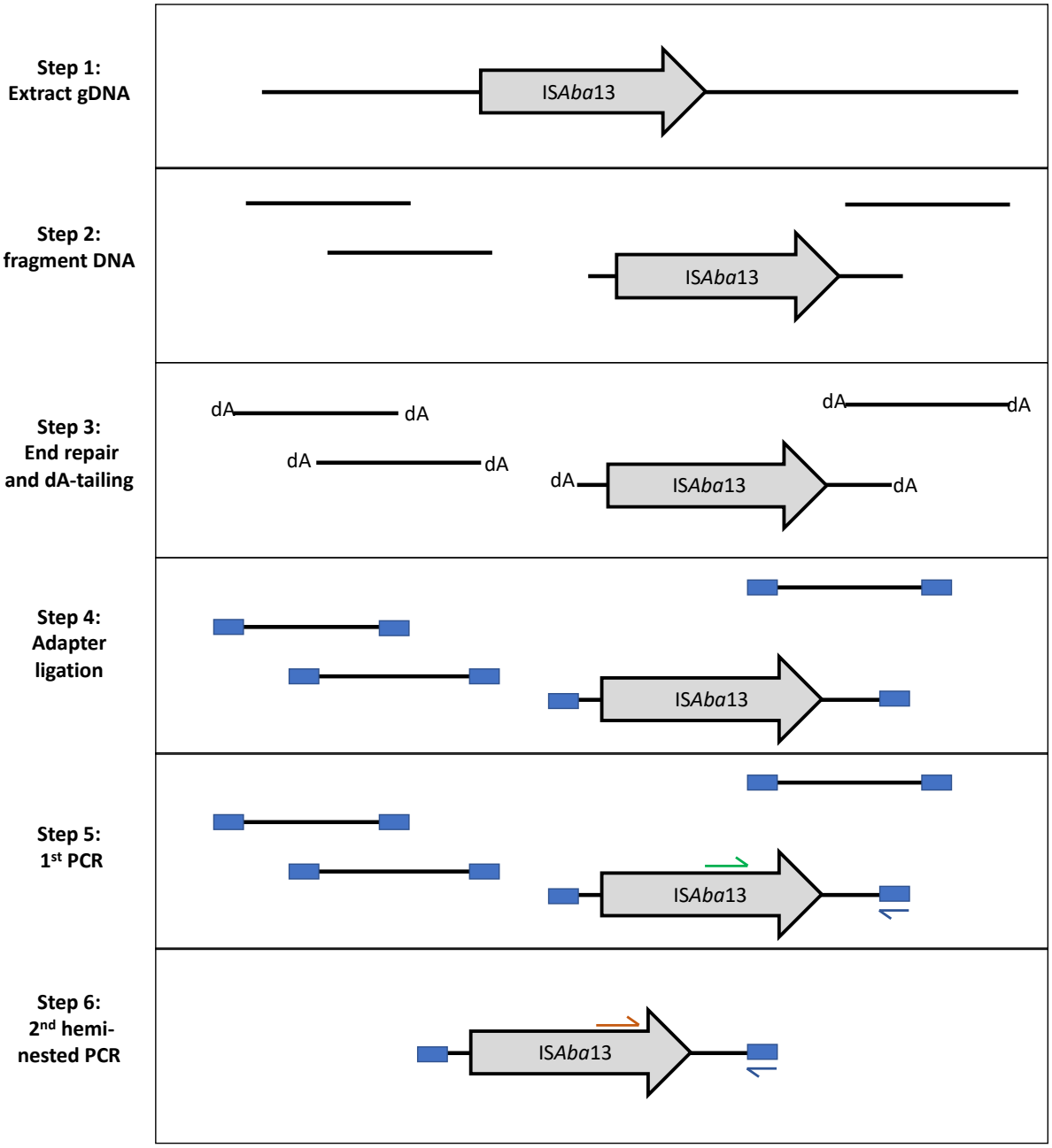

Fig.5.1. The method of native Tn-seq

Genomic DNA (gDNA) is sheared with dsDNA fragmentase. Following end repair and dA-tailing, adaptors are ligated on. This is followed by a PCR using a primer specific for the adaptor (blue arrow) and a primer complementary to the end of IS*Aba*13 (green arrow). A 2nd hemi-nested PCR is done with the same adaptor primer and a primer complementary to IS*Aba*13 further downstream from the previous binding site (red arrow).

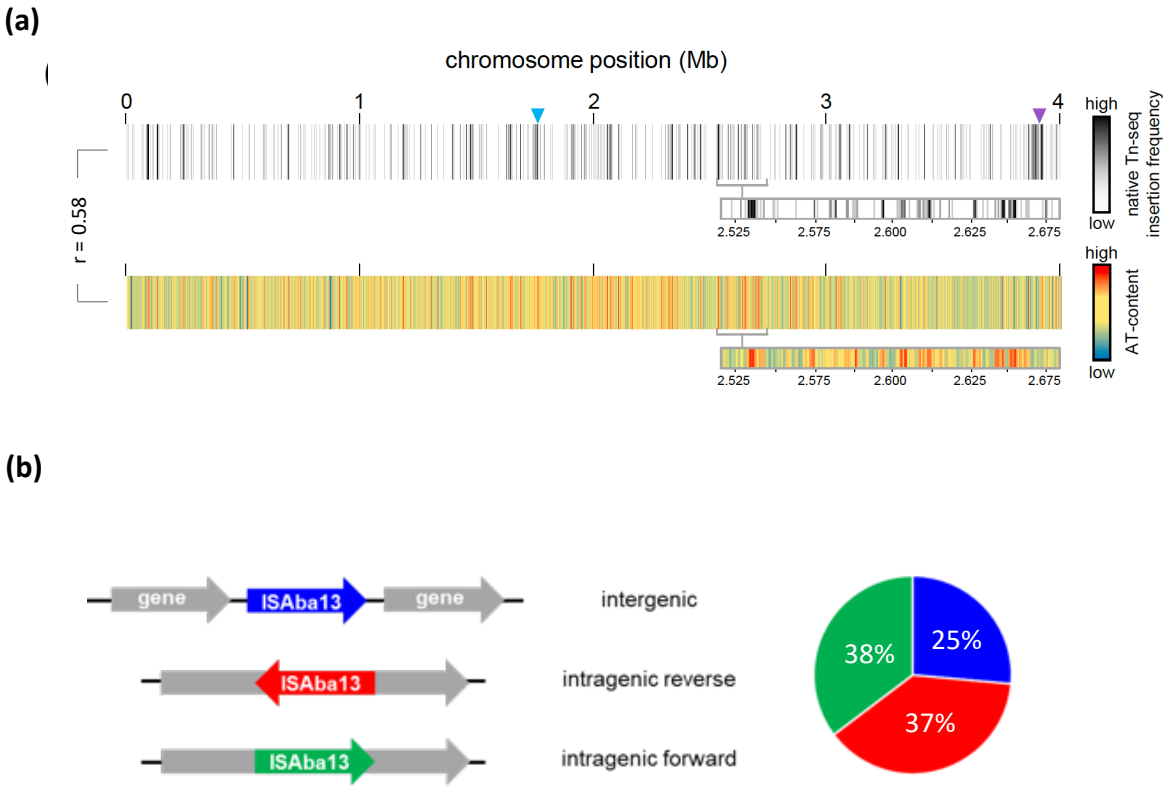

Fig.5.2. Global insertion of IS*Aba*13 in AB5075

(a) Heat map of global insertion sites of IS*Aba*13. The chromosome is divided up into 1 kb regions, coloured from white to black indicating the frequency of insertions in those regions. Chromosomal position of two starting copies of IS*Aba*13 highlighted by blue and purple triangles. AT content heat map shows regions of high (red) and low (blue) AT content. (b) Locations of IS*Aba*13 insertions relative to genes.

insertion (Fig.5.2a, blue and purple triangles). Additionally, a striking correlation (r = 0.58) was seen between sites of insertion and DNA AT-content (Fig.5.2a). We also determined the position and orientation of insertions with respect to genes (Fig.5.2b). There is a small bias towards insertions occurring in intergenic regions. These account for only 13 % of the AB5075 chromosome, yet harbour 25% of total IS*Aba*13 insertions. Within intragenic DNA, the orientation of IS*Aba*13 with respect to the disrupted gene is similar in the reverse (37 %) and forward (38 %) directions.

5.3. Preferential insertion of IS*Aba*13 into the K-locus

Given that we had previously identified IS*Aba*13 in *gtr52* at the K-locus of grey variants, we expected to detect this by native Tn-seq. This was the case, (grey arrows in Fig.5.3a and Fig.5.3b.) In AB5075, *gtr52,* contains a high number of insertions (143, 1395 and 37,344 reads mapping to this locus in three replicates.) The exact site of insertion in the K-locus described by Whiteway *et al.* is also found in our native Tn-seq data (red arrows, Fig.5.3a and Fig.5.3b) (Whiteway *et al.*, 2022). However, the number of insertions at this site is much lower (21, 29 and 969 reads mapping to this locus in the respective three replicates.) Interestingly, in *gtr52* there is a sequence matching bases immediately downstream of the IS*Aba*13 transposase stop codon (Fig.5.3c, blue). In *gtr52*, this sequence forms an inverted repeat that occurs nowhere else in the chromosome (Fig.5.3c, blue and green arrows). This may be coincidental, or could play some role in the preferential targeting of IS*Aba*13 to this region.

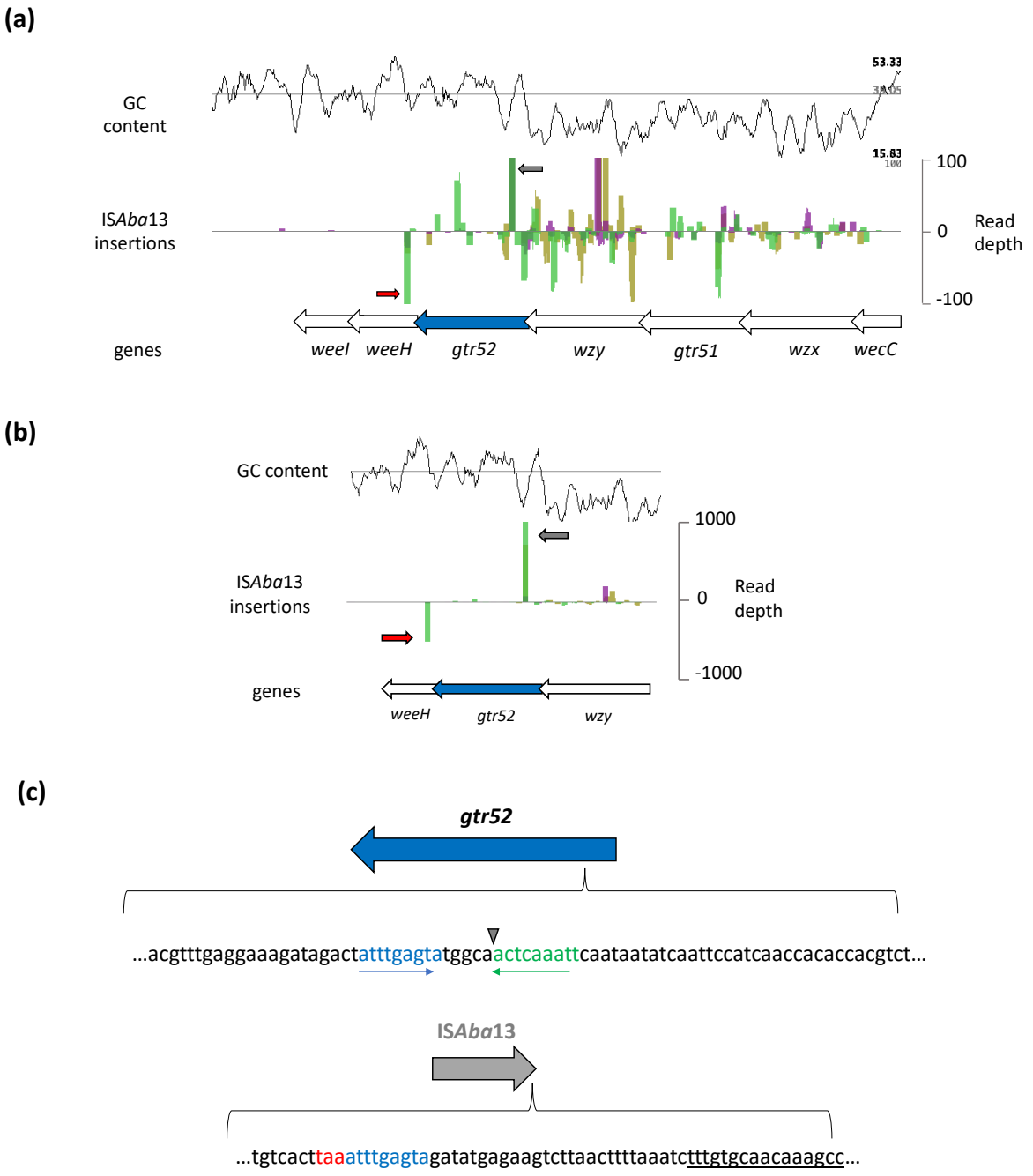

Fig.5.3. Insertion of IS*Aba*13 into the K-locus identified by native Tn-seq
(a) Insertions across the K-locus. Top panel shows % GC content, middle panel shows insertions of IS*Aba*13, with red arrows indicating the site of insertion identified in *weeH* (Whiteway *et al.,* 2022) and grey arrows indicating site of insertion identified in *gtr52* (this study.) Bottom panel shows genes. (b) Zoomed in view of K-locus insertions to show high frequency of insertions at the two positions previously mentioned. (c) Top: sequence of *gtr52* gene. Blue indicates region of homology, green indicates DTR sequence generated following transposition. Grey triangle shows point of IS*Aba*13 insertion following transposition. Blue and green arrows highlight inverted repeat sequences. Bottom: sequence of end of IS*Aba*13, red highlights transposase stop codon, blue indicates region of homology. Underlined region indicates terminal IRR.

5.4. IS*Aba*13 inserts into *ompW* and *ABUW_1221*

The phenotypic impact of IS*Aba*13 insertion into *gtr52* was characterised in Chapter 3. We next wanted to examine how insertion of IS*Aba*13 into other regions, identified by native Tn-seq, could affect phenotype. Two AT-rich genes with a high density of insertions were selected (Fig.5.4). We speculated these genes, *ompW* and *ABUW_1221*, would affect phenotype if inactivated. The first of these, *ompW*, is an outer membrane porin involved in iron homeostasis (Catel-Ferreira *et al.*, 2016). The gene has been shown to have roles in biofilm formation, host cell adherence/invasion, and persistence (Gil-Marqués, Pachón and Smani, 2022; Schmitt *et al.*, 2023). The second gene, *ABUW_1221*, is an EAL domain containing protein. EAL domains are found in diverse bacterial signal transduction proteins, and have cyclic di-GMP phosphodiesterase activity (Schmidt, Ryjenkov and Gomelsky, 2005). The *ABUW_1221* encoded protein also has a RhaT domain, a permease of the drug/metabolite transporter family.

It is not possible to isolate single IS mutants from our sequencing libraries, as the method uses a mixed population of cells. For *ompW*, we recreated an *ompW*::IS*Aba*13 insertion identified by native Tn-seq using genome editing (Fig.2.2) (Godeux *et al.*, 2020). Additionally, an *ABUW_1221*:T26 mutant was obtained from the T26 mutant library (Gallagher *et al.*, 2015).

(a)

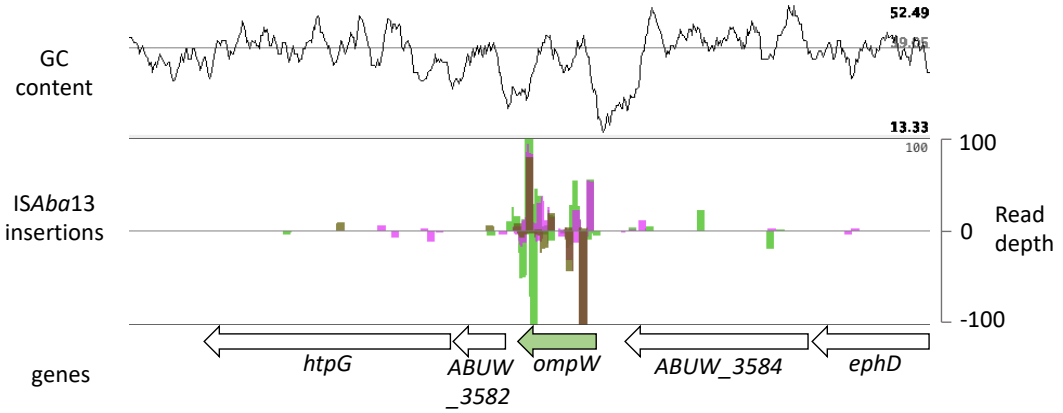

(b)

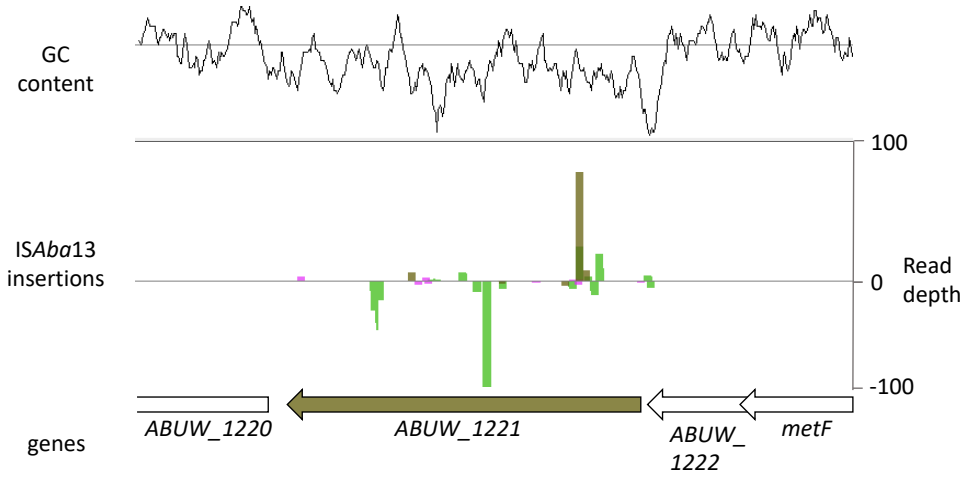

Fig.5.4. IS*Aba*13 insertion into *ompW* and *ABUW_1221*
Top panel: % GC content across locus. Middle panel: IS*Aba*13 insertions, peaks up indicate insertions on top DNA strand, peaks down indicate insertions on bottom DNA strand. Bottom panel: annotated genes at locus of interest. Peaks shown are for three biological replicates.

5.4.1. Phenotypes of IS*Aba*13 insertion into *ompW* and *ABUW_1221*

We compared the *ompW*::IS*Aba*13 and *ABUW_1221*::T26 mutants to wild-type cells. We saw no difference in growth rate in LB medium (Fig.5.5a) or growth rate for *ompW*::IS*Aba*13 in the presence of human serum compared to wild-type cells (Fig.5.5b). Similarly, these strains were able to form biofilms equally well (Fig.5.6). Comparing wild-type to *ompW*::IS*Aba*13, no statistically significant difference is seen either at 37 °C ($p = 0.9814$) or room temperature ($p = 0.9365$). Although there appears to be slightly improved biofilm formation for *ABUW_1221*:T26, this does not reach statistical significance at 37 °C ($p = 0.1252$) or room temperature ($p = 0.0979$).

In *A. baumannii,* although *ompW* has been shown to bind colistin, and has reduced expression in colistin-resistant strains, deletion of *ompW* does not change the MIC for colistin (Catel-Ferreira *et al.*, 2016). We tested our *ompW*::IS*Aba*13 mutant against tetracycline, zeocin and polymyxin B, which has a slightly different structure to colistin (polymyxin E). As seen in table 5.1, the *ompW*::IS*Aba*13 mutant shows no difference in MIC except for polymyxin B, however there is only a 2-fold increase in susceptibility. More repeat experiments would be required in order to confirm a difference in MIC for polymyxin B.

5.4.2. The impact of *ompW*::IS*Aba*13 on transposition

As seen in Fig 5.2, as well as the propensity for insertion into AT-rich regions, there are hotspots around the two native locations of IS*Aba*13. This suggests chromosomal regions in close proximity to IS*Aba*13 may be attractive targets for insertion. To test this, we repeated

(a)

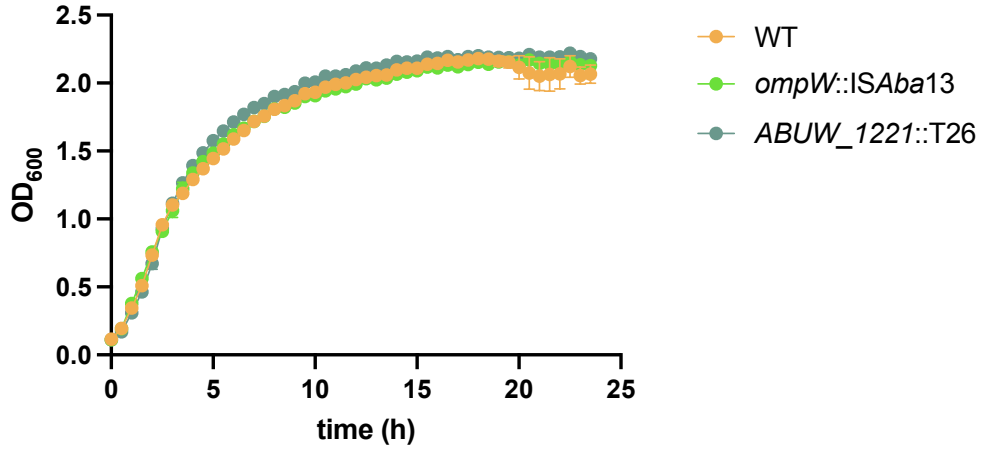

(b)

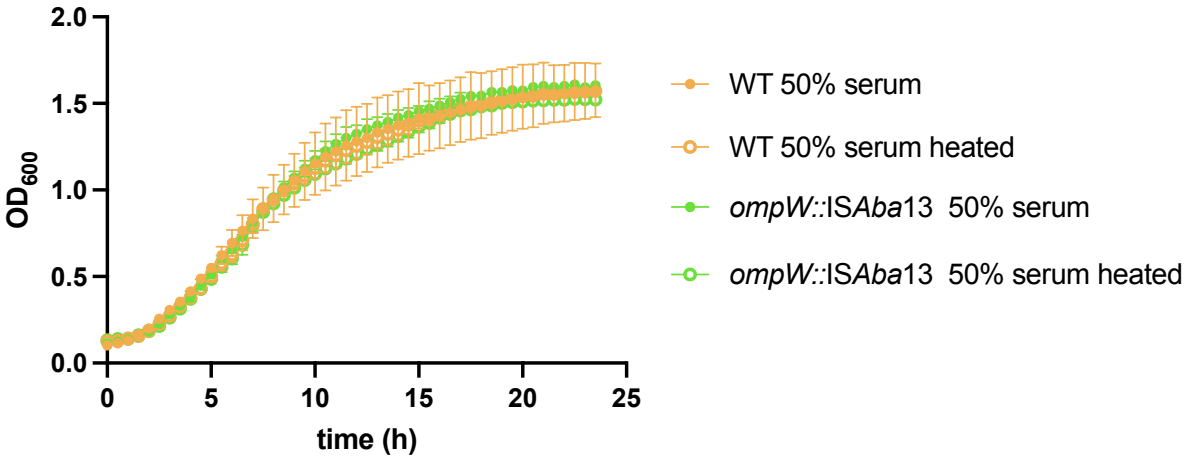

Fig.5.5. Growth curves of *ompW*::IS*Aba*13 and *ABUW_1221*::T26 cells
OD_{600} was measured by a plate reader in a 96-well plate for 24 hours in (a) LB medium or (b) 50 % normal human serum or 50 % heat-treated normal human serum. Points represent mean of three biological replicates, error bars represent standard deviation.

(a)

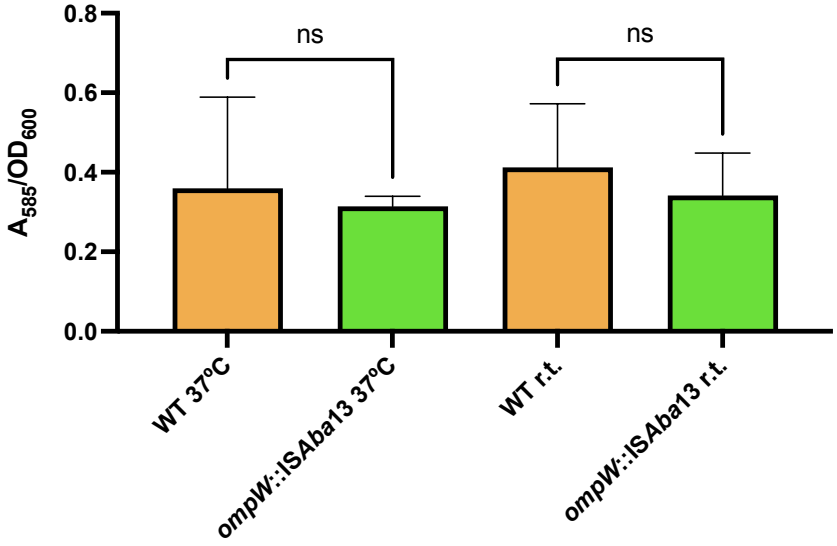

(b)

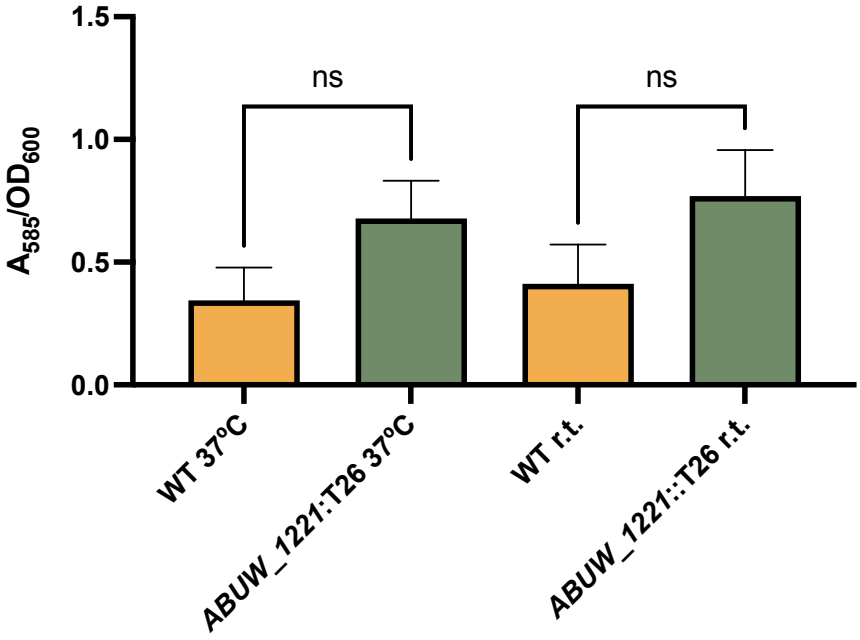

Fig.5.6. *ompW*::IS*Aba*13 and *ABUW_1221*::T26 biofilm assay

Crystal violet staining measured by absorbance at A_{585} and normalised by OD_{600}. Initial inoculum for overnight culture was OD_{600} = 0.3. Tubes were incubated overnight at 37 °C or room temperature. Ordinary one-way ANOVA with Tukey's multiple comparisons test used to assess significance. Bars represent mean of three biological replicates with error bars representing standard deviation (a) biofilm formation of *ompW*::IS*Aba*13 (b) biofilm formation of *ABUW_1221*::T26.

Strain	MIC of antibiotic (μg/ml)			
	gentamicin	polymyxin B	zeocin	tetracycline
WT	4096	2	64	0.5
ompW::IS*Aba*13	4096	1	64	0.5

Table 5.1. MIC of WT and *ompW*::IS*Aba*13 measured by broth microdilution
Strains were tested in a 96-well plate in at least triplicate on at least two separate occasions. Reference ATCC 25922 and NCTC10418 control strains were included.

the native Tn-seq experiment using the *ompW*::IS*Aba*13 strain generated (Fig.5.7). An increased density of insertions around *ompW* is observed.

5.5. IS*Aba*13 inserts into *hns*

In addition to *ompW* and *ABUW_1221*, a further AT-rich target of IS*Aba*13 is *hns,* which encodes the global transcriptional regulator, and chromosome folding protein, H-NS (Fig.5.8). Given its role in chromosome organization, and the transcriptional regulation of multiple genes, we expected disruption of *hns* to affect multiple phenotypes. Given time constraints, an *hns*::T26 mutant was obtained from the T26 mutant library for use in subsequent phenotypic assays (Gallagher *et al.*, 2015).

5.5.1. Phenotypes of the *hns*::T26 mutant

We first assessed the impact of *hns* inactivation on growth in LB medium compared to wild-type. The *hns*::T26 mutant has a slower growth rate, eventually reaching a similar final OD_{600} (Fig.5.9a). *hns*::T26 cells have a smaller growth rate constant (k = 0.422, 95 % confidence intervals = 0.396 to 0.451) compared with VIR-O cells (k = 0.486, 95 % confidence intervals = 0.453 to 0.522).

Human serum albumin (HSA) has been shown to down-regulate the expression of H-NS in *A. baumannii* (Escalante *et al.*, 2022). We tested whether growth in human serum with *hns*::T26 would differ from wild-type. Fig.5.9b shows that growth is impaired for *hns*::T26 in both serum and heated serum. *hns*::T26 cells have a smaller growth rate constant (k = 0.247, 95 % confidence intervals = 0.239 to 0.254) compared with VIR-O cells (k = 0.344, 95 % confidence intervals = 0.305 to 0.389). Inactivating *hns* by transposon insertion therefore may limit the

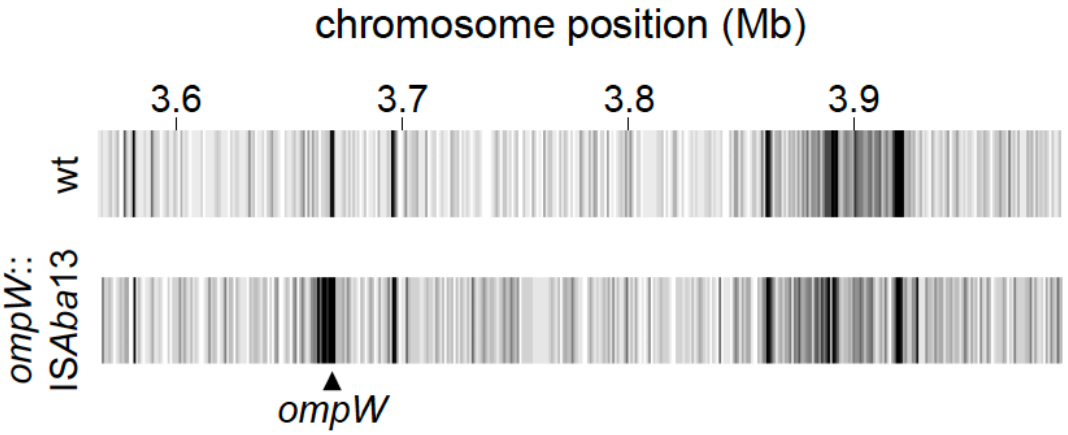

Fig.5.7. IS*Aba*13 insertion in *ompW*::IS*Aba*13

Heat map of insertion sites of IS*Aba*13 near the *ompW* gene in wild-type (wt) and *ompW*::IS*Aba*13. Chromosome is divided up into 1 kb regions, coloured from white to black indicating the frequency of insertions in those regions. Chromosomal position of *ompW* highlighted by black triangle**.**

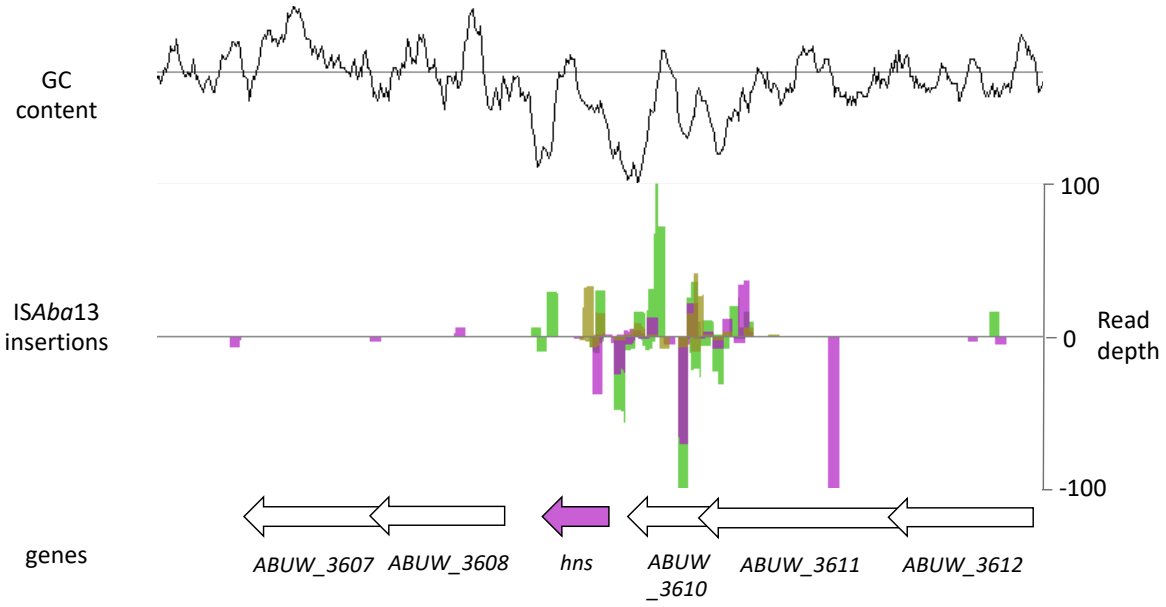

Fig.5.8. IS*Aba*13 insertion into *hns*

Top panel % GC content across locus. Middle panel IS*Aba*13 insertions, peaks up indicate insertions on top DNA strand, peaks down indicate insertions on bottom DNA strand. Bottom panel annotated with genes at locus of interest. Of note *ABUW_3610* encodes a FadM Acyl-CoA thioesterase family protein and *ABUW_3611* encodes a hypothetical protein with a putative protoheme IX biogenesis protein conserved domain. Peaks represent three biological replicates.

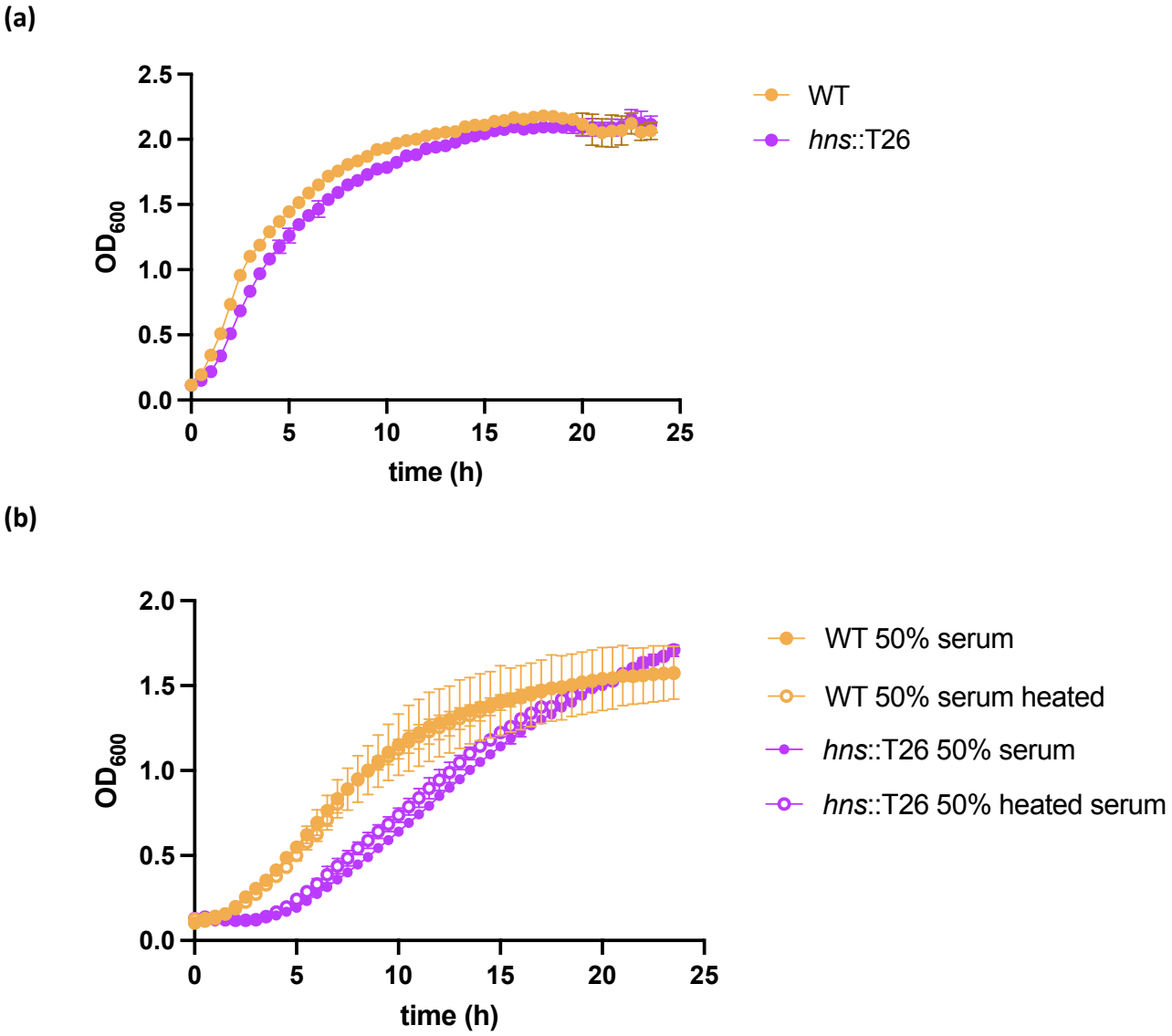

Fig.5.9. Growth curves of wild-type and *hns*::T26 cells
OD_{600} was measured by a plate reader in a 96-well plate for 24 hours in (a) LB medium or (b) 50 % normal human serum or 50 % heat-treated normal human serum. Points represent mean of three biological replicates, error bars represent standard deviation. Logistic growth analysis using nonlinear regression was used to calculate the growth rate constant (k).

ability to adapt to growth in human serum. We also assessed whether *hns* disruption would impact biofilm formation at 37 °C, or room temperature. Fig.5.10 shows there is no significant difference in biofilm formation between wild-type and *hns*::T26 cells at 37 °C ($p = 0.9538$). However, a 6-fold increase in biofilm formation by *hns*::T26 cells was detected at room temperature ($p < 0.0001$). Finally, because *hns* has been shown to regulate antibiotic resistance in *A. baumanii*, we investigated the susceptibility of *hns*::T26 to gentamicin, polymyxin B and zeocin (Table 5.2). No difference in susceptibility to polymyxin B was observed. However, there was a 128 and 16-fold decrease in MIC for gentamicin and zeocin respectively.

5.6. Discussion

Various methods have been used to track IS movement in prokaryotes. These have included papillation assays and plasmid-based targeting. These inform on the frequency of transposition, but there are caveats. Papillation assays use a promoter-less, and cryptic, *lacZ* gene placed between TIR. Transposition causes integration of cryptic *lacZ* into other regions, and if these regions are expressed, and *lacZ* is in the correct orientation and reading frame, cells become lac^+ (Swingle *et al.*, 2004). Plasmid based targeting uses a transposon with an antibiotic resistance cassette. Transposition into plasmids is detected after their isolation, by using them to transform fresh cells that are then plated on selective media (Ravasi *et al.*, 2011). These methods are laborious, with multiple steps, and are limited by the number of transposition events that can be observed. Furthermore, neither reports global patterns of transposition.

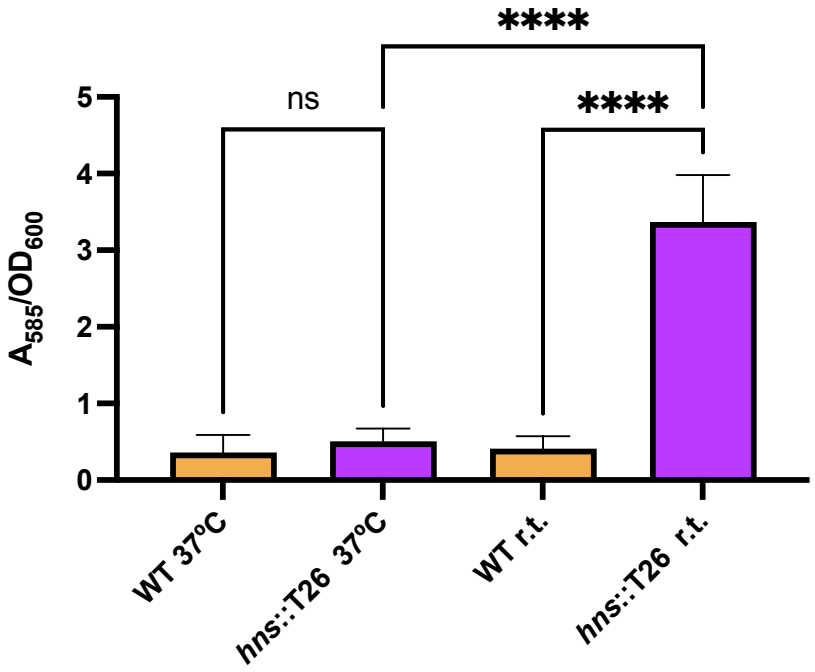

Fig.5.10. *hns*::T26 biofilm assay

Crystal violet staining measured by absorbance at A_{585} and normalised by OD_{600}. Initial inoculum for overnight culture was OD_{600} = 0.3. Tubes were incubated overnight at 37 °C or room temperature. Ordinary one-way ANOVA with Tukey's multiple comparisons test used to assess significance. Bars represent mean of three biological replicates with error bars representing standard deviation.

Strain	MIC of antibiotic (µg/ml)		
	gentamicin	polymyxin B	zeocin
WT	4096	2	64
hns::T26	32	2	4

Table 5.2. MIC of WT and *hns*::T26 measured by broth microdilution
Strains were tested in a 96-well plate in at least triplicate on at least two separate occasions. Reference ATCC 25922 and NCTC10418 control strains were included.

Native Tn-seq and IS-seq use next generation sequencing to allow a comprehensive in-depth analysis of global insertion sites. As well as the LAC-4 study, discussed earlier, IS-seq has been applied to IS6110 in *Mycobacterium Tuberculosis* isolates (Reyes *et al.*, 2012). In this study, individual colonies from agar plates were used for analysis, limiting the genetic heterogeneity of the population. Hence, only an average of 13 insertions per isolate were identified (Reyes *et al.*, 2012). A disadvantage of native Tn-seq is that the number of sequence reads from a given insertion may not necessarily represent frequent IS*Aba*13 insertion at that site. For instance, an insertion event which occurred early during growth of the population could propagate to high numbers and so be over-represented in the final population. For this reason, we counted each insertion position only once in our global analysis. To improve specificity of the technique, both ends of the IS could be mapped instead of one. However, this would greatly reduce sensitivity (Reyes *et al.*, 2012).

The sequence homology between the *gtr52* insertion site for IS*Aba*13 and IS*Aba*13 itself may explain why this region is a particularly strong hotspot for insertion. Homology between the terminal ends of an IS, and preferential sites of insertion, has been noted for multiple ISs which form excised circular intermediates (Loot, Turlan and Chandler, 2004). It is speculated that transposases of such IS elements are able to create a synaptic complex, involving one IR of the excised IS and a sequence resembling an IR in the target DNA (Siguier *et al.*, 2015). Of note, the sequence within *gtr52* also forms an inverted repeat. The downstream half of this repeat, following transposition, becomes the DTR. Inverted repeats and the secondary structures they form could play a role in transposition of IS*Aba1*3. Indeed, the insertion of some TEs, across multiple domains of life, has been associated with palindromic motifs, including IS903 of *E.*

coli (Hu *et al.*, 2001; Linheiro and Bergman, 2008). Palindromic sequences, (particularly AT-rich repeats) are inherently unstable and may encourage chromosomal rearrangement as they can form hairpin/cruciform structures prone to double stranded breaks (Kato, Kurahashi and Emanuel, 2012). Some IS members of the families IS110 and IS3 show preference for insertion into repetitive extragenic palindromes (Choi, Ohta and Ohtsubo, 2003; Wilde *et al.*, 2003).

Despite the role of *ompW* in protecting *E. coli* from phagocytosis, and the alternative complement pathway mediated attack, we found no change in growth of AB5075 *ompW*::IS*Aba*13 in human serum (Fig.5.5b) (Li *et al.*, 2016). Both *ompW* and EAL domain-containing proteins have roles in biofilm formation in *A. baumannii* ATCC 17978 (Ahmad *et al.*, 2020; Gil-Marqués, Pachón and Smani, 2022). However, we found no significant difference in biofilm formation for *ompW*::IS*Aba*13 or *ABUW_1221*::T26 in AB5075 (Fig.5.6). OmpW from *A. baumannii* ATCC 19606 has been shown to interact with colistin, despite no difference in MIC for colistin in a Δ*ompW* mutant (Catel-Ferreira *et al.*, 2016). This is in contrast to *K. pneumoniae*, where *ompW* disruption mediated by an IS leads to colistin resistance (Macesic *et al.*, 2020). The antibiotics used in the MIC assays in this study (Table 5.1) are of limited clinical relevance, and meropenem should be tested, with susceptibility to meropenem expected to decrease in AB5075 *ompW::ISAba13* (Wu *et al.*, 2016). Further characterisation of the *ompW*::IS*Aba*13 mutant used in this study could involve measuring persistence, iron incorporation, and adhesion to or invasion of A549 cells, which are known roles for *ompW* in *A. baumannii* (Catel-Ferreira et al., 2016; Gil-Marqués, Pachón and Smani, 2022; Schmitt et al., 2023). The increased density of IS*Aba*13 insertions around the *ompW*::IS*Aba*13 locus observed in native Tn-seq (Fig.5.7) supports the initial observation that IS*Aba*13 is more likely

to be transposed to nearby adjacent sites. This could be because cis-activity of transposases requires rapid formation of the transpososome at the site of excision (Derbyshire, Kramer and Grindley, 1990). Upon transpososome formation, immediate AT-rich regions near the starting location represent attractive sites of insertion.

In *A. baumannii,* The *hns* gene is a target for various ISs including IS*Aba*1, IS*Aba*12, IS*Aba*13 (as confirmed in this study), and IS*Aba*125 (Eijkelkamp *et al.*, 2013; Deveson Lucas *et al.*, 2018; Penesyan *et al.*, 2019). The non-autonomous element $MITE_{Aba12}$ has also been found disrupting *hns* in ATCC 17978 (Adams and Brown, 2019). In regards to the *hns*::T26 phenotypes observed, if reduced growth in human serum is due to albumin, heat inactivation of this protein may not be important. It has previously been reported bovine serum albumin (BSA) increases transformability of *A. baumannii* A118, and that heat inactivation further increases transformability (Traglia *et al.*, 2016). The slow growth could also be more pronounced in serum as nutrient levels are lower than in LB (Fig.5.9a and Fig.5.9b). Loss of *hns* was previously reported to have conflicting impacts on biofilm formation. In A118 and AB5075, an *hns* mutant shows reduced biofilm formation (Rodgers *et al.*, 2021; Escalante *et al.*, 2022). However, in ATCC 17978, knocking out *hns* increases biofilm formation (Eijkelkamp *et al.*, 2013). These assays were done at 37 °C whereas, in this study with AB5075, the marked increase in biofilm formation was only seen at room temperature (Fig.5.10). Additionally, the change in MIC of gentamicin for a Δ*hns* mutant has been described before, but only a 24-fold change was reported (measured by E-strips) in contrast to the 128-fold difference reported in this study (Rodgers *et al.*, 2021). As well as differences in agar and broth dilution methods, results from broth dilution MIC assays can vary between laboratories due to differences in

starting culture density, choice of optical density versus cell counts, and length of measurement (Schuurmans *et al.*, 2009).

IS-mediated mutations offer the potential to generate huge phenotypic diversity in populations, which may enable adaptation to specific niches. As a mechanism of generating genetic diversity, transposition offers many advantages. First, a transposition event is more likely to inactivate a gene than a SNP, which in turn makes phenotypic change more likely. Second, transposition is reversible, and so gene function can be subsequently restored. Third, outwardly directed promoters, in TEs, can drive transcription of adjacent genes, upregulating their expression. A "bet-hedging" strategy is beneficial when most cells remain wild-type, but rare mutants can clonally expand under the right circumstances. In one study, examining the evolution of *A. baumannii* in response to sub-inhibitory levels of ciprofloxacin and tetracycline, IS*Aba*13 was the largest driver of mutations (30 % of total mutations, compared with IS*Aba*1 (4.4 %) or IS*Aba*125 (2.8 %)) (Penesyan *et al.*, 2019). Additionally, despite mapping five different IS elements, 73 % of low-abundance novel insertion sites found during IS-seq in LAC-4 were from IS*Aba*13 (Wright *et al.*, 2017). Further characterised phenotypic consequences from IS*Aba*13 transposition include insertion upstream of the transcriptional regulator *adeN,* increasing *adeIJK* mediated efflux and resistance to erythromycin and tetracycline (Zang *et al.*, 2021). Intriguingly, IS*Aba*13 has also been found in colistin-dependent *A. baumanniii,* interrupting the *pldA* gene encoding an outer membrane phospholipase (Chamoun *et al.*, 2021).

Here, we show that IS*Aba*13 preferentially inserts into AT-rich regions of the chromosome. The AT-preference of various ISs have been noted before, including IS903 and IS5 in *E. coli,* and IS*Aba*825 and IS*Aba*11 in *A. baumannii* (Hu and Derbyshire, 1998; Ravasi *et al.*, 2011; Humayun *et al.*, 2017; Olmeda-López, Corral-Lugo and McConnell, 2021). AT-rich regions are typically bound by H-NS in γ-proteobacteria (Singh *et al.*, 2014). However, H-NS is typically thought to exclude factors from bound DNA. We hypothesize that H-NS is either removed temporarily to allow transposition, or directly facilitates the process. This idea is explored in the next chapter.

Chapter 6: H-NS directs transposition of IS*Aba*13 by DNA bridging

6.1. Introduction

H-NS is a global transcriptional regulator and chromosome folding protein, typically binding AT-rich regions of horizontally acquired DNA (Dame, Rashid and Grainger, 2020). H-NS has two modes of binding following nucleation, and subsequent oligomerisation, at an AT-rich site (Lang *et al.*, 2007). The first is formation of extended nucleoprotein filaments, along a single double stranded DNA region, causing DNA stiffening (Amit, Oppenheim and Stavans, 2003). Alternatively, in a different conformation, H-NS can bridge between separate DNA sections (Dame, Noom and Wuite, 2006).

There is no structure of *A. baumannii* H-NS, but the protein is 25 % identical and 59 % similar to *E. coli* H-NS (Fig.6.1a). AlphaFold prediction suggests a very similar organization, including a C-terminal DNA binding domain, N-terminal dimerization domain (for site 1 interactions), and central multimerization domain (for site 2 interactions) (Fig.6.1b). The structure of H-NS from *S. enterica* Serovar Typhimurium (differing in only 7 amino acids from *E. coli* H-NS) reveals intermolecular salt bridges involving residues K57 and R54 from one protomer interacting with D68 and E74, respectively, of the other protomer (Arold *et al.*, 2010). These interactions form the site 2 interface, key for multimerization (Arold *et al.*, 2010). These residues are missing in the *A. baumannii* sequence (Fig.6.1a), and the AlphaFold prediction indicates interactions at site 2 instead involve amino acid pairs R61-E51 and K60-E33 in each protomer (Fig.6.1c).

Given that native Tn-seq showed a positive correlation between IS*Aba*13 insertion, and AT-content, we hypothesized that H-NS might affect transposition in some way. To investigate

(a)

```
A. baumannii   ------------MKPDISELSVEELKRLQEEAEALIASKKDQA------IED---AYNQ
E. coli        MSEALKILNNIRTLRAQARECTLETLEEMLEKLEVVVNERREEESAAAAEVEERTRKLQQ
                           :: :  * ::* *:.: *: *.:: .:::::       :*:     :*

A. baumannii   IIEIAENVGFSVEQLLE----FGAQKRKKTTRKSVEPRYRNKNNAEETWTGRGKQPRWLV
E. coli        YREMLIADGIDPNELLNSLAAVKSGTKAKRAQRPAKYSYVDENGETKTWTGQGRTPAVIK
                 *:    *:. ::**:    . : .: * ::: .:  * ::*.  :****:*: *  :

A. baumannii   AEI-EKGAKLEDFLI--
E. coli        KAMDEQGKSLDDFLIKQ
                 : *:* .*:****
```

(b)

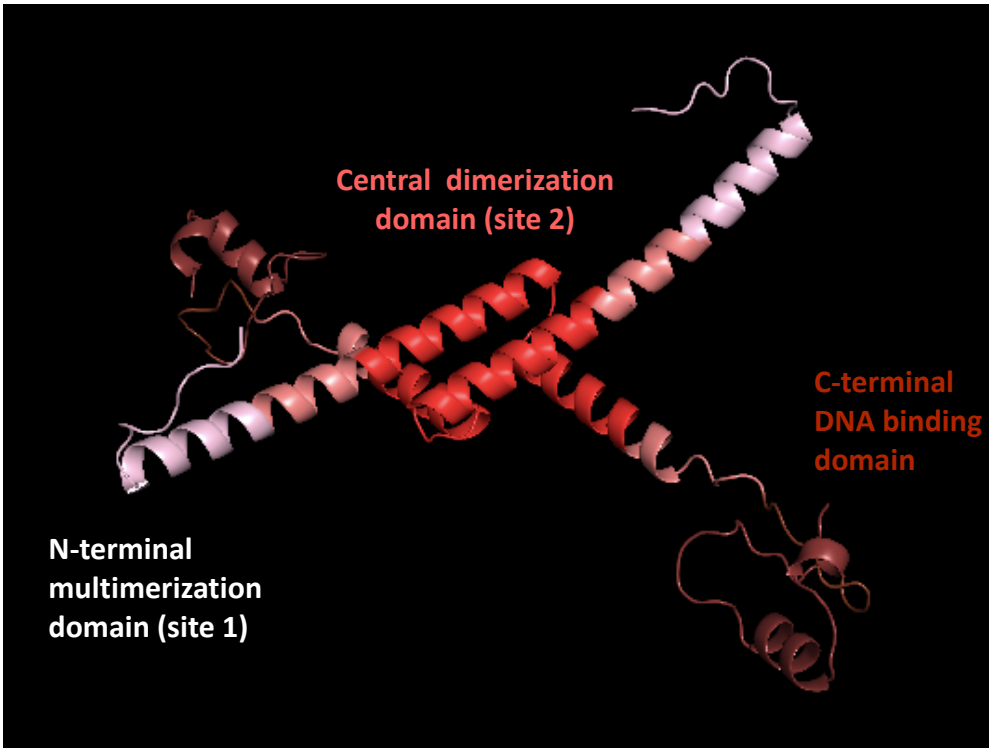

(c)

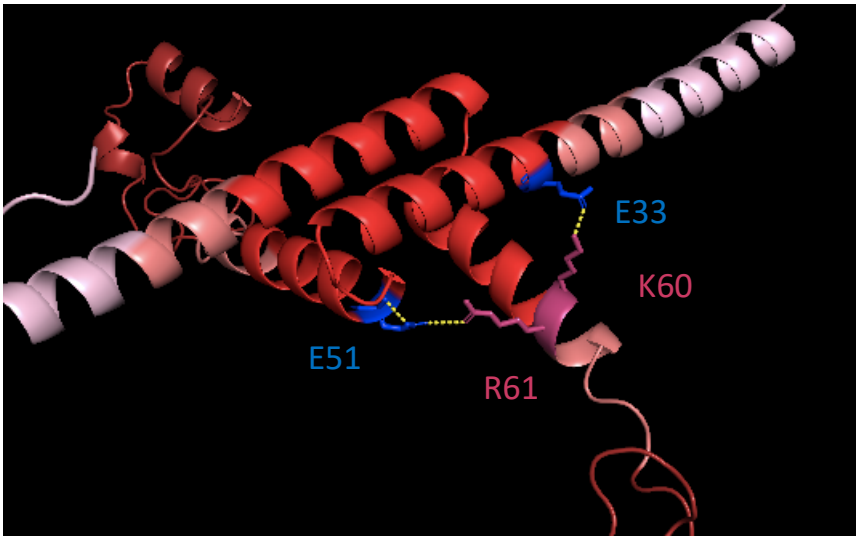

Fig.6.1. Sequence and putative structure of *A. baumannii* H-NS
(a) Clustal Omega sequence alignment (v1.2.4) of AB5075 and *E. coli* MG1655 H-NS. Asterisk indicates residues which are fully conserved, two dots indicate conservation between residues of highly similar properties, single dots indicate conservation between residues of weakly similar properties. (b) Alphafold2 model created in UCSF ChimeraX v1.6.1 (Mirdita *et al.*, 2022). Viewed in PyMOL v2.5.3. (c) Zoomed in view of site 2 interaction highlighting key residues involved.

this, we used a combination of genomic and genetic tools. These included *in vivo* assays, such as native Tn-seq, to measure the distribution of IS*Aba*13 insertions in different mutants, and a BACTH assay, to measure protein-protein interactions between H-NS and IS*Aba*13 transposase. We also made use of chromatin immunoprecipitation sequencing (ChIP-seq) data for H-NS binding (by Dr. Simon LeGood) to allow comparisons between transposition and H-NS binding. Furthermore, *in vitro* assays, including EMSAs and DNA bridging measurements, were used. These assays confirm H-NS is essential for transposition directed into AT-rich DNA, and that the ability for H-NS to drive DNA bridging is important to achieve this.

6.2. H-NS directs transposition of IS*Aba*13 to AT-rich regions

To test if IS*Aba*13 insertion bias was driven by an intrinsic property of AT-rich sequence, or H-NS, we repeated native Tn-seq with the *A. baumannii hns*::T26 mutant. Fig.6.2a shows that, in *hns*::T26 cells, sites of insertion are evenly spread across the chromosome, and the correlation between AT-content and IS*Aba*13 insertion frequency is greatly reduced (r = 0.23). In the figure, a 115 kb section of the chromosome is shown as an expansion, to aid comparison of transposition patterns and DNA AT-content (Fig.6.2b). We conclude that H-NS drives transposition into AT-rich regions. Interestingly, in the *hns* mutant, the preference for IS*Aba*13 insertion around the two starting copies of IS*Aba*13 (Fig.6.2a blue and purple arrows) is maintained. This suggests, in the absence of H-NS, proximity to starting chromosomal location plays the most important role in directing transposition. Additionally, a dark section in the

(a)

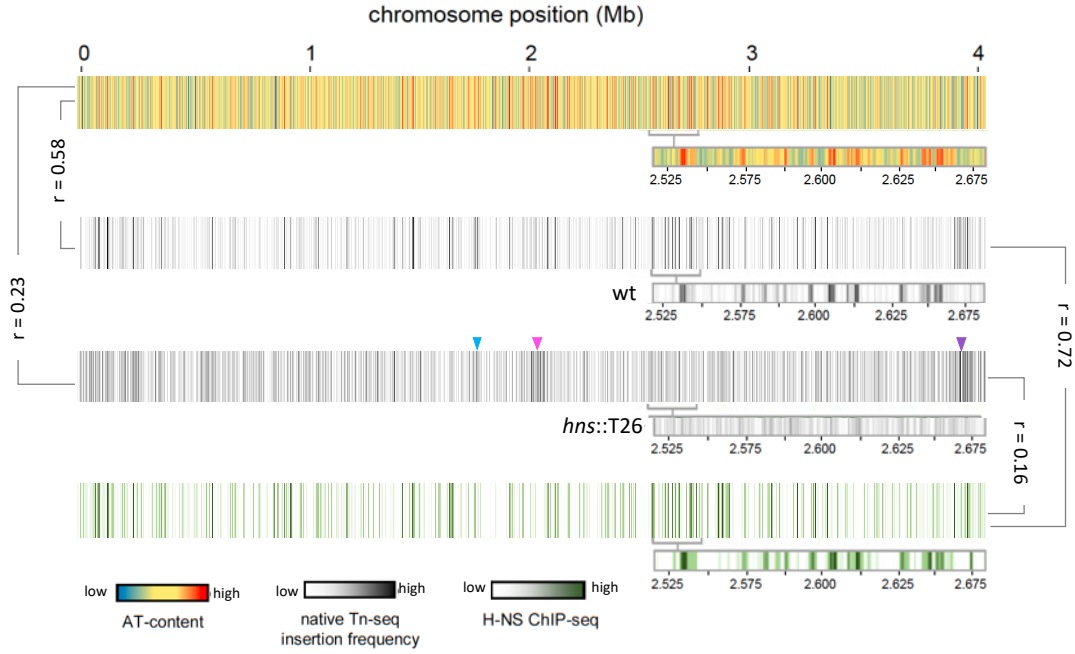
chromosome position (Mb)
0
1
2
3
4
r = 0.58
2.525
2.575
2.600
2.625
2.675
wt
r = 0.23
r = 0.72
hns::T26
r = 0.16
low
high
AT-content
native Tn-seq
insertion frequency
H-NS ChIP-seq

(b)

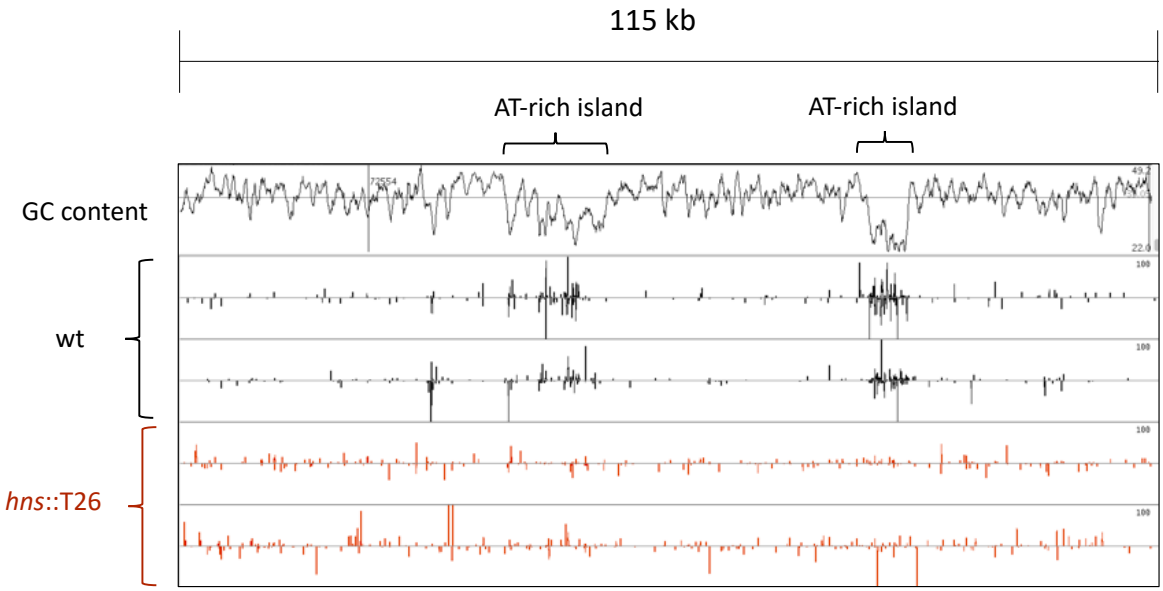
115 kb
AT-rich island
AT-rich island
GC content
wt
hns::T26

(c)

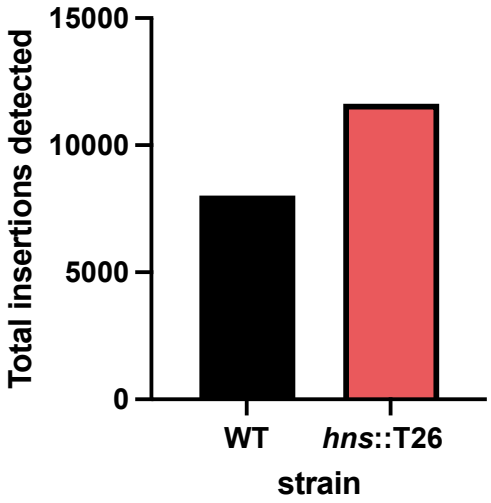

Fig.6.2. IS*Aba*13 hotspots are lost in an *hns*::T26 mutant

(a) First panel: heat map of AT-content. IS*Aba*13 insertions were binned into 1 kb regions (compiled from both top and bottom DNA strands). Second panel: wild-type insertions and third panel: (*hns*::T26) insertions. Fourth panel: ChIP-seq binding profile of H-NS, binned into 1 kb regions (b) Zoomed in region showing insertion sites for *hns*::T26 and WT in two biological replicates across a 115 kb section of chromosome. Coverage cut-off set to 200 reads. Peaks upwards indicate insertions in top DNA strand, peaks downwards indicate insertions in bottom DNA strand. (c) Total number of sites of IS*Aba*13 insertion recorded for each strain.

middle of the plot arises in the *hns* mutant, corresponding to the terminus of replication (Fig.6.2a pink arrow). In parallel to work in this thesis, Dr. Simon LeGood used ChIP-seq to map global H-NS binding *in vivo*. Briefly, this technique involves expressing C-terminally FLAG-tagged H-NS, which is cross-linked to DNA. Following DNA fragmentation, an anti-FLAG antibody is used to immunoprecipitate H-NS and associated DNA, which is sequenced. ChIP-seq confirmed a strong correlation between sites bound by H-NS and IS*Aba*13 insertion (r = 0.72) (Fig.6.2a). This was abolished in the *hns* mutant (r = 0.16.) (Fig.6.2a). Importantly, the number of total insertion events detected for *hns*::T26 and wild-type cells is similar (Fig.6.2c). Hence, H-NS does not alter overall transposition efficiency.

6.3. Attempted purification of IS*Aba*13 transposase

To investigate the mechanism of targeting, we first wanted to purify the IS*Aba*13 transposase. Transposases are notoriously difficult to purify as they are typically made in very small amounts and are often insoluble. We first attempted to purify His_6-tagged recombinant transposase in Lemo21 DE3 cells using the tuneable T7 expression system for challenging proteins. In this system, as the amount of L-rhamnose added to the culture is increased, the level of lysozyme, which inhibits T7 RNA polymerase expression, rises. This permits better control of protein expression and folding. The IS*Aba*13 transposase sequence was cloned into plasmids pET21 and pET28 to allow expression of N- and C-terminal His_6 fusions respectively, under the control of an IPTG-inducible promoter.

Fig.6.3a shows an SDS-PAGE gel on which lysates from cells carrying pET21 IS*Aba*13 encoded transposase were analysed. Expression of the pET21 IS*Aba*13 encoded transposase (expected size 37 kDa) was induced best with 400 µM IPTG and 0 mM L-rhamnose, and the protein was recovered from the insoluble fraction (red triangle, Fig.6.3a). Fig.6.4b shows that an equivalent experiment with pET28 IS*Aba*13 encoded transposase (expected size of 38 kDa) did not yield any expression. Given this, we attempted to optimise conditions of growth for cells expressing pET21 IS*Aba*13 encoded transposase. Cells were grown at 37 °C for 5 h, or at 16 °C overnight, with either 0 mM, 100 mM or 500 mM rhamnose. This was to further slow protein expression and reduce any misfolding. As seen in Fig.6.3c (red triangles), the transposase remained in the insoluble fraction regardless of conditions used. To confirm the band expected was not a result of IPTG induction of a different protein, we used an empty plasmid control (Fig.6.3d.) Despite using 8 M Urea, when doing a large-scale preparation of the transposase, the insoluble inclusion body containing the transposase could not be resolubilised.

In an attempt to make the transposase soluble, we fused it to Maltose Binding Protein (MBP). This method was the only successful method of purifying the IS5 family IS903 transposase after several years of attempts (Derbyshire and Grindley, 1992). The IS*Aba*13 transposase gene was cloned into pMAL-C6T to create an N-terminal MBP tag fusion. Fig.6.4 shows that, despite the MBP tag, IS*Aba*13 transposase remained insoluble in all conditions tested (expected size 78 kDa, red triangles).

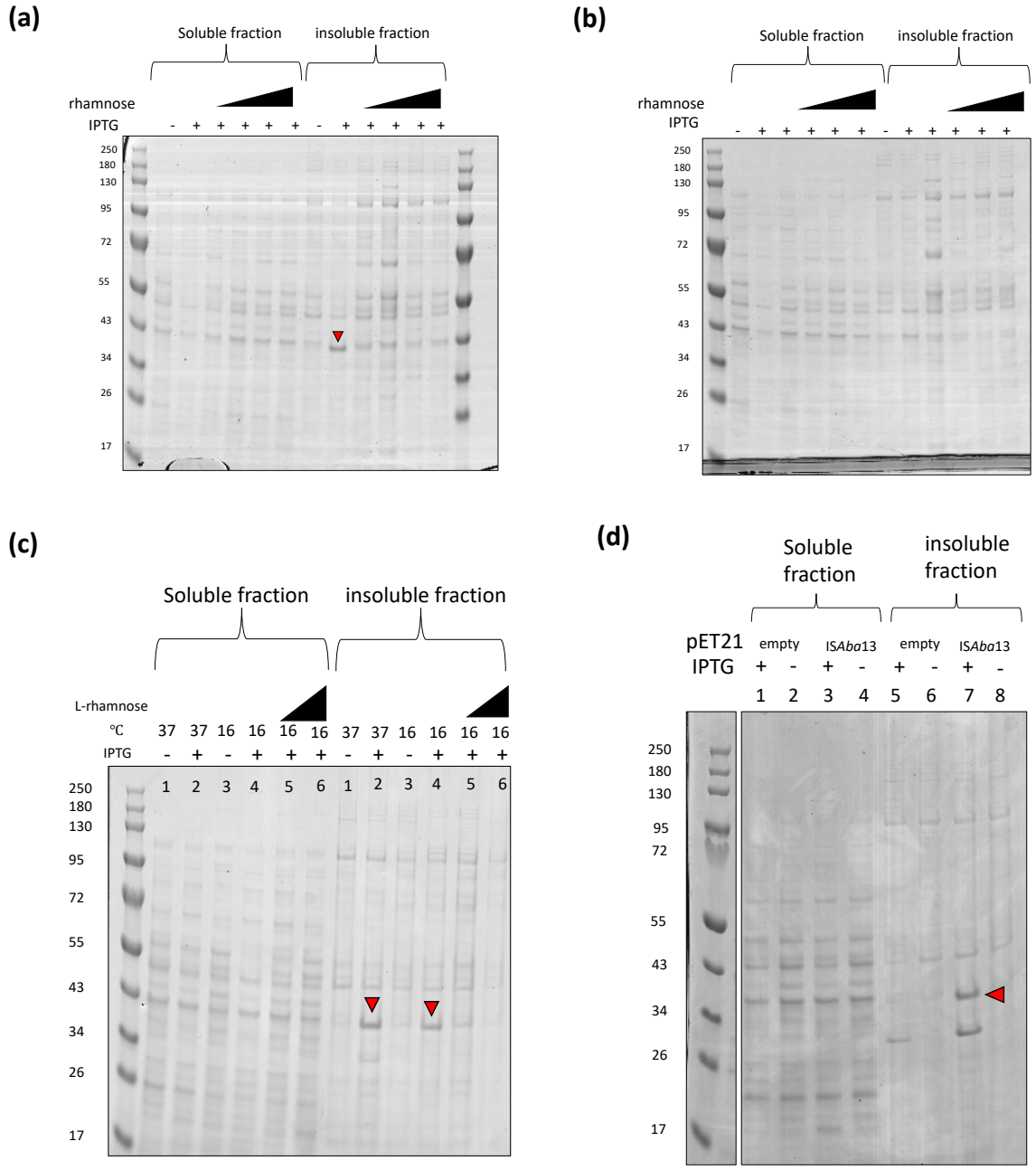

Fig.6.3. SDS-PAGE of pET21-IS*Aba*13 and pET28-IS*Aba*13 expression

Coomassie stained gel with and without IPTG induction of (a) pET21 IS*Aba*13 encoded transposase grown at 37 °C for 3 h following induction with 0, 250, 750, 1000, or 2000 mM L-rhamnose (b) pET28 IS*Aba*13 encoded transposase grown at 37 °C for 3 h following induction with 0, 250, 750, 1000, or 2000 mM L-rhamnose. (c) pET21 IS*Aba*13 encoded transposase grown at 37 °C for 5 h or 16 °C overnight following induction, with or without 100 mM or 500 mM L-rhamnose. (d) pET21 empty or pET21 IS*Aba*13 encoded transposase grown at 37 °C for 5 h.

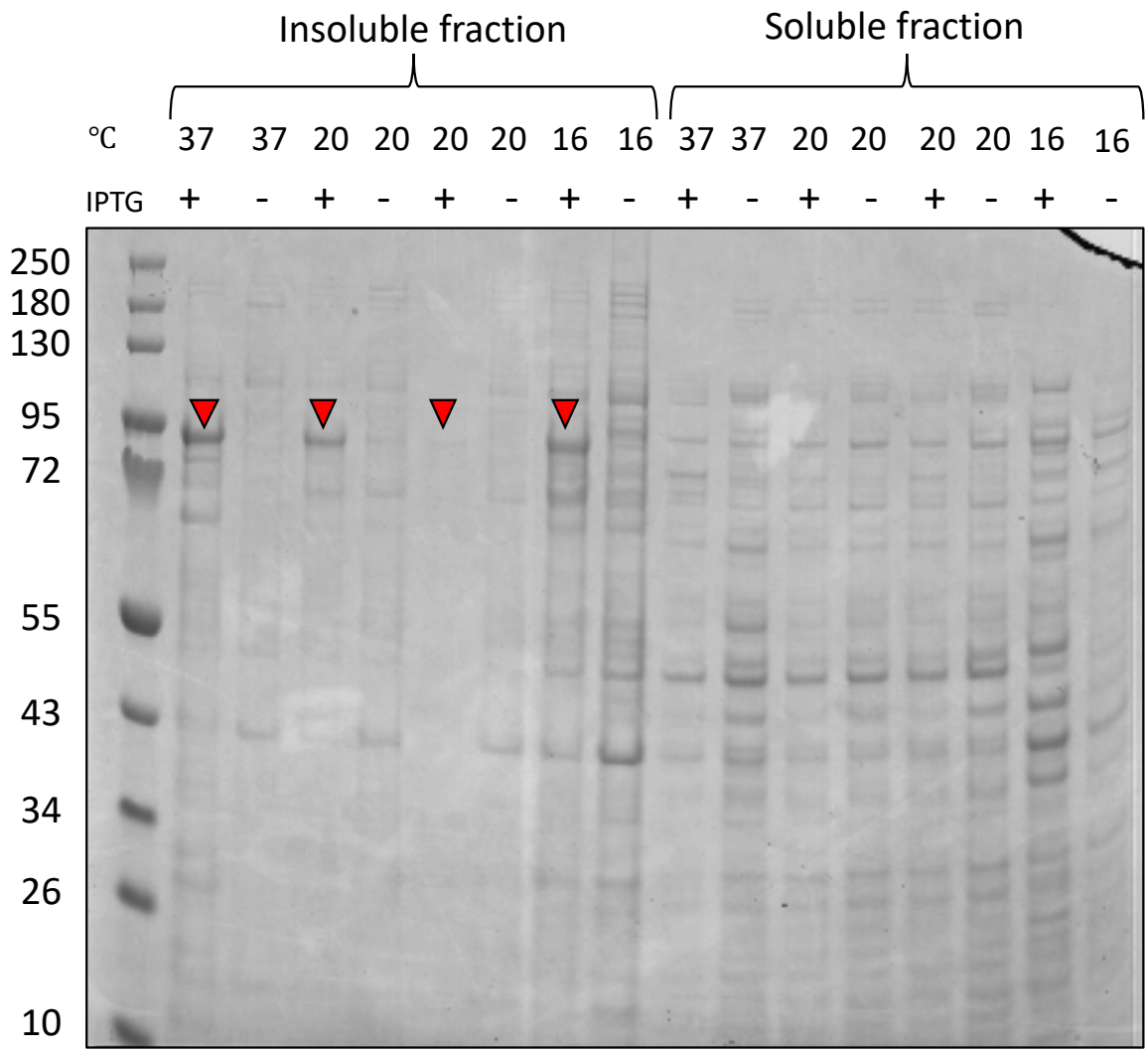

Fig.6.4. SDS-PAGE of MBP-IS*Aba*13 fusion expression
Coomassie stained gel of cells expressing MBP-tagged IS*Aba*13 encoded transposase with and without IPTG induction. Following induction, cells were grown at 37 °C for 2 h, 20 °C for 2 h or 5 h, or 16 °C overnight.

6.4. H-NS does not interact with IS*Aba*13 encoded transposase

H-NS bound at AT-rich DNA could direct transposition by capturing the transpososome. There are two models to explain how this could occur. First H-NS could directly interact with the IS*Aba*13 encoded transposase. Second, H-NS could bridge between target DNA and IS*Aba*13 DNA. To test the first model, a bacterial 2-hybrid (BACTH) assay was used. In this assay, proteins of interest are separately fused to T18 or T25 domains of adenylate cyclase. If the two proteins of interest interact in *E. coli*, the T18 and T25 domains are brought into close proximity, where they form a functional adenylate cyclase which can convert ATP into cAMP. This activates *lacZ* expression which can be quantified. All possible combinations of protein fusion were tested, including N- and C-terminal fusion of T18/T25 to IS*Aba*13 encoded transposase, and N- and C-terminal fusion of T18/T25 to H-NS. Fig.6.5a shows none of the tagged protein combinations were able to interact to reconstitute *lacZ* activity. The positive control of T25 and T18 fused to leucine zipper domains shows a large amount of activity, confirming the assay is functional. This suggests no interaction between IS*Aba*13 encoded transposase and H-NS. We also included a control of C-terminal fusions of H-NS to T18 and T25, which we expected to interact. Whilst no activity was detected in the *lacZ* assays (Fig.6.5a), colonies containing these constructs did turn blue on X-gal plates (Fig.6.5b). Such "plate-only" phenotypes have been reported previously with BACTH assays (Cosgriff *et al.*, 2010; Sobe *et al.*, 2022).

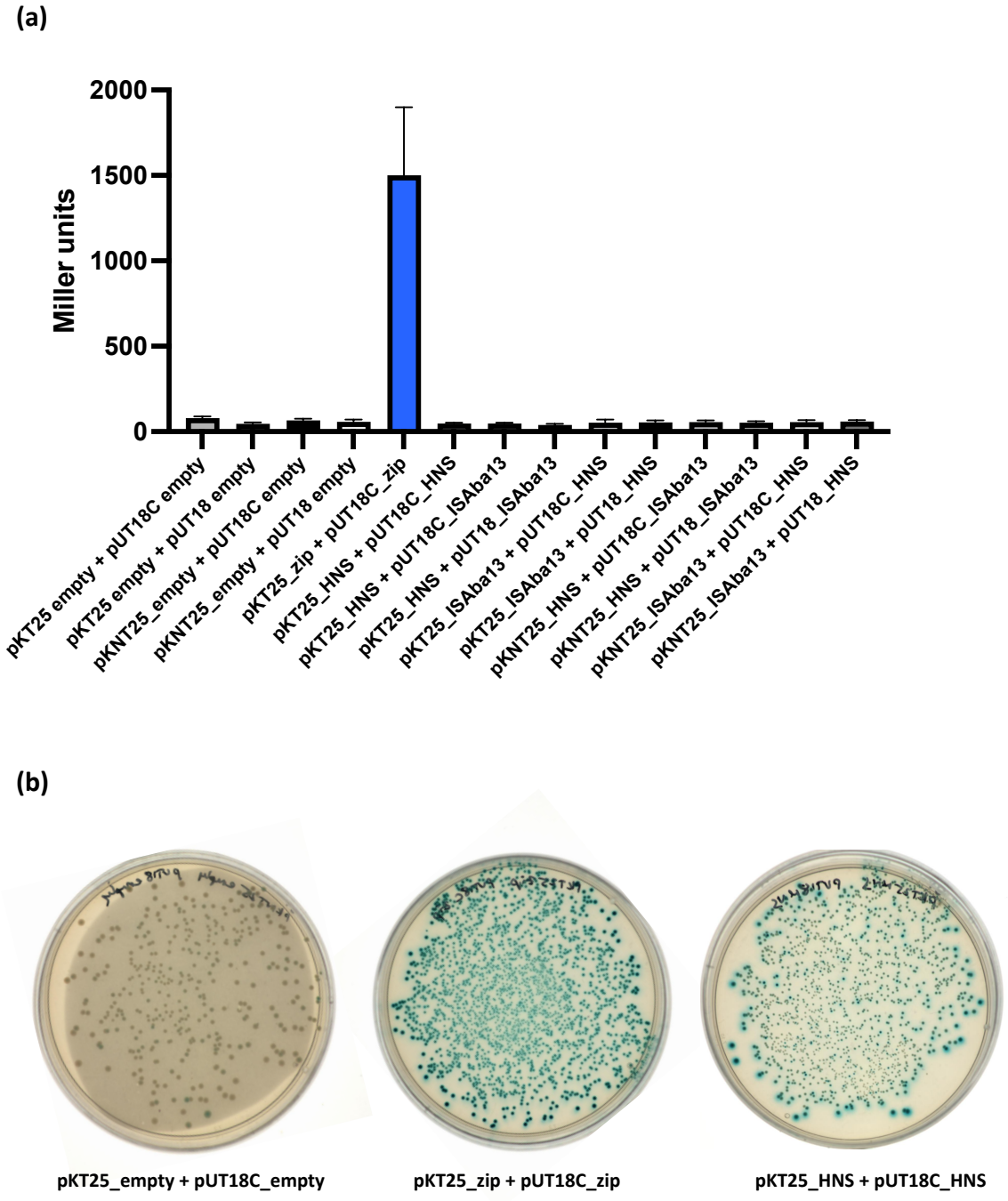

Fig.6.5. BACTH assay for H-NS and IS*Aba*13 encoded transposase

(a) *lacZ* assay for all constructs tested. Bars represent mean of three biological replicates. Error bars = standard deviation. (b) Colonies of empty plasmid negative control, leucine zipper positive control and H-NS dimer interaction on X-gal LBA after a few days of incubation at 30°C.

6.5. Purification of *A. baumannii* H-NS

To test the DNA bridging model, we purified H-NS from *A. baumannii*. An SDS-PAGE analysis of cell lysates showed expression of the 12.5 kDa H-NS protein upon IPTG induction. The protein was recovered in the soluble fraction (Fig.6.6, red arrows). Given that protein production was similar following induction for 2 h or 5 h, large scale purification was done using a 2 h induction step. The H-NS in lysates was bound to a heparin column and eluted fractions containing H-NS (Fig.6.7a) were pooled and used in cation exchange chromatography. Based on the isoelectric point of H-NS (5.33) and the pH of the buffer used (7.2), H-NS did not bind to the column whilst other proteins remained attached (Fig.6.7b). As *A. baumannii* H-NS was expressed in *E. coli* T7 Express cells, there was a possibility of cross-contamination of *E. coli* H-NS. To check for this, a sample of *E. coli* H-NS (Fig.6.7c lanes 1 and 3) was subjected to electrophoresis alongside *A. baumannii* H-NS (Fig.6.7c lanes 2, 4, 5, and 6). *E. coli* H-NS has an expected size of 15.5 kDa, and has a different migration pattern, making it easily distinguishable from the *A. baumannii* protein.

6.6. H-NS binds to IS*Aba*13 insertion hotspots *in vitro*

We chose two AT-rich DNA regions to confirm purified H-NS binding using EMSAs. The DNA fragments used each had a high density of IS*Aba*13 insertions in wild-type *A. baumannii* and a low density of IS*Aba*13 insertions in *hns*::T26 cells (Fig.6.8). The encoded genes are also known to be H-NS regulated (Eijkelkamp *et al.*, 2013; Escalante *et al.*, 2022). ChIP-seq also confirmed that these DNA regions are bound by H-NS *in vivo* (Appendix 6). The first fragment used for EMSAs was the 631 bp region preceding the gene *csuAB,* encoding the Csu major

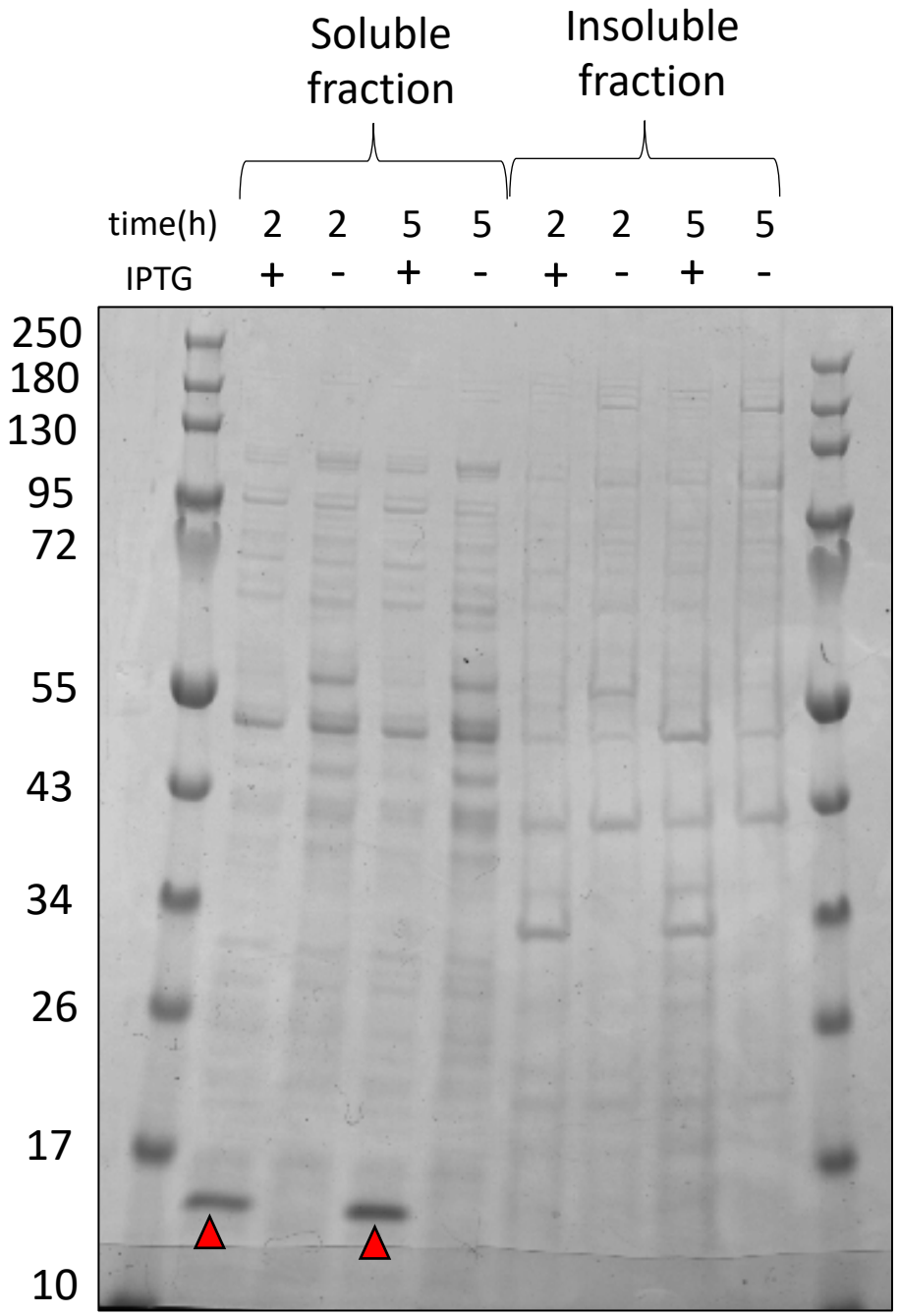

Fig.6.6. SDS-PAGE of expression of *A. baumannii* H-NS
Coomassie stained gel of cells expressing *A. baumannii* H-NS with and without IPTG induction. Following induction all cells were grown at 37 °C.

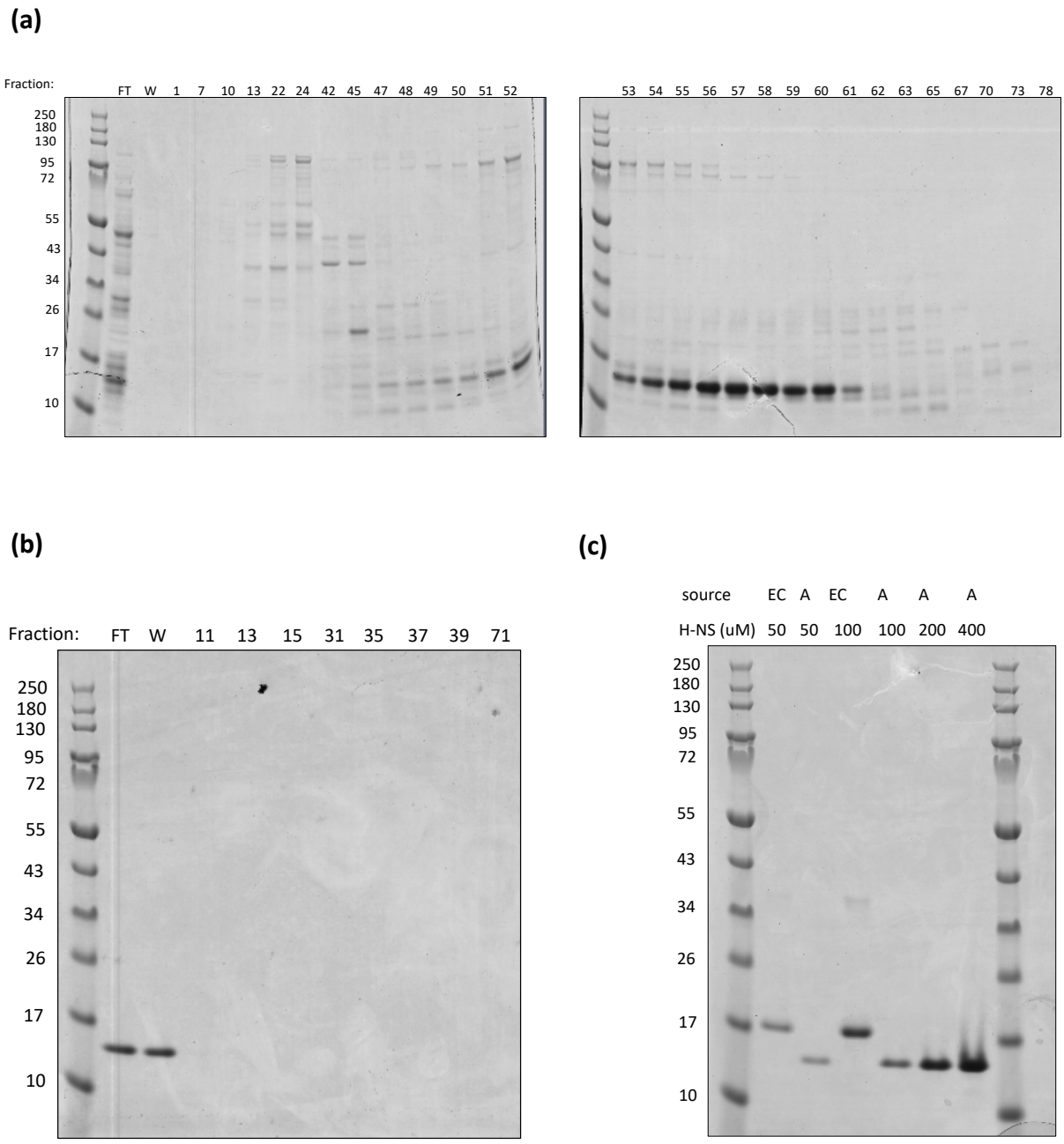

Fig.6.7. SDS-PAGE of *A. baumannii* H-NS purification

Coomassie stained gel of cells expressing *A. baumannii* H-NS. Following induction all cells were grown at 37 °C. (a) Fractions which eluted from heparin column are indicated. (b) Fractions following elution from cation exchange column. FT = flow through, W = wash. (c) Purified *A. baumannii* H-NS (source "A") compared with purified *E. coli* H-NS (source "EC").

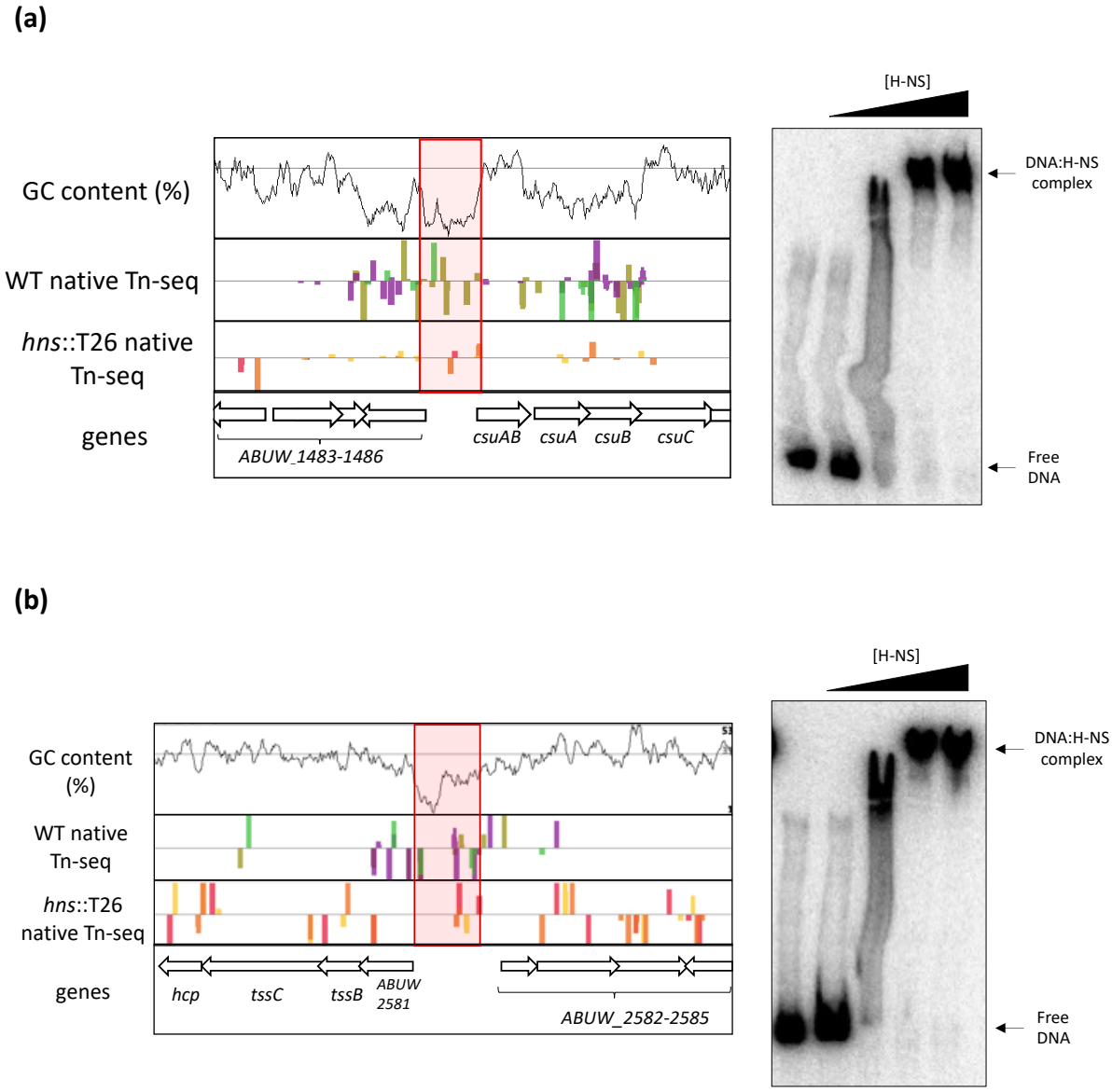

Fig.6.8. H-NS EMSA for *csuAB* and T6SS intergenic regions.
(a) *csuAB* and (b) T6SS intergenic loci. Left shows GC content, IS*Aba*13 insertions in wild-type cells and *hns*::T26 mutant and genes of associated regions. For (a) *csuAB* and (b) T6SS intergenic loci. EMSAs were done using 0, 1.25, 2.5, 5, and 10 µM purified *A. baumannii* H-NS.

fimbrial subunit (Fig.6.8a). The second fragment was the 780 bp region in front of the gene *ABUW_2581* (Fig.6.8b). This gene is annotated as a putative *yedL* acetyltransferase, however it is likely to be a signal peptide as the adjacent genes are used for the T6SS. This region is equivalent to the region of the H-NS regulated T6SS locus in ATCC 17978 (Escalante *et al.*, 2022). The EMSA for both of these regions shows that at least 2.5 µM H-NS is required to bind these DNA fragments *in vitro*.

6.7. H-NS bridges DNA *in vitro*

Next, we used DNA bridging assays to determine if H-NS could stabilise interactions between chromosomal sites and IS*Aba*13. Briefly, this assay uses radiolabelled prey DNA, and biotinylated bait DNA recoverable with streptavidin beads. If bridging between the DNA fragments occurs, a radioactive signal is evident following streptavidin mediated DNA recovery. A 1060 bp section of DNA, encompassing the entirety of IS*Aba*13, was used as bait DNA (Appendix 7). The T6SS encoding region, used in the EMSA, was radiolabelled and used as prey DNA. Samples were incubated with increasing amounts of H-NS. As seen in Fig.6.9a, As the concentration of H-NS increases, the amount of radioactivity retained, and so the amount of bridging, increases. A nearly 4-fold increase in bridging is seen between 2 µM and 4 µM H-NS ($p = 0.0134$) which reaches a maximum bridging at 6 µM ($p = 0.0001$). Hence, 6 µM H-NS was used in future assays to ensure maximal bridging.

It has previously been shown that *E. coli* H-NS bridging requires the divalent cation Mg^{2+}, reaching a maximum bridging at 8 – 10 mM of the metal (van der Valk *et al.*, 2017).

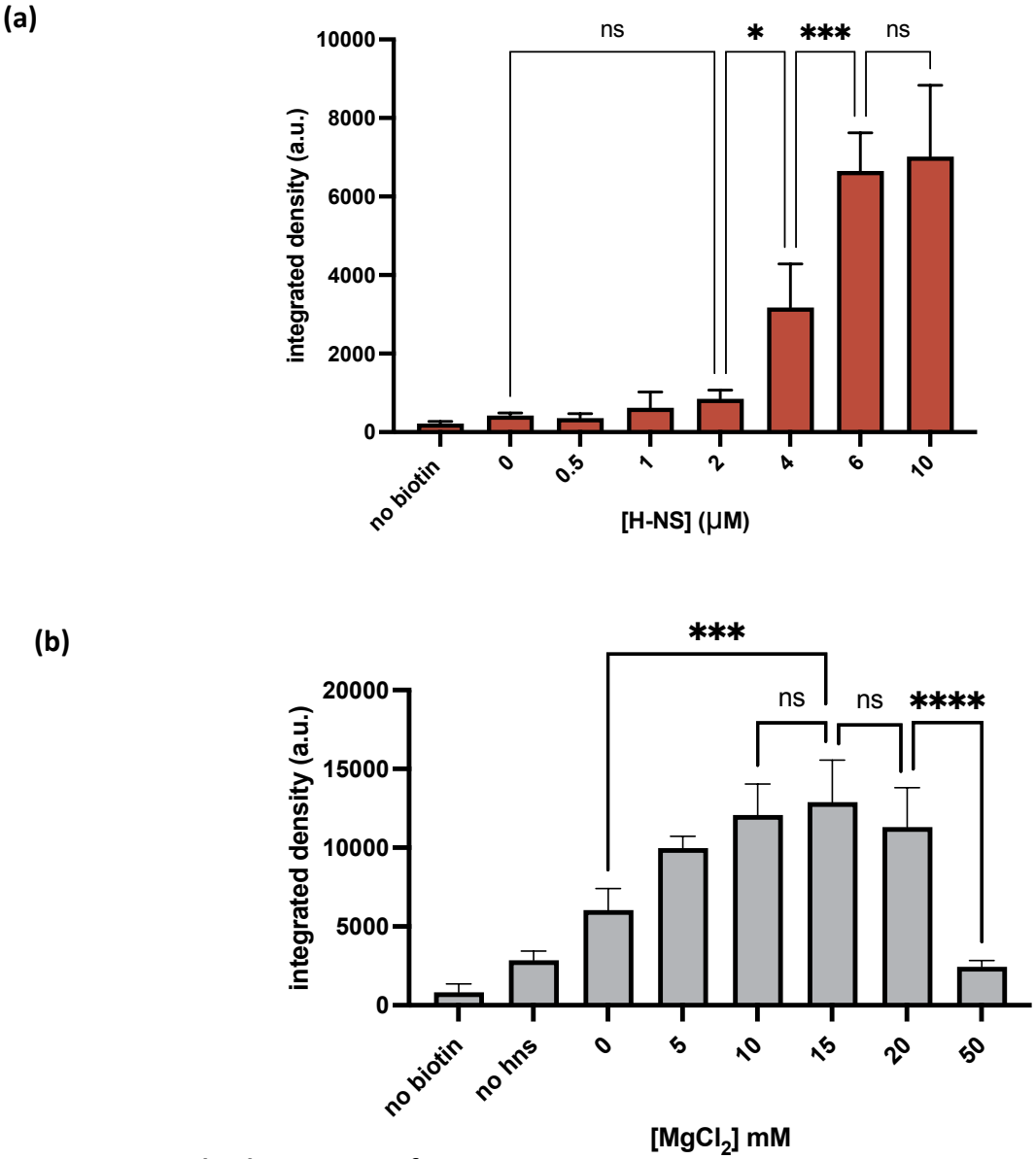

Fig.6.9. *in vitro* bridging assay of H-NS

(a) Bridging as a function of varying concentration of H-NS, 10 mM $MgCl_2$ was used in each condition. (b) Bridging as a function of varying concentration of $MgCl_2$, 6 µM H-NS was used in each condition, except in the no H-NS control. Bars represent the mean of four replicates. Error bars = standard deviation. Of note, this assay varying $MgCl_2$ used the T6SS region as both biotinylated prey and bait DNA. Statistical significance assessed by one-way ANOVA. Integrated density, the sum of values of pixels on a scanned image of an exposed phosphor screen, is calculated by circling radioactive spots and measurement using ImageJ.

Interestingly, with the *P. aeruginosa* functional homologue of H-NS (MvaT), bridging increases from 0 – 15 mM $MgCl_2$, and decreases at concentrations > 15 mM (Qin *et al.*, 2020). To show that *A. baumannii* H-NS bridging also varies with $MgCl_2$ concentration, we repeated the experiment while varying the amount of $MgCl_2$. As the concentration of $MgCl_2$ increases, from 0 mM to 15 mM $MgCl_2$, bridging doubles ($p = 0.0006$). Bridging then decreases at higher concentrations ($p < 0.0001$).

6.8. H-NS^{39aa} disrupts bridging of H-NS *in vitro*

It was previously shown that amino acids 56 – 83 of *E. coli* H-NS, comprising the site 2 domain, disrupted DNA bridging but not filamentation *in vitro* (Fig.6.10a) (van der Valk *et al.*, 2017). We repeated the bridging assay with increasing amounts of the equivalent 39 amino acid region of *A. baumannii* H-NS (H-NS^{39aa}). Fig.6.10b shows H-NS^{39aa} decreases bridging roughly 3-fold ($p < 0.0001$). H-NS^{39aa} alone cannot stimulate any DNA bridging.

6.9. H-NS^{39aa} disrupts bridging of H-NS *in vivo*

To test the effect of disrupting H-NS bridging *in vivo*, we next expressed H-NS^{39aa} from plasmid pVRL1Z and repeated the native Tn-seq assay. As a negative control we used *A. baumannii* harbouring an empty pVRL1Z plasmid. The results are shown as heatmaps in Fig.6.11, alongside ChIP-seq data for H-NS. In the strain with pVRL1Z encoding H-NS^{39aa}, IS*Aba*13 insertion at H-NS bound DNA is reduced compared to the strain with the empty plasmid, and there is a more even distribution of insertions, similar to the *hns*::T26 mutant (Fig.6.2a). Also note, that with expression of H-NS^{39aa}, increased insertion around the DNA replication

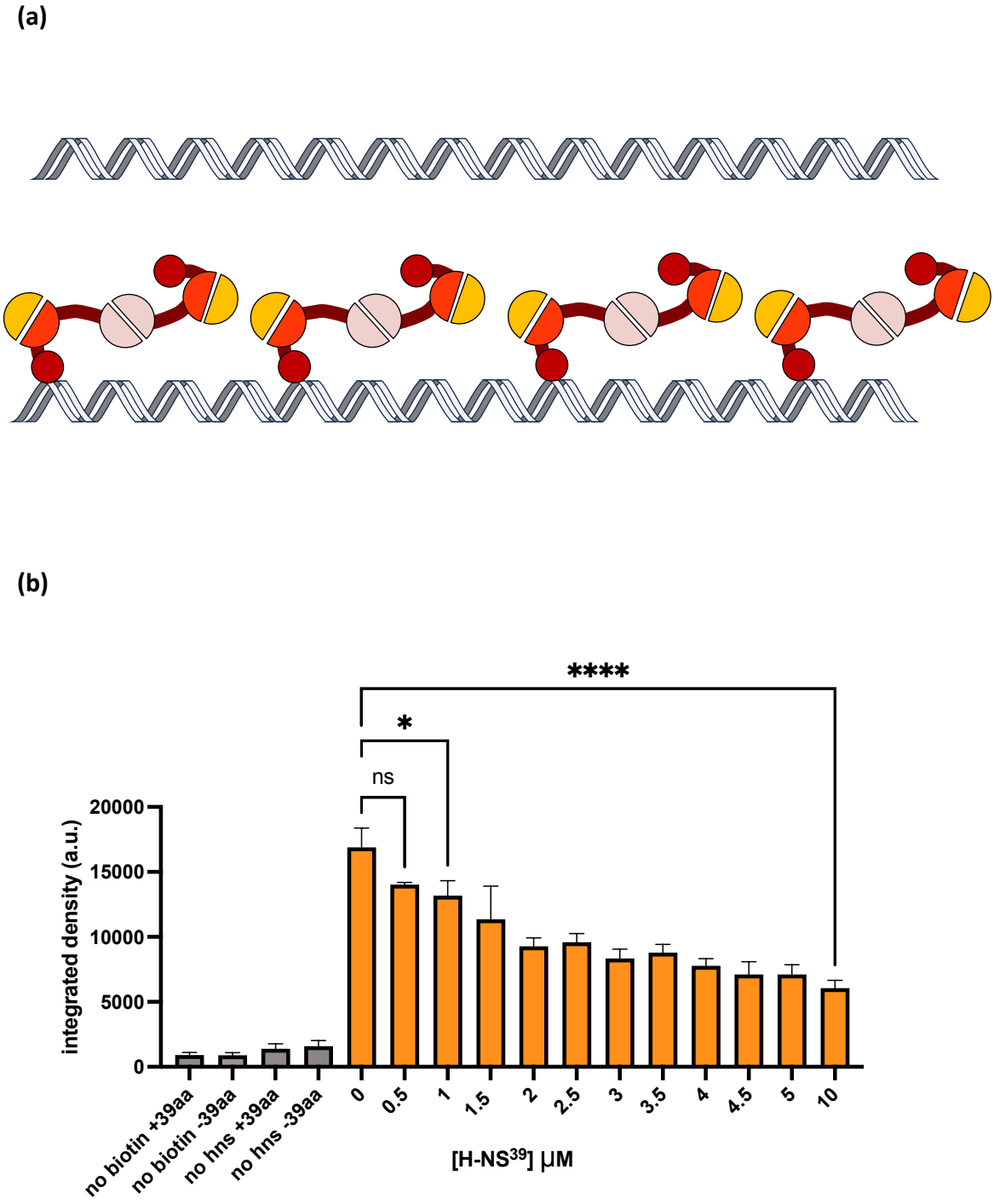

Fig.6.10. *in vitro* bridging assay of H-NS with H-NS^{39aa}
(a) Cartoon schematic showing the impact on bridging of targeting the site 2 domain of H-NS. Orange semi-circle represents H-NS^{39aa}. (b) *in vitro* bridging assay with varying amounts of H-NS^{39aa}. $MgCl_2$ concentration of 10mM and 6µM H-NS used throughout except in no H-NS controls. Bars represent the mean of four replicates, error bars = standard deviation. Statistical significance assessed by one-way ANOVA.

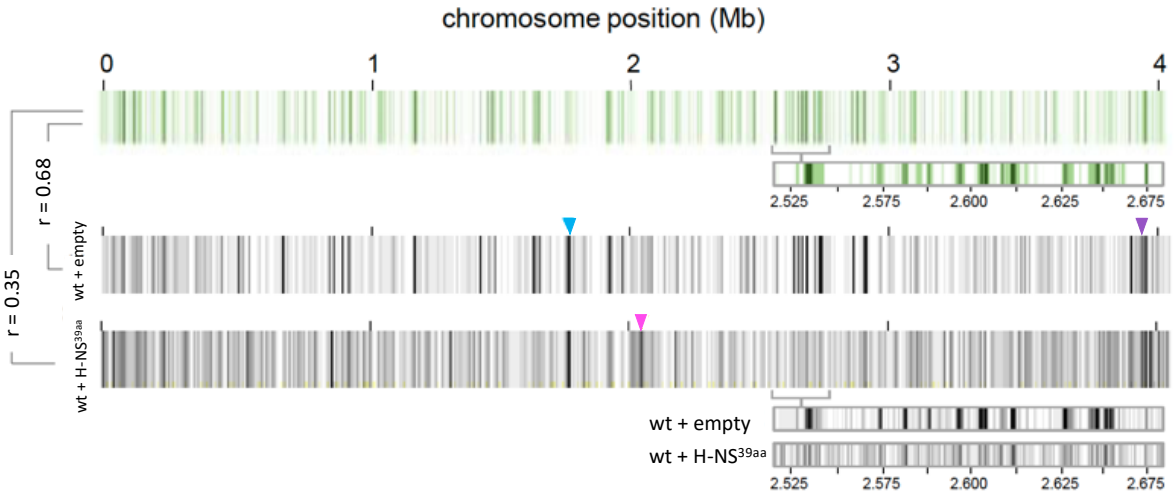

Fig.6.11.Native Tn-seq with wild-type cells expressing H-NS^{39aa}

Green heat map shows H-NS ChIP-seq binding profile binned into 1 kb regions across the chromosome. Darker regions indicate greater degree of H-NS binding. Black heat maps indicate sites of IS*Aba*13 insertion binned into 1 kb regions across the chromosome. Darker regions indicate greater frequency of IS*Aba*13 insertions. Blue and purple arrows show the position of the two starting native copies of IS*Aba1*3. Pink arrow shows site of chromosomal terminus.

terminus was observed, similar to our observations with the *hns* mutant (Fig.6.11 pink arrow). The correlation between sites of H-NS binding and transposition is greater for the strain containing the empty plasmid (r = 0.68) compared to the strain expressing H-NS^{39aa} (r = 0.35).

6.10. H-NS^{39aa} does not inhibit H-NS binding to DNA

Given that H-NS^{39aa} targets only the H-NS multimerization domain, H-NS should remain able to dimerise and bind DNA. To show this, we repeated the EMSA analysis of the T6SS DNA fragment used above, including the H-NS^{39aa} peptide. Fig.6.12a shows that H-NS^{39aa} cannot bind DNA nor perturb DNA binding by wild-type H-NS. This is confirmed *in vivo* by ChIP-seq data; patterns of H-NS binding are almost identical with and without H-NS^{39aa} expression (Fig.6.12b, r = 0.99). Taken together, these data show that H-NS^{39aa} does not affect the ability of H-NS to bind DNA but does affect the ability of H-NS to bridge DNA, changing the profile of IS*Aba*13 insertion targeting.

6.11. Discussion

The role of chromosome folding proteins in promoting transposition, including H-NS, IHF, Fis, HU, StpA and Dps has previously been investigated (Swingle et al., 2004). Notably, H-NS was the only nucleoid protein essential for efficient transposition of IS903, Tn10 and Tn552, all of which transpose via different mechanisms (Swingle et al., 2004). H-NS has been shown to bind strongly to the unfolded form of the Tn10 transpososome, stabilizing it via direct interaction with the transposase (Ward *et al.*, 2007; Wardle, Chan and Haniford, 2009). This further

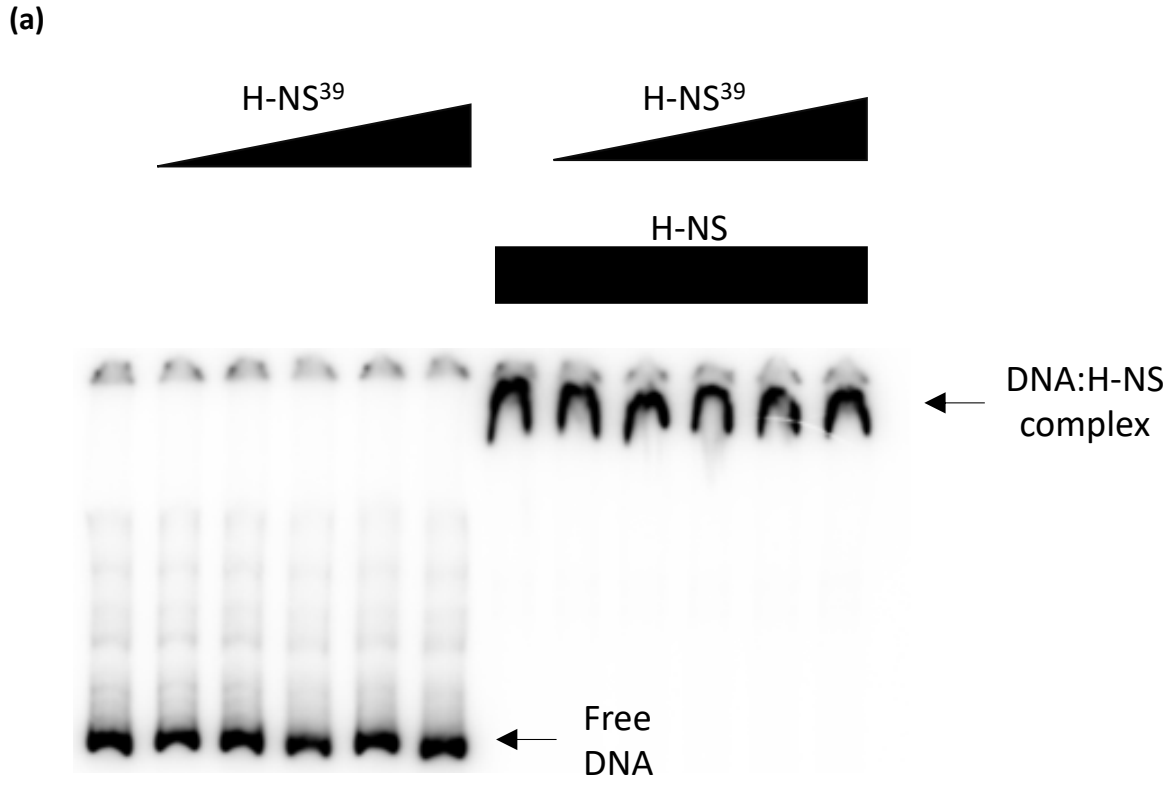

Fig.6.12. H-NS^{39aa} does not impair H-NS binding to DNA
(a) EMSAs were done using 0, 1, 2, 4, 6 and 10 µM H-NS^{39} peptide and where purified *A. baumannii* H-NS was used, this was at a concentration of 6 µM. (b) Heat maps show H-NS binding of regions across the chromosome which are divided into 1 kb sections, in the absence and presence of H-NS^{39aa}.

extends to the Tn5 composite transposon, with H-NS promoting transpososome formation (Whitfield, Wardle and Haniford, 2009). Interestingly, data also suggest Hha, which stabilises H-NS binding, and increases DNA bridging, promotes transposition of IS1, IS5 and IS10 in a concentration-dependent manner (Mikulskis and Cornetis, 1994; van der Valk *et al.*, 2017). H-NS has been shown to promote transposition of IS1 indirectly, with loss of H-NS decreasing transposase levels (Rouquette, Serre and Lane, 2004). In our native Tn-seq experiment comparing wild-type and the *hns* mutant, target preference for transposition is changed (Fig.6.2a, Fig.6.2b) but the total number of transposition events does not decrease (Fig.6.2c). This suggests the overall transposition efficiency is not modified, as would be the case with IS1.

Preferential targeting of the IS5 family has been noted before, with hotspots of insertion into superhelical stress-induced duplex destabilization (SIDD) regions which have high AT-content, and are likely to bind H-NS (Humayun *et al.*, 2017). For the IS5 family member IS903 in *E. coli,* the deletion of H-NS was shown to modify target preference, drastically reducing insertion into hot spots (Swingle *et al.*, 2004). Given that H-NS is normally considered an exclusionary factor - for example occluding RNAP (Singh and Grainger, 2013), the authors proposed that H-NS bound regions could occlude IS903 transposition (Swingle *et al.*, 2004). The data that Swingle *et al* acquired is consistent with our data, as the hotspots observed do correspond to H-NS bound regions, though they could not have known, as genome wide H-NS ChIP-seq data was not available at the time. Additionally, while H-NS has been shown to occlude the mariner transposon in *V. cholerae*, this is a eukaryotic transposon, with a stringent requirement for insertion into TA dinucleotides, that are sequestered by H-NS (Kimura *et al.*, 2016). Target

capture by H-NS could occur either through stabilizing binding of the transpososome, or increasing DNA accessibility by forming looped out segments of DNA, attractive for insertion (Swingle *et al.*, 2004). Both of these mechanisms could be explained by the propensity for H-NS to undergo DNA bridging. Recently, it was proposed that bridging by MucR, the nucleoid associated silencer of *Sinorhizobium fredii,* is important for targeting IS5 family insertions into AT-rich DNA (Guo *et al.*, 2023).

For the IS5 family member IS*Aba*13, investigated in this study, we have shown that DNA bridging by H-NS, bound at AT-rich DNA, is important for target capture. There are three potential models, which are not mutually exclusive, to explain this: H-NS could interact with the transposase protein, bridge DNA between the transpososome and the site of insertion, or create attractive sites for insertion of IS*Aba*13 by local DNA looping and bending (Fig.6.13). Given the importance of DNA bridging, and the lack of evidence of an interaction between H-NS and IS*Aba*13 using the BACTH assay (Fig.6.5), the first model is unlikely. However, it is important to note that the BACTH assay is done in *E. coli*. The IS*Aba*13 transposase ORF is fused to the adenylate cyclase domain, omitting the presence of the inverted repeats required for transposase binding, so no transpososome structure is formed. It may be that conformational changes following transpososome formation are necessary for a protein interaction between H-NS and IS*Aba*13. For the second model, H-NS could also bridge between target DNA and the native IS*Aba*13 copies prior to excision, rather than as part of the transpososome, bringing the target site into close proximity to where transposase is synthesised. However, 3C-seq analysis of *A. baumannii* (Rachel Hoare, unpublished data) show few interactions between native copies of IS*Aba*13 and other parts of the chromosome

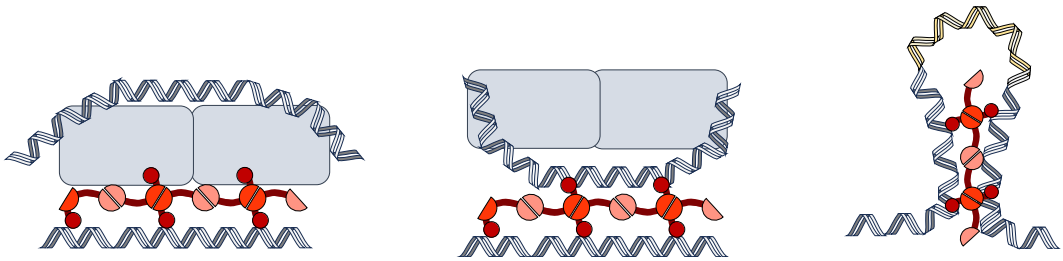

Fig.6.13. Potential models for how H-NS directs transposition
Left: H-NS bound to target DNA interacts with the transpososome via direct protein-protein interaction to IS*Aba*13 transposase. Middle: H-NS bound to target DNA interacts with the transpososome by bridging to excised IS*Aba*13 DNA. Right: H-NS bound to target DNA creates a loop of bent DNA. Yellow DNA highlights region made more accessible for transposition.

(Appendix 8). Although we successfully purified *A. baumannii* H-NS and show it can bind AT-rich DNA *in vitro*, a limitation of the EMSA experiment (Fig.6.8) is the omission of a non-binding DNA control (such as a GC-rich fragment), to confirm that purified H-NS does not bind any DNA fragment promiscuously. Additionally, while the *in vivo* data supports a role for bridging in directing transposition to H-NS bound regions (Fig. 6.11), a Western blot should be done to confirm expression of the H-NS^{39aa} peptide.

The role of chromosomal proximity in directing transposition is still a question to be explored. Tn7 and IS903 in *E. coli,* and Tn917 in *E. faecalis* and *B. subtilis* show a preference for insertion into sites of replication termination, where regions of dsDNA breakage are prominent (Peters and Craig, 2000; Garsin *et al.*, 2004; Swingle *et al.*, 2004). The preference for insertion into the chromosomal terminus in the absence of H-NS directed targeting (Fig.6.2a, Fig.6.11) could be explained by an underlying regional preference of IS*Aba*13. Future work will also require purification of IS*Ab*a13 encoded transposase in order to fully understand the mechanism of H-NS directed targeting. Potential solubility tags to test include green fluorescent protein (GFP), Small Ubiquitin-lilke Modifier (SUMO), or Glutathione-S-transferase (GST). These have been used successfully with IS2 and Tn7 (Lewis *et al.*, 2011; Hennig *et al.*, 2017; Kaczmarska *et al.*, 2022). Alternatively, *in vitro* transcription-translation of transposase may avoid protein toxicity effects, and allow environmental conditions to be modified for enhanced solubility (Iskakova *et al.*, 2006).

Given that H-NS typically binds at intergenic regions, a further mechanism of transcriptional control mediated by H-NS may be protection of highly transcribed genes by diverting

transposition away from intragenic regions. Exclusion of Mu transposition into highly transcribed operons has been noted before in *S. enterica* and *E. coli* (Manna *et al.*, 2007). Additionally, H-NS mediated targeting of IS*Aba1*3 may represent another level at which H-NS can silence the expression of horizontally acquired DNA, and prevent spurious transcription (Singh *et al.*, 2014). Plasmids and bacteriophage DNA are frequently AT-rich and may represent prospective hotspots for insertion (Daubin, Lerat and Perrière, 2003). Directed transposition into plasmids could serve as a mechanism of spreading IS*Aba*13 into new hosts. Whereas, directed transposition into prophages (which make up a significant portion of *Acinetobacter* genomes) could inactivate them and protect the cell by preventing lysis (Touchon *et al.*, 2014). This could be particularly important in the context of stressful conditions such as antibiotic treatments, which promote phage lysis and transposition (Torres-Barceló, 2018; Penesyan *et al.*, 2019). Finally, because H-NS has a pivotal role in targeting IS*Aba*13, yet the *hns* gene itself is a target of IS*Aba*13 (Fig.5.8) this raises an interesting possibility. If IS*Aba*13 inserts into *hns* inactivating it, this cell may then undergo an evolutionary trajectory of more widespread transposition, with insertions into rarer locations with various consequences.

Chapter 7: Final discussion

A. baumannii is a highly concerning opportunistic pathogen, resistant to multiple antibiotics and able to persist on hospital surfaces and equipment for extended periods of time (Espinal, Martí and Vila, 2012). The ability of *A. baumannii* to adapt to specific niches can be attributed to its genetic malleability; the ability to acquire new genes and undergo frequent genome mutations and rearrangements (Zhu *et al.*, 2013; Touchon *et al.*, 2014).

In this study we identified an *A. baumannii* atypical colony morphology on agar plates. Long read genome sequencing determined that this resulted from insertion of IS*Aba*13, an IS5 family insertion sequence, into the K-locus of grey colonies. This insertion was shown to affect multiple clinically relevant phenotypes. Grey colonies made less capsule, were less motile, more susceptible to gentamicin, showed reduce tolerance to desiccation, had slower growth in human serum, and had an increased capacity to form biofilms. In an abiotic environment where biofilm formation is favourable, it may be advantageous for cells to reduce capsule production via this mechanism. Mutations of K-locus genes, including IS-mediated disruption, frequently provide resistance to bacteriophages (Gordillo Altamirano *et al.*, 2021; Bai *et al.*, 2023). Exploring how IS*Aba*13 disruption of *gtr52* in AB5075 could confer phage resistance will require isolation of a phage unaffected by the VIR-O to AV-T switch.

Using RNA-seq, we were able to show how IS*Aba*13 insertion blocks transcription of the capsule synthesis operon, preventing the expression of adjacent genes. Additionally, Cappable-seq revealed the lack of a leader sequence of IS*Aba*13 transposase, suggesting poor translation may be a method to limit its levels in the cell (Nagy and Chandler, 2004). The impediment to transcriptional readthrough is not dependent on orientation of IS*Aba*13, and

in vitro and *in vivo* data point towards a Rho-dependent mechanism of transcriptional termination. Additionally, we discovered the first example of a bidirectional promoter residing with an IS, with the potential to couple expression of the IS*Aba*13 transposase to outward transcription of adjacent DNA.

Surprised by the wide range of phenotypes affected by a single insertion event, we developed a novel sequencing method, called native Tn-seq, to enable us to map other sites of IS*Aba*13 insertion across the genome and population. We analysed the potential phenotypic impact of inactivation of three genes targeted by IS*Aba*13 and show inactivation of *hns* results in increased susceptibility to gentamicin and zeocin, impaired growth, and increased biofilm formation at room temperature. Hotspots of IS*Aba*13 insertion strongly correlated with AT-rich regions which were also shown to bind H-NS, suggesting a crucial role for H-NS in directing transposition. We showed that H-NS was essential for targeted transposition, and that disruption of the DNA bridging ability of H-NS impairs target preference of IS*Aba*13.

Purifying the IS*Aba*13 encoded transposase will be essential in order to better characterise its mechanism of action and to fully reconstitute the proposed DNA bridging complex involving H-NS, the transposase and DNA *in vitro*. Purified transposase would also enable DNase footprinting and EMSAs to see which bases are critical for transposase binding and help elucidate the requirements for IS*Aba*13 transposition, very little of which is currently known. Further future work will focus on identifying the impact of insertion of IS*Aba*13 into other targets. This encompasses both phenotypic effects from inactivation of the gene, as well as transcriptional effects on adjacent genes (both upregulation and downregulation). It may be

that adjoined to certain locations in the genome, the bidirectional transcriptional activity of IS*Aba*13 can be increased (e.g. if the resulting RNA is translated). Particularly intriguing are the potential roles of H-NS in targeting ISs to horizontally acquired DNA, which frequently encodes pathogenicity traits, antibiotic resistance determinants and virulence factors (Schmidt and Hensel, 2004). How this may modulate survival in nosocomial environments, and in the context of human infection remains to be investigated. There has been substantial proliferation of IS*Aba*13 in the hypervirulent hospital outbreak isolate LAC-4, which contains 22 copies of IS*Aba*13 that mostly reside within prophage and cell-surface related genes (Ou *et al.*, 2015). A further direction to explore is the role of H-NS in directing transposition of ISs in other bacteria, as well as the role of other chromosome folding proteins in transposition and the role of chromosome proximity on directing transposition.

Appendices

Appendix 1: Code for differential gene expression analysis written by Dr. David Forrest

```
#code written by Dr. David Forrest

```{r setup, include=FALSE}
knitr::opts_chunk$set(echo = TRUE)
```

######################### Determining differential expression
######################

We have the BAM files so we can use feature counts and edgeR to determine fold
changes:

```{r}
setwd("C:/Users/foz_2/Acinetobacter/Acinetobacter_RNA/BAM_alignments/")

library(Rsubread)
library(dplyr)
library(edgeR)
library(ggplot2)

O_a_RNAseq <-
featureCounts(files="O_a_RNAseq.bam",annot.ext="CP0008706.1.GTF",isGTFAnnotation
File=TRUE,GTF.featureType="gene",GTF.attrType="Name")
O_b_RNAseq <-
featureCounts(files="O_b_RNAseq.bam",annot.ext="CP0008706.1.GTF",isGTFAnnotation
File=TRUE,GTF.featureType="gene",GTF.attrType="Name")
T_a_RNAseq <-
featureCounts(files="T_a_RNAseq.bam",annot.ext="CP0008706.1.GTF",isGTFAnnotation
File=TRUE,GTF.featureType="gene",GTF.attrType="Name")
T_b_RNAseq <-
featureCounts(files="T_b_RNAseq.bam",annot.ext="CP0008706.1.GTF",isGTFAnnotation
File=TRUE,GTF.featureType="gene",GTF.attrType="Name")

### Just need to select the information we want and rename the columns.

O_a_counts <- cbind(O_a_RNAseq$annotation, O_a_RNAseq$counts)
O_a_counts <- O_a_counts[,c(1,7)]
colnames(O_a_counts) <- c("GeneID", "counts")

O_b_counts <- cbind(O_b_RNAseq$annotation, O_b_RNAseq$counts)
O_b_counts <- O_b_counts[,c(1,7)]
colnames(O_b_counts) <- c("GeneID", "counts")

T_a_counts <- cbind(T_a_RNAseq$annotation, T_a_RNAseq$counts)
T_a_counts <- T_a_counts[,c(1,7)]
colnames(T_a_counts) <- c("GeneID", "counts")

T_b_counts <- cbind(T_b_RNAseq$annotation, T_b_RNAseq$counts)
T_b_counts <- T_b_counts[,c(1,7)]
colnames(T_b_counts) <- c("GeneID", "counts")
```
```

```
setwd("C:/Users/cxc1036/Acinetobacter/edgeR/")

write.table(O_a_counts, "O_a_counts.csv", sep=",")
write.table(O_b_counts, "O_b_counts.csv", sep=",")
write.table(T_a_counts, "T_a_counts.csv", sep=",")
write.table(T_b_counts, "T_b_counts.csv", sep=",")


setwd("C:/Users/cxc1036/Acinetobacter/edgeR/")

readDGE <- c("O_a_counts.csv", "O_b_counts.csv", "T_a_counts.csv",
"T_b_counts.csv")
counts_combined <- readDGE(readDGE, columns = c(1,2), group = c(1,1,2,2),
sep=",")
DGE_list <- DGEList(counts_combined, group = c(1,1,2,2))
Y <- estimateDisp(DGE_list)
exact_test <- exactTest(Y)
O_vs_T_RNAseq <- exact_test
write.table(exact_test, "O_vs_T_RNAseq.csv", sep = ",")


O_vs_T_RNAseq$table$log10_Pvalue <- -log10(O_vs_T_RNAseq$table$PValue)

#selecting the genes which have interesting differential expression

O_vs_T_upregulated <- filter(O_vs_T_RNAseq$table, logFC >= 2, PValue <= 0.05)
O_vs_T_upregulated$Differential_expression <- "upregulated"

O_vs_T_downregulated <- filter(O_vs_T_RNAseq$table, logFC <= -2, PValue <= 0.05)
O_vs_T_downregulated$Differential_expression <- "downregulated"

#Combining the up and down expressed together. this table will show you those
genes of interest

O_vs_T_differentially_expressed <- rbind(O_vs_T_upregulated,
O_vs_T_downregulated)

ggplot(O_vs_T_RNAseq$table, aes(x = logFC, y = log10_Pvalue)) + geom_point() +
geom_point(data = O_vs_T_differentially_expressed, aes(col =
Differential_expression)) + labs(title = "Opaque vs Grey Differential Gene
Expression") + scale_color_manual(values = c("blue", "red")) +
theme(panel.border = element_blank(), panel.grid.major =
element_blank(),panel.grid.minor = element_blank(), axis.line =
element_line(colour = "black"), axis.text = element_text(size = 12))

setwd("C:/Users/cxc1036/Acinetobacter/edgeR/")

ggsave(filename = "O_vs_T_RNAseq_volcano.png",
       plot = last_plot(),
       width = 12.78,
       height = 8.94,
       device='png',
       dpi=1500)


```

```{r setup, include=FALSE}
```

Appendix 2: Code for determining TSSs written by Dr. David Forrest and Zuzana Palečková

```
# 11. May 2021, Zuzana Palečková, Cappable-Seq Template

# Original code was written by Dr. David Forrest and adjusted by Zuzana
Palečková

# R Packages

library(tidyverse)
library(dplyr)
library(plyr)

################################################
#### PLEASE FILL IN PRIOR TO STARTING THE CODE ####
################################################


######################
#### 1. Directories ####
######################

# 1. In this code, the following files will be stored to your computer. Please
fill in the location where you would like to store them on your computer.

# Example:

# CapSeqTSS <- ""/Users/cxc1036/Downloads/R/Cappable-seq""


# - List of Transcription Start Sites (TSSs) - a file per sample
dir_TSSs <- "/Users/cxc1036/Downloads/R/Cappable-seq/CapSeqTSS"

# - List of TSSs containing TSS for each replicate per treatment and TSSs they
share
dir_sharedTSSs <- "/Users/cxc1036/Downloads/R/Cappable-seq/CapSeqTSS"



# 2. Location of the folder where the files you are loading into R are stored.
dir_cov <- "/Users/cxc1036/Downloads/R/Cappable-seq"

#######################################
#### 2. Input Raw Data File Extension ####
#######################################

# Write down the extension of your input raw files for e.g. if you wish to
import a a text file, write:

# ext <- ".txt"

ext <- ".txt"
```

```
################################################
#### 3. Strand, Treatment and Replicate Labels ####
################################################

# Fill in how your strand, treatment and replicates are named in your file names
# E.g. in file name "min_delta_a_test.txt", strand is denoted as "min",
treatment as "delta" and replicate as _a_. All strand, treatment and replicate
types should be mentioned in the vectors below. ***Make sure the name is unique,
using only "a" for replicate for e.g. is not unique, as a is also present in
"delta".

# fill in strand labels in this order:



# c("positivestrandlabel", "negativestrandlabel")
strand <- c("plus", "negative")

treatment <- c("O", "T")
# number of elements in vector must correspond to number of treatments

replicates <- c("A", "B")
# number of elements in vector must correspond to number of replicates in
experiment


# IF UNSURE ABOUT THE FILE NAMES, RUN THE myFiles CODE BELOW, THEN TYPE myFiles
INTO THE CONSOLE AND IT WILL SHOW YOU THE NAMES OF ALL FILES.
myFiles <- list.files(path=dir_cov,
                      pattern = ext)

#############################################################################
#############################################################################
#### NOW YOU MAY RUN THE ENTIRE CODE FROM HERE TO THE BOTTOM OF THE SCRIPT ####
#############################################################################
#############################################################################

setwd(dir_cov)

myFiles <- list.files(path=dir_cov,
                      pattern = ext)

files_ls <- list()

for (i in 1:length(myFiles)) {

  filename <- myFiles[i]

  filename2 <- str_remove(filename, ext)

  files_ls[[filename2]] <- assign(filename2, read.delim(filename,
                                                        header = FALSE))
}

myFiles <- str_remove(myFiles, ext)
```

```
#######################
#### Isolating TSSs ####
#######################

setwd(dir_TSSs)

TSS_ls <- list()

for(i in 1:length(myFiles)) {

  filename <- myFiles[i]

  if((grepl(strand[1], filename) == TRUE)) {

    name3 <- str_glue(filename, "_new")

    TSS_ls[[name3]] <- assign(name3, (files_ls[[i]] %>%
                                        mutate(NewCol = ifelse(lag(V3*3) < V3 &
V3 >= 4, "yes", "no")) %>% filter(NewCol == "yes")))

    mat = TSS_ls[[i]]

    form = sprintf('%s.csv', filename)

    write.csv(mat, file = form)

  }

  else if((grepl(strand[2], filename) == TRUE)) {

    name3 <- str_glue(filename, "_new")

    TSS_ls[[name3]] <- assign(name3, (files_ls[[i]] %>%
                                        mutate(NewCol = ifelse(lead(V3*3) < V3 &
V3 >= 4, "yes", "no")) %>% filter(NewCol == "yes")))

    mat = TSS_ls[[i]]

    form = sprintf('%s.csv', filename)

    write.csv(mat, file = form)

  }
}
```

```
####################################
#### Compiled Replicate CSV Files ####
####################################

setwd(dir_sharedTSSs)

lengths <- lapply(TSS_ls, nrow)

longest <- as.data.frame(which.max(lengths))

longest_nrow <- nrow(TSS_ls[[longest[1,1]]])



replicates_ls <- list()

ma <- matrix(, nrow = longest_nrow, ncol = length(replicates) + 1)


for(s in 1:length(strand)) {

  for(t in 1:length(treatment)) {

    replicates2 <- which((grepl(treatment[t], myFiles)) & grepl(strand[s],
myFiles))

    for(r in 1:length(replicates)) {

      idx <- which(grepl(replicates[r], myFiles[replicates2]))

      for(m in 1:nrow(ma)) {

        ma[m,r] <- (TSS_ls[[replicates2[idx]]])[m,2]

      }

    }

    name4 <- str_glue(strand[s], treatment[t], .sep = "_")

    replicates_ls[[name4]] <- assign(name4, ma)

  }
}

shared_ls <- list()
```

```
for(d in 1:length(replicates_ls)) {
  ma <- replicates_ls[[d]]
  for(i in 1:nrow(ma)) {
    shared <- which(ma[i,1] == ma)
    if(length(shared) == (ncol(ma) - 1)) {
      ma[i,(ncol(ma))] <- ma[i,1]
    }
  }
  ma2 <- na.omit(ma[,length(replicates)+1])
  ma[,length(replicates)+1] <- NA
  for(i in 1:length(ma2)) {
    ma[i,length(replicates)+1] <- ma2[i]
  }
  shared_ls[[(names(replicates_ls))[d]]] <- ma
  mat = shared_ls[[d]]
  form = sprintf('%s.csv', (names(replicates_ls))[d])
  write.csv(mat, file = form)
}
```

Appendix 3: SNPs identified in VIR-O and grey cells

SNP analysis by Varscan. Genomes assembled from Illumina sequencing were compared to the reference genome

Position	Ref_Allele_Forward_Strand	Alt_Allele_Fwd_Strand	Average_Depth	Mutation_Type	AminoAcid_Subst	Locus_Tag	VIR-O	grey	Max_Freq
876116	C	A	92	NON_SYNONYMOUS_CODING	A2904E	ABUW_0885		C/A	10.26
877097	C	A	140	NON_SYNONYMOUS_CODING	A3231E	ABUW_0885	C/A		11.11
1552067	G	C	104	NON_SYNONYMOUS_CODING	I47M	ABUW_1563	G/C		10.26
1552651	G	T	134	NON_SYNONYMOUS_CODING	H72N	ABUW_1564		G/T	10.53
3413575	A	C	86	NON_SYNONYMOUS_CODING	N319K	ABUW_3374		A/C	12.07
3862534	A	G	137	NON_SYNONYMOUS_CODING	I6T	ABUW_3801		A/G	24.83
462369	G	A	110	SYNONYMOUS_CODING	G384	ABUW_0449		G/A	13.83
462378	C	T	115	SYNONYMOUS_CODING	T381	ABUW_0449		C/T	13.33
462396	G	A	95	SYNONYMOUS_CODING	F375	ABUW_0449		G/A	12.64
462414	G	A	104	SYNONYMOUS_CODING	D369	ABUW_0449		G/A	10.75
462561	A	T	101	SYNONYMOUS_CODING	V320	ABUW_0449		A/T	10.34
462567	C	A	93	SYNONYMOUS_CODING	S318	ABUW_0449		C/A	12.99
869469	G	A	138	SYNONYMOUS_CODING	A688	ABUW_0885		G/A	13.91
869490	T	A	151	SYNONYMOUS_CODING	T695	ABUW_0885		T/A	14.4
869544	A	G	120	SYNONYMOUS_CODING	V713	ABUW_0885		A/G	11.24
870066	A	T	134	SYNONYMOUS_CODING	T887	ABUW_0885	A/T	A/T	13.39
870120	G	A	141	SYNONYMOUS_CODING	V905	ABUW_0885	G/A		10.19
871200	A	G	176	SYNONYMOUS_CODING	P1265	ABUW_0885		A/G	13.61
871212	T	C	178	SYNONYMOUS_CODING	D1269	ABUW_0885		T/C	10.67
871215	C	T	181	SYNONYMOUS_CODING	G1270	ABUW_0885		C/T	10.46
871221	G	A	169	SYNONYMOUS_CODING	V1272	ABUW_0885	G/A		13.47
871254	A	T	139	SYNONYMOUS_CODING	T1283	ABUW_0885	A/T		10.69
871845	T	C	62	SYNONYMOUS_CODING	G1480	ABUW_0885		T/C	10
872157	T	C	102	SYNONYMOUS_CODING	D1584	ABUW_0885	T/C		10.74
872961	G	A	87	SYNONYMOUS_CODING	T1852	ABUW_0885		G/A	10.13
873561	A	T	73	SYNONYMOUS_CODING	V2052	ABUW_0885		A/T	11.11
874677	T	C	150	SYNONYMOUS_CODING	D2424	ABUW_0885		T/C	11.81
874806	T	A	134	SYNONYMOUS_CODING	A2467	ABUW_0885		T/A	10.74
874998	A	T	80	SYNONYMOUS_CODING	A2531	ABUW_0885	A/T		10.47
875004	T	C	81	SYNONYMOUS_CODING	D2533	ABUW_0885	T/C		10.99
875331	C	T	102	SYNONYMOUS_CODING	D2642	ABUW_0885	C/T		10.09
876300	T	C	92	SYNONYMOUS_CODING	D2965	ABUW_0885		T/C	13.41
876627	C	T	81	SYNONYMOUS_CODING	D3074	ABUW_0885	C/T		14.71
914341	G	A	42	SYNONYMOUS_CODING	L180	ABUW_0916		G/A	19.23
1552037	T	A	100	SYNONYMOUS_CODING	A57	ABUW_1563	T/A		10.48
1552634	T	A	117	SYNONYMOUS_CODING	A77	ABUW_1564		T/A	10.78
2421010	A	G	81	SYNONYMOUS_CODING	R365	ABUW_2433		A/G	10.17
2421745	G	A	73	SYNONYMOUS_CODING	D120	ABUW_2433		G/A	10.2

Appendix 4: Schematic of duplicated prophage sequence

VIR-O (top) and grey (bottom) cells. Length of gene regions annotated. Colours and order correspond to genes in table of Appendix 5. Dashes illustrate continuation of duplicated prophage sequence. Dots illustrate continuation of the rest of the chromosome sequence.

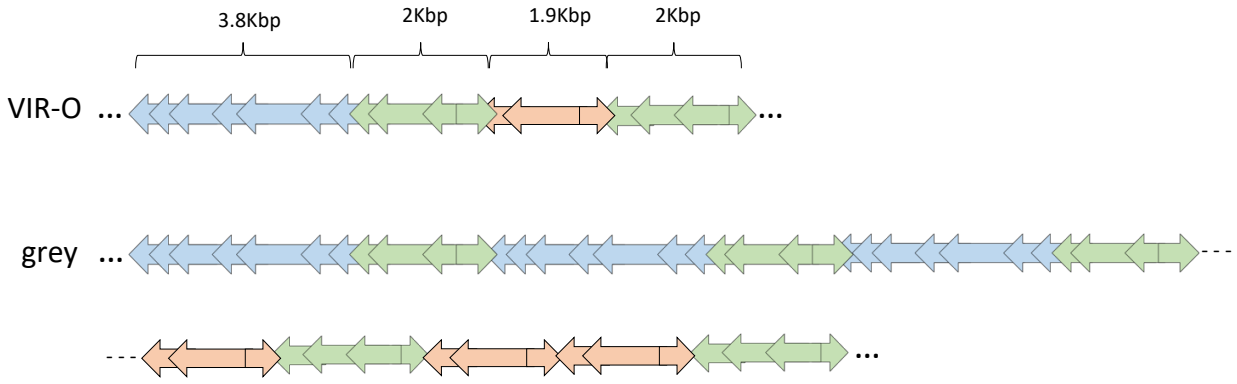

Appendix 5: Genes of duplicated prophage region
Annotated by conserved domains search. Colour relates to colours in Appendix 4.

Gene annotation	Putative function/conserved domains identified
ABUW_2023	Hypothetical protein
ABUW_2024	Hypothetical protein
ABUW_2025	P-loop, NTPase super family. Walker A/B motifs which bind ATP/GTP and Mg^{2+} respectively. CRISPR/cas system-associated protein Cas3 – host defence against phage, DEAD/DEAH box DNA helicase
ABUW_2026	DUF2523 phage related protein with uncharacterised function
ABUW_2027	Virulence factor TspB C-terminal domain-related protein
ABUW_2028	Phage coat protein B
ABUW_2029	Hypothetical protein
ABUW_2030	None
ABUW_2031	DNA relaxase NicK
ABUW_2032	Hypothetical protein
ABUW_2033	Hypothetical protein
ABUW_2034	Hypothetical protein
ABUW_2035	Replication initiaton protein
ABUW_2036	Hypothetical protein
ABUW_2037	Hypothetical protein
ABUW_2038	DNA relaxase NicK
ABUW_2039	Hypothetical protein
ABUW_2040	Hypothetical protein

Appendix 6: ChIP-seq profile of H-NS binding to *csuAB* and T6SS intergenic regions.
Plots show GC content, H-NS ChIP-seq binding profile and annotated genes of relevant locus. Red bar indicates section of DNA used in *in vitro* assays.

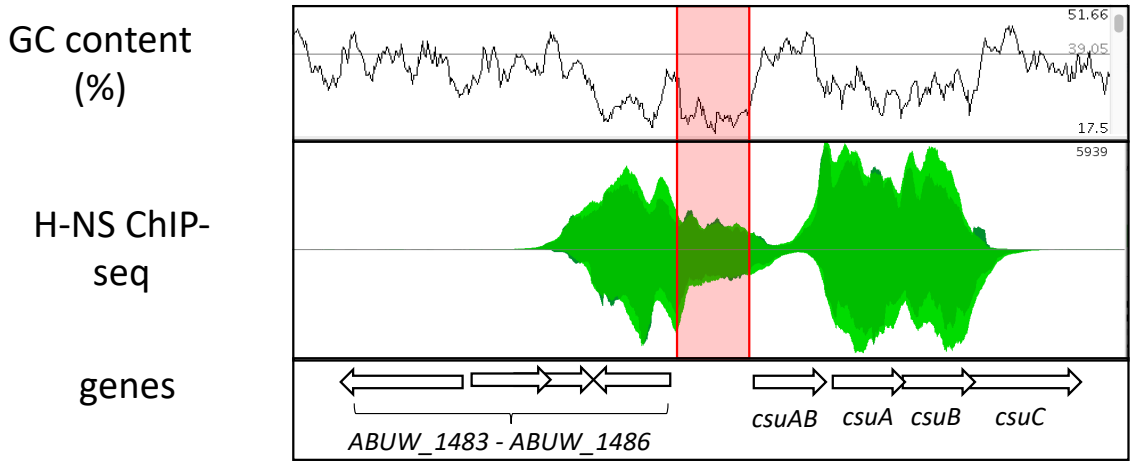

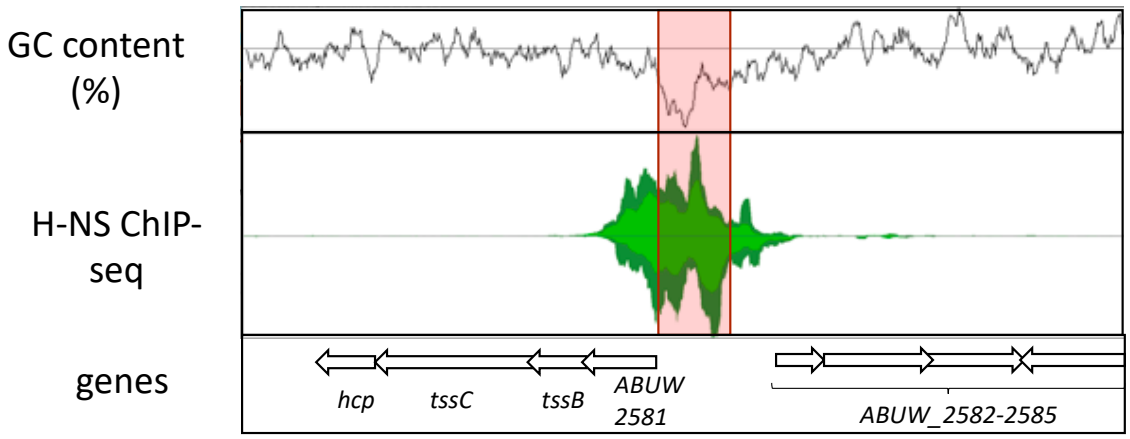

Appendix 7: ChIP-seq profile of H-NS binding to IS*Aba*13 chromosomal regions.
Plots show GC content, H-NS ChIP-seq binding profile and annotated genes of relevant locus. Red bar indicates section of DNA used in bridging assays.

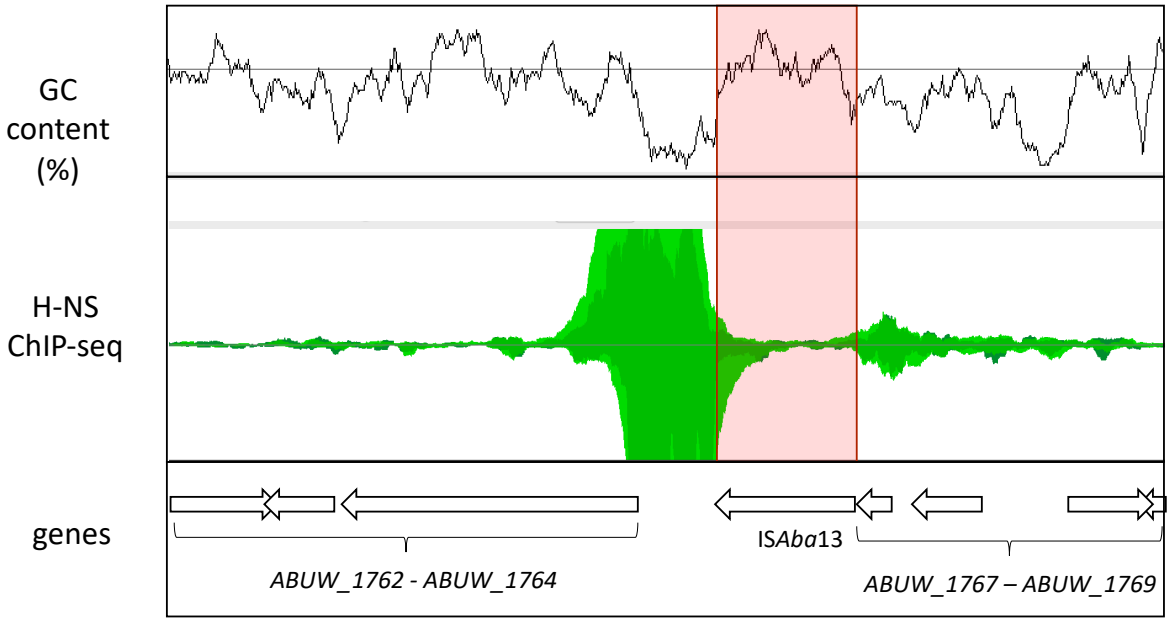

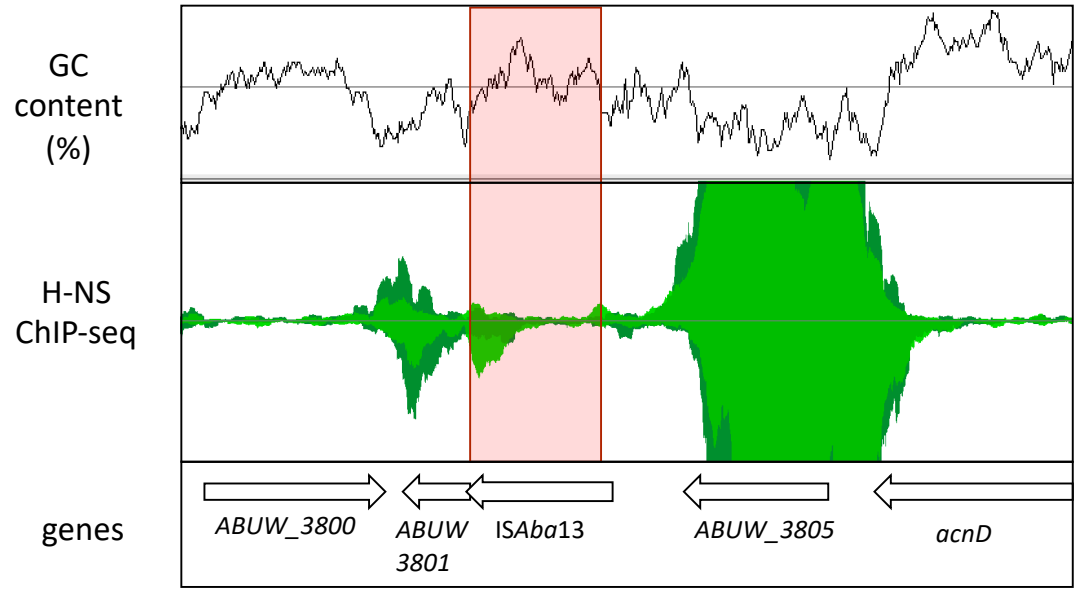

Appendix 8: Chromosomal contacts of IS*Aba*13 with other regions of the chromosome.
3C done by Ms. Rachel Hoare. Left: The chromosome was divided into 1 kb bins and the number of contacts in each bin assessed from 3C-seq was ranked from high to low. Top right: Number and location of contacts in 1 kb bins, involving each IS*Aba*13 copy at starting positions in the chromosome. Bottom right: IS*Aba*13 transposition frequency in 1 kb bins across the chromosome.

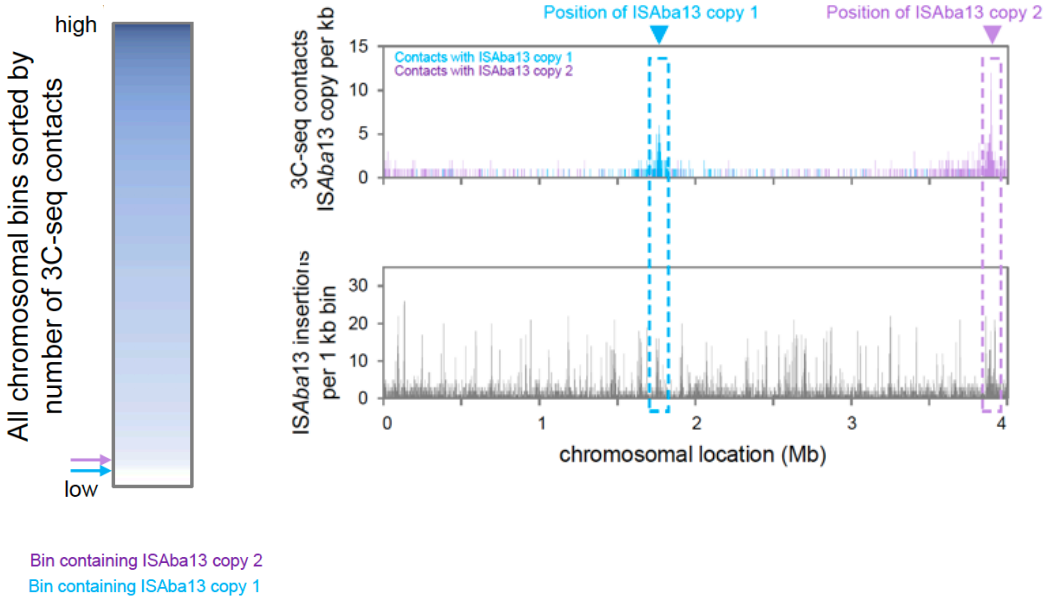

References

Adams, F.G. and Brown, M.H. (2019) 'MITEAba12, a Novel Mobile Miniature Inverted-Repeat Transposable Element Identified in *Acinetobacter baumannii* ATCC 17978 and Its Prevalence across the Moraxellaceae Family', *mSphere*, 4(1), pp. e00028-19. Available at: https://doi.org/10.1128/mSphereDirect.00028-19.

Adams, M.D. *et al.* (2019) 'Rapid Replacement of *Acinetobacter baumannii* Strains Accompanied by Changes in Lipooligosaccharide Loci and Resistance Gene Repertoire', *mBio*, 10(2), pp. e00356-19. Available at: https://doi.org/10.1128/mBio.00356-19.

Adams, M.D., Bishop, B. and Wright, M.S. (2016) 'Quantitative assessment of insertion sequence impact on bacterial genome architecture', *Microbial Genomics*, 2(7), p. e000062. Available at: https://doi.org/10.1099/mgen.0.000062.

Afgan, E. *et al.* (2018) 'The Galaxy platform for accessible, reproducible and collaborative biomedical analyses: 2018 update', *Nucleic Acids Research*, 46(Web Server issue), pp. W537–W544. Available at: https://doi.org/10.1093/nar/gky379.

Ahmad, I. *et al.* (2019) 'Analysis of colony phase variation switch in *Acinetobacter baumannii* clinical isolates', *PLoS ONE*, 14(1), p. e0210082. Available at: https://doi.org/10.1371/journal.pone.0210082.

Ahmad, I. *et al.* (2020) 'A Cyclic-di-GMP signalling network regulates biofilm formation and surface associated motility of *Acinetobacter baumannii* 17978', *Scientific Reports*, 10, p. 1991. Available at: https://doi.org/10.1038/s41598-020-58522-5.

Ahmad, I. *et al.* (2023) 'Csu pili dependent biofilm formation and virulence of *Acinetobacter baumannii*', *npj Biofilms and Microbiomes*, 9(1), pp. 1–17. Available at: https://doi.org/10.1038/s41522-023-00465-6.

Álvarez, V.E. *et al.* (2020) 'Crucial Role of the Accessory Genome in the Evolutionary Trajectory of *Acinetobacter baumannii* Global Clone 1', *Frontiers in Microbiology*, 11. Available at: https://www.frontiersin.org/article/10.3389/fmicb.2020.00342 (Accessed: 22 May 2022).

Amit, R., Oppenheim, A.B. and Stavans, J. (2003) 'Increased Bending Rigidity of Single DNA Molecules by H-NS, a Temperature and Osmolarity Sensor', *Biophysical Journal*, 84(4), pp. 2467–2473. Available at: https://doi.org/10.1016/S0006-3495(03)75051-6.

Anderson, S.E. *et al.* (2018) 'Aminoglycoside Heteroresistance in *Acinetobacter baumannii* AB5075', *mSphere*, 3(4), pp. e00271-18. Available at: https://doi.org/10.1128/mSphere.00271-18.

Anderson, S.E. *et al.* (2020) 'Copy Number of an Integron-Encoded Antibiotic Resistance Locus Regulates a Virulence and Opacity Switch in *Acinetobacter baumannii* AB5075', *mBio*, 11(5), p. 10.1128/mbio.02338-20. Available at: https://doi.org/10.1128/mbio.02338-20.

Arold, S.T. *et al.* (2010) 'H-NS forms a superhelical protein scaffold for DNA condensation', *Proceedings of the National Academy of Sciences*, 107(36), pp. 15728–15732. Available at: https://doi.org/10.1073/pnas.1006966107.

Ayoub Moubareck, C. and Hammoudi Halat, D. (2020) 'Insights into *Acinetobacter baumannii*: A Review of Microbiological, Virulence, and Resistance Traits in a Threatening Nosocomial Pathogen', *Antibiotics*, 9(3). Available at: https://doi.org/10.3390/antibiotics9030119.

Bai, J. *et al.* (2023) 'Genome-wide phage susceptibility analysis in *Acinetobacter baumannii* reveals capsule modulation strategies that determine phage infectivity', *PLOS Pathogens*, 19(6), p. e1010928. Available at: https://doi.org/10.1371/journal.ppat.1010928.

Beck, H.J. and Moll, I. (2018) 'Leaderless mRNAs in the Spotlight: Ancient but Not Outdated!', *Microbiology Spectrum*, 6(4), p. 10.1128/microbiolspec.rwr-0016–2017. Available at: https://doi.org/10.1128/microbiolspec.rwr-0016-2017.

Becker, N.A., Kahn, J.D. and Maher, L.J. (2007) 'Effects of nucleoid proteins on DNA repression loop formation in *Escherichia coli*', *Nucleic Acids Research*, 35(12), pp. 3988–4000. Available at: https://doi.org/10.1093/nar/gkm419.

Benomar, S., Di Venanzio, G. and Feldman, M.F. (2021) 'Plasmid-Encoded H-NS Controls Extracellular Matrix Composition in a Modern *Acinetobacter baumannii* Urinary Isolate', *Journal of Bacteriology*, 203(21), p. 10.1128/jb.00277-21. Available at: https://doi.org/10.1128/jb.00277-21.

Bergogne-Bérézin, E. and Towner, K.J. (1996) '*Acinetobacter* spp. as nosocomial pathogens: microbiological, clinical, and epidemiological features.', *Clinical Microbiology Reviews*, 9(2), pp. 148–165.

Bertin, P. *et al.* (2001) 'H-NS and H-NS-like proteins in Gram-negative bacteria and their multiple role in the regulation of bacterial metabolism', *Biochimie*, 83(2), pp. 235–241. Available at: https://doi.org/10.1016/S0300-9084(01)01247-0.

Beyhan, S. and Yildiz, F.H. (2007) 'Smooth to rugose phase variation in *Vibrio cholerae* can be mediated by a single nucleotide change that targets c-di-GMP signalling pathway', *Molecular Microbiology*, 63(4), pp. 995–1007. Available at: https://doi.org/10.1111/j.1365-2958.2006.05568.x.

Blaschke, U., Skiebe, E. and Wilharm, G. (2021) 'Novel Genes Required for Surface-Associated Motility in *Acinetobacter baumannii*', *Current Microbiology*, 78(4), pp. 1509–1528. Available at: https://doi.org/10.1007/s00284-021-02407-x.

Bohlin, J. *et al.* (2017) 'The nucleotide composition of microbial genomes indicates differential patterns of selection on core and accessory genomes', *BMC Genomics*, 18(1), p. 151. Available at: https://doi.org/10.1186/s12864-017-3543-7.

Borukhov, S. and Nudler, E. (2008) 'RNA polymerase: the vehicle of transcription', *Trends in Microbiology*, 16(3), pp. 126–134. Available at: https://doi.org/10.1016/j.tim.2007.12.006.

Browning, D.F. and Busby, S.J.W. (2004) 'The regulation of bacterial transcription initiation', *Nature Reviews Microbiology*, 2(1), pp. 57–65. Available at: https://doi.org/10.1038/nrmicro787.

Browning, D.F. and Busby, S.J.W. (2016) 'Local and global regulation of transcription initiation in bacteria', *Nature Reviews Microbiology*, 14(10), pp. 638–650. Available at: https://doi.org/10.1038/nrmicro.2016.103.

Browning, D.F., Butala, M. and Busby, S.J.W. (2019) 'Bacterial Transcription Factors: Regulation by Pick "N" Mix', *Journal of Molecular Biology*, 431(20), pp. 4067–4077. Available at: https://doi.org/10.1016/j.jmb.2019.04.011.

Busby, S.J.W. (2019) 'Transcription activation in bacteria: ancient and modern', *Microbiology*, 165(4), pp. 386–395. Available at: https://doi.org/10.1099/mic.0.000783.

Cagliero, C. *et al.* (2013) 'Genome conformation capture reveals that the *Escherichia coli* chromosome is organized by replication and transcription', *Nucleic Acids Research*, 41(12), pp. 6058–6071. Available at: https://doi.org/10.1093/nar/gkt325.

Calhoun, J.H., Murray, C.K. and Manring, M.M. (2008) 'Multidrug-resistant Organisms in Military Wounds from Iraq and Afghanistan', *Clinical Orthopaedics and Related Research*, 466(6), pp. 1356–1362. Available at: https://doi.org/10.1007/s11999-008-0212-9.

Callahan, B.J. *et al.* (2016) 'DADA2: High-resolution sample inference from Illumina amplicon data', *Nature Methods*, 13(7), pp. 581–583. Available at: https://doi.org/10.1038/nmeth.3869.

Carruthers, M.D. *et al.* (2013) '*Acinetobacter baumannii* Utilizes a Type VI Secretion System for Bacterial Competition', *PLoS ONE*, 8(3), p. e59388. Available at: https://doi.org/10.1371/journal.pone.0059388.

Carver, T. *et al.* (2012) 'Artemis: an integrated platform for visualization and analysis of high-throughput sequence-based experimental data', *Bioinformatics*, 28(4), pp. 464–469. Available at: https://doi.org/10.1093/bioinformatics/btr703.

Catel-Ferreira, M. *et al.* (2016) 'The outer membrane porin OmpW of *Acinetobacter baumannii* is involved in iron uptake and colistin binding', *FEBS Letters*, 590(2), pp. 224–231. Available at: https://doi.org/10.1002/1873-3468.12050.

Chabane, Y.N. *et al.* (2014) 'Characterisation of Pellicles Formed by *Acinetobacter baumannii* at the Air-Liquid Interface', *PLOS ONE*, 9(10), p. e111660. Available at: https://doi.org/10.1371/journal.pone.0111660.

Chalmers, R. *et al.* (1998) 'IHF Modulation of Tn10 Transposition: Sensory Transduction of Supercoiling Status via a Proposed Protein/DNA Molecular Spring', *Cell*, 93(5), pp. 897–908. Available at: https://doi.org/10.1016/S0092-8674(00)81449-X.

Chamoun, S. *et al.* (2021) 'Colistin Dependence in Extensively Drug-Resistant *Acinetobacter baumannii* Strain Is Associated with IS*Ajo*2 and IS*Aba*13 Insertions and Multiple Cellular Responses', *International Journal of Molecular Sciences*, 22(2), p. 576. Available at: https://doi.org/10.3390/ijms22020576.

Chen, J., Boyaci, H. and Campbell, E.A. (2021) 'Diverse and Unified Mechanisms of Transcription Initiation in Bacteria', *Nature reviews. Microbiology*, 19(2), pp. 95–109. Available at: https://doi.org/10.1038/s41579-020-00450-2.

Cheng, Y.-S. *et al.* (2019) 'Repurposing Screen Identifies Unconventional Drugs With Activity Against Multidrug Resistant *Acinetobacter baumannii*', *Frontiers in Cellular and Infection Microbiology*, 8, p. 438. Available at: https://doi.org/10.3389/fcimb.2018.00438.

Chin, C.Y. *et al.* (2018) 'A high-frequency phenotypic switch links bacterial virulence and environmental survival in *Acinetobacter baumannii*', *Nature microbiology*, 3(5), pp. 563–569. Available at: https://doi.org/10.1038/s41564-018-0151-5.

Choi, S., Ohta, S. and Ohtsubo, E. (2003) 'A Novel IS Element, IS621, of the IS110/IS492 Family Transposes to a Specific Site in Repetitive Extragenic Palindromic Sequences in *Escherichia coli*', *Journal of Bacteriology*, 185(16), p. 4891. Available at: https://doi.org/10.1128/JB.185.16.4891-4900.2003.

Chong, P. *et al.* (1985) 'Structural analysis of a new GC-specific insertion element IS186', *FEBS Letters*, 192(1), pp. 47–52. Available at: https://doi.org/10.1016/0014-5793(85)80040-5.

Clemmer, K.M., Bonomo, R.A. and Rather, P.N. (2011) 'Genetic analysis of surface motility in *Acinetobacter baumannii*', *Microbiology*, 157(Pt 9), pp. 2534–2544. Available at: https://doi.org/10.1099/mic.0.049791-0.

Consuegra, J. *et al.* (2021) 'Insertion-sequence-mediated mutations both promote and constrain evolvability during a long-term experiment with bacteria', *Nature Communications*, 12(1), p. 980. Available at: https://doi.org/10.1038/s41467-021-21210-7.

Corral, J. *et al.* (2021) 'Importance of twitching and surface-associated motility in the virulence of *Acinetobacter baumannii*', *Virulence*, 12(1), pp. 2201–2213. Available at: https://doi.org/10.1080/21505594.2021.1950268.

Cosgriff, S. *et al.* (2010) 'Dimerization and DNA-dependent aggregation of the *Escherichia coli* nucleoid protein and chaperone CbpA', *Molecular Microbiology*, 77(5), pp. 1289–1300. Available at: https://doi.org/10.1111/j.1365-2958.2010.07292.x.

de la Cruz, N.B. *et al.* (1993) 'Characterization of the Tn5 transposase and inhibitor proteins: a model for the inhibition of transposition.', *Journal of Bacteriology*, 175(21), pp. 6932–6938.

Curcio, M.J. and Derbyshire, K.M. (2003) 'The outs and ins of transposition: from Mu to Kangaroo', *Nature Reviews Molecular Cell Biology*, 4(11), pp. 865–877. Available at: https://doi.org/10.1038/nrm1241.

Da Silva, G.J. and Domingues, S. (2016) 'Insights on the Horizontal Gene Transfer of Carbapenemase Determinants in the Opportunistic Pathogen *Acinetobacter baumannii*', *Microorganisms*, 4(3), p. 29. Available at: https://doi.org/10.3390/microorganisms4030029.

Dame, R.T. *et al.* (2002) 'Structural Basis for H-NS-mediated Trapping of RNA Polymerase in the Open Initiation Complex at the rrnB P1 *', *Journal of Biological Chemistry*, 277(3), pp. 2146–2150. Available at: https://doi.org/10.1074/jbc.C100603200.

Dame, R.T., Noom, M.C. and Wuite, G.J.L. (2006) 'Bacterial chromatin organization by H-NS protein unravelled using dual DNA manipulation', *Nature*, 444(7117), pp. 387–390. Available at: https://doi.org/10.1038/nature05283.

Dame, R.T., Rashid, F.-Z.M. and Grainger, D.C. (2020) 'Chromosome organization in bacteria: mechanistic insights into genome structure and function', *Nature Reviews Genetics*, 21(4), pp. 227–242. Available at: https://doi.org/10.1038/s41576-019-0185-4.

Dame, R.T., Wyman, C. and Goosen, N. (2000) 'H-NS mediated compaction of DNA visualised by atomic force microscopy', *Nucleic Acids Research*, 28(18), pp. 3504–3510.

Danson, A.E. *et al.* (2019) 'Mechanisms of σ54-Dependent Transcription Initiation and Regulation', *Journal of Molecular Biology*, 431(20), pp. 3960–3974. Available at: https://doi.org/10.1016/j.jmb.2019.04.022.

Dar, D. *et al.* (2016) 'Term-seq reveals abundant ribo-regulation of antibiotics resistance in bacteria', *Science (New York, N.Y.)*, 352(6282), p. aad9822. Available at: https://doi.org/10.1126/science.aad9822.

Darling, A.C.E. *et al.* (2004) 'Mauve: Multiple Alignment of Conserved Genomic Sequence With Rearrangements', *Genome Research*, 14(7), pp. 1394–1403. Available at: https://doi.org/10.1101/gr.2289704.

Daubin, V., Lerat, E. and Perrière, G. (2003) 'The source of laterally transferred genes in bacterial genomes', *Genome Biology*, 4(9), p. R57.

De Silva, P.M. *et al.* (2017) 'Effect of Incubation Temperature on Antibiotic Resistance and Virulence Factors of *Acinetobacter baumannii* ATCC 17978', *Antimicrobial Agents and Chemotherapy*, 62(1), pp. e01514-17. Available at: https://doi.org/10.1128/AAC.01514-17.

Derbyshire, K.M. and Grindley, N.D. (1992) 'Binding of the IS903 transposase to its inverted repeat in vitro.', *The EMBO Journal*, 11(9), pp. 3449–3455.

Derbyshire, K.M., Kramer, M. and Grindley, N.D. (1990) 'Role of instability in the cis action of the insertion sequence IS903 transposase.', *Proceedings of the National Academy of Sciences of the United States of America*, 87(11), pp. 4048–4052.

Deveson Lucas, D. *et al.* (2018) 'Emergence of High-Level Colistin Resistance in an *Acinetobacter baumannii* Clinical Isolate Mediated by Inactivation of the Global Regulator H-NS', *Antimicrobial Agents and Chemotherapy*, 62(7), pp. e02442-17. Available at: https://doi.org/10.1128/AAC.02442-17.

Dexter, C. *et al.* (2015) 'Community-acquired *Acinetobacter baumannii* : clinical characteristics, epidemiology and pathogenesis', *Expert Review of Anti-infective Therapy*, 13(5), pp. 567–573. Available at: https://doi.org/10.1586/14787210.2015.1025055.

Dillon, S.C. and Dorman, C.J. (2010) 'Bacterial nucleoid-associated proteins, nucleoid structure and gene expression', *Nature Reviews Microbiology*, 8(3), pp. 185–195. Available at: https://doi.org/10.1038/nrmicro2261.

Eijkelkamp, B.A. *et al.* (2013) 'H-NS Plays a Role in Expression of *Acinetobacter baumannii* Virulence Features', *Infection and Immunity*, 81(7), pp. 2574–2583. Available at: https://doi.org/10.1128/IAI.00065-13.

Ellison, C.K. *et al.* (2021) '*Acinetobacter baylyi* regulates type IV pilus synthesis by employing two extension motors and a motor protein inhibitor', *Nature Communications*, 12(1), p. 3744. Available at: https://doi.org/10.1038/s41467-021-24124-6.

Engler, J.A. and Van Bree, M.P. (1981) 'The nucleotide sequence and protein-coding capability of the transposable element IS5', *Gene*, 14(3), pp. 155–163. Available at: https://doi.org/10.1016/0378-1119(81)90111-6.

Escalante, J. *et al.* (2022) Human Serum Albumin (HSA) Regulates the Expression of Histone-like Nucleoid Structure Protein (H-NS) in *Acinetobacter baumannii*. preprint. In Review. Available at: https://doi.org/10.21203/rs.3.rs-1293237/v1.

Espinal, P., Martí, S. and Vila, J. (2012) 'Effect of biofilm formation on the survival of *Acinetobacter baumannii* on dry surfaces', *Journal of Hospital Infection*, 80(1), pp. 56–60. Available at: https://doi.org/10.1016/j.jhin.2011.08.013.

Ettwiller, L. *et al.* (2016) 'A novel enrichment strategy reveals unprecedented number of novel transcription start sites at single base resolution in a model prokaryote and the gut microbiome', *BMC Genomics*, 17(1), p. 199. Available at: https://doi.org/10.1186/s12864-016-2539-z.

Falconi, M. *et al.* (1991) 'Mutations altering chromosomal protein H-NS induce mini-Mu transposition', *The New biologist*, 3, pp. 615–25.

Falconi, M. *et al.* (1998) 'Thermoregulation of *Shigella* and *Escherichia coli* EIEC pathogenicity. A temperature-dependent structural transition of DNA modulates

accessibility of *virF* promoter to transcriptional repressor H-NS.', *The EMBO Journal*, 17(23), pp. 7033–7043. Available at: https://doi.org/10.1093/emboj/17.23.7033.

Feklistov, A. and Darst, S.A. (2011) 'Structural basis for promoter –10 element recognition by the bacterial RNA polymerase σ subunit', *Cell*, 147(6), pp. 1257–1269. Available at: https://doi.org/10.1016/j.cell.2011.10.041.

Feschotte, C. (2023) 'Transposable elements: McClintock's legacy revisited', *Nature Reviews Genetics*, 24(11), pp. 797–800. Available at: https://doi.org/10.1038/s41576-023-00652-3.

Figurski, D.H. and Helinski, D.R. (1979) 'Replication of an origin-containing derivative of plasmid RK2 dependent on a plasmid function provided in trans', *Proceedings of the National Academy of Sciences*, 76(4), pp. 1648–1652. Available at: https://doi.org/10.1073/pnas.76.4.1648.

Fitzgerald, S. *et al.* (2020) 'Redefining the H-NS protein family: a diversity of specialized core and accessory forms exhibit hierarchical transcriptional network integration', *Nucleic Acids Research*, 48(18), pp. 10184–10198. Available at: https://doi.org/10.1093/nar/gkaa709.

Florek, M.C., Gilbert, D.P. and Plague, G.R. (2014) 'Insertion sequence distribution bias in Archaea', *Mobile Genetic Elements*, 4, p. e27829. Available at: https://doi.org/10.4161/mge.27829.

Forrest, D. *et al.* (2022) 'Xenogeneic silencing strategies in bacteria are dictated by RNA polymerase promiscuity', *Nature Communications*, 13, p. 1149. Available at: https://doi.org/10.1038/s41467-022-28747-1.

Gaiarsa, S. *et al.* (2019) 'Can Insertion Sequences Proliferation Influence Genomic Plasticity? Comparative Analysis of *Acinetobacter baumannii* Sequence Type 78, a Persistent Clone in Italian Hospitals', *Frontiers in Microbiology*, 10. Available at: https://www.frontiersin.org/article/10.3389/fmicb.2019.02080 (Accessed: 23 May 2022).

Gallagher, L.A. *et al.* (2015) 'Resources for Genetic and Genomic Analysis of Emerging Pathogen *Acinetobacter baumannii*', *Journal of Bacteriology*, 197(12), pp. 2027–2035. Available at: https://doi.org/10.1128/JB.00131-15.

Garsin, D.A. *et al.* (2004) 'Construction of an *Enterococcus faecalis* Tn917-Mediated-Gene-Disruption Library Offers Insight into Tn917 Insertion Patterns', *Journal of Bacteriology*, 186(21), pp. 7280–7289. Available at: https://doi.org/10.1128/JB.186.21.7280-7289.2004.

Gebhardt, M.J. *et al.* (2015) 'Joint Transcriptional Control of Virulence and Resistance to Antibiotic and Environmental Stress in *Acinetobacter baumannii*', *mBio*, 6(6), pp. e01660-15. Available at: https://doi.org/10.1128/mBio.01660-15.

Gerson, S. *et al.* (2018) 'Diversity of mutations in regulatory genes of resistance-nodulation-cell division efflux pumps in association with tigecycline resistance in *Acinetobacter*

baumannii', *Journal of Antimicrobial Chemotherapy*, 73(6), pp. 1501–1508. Available at: https://doi.org/10.1093/jac/dky083.

Gil-Marqués, M.L., Pachón, J. and Smani, Y. (2022) 'iTRAQ-Based Quantitative Proteomic Analysis of *Acinetobacter baumannii* under Hypoxia and Normoxia Reveals the Role of OmpW as a Virulence Factor', *Microbiology Spectrum*. Edited by J.M. Atack, 10(2), pp. e02328-21. Available at: https://doi.org/10.1128/spectrum.02328-21.

Godeux, A.-S. *et al.* (2020) 'Scarless Removal of Large Resistance Island AbaR Results in Antibiotic Susceptibility and Increased Natural Transformability in *Acinetobacter baumannii*', *Antimicrobial Agents and Chemotherapy*, 64(10), pp. e00951-20. Available at: https://doi.org/10.1128/AAC.00951-20.

Gómez, M.J. *et al.* (2014) 'Chromosomal Replication Dynamics and Interaction with the β Sliding Clamp Determine Orientation of Bacterial Transposable Elements', *Genome Biology and Evolution*, 6(3), pp. 727–740. Available at: https://doi.org/10.1093/gbe/evu052.

Gordillo Altamirano, F. *et al.* (2021) 'Bacteriophage-resistant *Acinetobacter baumannii* are resensitized to antimicrobials', *Nature Microbiology*, 6(2), pp. 157–161. Available at: https://doi.org/10.1038/s41564-020-00830-7.

Gordillo Altamirano, F.L. *et al.* (2022) 'Phage-antibiotic combination is a superior treatment against *Acinetobacter baumannii* in a preclinical study', *eBioMedicine*, 80, p. 104045. Available at: https://doi.org/10.1016/j.ebiom.2022.104045.

Gordon, B.R.G. *et al.* (2011) 'Structural basis for recognition of AT-rich DNA by unrelated xenogeneic silencing proteins', *Proceedings of the National Academy of Sciences of the United States of America*, 108(26), p. 10690. Available at: https://doi.org/10.1073/pnas.1102544108.

Grindley, N.D. and Joyce, C.M. (1980) 'Genetic and DNA sequence analysis of the kanamycin resistance transposon Tn903.', *Proceedings of the National Academy of Sciences of the United States of America*, 77(12), pp. 7176–7180.

Guédon, G. *et al.* (2017) 'The Obscure World of Integrative and Mobilizable Elements, Highly Widespread Elements that Pirate Bacterial Conjugative Systems', *Genes*, 8(11), p. 337. Available at: https://doi.org/10.3390/genes8110337.

Gunn, J.S., Bakaletz, L.O. and Wozniak, D.J. (2016) 'What's on the Outside Matters: The Role of the Extracellular Polymeric Substance of Gram-negative Biofilms in Evading Host Immunity and as a Target for Therapeutic Intervention', *The Journal of Biological Chemistry*, 291(24), pp. 12538–12546. Available at: https://doi.org/10.1074/jbc.R115.707547.

Guo, H. *et al.* (2023) 'Intracellular common gardens reveal niche differentiation in transposable element community during bacterial adaptive evolution', *The ISME Journal*, 17(2), pp. 297–308. Available at: https://doi.org/10.1038/s41396-022-01344-2.

Guo, T. *et al.* (2022) 'Whole-Genome Analysis of *Acinetobacter baumannii* Strain AB43 Containing a Type I-Fb CRISPR-Cas System: Insights into the Relationship with Drug Resistance', *Molecules*, 27(17), p. 5665. Available at: https://doi.org/10.3390/molecules27175665.

Gupta, N. *et al.* (2015) 'Isolation and identification of *Acinetobacter* species with special reference to antibiotic resistance', *Journal of Natural Science, Biology, and Medicine*, 6(1), pp. 159–162. Available at: https://doi.org/10.4103/0976-9668.149116.

Gusarov, I. and Nudler, E. (1999) 'The Mechanism of Intrinsic Transcription Termination', *Molecular Cell*, 3(4), pp. 495–504. Available at: https://doi.org/10.1016/S1097-2765(00)80477-3.

Hagemann, A.T. and Craig, N.L. (1993) 'Tn7 transposition creates a hotspot for homologous recombination at the transposon donor site.', *Genetics*, 133(1), pp. 9–16. Available at: https://doi.org/10.1093/genetics/133.1.9.

Hamidian, M. *et al.* (2019) 'Complete Genome Sequence of A388, an Antibiotic-Resistant *Acinetobacter baumannii* Global Clone 1 Isolate from Greece', *Microbiology Resource Announcements*, 8(41), p. 10.1128/mra.00971-19. Available at: https://doi.org/10.1128/mra.00971-19.

Hamidian, M. and Hall, R.M. (2013) 'IS*Aba*1 targets a specific position upstream of the intrinsic *ampC* gene of *Acinetobacter baumannii* leading to cephalosporin resistance', *Journal of Antimicrobial Chemotherapy*, 68(11), pp. 2682–2683. Available at: https://doi.org/10.1093/jac/dkt233.

Hamidian, M. and Hall, R.M. (2014) 'Tn6168, a transposon carrying an IS*Aba*1-activated *ampC* gene and conferring cephalosporin resistance in *Acinetobacter baumannii*', *Journal of Antimicrobial Chemotherapy*, 69(1), pp. 77–80. Available at: https://doi.org/10.1093/jac/dkt312.

Hammerschmidt, S. *et al.* (1996) 'Modulation of cell surface sialic acid expression in *Neisseria meningitidis* via a transposable genetic element.', *The EMBO Journal*, 15(1), pp. 192–198.

Hannon, G. and Assaf, G. (2010) *FASTX-Toolkit*. Available at: http://hannonlab.cshl.edu/fastx_toolkit/ (Accessed: 19 January 2024).

Harding, C.M. *et al.* (2013) '*Acinetobacter baumannii* Strain M2 Produces Type IV Pili Which Play a Role in Natural Transformation and Twitching Motility but Not Surface-Associated Motility', *mBio*, 4(4), pp. e00360-13. Available at: https://doi.org/10.1128/mBio.00360-13.

Harding, C.M. *et al.* (2015) '*Acinetobacter* strains carry two functional oligosaccharyltransferases, one devoted exclusively to type IV pilin, and the other one dedicated to O-glycosylation of multiple proteins', *Molecular Microbiology*, 96(5), pp. 1023–1041. Available at: https://doi.org/10.1111/mmi.12986.

Harding, C.M. *et al.* (2018) 'Distinct amino acid residues confer one of three UDP-sugar substrate specificities in *Acinetobacter baumannii* PglC phosphoglycosyltransferases', *Glycobiology*, 28(7), pp. 522–533. Available at: https://doi.org/10.1093/glycob/cwy037.

Hardy, C.D. and Cozzarelli, N.R. (2005) 'A genetic selection for supercoiling mutants of *Escherichia coli* reveals proteins implicated in chromosome structure', *Molecular Microbiology*, 57(6), pp. 1636–1652. Available at: https://doi.org/10.1111/j.1365-2958.2005.04799.x.

Haren, L., Ton-Hoang, B. and Chandler, M. (1999) 'Integrating DNA: Transposases and Retroviral Integrases', *Annual Review of Microbiology*, 53(1), pp. 245–281. Available at: https://doi.org/10.1146/annurev.micro.53.1.245.

Harris, G. *et al.* (2013) 'A Mouse Model of *Acinetobacter baumannii*-Associated Pneumonia Using a Clinically Isolated Hypervirulent Strain', *Antimicrobial agents and chemotherapy*, 57. Available at: https://doi.org/10.1128/AAC.00944-13.

Haycocks, J.R.J. *et al.* (2019) 'The quorum sensing transcription factor AphA directly regulates natural competence in *Vibrio cholerae*', *PLOS Genetics*. Edited by M. Blokesch, 15(10), p. e1008362. Available at: https://doi.org/10.1371/journal.pgen.1008362.

He, S. *et al.* (2015) 'Insertion Sequence IS26 Reorganizes Plasmids in Clinically Isolated Multidrug-Resistant Bacteria by Replicative Transposition', *mBio*, 6(3). Available at: https://doi.org/10.1128/mBio.00762-15.

Helgesen, E., Fossum, S. and Skarstad, K. (2016) 'Lack of the H-NS Protein Results in Extended and Aberrantly Positioned DNA during Chromosome Replication and Segregation in *Escherichia coli*', *Journal of Bacteriology*, 198, p. JB.00919-15. Available at: https://doi.org/10.1128/JB.00919-15.

Hennig, B.P. *et al.* (2017) 'Large-Scale Low-Cost NGS Library Preparation Using a Robust Tn5 Purification and Tagmentation Protocol', *G3: Genes|Genomes|Genetics*, 8(1), pp. 79–89. Available at: https://doi.org/10.1534/g3.117.300257.

Hickan, A.B. and Dyda, F. (2015) 'Mechanisms of DNA Transposition', *Microbiology spectrum*, 3(2), pp. MDNA3-0034–2014. Available at: https://doi.org/10.1128/microbiolspec.MDNA3-0034-2014.

Hickman, A.B. and Dyda, F. (2015) 'Mechanisms of DNA Transposition', *Microbiology spectrum*, 3(2), pp. MDNA3-0034–2014. Available at: https://doi.org/10.1128/microbiolspec.MDNA3-0034-2014.

Hu, W.-Y. *et al.* (2001) 'Anatomy of a preferred target site for the bacterial insertion sequence IS903', *Journal of Molecular Biology*, 306(3), pp. 403–416. Available at: https://doi.org/10.1006/jmbi.2000.4421.

Hu, W.-Y. and Derbyshire, K.M. (1998) 'Target Choice and Orientation Preference of the Insertion Sequence IS903', *Journal of Bacteriology*, 180(12), pp. 3039–3048. Available at: https://doi.org/10.1128/jb.180.12.3039-3048.1998.

Hu, Y. *et al.* (2019) 'High DNA Uptake Capacity of International Clone II *Acinetobacter baumannii* Detected by a Novel Planktonic Natural Transformation Assay', *Frontiers in Microbiology*, 10, p. 2165. Available at: https://doi.org/10.3389/fmicb.2019.02165.

Huang, F. *et al.* (2020) 'The H-NS Regulator Plays a Role in the Stress Induced by Carbapenemase Expression in *Acinetobacter baumannii*', *mSphere*. Edited by A.C. Gales, 5(4), pp. e00793-20. Available at: https://doi.org/10.1128/mSphere.00793-20.

Huang, W. *et al.* (2015) 'OmpW is a potential target for eliciting protective immunity against *Acinetobacter baumannii* infections', *Vaccine*, 33(36), pp. 4479–4485. Available at: https://doi.org/10.1016/j.vaccine.2015.07.031.

Hübner, P., Iida, S. and Arber, W. (1987) 'A transcriptional terminator sequence in the prokaryotic transposable element IS1', *Molecular & general genetics: MGG*, 206(3), pp. 485–490. Available at: https://doi.org/10.1007/BF00428889.

Humayun, M.Z. *et al.* (2017) 'Hopping into a hot seat: Role of DNA structural features on IS5-mediated gene activation and inactivation under stress', *PLoS ONE*, 12(6), p. e0180156. Available at: https://doi.org/10.1371/journal.pone.0180156.

Hutchison, C.A. *et al.* (2019) 'Polar Effects of Transposon Insertion into a Minimal Bacterial Genome', *Journal of Bacteriology*. Edited by T.J. Silhavy, 201(19). Available at: https://doi.org/10.1128/JB.00185-19.

Ikuta, K.S. *et al.* (2022) 'Global mortality associated with 33 bacterial pathogens in 2019: a systematic analysis for the Global Burden of Disease Study 2019', *The Lancet*, 400(10369), pp. 2221–2248. Available at: https://doi.org/10.1016/S0140-6736(22)02185-7.

Iskakova, M.B. *et al.* (2006) 'Troubleshooting coupled *in vitro* transcription–translation system derived from *Escherichia coli* cells: synthesis of high-yield fully active proteins', *Nucleic Acids Research*, 34(19), p. e135. Available at: https://doi.org/10.1093/nar/gkl462.

Jacobs, A.C. *et al.* (2014) 'AB5075, a Highly Virulent Isolate of *Acinetobacter baumannii*, as a Model Strain for the Evaluation of Pathogenesis and Antimicrobial Treatments', *mBio*, 5(3), pp. e01076-14. Available at: https://doi.org/10.1128/mBio.01076-14.

Jain, S., Gupta, R. and Sen, R. (2019) 'Rho-dependent transcription termination in bacteria recycles RNA polymerases stalled at DNA lesions', *Nature Communications*, 10(1), p. 1207. Available at: https://doi.org/10.1038/s41467-019-09146-5.

Johnson, E.N. *et al.* (2007) 'Infectious Complications of Open Type III Tibial Fractures among Combat Casualties', *Clinical Infectious Diseases*, 45(4), pp. 409–415. Available at: https://doi.org/10.1086/520029.

Jung, J. and Park, W. (2015) '*Acinetobacter* species as model microorganisms in environmental microbiology: current state and perspectives', *Applied Microbiology and Biotechnology*, 99(6), pp. 2533–2548. Available at: https://doi.org/10.1007/s00253-015-6439-y.

Juni, E. (1978) 'Genetics and Physiology of *Acinetobacter*', *Annual Review of Microbiology*, 32(1), pp. 349–371. Available at: https://doi.org/10.1146/annurev.mi.32.100178.002025.

Kaczmarska, Z. *et al.* (2022) 'Structural basis of transposon end recognition explains central features of Tn7 transposition systems', *Molecular Cell*, 82(14), pp. 2618-2632.e7. Available at: https://doi.org/10.1016/j.molcel.2022.05.005.

Kamuyu, G. *et al.* (2022) 'Strain Specific Variations in *Acinetobacter baumannii* Complement Sensitivity', *Frontiers in Immunology*, 13, p. 853690. Available at: https://doi.org/10.3389/fimmu.2022.853690.

Karakonstantis, S. (2021) 'A systematic review of implications, mechanisms, and stability of in vivo emergent resistance to colistin and tigecycline in *Acinetobacter baumannii*', *Journal of Chemotherapy*, 33(1), pp. 1–11. Available at: https://doi.org/10.1080/1120009X.2020.1794393.

Karimova, G. *et al.* (1998) 'A bacterial two-hybrid system based on a reconstituted signal transduction pathway', *Proceedings of the National Academy of Sciences of the United States of America*, 95(10), pp. 5752–5756.

Kato, T., Kurahashi, H. and Emanuel, B.S. (2012) 'Chromosomal translocations and palindromic AT-rich repeats', *Current opinion in genetics & development*, 22(3), pp. 221–228. Available at: https://doi.org/10.1016/j.gde.2012.02.004.

Kenyon, J.J. *et al.* (2014) 'Insertions in the OCL1 locus of *Acinetobacter baumannii* lead to shortened lipooligosaccharides', *Research in Microbiology*, 165(6), pp. 472–475. Available at: https://doi.org/10.1016/j.resmic.2014.05.034.

Kenyon, J.J. and Hall, R.M. (2013) 'Variation in the Complex Carbohydrate Biosynthesis Loci of *Acinetobacter baumannii* Genomes', *PLoS ONE*, 8(4), p. e62160. Available at: https://doi.org/10.1371/journal.pone.0062160.

Kimura, S. *et al.* (2016) 'The Nucleoid Binding Protein H-NS Biases Genome-Wide Transposon Insertion Landscapes', *mBio*, 7(4), pp. e01351-16. Available at: https://doi.org/10.1128/mBio.01351-16.

Kirsch, J.M. *et al.* (2023) 'Targeted IS-element sequencing uncovers transposition dynamics during selective pressure in enterococci', *PLOS Pathogens*, 19(6), p. e1011424. Available at: https://doi.org/10.1371/journal.ppat.1011424.

Kon, H. *et al.* (2020) 'Rapid identification of capsulated *Acinetobacter baumannii* using a density-dependent gradient test', *BMC Microbiology*, 20(1), p. 285. Available at: https://doi.org/10.1186/s12866-020-01971-9.

Kotlajich, M.V. *et al.* (2015) 'Bridged filaments of histone-like nucleoid structuring protein pause RNA polymerase and aid termination in bacteria', *Genes and chromosomes* [Preprint].

Lamberte, L.E. *et al.* (2017) 'Horizontally acquired AT-rich genes in *Escherichia coli* cause toxicity by sequestering RNA polymerase', *Nature Microbiology*, 2(3), p. 16249. Available at: https://doi.org/10.1038/nmicrobiol.2016.249.

Lang, B. *et al.* (2007) 'High-affinity DNA binding sites for H-NS provide a molecular basis for selective silencing within proteobacterial genomes', *Nucleic Acids Research*, 35(18), pp. 6330–6337. Available at: https://doi.org/10.1093/nar/gkm712.

Langmead, B. and Salzberg, S.L. (2012) 'Fast gapped-read alignment with Bowtie 2', *Nature Methods*, 9(4), pp. 357–359. Available at: https://doi.org/10.1038/nmeth.1923.

Le, C. *et al.* (2021) 'Involvement of the Histone-Like Nucleoid Structuring Protein (H-NS) in *Acinetobacter baumannii*'s Natural Transformation', *Pathogens*, 10(9), p. 1083. Available at: https://doi.org/10.3390/pathogens10091083.

Lee, C.-R. *et al.* (2017) 'Biology of *Acinetobacter baumannii*: Pathogenesis, Antibiotic Resistance Mechanisms, and Prospective Treatment Options', *Frontiers in Cellular and Infection Microbiology*, 7. Available at: https://doi.org/10.3389/fcimb.2017.00055.

Lee, S.Y., Butler, D. and Kleckner, N. (1987) 'Efficient Tn10 transposition into a DNA insertion hot spot *in vivo* requires the 5-methyl groups of symmetrically disposed thymines within the hot-spot consensus sequence.', *Proceedings of the National Academy of Sciences of the United States of America*, 84(22), pp. 7876–7880.

Lees-Miller, R.G. *et al.* (2013) 'A common pathway for O-linked protein-glycosylation and synthesis of capsule in *Acinetobacter baumannii*', *Molecular Microbiology*, 89(5), pp. 816–830. Available at: https://doi.org/10.1111/mmi.12300.

Lewis, L.A. *et al.* (2011) 'Soluble expression, purification and characterization of the full length IS2 Transposase', *Mobile DNA*, 2, p. 14. Available at: https://doi.org/10.1186/1759-8753-2-14.

Li, H. *et al.* (2015) 'Evolution of Carbapenem-Resistant *Acinetobacter baumannii* Revealed through Whole-Genome Sequencing and Comparative Genomic Analysis', *Antimicrobial Agents and Chemotherapy*, 59(2), pp. 1168–1176. Available at: https://doi.org/10.1128/aac.04609-14.

Li, J. and Zhang, J.-R. (2019) 'Phase Variation of *Streptococcus pneumoniae*', *Microbiology Spectrum*, 7(1), p. 7.1.11. Available at: https://doi.org/10.1128/microbiolspec.GPP3-0005-2018.

Li, W. *et al.* (2016) 'Contribution of the outer membrane protein OmpW in *Escherichia coli* to complement resistance from binding to factor H', *Microbial Pathogenesis*, 98, pp. 57–62. Available at: https://doi.org/10.1016/j.micpath.2016.06.024.

Liang, Y. *et al.* (2017) 'Probing the mechanical stability of bridged DNA-H-NS protein complexes by single-molecule AFM pulling', *Scientific Reports*, 7(1), p. 15275. Available at: https://doi.org/10.1038/s41598-017-15477-4.

Liao, Y., Smyth, G.K. and Shi, W. (2019) 'The R package Rsubread is easier, faster, cheaper and better for alignment and quantification of RNA sequencing reads', *Nucleic Acids Research*, 47(8), p. e47. Available at: https://doi.org/10.1093/nar/gkz114.

Lim, C.J., Kenney, L.J. and Yan, J. (2014) 'Single-molecule studies on the mechanical interplay between DNA supercoiling and H-NS DNA architectural properties', *Nucleic Acids Research*, 42(13), pp. 8369–8378. Available at: https://doi.org/10.1093/nar/gku566.

Linheiro, R.S. and Bergman, C.M. (2008) 'Testing the palindromic target site model for DNA transposon insertion using the *Drosophila melanogaster* P-element', *Nucleic Acids Research*, 36(19), pp. 6199–6208. Available at: https://doi.org/10.1093/nar/gkn563.

Lioy, V.S. *et al.* (2018) 'Multiscale Structuring of the *E. coli* Chromosome by Nucleoid-Associated and Condensin Proteins', *Cell*, 172(4), pp. 771-783.e18. Available at: https://doi.org/10.1016/j.cell.2017.12.027.

Liu, M. *et al.* (2022) 'Comparative genomics of *Acinetobacter baumannii* and therapeutic bacteriophages from a patient undergoing phage therapy', *Nature Communications*, 13(1), p. 3776. Available at: https://doi.org/10.1038/s41467-022-31455-5.

Liu, Y. *et al.* (2010) 'A divalent switch drives H-NS/DNA-binding conformations between stiffening and bridging modes', *Genes & Development*, 24(4), pp. 339–344. Available at: https://doi.org/10.1101/gad.1883510.

Loot, C., Turlan, C. and Chandler, M. (2004) 'Host processing of branched DNA intermediates is involved in targeted transposition of IS911', *Molecular Microbiology*, 51(2), pp. 385–393. Available at: https://doi.org/10.1046/j.1365-2958.2003.03850.x.

López-Martín, M. *et al.* (2021) 'AbaM Regulates Quorum Sensing, Biofilm Formation, and Virulence in *Acinetobacter baumannii*', *Journal of Bacteriology*, 203(8), pp. e00635-20. Available at: https://doi.org/10.1128/JB.00635-20.

Lucchini, S. *et al.* (2006) 'H-NS Mediates the Silencing of Laterally Acquired Genes in Bacteria', *PLoS Pathogens*, 2(8), p. e81. Available at: https://doi.org/10.1371/journal.ppat.0020081.

Lucidi, M. *et al.* (2018) 'New Shuttle Vectors for Gene Cloning and Expression in Multidrug-Resistant *Acinetobacter* Species', *Antimicrobial Agents and Chemotherapy*, 62(4). Available at: https://doi.org/10.1128/AAC.02480-17.

Luo, J. *et al.* (2023) '*Acinetobacter baumannii* Kills Fungi via a Type VI DNase Effector', *mBio*. Edited by M. Parsek, 14(1), pp. e03420-22. Available at: https://doi.org/10.1128/mbio.03420-22.

Ma, C. and Simons, R.W. (1990) 'The IS10 antisense RNA blocks ribosome binding at the transposase translation initiation site.', *The EMBO Journal*, 9(4), pp. 1267–1274.

Macesic, N. *et al.* (2020) 'Emergence of Polymyxin Resistance in Clinical *Klebsiella pneumoniae* Through Diverse Genetic Adaptations: A Genomic, Retrospective Cohort Study', *Clinical Infectious Diseases: An Official Publication of the Infectious Diseases Society of America*, 70(10), pp. 2084–2091. Available at: https://doi.org/10.1093/cid/ciz623.

Manna, D. *et al.* (2007) 'Microarray analysis of Mu transposition in *Salmonella enterica*, serovar Typhimurium: transposon exclusion by high-density DNA binding proteins', *Molecular Microbiology*, 66(2), pp. 315–328. Available at: https://doi.org/10.1111/j.1365-2958.2007.05915.x.

Marchler-Bauer, A. *et al.* (2017) 'CDD/SPARCLE: functional classification of proteins via subfamily domain architectures', *Nucleic Acids Research*, 45(Database issue), pp. D200–D203. Available at: https://doi.org/10.1093/nar/gkw1129.

Martí, S. *et al.* (2011) 'Biofilm formation at the solid-liquid and air-liquid interfaces by *Acinetobacter* species', *BMC Research Notes*, 4, p. 5. Available at: https://doi.org/10.1186/1756-0500-4-5.

Martinez, J. *et al.* (2019) 'Human pleural fluid triggers global changes in the transcriptional landscape of *Acinetobacter baumannii* as an adaptive response to stress', *Scientific Reports*, 9(1), p. 17251. Available at: https://doi.org/10.1038/s41598-019-53847-2.

Maslova, O. *et al.* (2022) 'Plasmids as Key Players in *Acinetobacter* Adaptation', *International Journal of Molecular Sciences*, 23(18), p. 10893. Available at: https://doi.org/10.3390/ijms231810893.

May, H.C., Yu, J.-J., Shrihari, S., *et al.* (2019) 'Thioredoxin Modulates Cell Surface Hydrophobicity in *Acinetobacter baumannii*', *Frontiers in Microbiology*, 10. Available at: https://www.frontiersin.org/article/10.3389/fmicb.2019.02849 (Accessed: 14 May 2022).

May, H.C., Yu, J.-J., Zhang, H., *et al.* (2019) 'Thioredoxin-A is a virulence factor and mediator of the type IV pilus system in *Acinetobacter baumannii*', *PLOS ONE*, 14(7), p. e0218505. Available at: https://doi.org/10.1371/journal.pone.0218505.

Mikulskis, A.V. and Cornetis, G.R. (1994) 'A new class of proteins regulating gene expression in enterobacteria', *Molecular Microbiology*, 11(1), pp. 77–86. Available at: https://doi.org/10.1111/j.1365-2958.1994.tb00291.x.

Mirdita, M. *et al.* (2022) 'ColabFold: making protein folding accessible to all', *Nature Methods*, 19(6), pp. 679–682. Available at: https://doi.org/10.1038/s41592-022-01488-1.

Mitra, P. *et al.* (2017) 'Rho Protein: Roles and Mechanisms', *Annual Review of Microbiology*, 71(1), pp. 687–709. Available at: https://doi.org/10.1146/annurev-micro-030117-020432.

Mohd Rani, F. *et al.* (2018) 'Prevalence and antimicrobial susceptibilities of *Acinetobacter baumannii* and non-*baumannii* Acinetobacters from Terengganu, Malaysia and their carriage of carbapenemase genes', *Journal of Medical Microbiology*, 67(11), pp. 1538–1543. Available at: https://doi.org/10.1099/jmm.0.000844.

Molodtsov, V. *et al.* (2023) 'Structural basis of Rho-dependent transcription termination', *Nature*, 614(7947), pp. 367–374. Available at: https://doi.org/10.1038/s41586-022-05658-1.

Monem, S. *et al.* (2020) 'Mechanisms Protecting *Acinetobacter baumannii* against Multiple Stresses Triggered by the Host Immune Response, Antibiotics and Outside-Host Environment', *International Journal of Molecular Sciences*, 21(15), p. 5498. Available at: https://doi.org/10.3390/ijms21155498.

Morris, F.C. *et al.* (2019) 'The Mechanisms of Disease Caused by *Acinetobacter baumannii*', *Frontiers in Microbiology*, 10. Available at: https://www.frontiersin.org/article/10.3389/fmicb.2019.01601 (Accessed: 8 May 2022).

Morrison, M.J. and Imperiali, B. (2013) 'Biosynthesis of UDP-N,N'-Diacetylbacillosamine in *Acinetobacter baumannii*: Biochemical Characterization and Correlation to Existing Pathways†', *Archives of biochemistry and biophysics*, 536(1), pp. 72–80. Available at: https://doi.org/10.1016/j.abb.2013.05.011.

Mukherjee, K. *et al.* (1999) 'GroEL is involved in activation of *Escherichia coli* RNA polymerase devoid of the ω subunit in vivo', *European Journal of Biochemistry*, 266(1), pp. 228–235. Available at: https://doi.org/10.1046/j.1432-1327.1999.00848.x.

Murayama, Y. *et al.* (2023) 'Structural basis of the transcription termination factor Rho engagement with transcribing RNA polymerase from *Thermus thermophilus*', *Science Advances*, 9(6), p. eade7093. Available at: https://doi.org/10.1126/sciadv.ade7093.

Murray, C.J.L. *et al.* (2022) 'Global burden of bacterial antimicrobial resistance in 2019: a systematic analysis', *The Lancet*, 399(10325), pp. 629–655. Available at: https://doi.org/10.1016/S0140-6736(21)02724-0.

Nagy, Z. and Chandler, M. (2004) 'Regulation of transposition in bacteria', *Research in microbiology*, 155, pp. 387–98. Available at: https://doi.org/10.1016/j.resmic.2004.01.008.

Navarre, W.W. *et al.* (2007) 'Silencing of xenogeneic DNA by H-NS—facilitation of lateral gene transfer in bacteria by a defense system that recognizes foreign DNA', *Genes & Development*, 21(12), pp. 1456–1471. Available at: https://doi.org/10.1101/gad.1543107.

Naville, M. *et al.* (2011) 'ARNold: A web tool for the prediction of Rho-independent transcription terminators', *RNA Biology*, 8(1), pp. 11–13. Available at: https://doi.org/10.4161/rna.8.1.13346.

Nieto, J.M. *et al.* (2002) 'Evidence for Direct Protein-Protein Interaction between Members of the Enterobacterial Hha/YmoA and H-NS Families of Proteins', *Journal of Bacteriology*, 184(3), pp. 629–635. Available at: https://doi.org/10.1128/JB.184.3.629-635.2002.

Nir-Paz, R. *et al.* (2019) 'Successful Treatment of Antibiotic-resistant, Poly-microbial Bone Infection With Bacteriophages and Antibiotics Combination', *Clinical Infectious Diseases*, 69(11), pp. 2015–2018. Available at: https://doi.org/10.1093/cid/ciz222.

Noel, H.R., Petrey, J.R. and Palmer, L.D. (2022) 'Mobile genetic elements in *Acinetobacter* antibiotic-resistance acquisition and dissemination', *Annals of the New York Academy of Sciences*, 1518(1), pp. 166–182. Available at: https://doi.org/10.1111/nyas.14918.

Noom, M.C. *et al.* (2007) 'H-NS promotes looped domain formation in the bacterial chromosome', *Current biology: CB*, 17(21), pp. R913-914. Available at: https://doi.org/10.1016/j.cub.2007.09.005.

Olmeda-López, H., Corral-Lugo, A. and McConnell, M.J. (2021) 'Effect of Subinhibitory Concentrations of Antibiotics and Disinfectants on IS*Aba*-Mediated Inactivation of Lipooligosaccharide Biosynthesis Genes in Acinetobacter baumannii', *Antibiotics*, 10(10), p. 1259. Available at: https://doi.org/10.3390/antibiotics10101259.

van Opijnen, T. and Levin, H.L. (2020) 'Transposon Insertion Sequencing, a Global Measure of Gene Function', *Annual review of genetics*, 54, pp. 337–365. Available at: https://doi.org/10.1146/annurev-genet-112618-043838.

Ou, H.-Y. *et al.* (2015) 'Complete genome sequence of hypervirulent and outbreak-associated *Acinetobacter baumannii* strain LAC-4: epidemiology, resistance genetic determinants and potential virulence factors', *Scientific Reports*, 5, p. 8643. Available at: https://doi.org/10.1038/srep08643.

Page, L., Griffiths, L. and Cole, J.A. (1990) 'Different physiological roles of two independent pathways for nitrite reduction to ammonia by enteric bacteria', *Archives of Microbiology*, 154(4), pp. 349–354. Available at: https://doi.org/10.1007/BF00276530.

Paget, M.S. and Helmann, J.D. (2003) 'The σ70 family of sigma factors', *Genome Biology*, 4(1), p. 203.

Park, H.-S. *et al.* (2010) 'Novel role for a bacterial nucleoid protein in translation of mRNAs with suboptimal ribosome-binding sites', *Genes & Development*, 24(13), pp. 1345–1350. Available at: https://doi.org/10.1101/gad.576310.

Park, K.-H. *et al.* (2014) 'The clinical characteristics, carbapenem resistance, and outcome of *Acinetobacter* bacteremia according to genospecies', *PloS One*, 8(6), p. e65026. Available at: https://doi.org/10.1371/journal.pone.0065026.

Penesyan, A. *et al.* (2019) 'Rapid microevolution of biofilm cells in response to antibiotics', *npj Biofilms and Microbiomes*, 5(1), p. 34. Available at: https://doi.org/10.1038/s41522-019-0108-3.

Pérez-Varela, M. *et al.* (2022) 'Stochastic activation of a family of TetR type transcriptional regulators controls phenotypic heterogeneity in *Acinetobacter baumannii*', *PNAS Nexus*, 1(5), p. pgac231. Available at: https://doi.org/10.1093/pnasnexus/pgac231.

Peters, J.E. and Craig, N.L. (2000) 'Tn7 Transposes Proximal to DNA Double-Strand Breaks and into Regions Where Chromosomal DNA Replication Terminates', *Molecular Cell*, 6(3), pp. 573–582. Available at: https://doi.org/10.1016/S1097-2765(00)00056-3.

Peters, J.M., Vangeloff, A.D. and Landick, R. (2011) 'Bacterial Transcription Terminators: The RNA 3′-End Chronicles', *Journal of molecular biology*, 412(5), pp. 793–813. Available at: https://doi.org/10.1016/j.jmb.2011.03.036.

Poirel, L., Bonnin, R.A. and Nordmann, P. (2011) 'Analysis of the Resistome of a Multidrug-Resistant NDM-1-Producing *Escherichia coli* Strain by High-Throughput Genome Sequencing', *Antimicrobial Agents and Chemotherapy*, 55(9), pp. 4224–4229. Available at: https://doi.org/10.1128/AAC.00165-11.

Porter, M.E. and Dorman, C.J. (1994) 'A role for H-NS in the thermo-osmotic regulation of virulence gene expression in *Shigella flexneri*.', *Journal of Bacteriology*, 176(13), pp. 4187–4191.

Pour, N.K. *et al.* (2011) 'Biofilm formation by *Acinetobacter baumannii* strains isolated from urinary tract infection and urinary catheters', *FEMS Immunology & Medical Microbiology*, 62(3), pp. 328–338. Available at: https://doi.org/10.1111/j.1574-695X.2011.00818.x.

Qin, L. *et al.* (2019) 'The architects of bacterial DNA bridges: a structurally and functionally conserved family of proteins', *Open Biology*, 9(12), p. 190223. Available at: https://doi.org/10.1098/rsob.190223.

Qin, L. *et al.* (2020) 'Structural basis for osmotic regulation of the DNA binding properties of H-NS proteins', *Nucleic Acids Research*, 48(4), pp. 2156–2172. Available at: https://doi.org/10.1093/nar/gkz1226.

Quinlan, A.R. and Hall, I.M. (2010) 'BEDTools: a flexible suite of utilities for comparing genomic features', *Bioinformatics*, 26(6), pp. 841–842. Available at: https://doi.org/10.1093/bioinformatics/btq033.

Rafailidis, P. *et al.* (2024) 'Current Therapeutic Approaches for Multidrug-Resistant and Extensively Drug-Resistant *Acinetobacter baumannii* Infections', *Antibiotics*, 13(3), p. 261. Available at: https://doi.org/10.3390/antibiotics13030261.

Rashid, F.-Z.M. *et al.* (2023) 'The environmentally-regulated interplay between local three-dimensional chromatin organisation and transcription of *proVWX* in *E. coli*', *Nature Communications*, 14, p. 7478. Available at: https://doi.org/10.1038/s41467-023-43322-y.

Ravasi, P. *et al.* (2011) 'IS*Aba*825, a Functional Insertion Sequence Modulating Genomic Plasticity and *bla*$_{OXA-58}$ Expression in *Acinetobacter baumannii*', *Antimicrobial Agents and Chemotherapy*, 55(2), pp. 917–920. Available at: https://doi.org/10.1128/AAC.00491-10.

Ray-Soni, A., Bellecourt, M.J. and Landick, R. (2016) 'Mechanisms of Bacterial Transcription Termination: All Good Things Must End', *Annual Review of Biochemistry*, 85(1), pp. 319–347. Available at: https://doi.org/10.1146/annurev-biochem-060815-014844.

Rebic, V. *et al.* (2018) 'The Importance of *Acinetobacter* Species in the Hospital Environment', *Medical Archives*, 72(5), pp. 325–329. Available at: https://doi.org/10.5455/medarh.2018.72.330-334.

Reichhardt, C. *et al.* (2015) 'Congo Red Interactions with Curli-Producing *E. coli* and Native Curli Amyloid Fibers', *PloS One*, 10(10), p. e0140388. Available at: https://doi.org/10.1371/journal.pone.0140388.

Repizo, G.D. *et al.* (2015) 'Differential Role of the T6SS in *Acinetobacter baumannii* Virulence', *PLOS ONE*, 10(9), p. e0138265. Available at: https://doi.org/10.1371/journal.pone.0138265.

Reyes, A. *et al.* (2012) 'IS-seq: a novel high throughput survey of *in vivo* IS6110 transposition in multiple *Mycobacterium tuberculosis* genomes', *BMC Genomics*, 13(1), p. 249. Available at: https://doi.org/10.1186/1471-2164-13-249.

Reynolds, A.E., Felton, J. and Wright, A. (1981) 'Insertion of DNA activates the cryptic *bgl* operon in *E. coli* K12', *Nature*, 293(5834), pp. 625–629. Available at: https://doi.org/10.1038/293625a0.

Rice, L.B. (2008) 'Federal Funding for the Study of Antimicrobial Resistance in Nosocomial Pathogens: No ESKAPE', *The Journal of Infectious Diseases*, 197(8), pp. 1079–1081. Available at: https://doi.org/10.1086/533452.

Roberts, J.W. (2019) 'Mechanisms of Bacterial Transcription Termination', *Journal of Molecular Biology*, 431(20), pp. 4030–4039. Available at: https://doi.org/10.1016/j.jmb.2019.04.003.

Robin, B. *et al.* (2022) 'MacAB-TolC Contributes to the Development of *Acinetobacter baumannii* Biofilm at the Solid–Liquid Interface', *Frontiers in Microbiology*, 12. Available at: https://www.frontiersin.org/articles/10.3389/fmicb.2021.785161 (Accessed: 5 October 2023).

Robinson, M.D., McCarthy, D.J. and Smyth, G.K. (2010) 'edgeR : a Bioconductor package for differential expression analysis of digital gene expression data', *Bioinformatics*, 26(1), pp. 139–140. Available at: https://doi.org/10.1093/bioinformatics/btp616.

Rodgers, D. *et al.* (2021) 'Histone-like nucleoid-structuring protein (H-NS) regulatory role in antibiotic resistance in *Acinetobacter baumannii*', *Scientific Reports*, 11(1), p. 18414. Available at: https://doi.org/10.1038/s41598-021-98101-w.

Ronish, L.A. *et al.* (2019) 'The structure of PilA from *Acinetobacter baumannii* AB5075 suggests a mechanism for functional specialization in *Acinetobacter* type IV pili', *The Journal of Biological Chemistry*, 294(1), pp. 218–230. Available at: https://doi.org/10.1074/jbc.RA118.005814.

Ross, K. *et al.* (2021) 'TnCentral: a Prokaryotic Transposable Element Database and Web Portal for Transposon Analysis', *mBio*, 12(5), p. 10.1128/mbio.02060-21. Available at: https://doi.org/10.1128/mbio.02060-21.

Rouquette, C., Serre, M.-C. and Lane, D. (2004) 'Protective Role for H-NS Protein in IS1 Transposition', *Journal of Bacteriology*, 186(7), pp. 2091–2098. Available at: https://doi.org/10.1128/JB.186.7.2091-2098.2004.

Santajit, S. and Indrawattana, N. (2016) 'Mechanisms of Antimicrobial Resistance in ESKAPE Pathogens', *BioMed Research International*, 2016, p. 2475067. Available at: https://doi.org/10.1155/2016/2475067.

Saranathan, R. *et al.* (2017) 'Disruption of *tetR* type regulator *adeN* by mobile genetic element confers elevated virulence in *Acinetobacter baumannii*', *Virulence*, 8(7), pp. 1316–1334. Available at: https://doi.org/10.1080/21505594.2017.1322240.

Saxena, S. *et al.* (2018) '*Escherichia coli* transcription factor NusG binds to 70S ribosomes', *Molecular Microbiology*, 108(5), pp. 495–504. Available at: https://doi.org/10.1111/mmi.13953.

Schmidt, A.J., Ryjenkov, D.A. and Gomelsky, M. (2005) 'The ubiquitous protein domain EAL is a cyclic diguanylate-specific phosphodiesterase: enzymatically active and inactive EAL domains', *Journal of Bacteriology*, 187(14), pp. 4774–4781. Available at: https://doi.org/10.1128/JB.187.14.4774-4781.2005.

Schmidt, H. and Hensel, M. (2004) 'Pathogenicity Islands in Bacterial Pathogenesis', *Clinical Microbiology Reviews*, 17(1), pp. 14–56. Available at: https://doi.org/10.1128/CMR.17.1.14-56.2004.

Schmitt, B.L. *et al.* (2023) 'Increased *ompW* and *ompA* expression and higher virulence of *Acinetobacter baumannii* persister cells', *BMC Microbiology*, 23(1), p. 157. Available at: https://doi.org/10.1186/s12866-023-02904-y.

Schnetz, K. and Rak, B. (1992) 'IS5: a mobile enhancer of transcription in *Escherichia coli*.', *Proceedings of the National Academy of Sciences of the United States of America*, 89(4), pp. 1244–1248.

Schuurmans, J.M. *et al.* (2009) 'Variations in MIC value caused by differences in experimental protocol', *Journal of Microbiological Methods*, 79(1), pp. 44–47. Available at: https://doi.org/10.1016/j.mimet.2009.07.017.

Sheck, E. *et al.* (2023) 'Acinetobacter Non-*baumannii* Species: Occurrence in Infections in Hospitalized Patients, Identification, and Antibiotic Resistance', *Antibiotics*, 12(8), p. 1301. Available at: https://doi.org/10.3390/antibiotics12081301.

Shin, M. *et al.* (2005) 'DNA looping-mediated repression by histone-like protein H-NS: specific requirement of Eσ70 as a cofactor for looping', *Genes & Development*, 19(19), pp. 2388–2398. Available at: https://doi.org/10.1101/gad.1316305.

Shin, M. *et al.* (2012) 'Gene silencing by H-NS from distal DNA site', *Molecular Microbiology*, 86(3), pp. 707–719. Available at: https://doi.org/10.1111/mmi.12012.

Siguier, P. *et al.* (2015) 'Everyman's Guide to Bacterial Insertion Sequences', *Microbiology Spectrum*, 3(2), pp. MDNA3-0030–2014. Available at: https://doi.org/10.1128/microbiolspec.MDNA3-0030-2014.

Siguier, P., Gagnevin, L. and Chandler, M. (2009) 'The new IS1595 family, its relation to IS1 and the frontier between insertion sequences and transposons', *Research in Microbiology*, 160(3), pp. 232–241. Available at: https://doi.org/10.1016/j.resmic.2009.02.003.

Siguier, P., Gourbeyre, E. and Chandler, M. (2014) 'Bacterial insertion sequences: their genomic impact and diversity', *FEMS Microbiology Reviews*, 38(5), pp. 865–891. Available at: https://doi.org/10.1111/1574-6976.12067.

Singh, J.K., Adams, F.G. and Brown, M.H. (2019) 'Diversity and Function of Capsular Polysaccharide in *Acinetobacter baumannii*', *Frontiers in Microbiology*, 9. Available at: https://www.frontiersin.org/article/10.3389/fmicb.2018.03301 (Accessed: 9 May 2022).

Singh, R.K. *et al.* (2008) 'The Nucleoid Binding Protein H-NS Acts as an Anti-Channeling Factor to Favor Intermolecular Tn10 Transposition and Dissemination', *Journal of Molecular Biology*, 376(4), pp. 950–962. Available at: https://doi.org/10.1016/j.jmb.2007.12.035.

Singh, S.S. *et al.* (2014) 'Widespread suppression of intragenic transcription initiation by H-NS', *Genes & Development*, 28(3), pp. 214–219. Available at: https://doi.org/10.1101/gad.234336.113.

Singh, S.S. and Grainger, D.C. (2013) 'H-NS Can Facilitate Specific DNA-binding by RNA Polymerase in AT-rich Gene Regulatory Regions', *PLOS Genetics*, 9(6), p. e1003589. Available at: https://doi.org/10.1371/journal.pgen.1003589.

Skordalakes, E. *et al.* (2005) 'Structural Mechanism of Inhibition of the Rho Transcription Termination Factor by the Antibiotic Bicyclomycin', *Structure*, 13(1), pp. 99–109. Available at: https://doi.org/10.1016/j.str.2004.10.013.

Snitkin, E.S. *et al.* (2011) 'Genome-wide recombination drives diversification of epidemic strains of *Acinetobacter baumannii*', *Proceedings of the National Academy of Sciences of the United States of America*, 108(33), pp. 13758–13763. Available at: https://doi.org/10.1073/pnas.1104404108.

Sobe, R.C. *et al.* (2022) 'FliL and its paralog MotF have distinct roles in the stator activity of the *Sinorhizobium meliloti* flagellar motor', *Molecular Microbiology*, 118(3), pp. 223–243. Available at: https://doi.org/10.1111/mmi.14964.

Spurio, R. *et al.* (1992) 'Lethal overproduction of the *Escherichia coli* nucleoid protein H-NS: ultramicroscopic and molecular autopsy', *Molecular & general genetics: MGG*, 231(2), pp. 201–211. Available at: https://doi.org/10.1007/BF00279792.

Sugawara, E. and Nikaido, H. (2012) 'OmpA is the principal nonspecific slow porin of *Acinetobacter baumannii*', *Journal of Bacteriology*, 194(15), pp. 4089–4096. Available at: https://doi.org/10.1128/JB.00435-12.

Sutherland, C. and Murakami, K.S. (2018) 'An Introduction to the Structure and Function of the catalytic core enzyme of *Escherichia coli* RNA polymerase', *EcoSal Plus*, 8(1), p. 10.1128/ecosalplus.ESP-0004–2018. Available at: https://doi.org/10.1128/ecosalplus.ESP-0004-2018.

Swingle, B. *et al.* (2004) 'The effect of host-encoded nucleoid proteins on transposition: H-NS influences targeting of both IS903 and Tn10', *Molecular Microbiology*, 52(4), pp. 1055–1067. Available at: https://doi.org/10.1111/j.1365-2958.2004.04051.x.

Tacconelli, E. *et al.* (2018) 'Discovery, research, and development of new antibiotics: the WHO priority list of antibiotic-resistant bacteria and tuberculosis', *The Lancet Infectious Diseases*, 18(3), pp. 318–327. Available at: https://doi.org/10.1016/S1473-3099(17)30753-3.

Talyansky, Y. *et al.* (2021) 'Capsule carbohydrate structure determines virulence in *Acinetobacter baumannii*', *PLoS Pathogens*, 17(2), p. e1009291. Available at: https://doi.org/10.1371/journal.ppat.1009291.

Tavakoli, N.P. and Derbyshire, K.M. (2001) 'Tipping the balance between replicative and simple transposition', *The EMBO Journal*, 20(11), pp. 2923–2930. Available at: https://doi.org/10.1093/emboj/20.11.2923.

Tenzen, T., Matsutani, S. and Ohtsubo, E. (1990) 'Site-specific transposition of insertion sequence IS630.', *Journal of Bacteriology*, 172(7), pp. 3830–3836.

Tipton, K.A., Dimitrova, D. and Rather, P.N. (2015) 'Phase-Variable Control of Multiple Phenotypes in *Acinetobacter baumannii* Strain AB5075', *Journal of Bacteriology*, 197(15), pp. 2593–2599. Available at: https://doi.org/10.1128/JB.00188-15.

Tiwari, V. *et al.* (2012) 'Comparative Proteomics of Inner Membrane Fraction from Carbapenem-Resistant *Acinetobacter baumannii* with a Reference Strain', *PLoS ONE*, 7(6), p. e39451. Available at: https://doi.org/10.1371/journal.pone.0039451.

Tobes, R. and Pareja, E. (2006) 'Bacterial repetitive extragenic palindromic sequences are DNA targets for Insertion Sequence elements', *BMC Genomics*, 7(1), p. 62. Available at: https://doi.org/10.1186/1471-2164-7-62.

Ton-Hoang, B., Turlan, C. and Chandler, M. (2004) 'Functional domains of the IS1 transposase: analysis in vivo and in vitro', *Molecular Microbiology*, 53(5), pp. 1529–1543. Available at: https://doi.org/10.1111/j.1365-2958.2004.04223.x.

Torres-Barceló, C. (2018) 'The disparate effects of bacteriophages on antibiotic-resistant bacteria', *Emerging Microbes & Infections*, 7(1), pp. 1–12. Available at: https://doi.org/10.1038/s41426-018-0169-z.

Touchon, M. *et al.* (2014) 'The Genomic Diversification of the Whole *Acinetobacter* Genus: Origins, Mechanisms, and Consequences', *Genome Biology and Evolution*, 6(10), pp. 2866–2882. Available at: https://doi.org/10.1093/gbe/evu225.

Traglia, G.M. *et al.* (2016) 'Serum Albumin and Ca^{2+} Are Natural Competence Inducers in the Human Pathogen *Acinetobacter baumannii*', *Antimicrobial Agents and Chemotherapy*, 60(8), pp. 4920–4929. Available at: https://doi.org/10.1128/AAC.00529-16.

Tupper, A.E. *et al.* (1994) 'The chromatin-associated protein H-NS alters DNA topology in vitro.', *The EMBO Journal*, 13(1), pp. 258–268.

Turton, J.F. *et al.* (2006) 'The role of IS*Aba*1 in expression of OXA carbapenemase genes in *Acinetobacter baumannii*', *FEMS Microbiology Letters*, 258(1), pp. 72–77. Available at: https://doi.org/10.1111/j.1574-6968.2006.00195.x.

Upmanyu, K., Haq, Q.Mohd.R. and Singh, R. (2022) 'Factors mediating *Acinetobacter baumannii* biofilm formation: Opportunities for developing therapeutics', *Current Research in Microbial Sciences*, 3, p. 100131. Available at: https://doi.org/10.1016/j.crmicr.2022.100131.

van der Valk, R.A. *et al.* (2017) Mechanism of environmentally driven conformational changes that modulate H-NS DNA-bridging activity, *eLife*. eLife Sciences Publications Limited. Available at: https://doi.org/10.7554/eLife.27369.

Vandecraen, J. *et al.* (2017) 'The impact of insertion sequences on bacterial genome plasticity and adaptability', *Critical Reviews in Microbiology*, 43(6), pp. 709–730. Available at: https://doi.org/10.1080/1040841X.2017.1303661.

Vesel, N. and Blokesch, M. (2021) 'Pilus Production in *Acinetobacter baumannii* Is Growth Phase Dependent and Essential for Natural Transformation', *Journal of Bacteriology*. Edited by T.J. Silhavy, 203(8). Available at: https://doi.org/10.1128/JB.00034-21.

Vijayakumar, S. *et al.* (2016) 'Biofilm Formation and Motility Depend on the Nature of the *Acinetobacter baumannii* Clinical Isolates', *Frontiers in Public Health*, 4, p. 105. Available at: https://doi.org/10.3389/fpubh.2016.00105.

Vijayakumar, S., Biswas, I. and Veeraraghavan, B. (2019) 'Accurate identification of clinically important *Acinetobacter* spp.: an update', *Future Science OA*, 5(6), p. FSO395. Available at: https://doi.org/10.2144/fsoa-2018-0127.

Vila, J., Martí, S. and Sánchez-Céspedes, J. (2007) 'Porins, efflux pumps and multidrug resistance in *Acinetobacter baumannii*', *Journal of Antimicrobial Chemotherapy*, 59(6), pp. 1210–1215. Available at: https://doi.org/10.1093/jac/dkl509.

Visca, P., Seifert, H. and Towner, K.J. (2011) '*Acinetobacter* infection – an emerging threat to human health', *IUBMB Life*, 63(12), pp. 1048–1054. Available at: https://doi.org/10.1002/iub.534.

Wan, B. *et al.* (2016) 'Global transcriptional regulation by H-NS and its biological influence on the virulence of Enterohemorrhagic *Escherichia coli*', *Gene*, 588(2), pp. 115–123. Available at: https://doi.org/10.1016/j.gene.2016.05.007.

Wang, L., Wang, S. and Li, W. (2012) 'RSeQC: quality control of RNA-seq experiments', *Bioinformatics*, 28(16), pp. 2184–2185. Available at: https://doi.org/10.1093/bioinformatics/bts356.

Wang, W. *et al.* (2011) 'Chromosome organization by a nucleoid-associated protein in live bacteria', *Science (New York, N.y.)*, 333(6048), pp. 1445–1449. Available at: https://doi.org/10.1126/science.1204697.

Ward, C.M. *et al.* (2007) 'The global regulator H-NS binds to two distinct classes of sites within the Tn10 transpososome to promote transposition', *Molecular Microbiology*, 64(4), pp. 1000–1013. Available at: https://doi.org/10.1111/j.1365-2958.2007.05708.x.

Wardle, S.J. *et al.* (2005) 'The global regulator H-NS acts directly on the transpososome to promote Tn10 transposition', *Genes & Development*, 19(18), pp. 2224–2235. Available at: https://doi.org/10.1101/gad.1338905.

Wardle, S.J., Chan, A. and Haniford, D.B. (2009) 'H-NS binds with high affinity to the Tn10 transpososome and promotes transpososome stabilization', *Nucleic Acids Research*, 37(18), pp. 6148–6160. Available at: https://doi.org/10.1093/nar/gkp672.

Warman, E.A. *et al.* (2021) 'Widespread divergent transcription from bacterial and archaeal promoters is a consequence of DNA sequence symmetry', *Nature microbiology*, 6(6), pp. 746–756. Available at: https://doi.org/10.1038/s41564-021-00898-9.

Weber, B.S., Harding, C.M. and Feldman, M.F. (2016) 'Pathogenic *Acinetobacter*: from the Cell Surface to Infinity and Beyond', *Journal of Bacteriology*, 198(6), pp. 880–887. Available at: https://doi.org/10.1128/JB.00906-15.

Weinreich, M.D., Gasch, A. and Reznikoff, W.S. (1994) 'Evidence that the cis preference of the Tn5 transposase is caused by nonproductive multimerization.', *Genes & Development*, 8(19), pp. 2363–2374. Available at: https://doi.org/10.1101/gad.8.19.2363.

Whiteway, C. *et al.* (2022) 'Scarless excision of an insertion sequence restores capsule production and virulence in *Acinetobacter baumannii*', *The ISME Journal*, 16(5), pp. 1473–1477. Available at: https://doi.org/10.1038/s41396-021-01179-3.

Whitfield, C.R., Wardle, S.J. and Haniford, D.B. (2009) 'The global bacterial regulator H-NS promotes transpososome formation and transposition in the Tn5 system', *Nucleic Acids Research*, 37(2), pp. 309–321. Available at: https://doi.org/10.1093/nar/gkn935.

Wickham, H. (2009) ggplot2: Elegant Graphics for Data Analysis. New York, NY: Springer. Available at: https://doi.org/10.1007/978-0-387-98141-3.

Wilde, C. *et al.* (2003) 'Transposases are responsible for the target specificity of IS1397 and ISKpn1 for two different types of palindromic units (PUs)', *Nucleic Acids Research*, 31(15), pp. 4345–4353.

Wilharm, G. *et al.* (2013) 'DNA Uptake by the Nosocomial Pathogen *Acinetobacter baumannii* Occurs during Movement along Wet Surfaces', *Journal of Bacteriology*, 195(18), pp. 4146–4153. Available at: https://doi.org/10.1128/JB.00754-13.

Wilharm, G. *et al.* (2017) 'Relatedness of wildlife and livestock avian isolates of the nosocomial pathogen *Acinetobacter baumannii* to lineages spread in hospitals worldwide: Avian Isolates of *Acinetobacter baumannii*', *Environmental Microbiology*, 19(10), pp. 4349–4364. Available at: https://doi.org/10.1111/1462-2920.13931.

Williamson, H.S. and Free, A. (2005) 'A truncated H-NS-like protein from enteropathogenic *Escherichia coli* acts as an H-NS antagonist', *Molecular Microbiology*, 55(3), pp. 808–827. Available at: https://doi.org/10.1111/j.1365-2958.2004.04421.x.

van der Woude, M.W. and Bäumler, A.J. (2004) 'Phase and Antigenic Variation in Bacteria', *Clinical Microbiology Reviews*, 17(3), pp. 581–611. Available at: https://doi.org/10.1128/CMR.17.3.581-611.2004.

Wright, M.S. *et al.* (2014) 'New Insights into Dissemination and Variation of the Health Care-Associated Pathogen *Acinetobacter baumannii* from Genomic Analysis', *mBio*, 5(1), p. 10.1128/mbio.00963-13. Available at: https://doi.org/10.1128/mbio.00963-13.

Wright, M.S. *et al.* (2017) 'Assessment of Insertion Sequence Mobilization as an Adaptive Response to Oxidative Stress in *Acinetobacter baumannii* Using IS-seq', *Journal of Bacteriology*, 199(9), pp. e00833-16. Available at: https://doi.org/10.1128/JB.00833-16.

Wu, X. *et al.* (2016) 'In vivo protein interaction network analysis reveals porin-localized antibiotic inactivation in *Acinetobacter baumannii* strain AB5075', *Nature Communications*, 7, p. 13414. Available at: https://doi.org/10.1038/ncomms13414.

You, L. *et al.* (2023) 'Structural basis for intrinsic transcription termination', *Nature*, 613(7945), pp. 783–789. Available at: https://doi.org/10.1038/s41586-022-05604-1.

Zang, M. *et al.* (2021) 'The Impact of Omega-3 Fatty Acids on the Evolution of *Acinetobacter baumannii* Drug Resistance', *Microbiology Spectrum*. Edited by A. Kumar, 9(3), pp. e01455-21. Available at: https://doi.org/10.1128/Spectrum.01455-21.

Zhang, G. *et al.* (1999) 'Crystal Structure of Thermus aquaticus Core RNA Polymerase at 3.3 Å Resolution', *Cell*, 98(6), pp. 811–824. Available at: https://doi.org/10.1016/S0092-8674(00)81515-9.

Zhang, H. *et al.* (2016) 'Identification and Characterization of *Staphylococcus aureus* Strains with an Incomplete Hemolytic Phenotype', *Frontiers in Cellular and Infection Microbiology*, 6. Available at: https://doi.org/10.3389/fcimb.2016.00146.

Zhu, L. *et al.* (2013) 'Complete Genome Analysis of Three *Acinetobacter baumannii* Clinical Isolates in China for Insight into the Diversification of Drug Resistance Elements', *PLoS ONE*, 8(6), p. e66584. Available at: https://doi.org/10.1371/journal.pone.0066584.